Radiocarbon Reservoir Effects on Shells from SE Arabia in the Context of Paleoenvironmental Studies

Dissertation

zur Erlangung des akademischen Grades

„Doktor der Naturwissenschaften“

Fachbereich Material- und Geowissenschaften

der Technischen-Universität Darmstadt

vorgelegt 2019 von

Susanne Lindauer

Prüfung am 01. Juli 2019

Erstprüfer/in:	Prof. Dr. Matthias Hinderer
Zweitprüfer/in:	Prof. Dr. Frank Preusser
Weitere Prüfer:	Prof. Dr. Stephan Kempe,
	Prof. Dr. Nico Blüthgen

Lindauer, Susanne: Radiocarbon Reservoir Effects on Shells from SE Arabia in the Context of Plaeoenvironmental Studies
Darmstadt, Technische Universität Darmstadt,
Year thesis published in Tuprints 2019
Date of the viva voce 01.07.2019

„When we try to pick out anything by itself, we find it hitched to everything else in the Universe”

- John Muir (My First Summer in the Sierra, 1911)

-

This thesis is dedicated to Jacqueline and Adrian Lindauer,

to Amy (†), Indra, Oskar, Lilith and Ella

Eidesstattliche Erklärung (Declaration of authorship)

Ich erkläre hiermit, die vorliegende Dissertation ohne Hilfe Dritter und nur mit den angegebenen Quellen und Hilfsmitteln angefertigt zu haben. Alle Stellen, die aus Quellen übernommen wurden, sind als solche kenntlich gemacht worden. Diese Arbeit hat in dieser oder ähnlicher Form noch keiner Prüfungsbehörde vorgelegen. Die schriftliche Fassung stimmt mit der elektronischen Fassung überein.

Darmstadt, den

Susanne Lindauer

Short CV

Since Feb 2011 – technical and scientific staff at Curt-Engelhorn-Zentrum Archäometrie gGmbH (radiocarbon and luminescence dating laboratories)

Juli 2006 – Jan 2011 – technical assistant at the Radiocarbon laboratory, Heidelberg Academy of Sciences

Aug 1993 – June 2006 – technical assistant at Luminescence laboratory, Heidelberg Academy of Sciences

From 1998 – 2005 studies in Physics, Astrophysics at Milton Keynes, UK (BSc honors, MSc Science with distinction)

Okt 1991 – July 1993 Berufsbildende Schule Naturwissenschaften (School for Technical staff) Ludwigshafen

1986 – 1989 – student at Heidelberg University (Physics and Astrophysics)

Born 1966

Foreword

This thesis is a cumulative dissertation, which comprises six publications in peer-reviewed journals.

The idea to work on this topic as a PhD thesis arose of problems regarding reservoir effects along the coast of the Gulf of Oman. I became interested in this subject and tried to construct a basic and systematic approach to investigate this topic further. Gladly, some people believed this was a good idea and supported me in various ways and I would like to take the chance to express my gratitude.

First I would like to thank my supervisors Prof. Dr. Matthias Hinderer, Institute of Applied Geosciences, Technical University Darmstadt, and Prof. Dr. Frank Preusser, Institute of Geology, University of Freiburg for their support and continuous encouragement to keep going although I had to do this thesis in my spare time. I´m glad they found time to accompany me to the United Arab Emirates to also teach me some geology on site. Especially Frank also shared his contacts with me which I´m absolutely grateful for. This allowed me to meet Prof. Adrian Parker, Brookes University Oxford, who was such a great help and supported me as much as he could.

Without Hans-Peter and Margarethe Uerpmann I probably would never have had the change to learn about this topic and even go to the UAE to sample the sites myself. Sabah Jasim and Eisa Yousif from the Directorate of Archaeology, Sharjah Emirate, UAE, were wonderful colleagues and invited me to come to Sharjah.

My colleagues Axel Steinhof, MPI Biogeochemistry, Jena and Guaciara Santos, KCCAMS, University Irvine, were the constant support when it came to helping out with radiocarbon measurements! I never before had experienced so wonderful unselfish support by colleagues who became good friends. In this context I would also like to thank my wonderful colleagues from the radiocarbon community who were always encouraging me and showed a lot of interest in my results. Fiona Petchey had introduced me into the calculations of the reservoir effect, although we never managed to meet in person so far.

I would like to thank Dr. Soraya Marali who taught me how to handle shells for stable isotopes. She was very patient, always willing to help and take some time to explain drilling, milling, taking photos, cutting and polishing and all sorts of things. Dr. Stefania Milano, too, was a great help and we both got carried away by burnt shells. It was wonderful to meet you ladies! Michael Maus is a very sophisticated colleague when it comes to stable isotope measurements and has my full admiration. Thanks for measuring my shells and providing wonderful insights into the measurements. Prof. Dr. Bernd Schöne was always encouraging and really got me interested in the stable isotopes on shells. Thanks you for allowing me to work at your lab and the many fruitful discussions and exchange of new ideas.

Carl Phillips shared his knowledge about Kalba with me and the enthusiasm to protect the mangroves in Arabia. Without his help we would not have found suitable samples in the Bronze Age settlement and we had wonderful discussions about the results via email. Marc Händel, Austrian Academy of Sciences, Vienna and Peter Magee, Bryn Mawr College, USA, thanks for being interested in my research and offering help. Although our results are not included here, they helped me to understand contexts.

I should also acknowledge the support from my employer, the Curt-Engelhorn-Centre for Archaeometry, though, who allowed me to do some measurements without funding. And from the technical staff there, Robin van Gyseghem, you know how you supported me. Our head of lab, Ronny Friedrich, should be acknowledged for letting me test the time-consuming and ear-battering high resolution measurements with our MICADAS AMS. Corina Knipper, wo also introduced me to Bernd Schöne, and Sandra Kraus were always interested and shared my enthusiasm.

Many friends and colleagues, especially Anni Begerock, Petra Würtz, Brigitte Heissner, Joachim Weylandt, Carmen Groß, Carmen Fontagnier, Lea Obrocki, Mike Krochmal, Lena Wittenstock, Christian Theis, Holger Mandel and his wife Carmen, Gösta Hoffmann, Ash Parton, Knut Bretzke, David Hindle, Andrew Green, Seppi Lehner, Heather Gill-Frerking and many more were a encouraging when I was desperate about the conditions and exhausted from not having a real holiday for so long. I owe you so much for not letting me down and encouraging me to continue. Some had to suffer while correcting my Germanisms. Especially Marc McClure always had an open door at conferences and cheered me up so often. I miss meeting you, Marc!

Last but not least I want to thank my wonderful little family that patiently endured a constantly exhausted family member. My mum Jacqueline who tried to help as good as she could and my son Adrian who always helped out with the pets when I had to travel or did not feel well. Amy (who sadly passed away 2018), Indra, Lilith, Oskar and Ella were absolutely gorgeous in helping to reduce stress and enjoy life besides working. They were patient when I practiced my talks and I´m sure they could give the talks meanwhile as well. By the way, Amy is hidden in one of the figures.

Abstract

Shells are among the most frequently used materials for dating coastal sites with radiocarbon, especially when no organic matter, such as bone collagen, is preserved. Shells are frequently used to constrain chronologies from archaeological sites or within palaeoenvironmental research. Sites throughout Arabia tend to lack organic material suitable for dating. Marine shells in upwelling areas, such as the Arabian Sea, show an older apparent age than contemporaneous terrestrial material, hence are most likely depleted in radiocarbon. In radiocarbon dating, this is referred to as marine reservoir effect. Correcting for this effect for a given period and location is required to establish reliable chronologies.

The aim of this research is to explore an understanding of the marine reservoir effect with respect to site-related factors and temporal variation. The suitability of shells for environmental monitoring is investigated using sclerochronology and stable isotopes and interpreted on the basis of background information on diet and habitat of respective mollusc species. A species-specific reservoir effect is then determined for radiocarbon chronologies and temporal variations are evaluated by assigning a species-specific reservoir effect to each period investigated. High resolution radiocarbon measurements along the shell are tested with the aim to support carbon isotope ($\delta^{13}C$) interpretation and determine a minimum amount of carbon necessary for reliable data. Shell foraging and subsequent heating provides an important aspect of this work with respect to its influence on the shell material and possible shifts in data, especially radiocarbon. A shift in data due to heating would prevent the use of heated shells for environmental monitoring and radiocarbon dating. Additionally, a pilot study sheds light on possible variations in hardwater effects on land and freshwater gastropods depending on the geological setting. Sampling sites range from archaeological excavations along the coast (Kalba) and inland (Wadi al-Hilo) to wadis throughout the Hajar Mountains in the United Arab Emirates.

The site of Kalba was chosen as the location for investigating the reservoir effect of marine shells and environmental conditions during their lifetime. Kalba is located between the Gulf of Oman and the Hajar Mountains and provides shells of different species from a mangrove forest that has existed since at least the mid-Holocene (ca. 7000 cal BP). Archaeological sites in Kalba dating to Neolithic and to the Bronze Age offer sediment layers rich in shells. Additionally, Kalba offers the unique possibility to monitor seasonal ocean circulation patterns where upwelling from the Arabian Sea to the South alternates with saline, dense outflow of Arabian Gulf waters. The Hajar Mountains reveal a diverse geology with ophiolites located southwest of Kalba and carbonates to the north. The Dibba Zone shows outcrops of shelf carbonates and metamorphic rocks and provides the greatest diversity of lithologies in the Hajar Mountains. For the study of terrestrial shells, this diversity conditioned the sampling sites in order to derive a dependence of possible hardwater effect on lithology involved.

The first part of the study concentrates on two shell species from Kalba, the bivalve *Anadara uropigimelana* and the gastropod *Terebralia palustris*, because they are often found in archaeological contexts. Shell and charcoal pairs were recovered from four layers representing two periods, Neolithic and Bronze Age, to evaluate temporal changes in the species-specific reservoir effect. For *A. uropigimelana*

a drop in ΔR from 576 ± 90 to 112 ± 44 years over this period was calculated, whereas for *T. palustris* the values decreases from 389 ± 66 to -19 ± 36 years. This species-specific reservoir effect likely reflects differences in habitat and/or dietary habits. *T. palustris* with a mainly terrestrial diet yielded a significantly lower ΔR compared to the mainly marine influenced *A. uropigimelana*. The temporal changes are probably explained by reduced upwelling in the Arabian Sea as observed in marine sediment cores, due to a decrease in summer monsoon strength.

High resolution ^{14}C measurements were performed in combination with stable isotopes $\delta^{13}C$ and $\delta^{18}O$ on two specimens of *A. uropigimelana*. Here, ^{14}C served to support the interpretation of the inconclusive $\delta^{13}C$ signal that has its origin in diet as well as water dissolved inorganic carbon (DIC). Sample sizes below 30 µg C did not result in reliable data due to elevated backgrounds for ^{14}C measurement and cross contamination from the previous sample. Nevertheless, trends in data could be identified and provided insights to help interpret changes in amplitude or extreme drifts of the isotopes as a result of changes in environmental conditions, such as freshwater input, or diet.

Shell foraging often includes heating of shells that inflicts a transformation from aragonite to calcite and also destroys the microstructural pattern of the shell material. Data indicates that the ^{14}C measurement is not shifted by heating of the shell material. Therefore, heated shell material like unheated shell carbonate provides reliable material for chronological purposes.

Land snails of species *Zootecus insularis* and freshwater snails of species *Melanoides tuberculata* were recovered from different geological substrates. A strong link between lithology and hard-water effect of the terrestrial species was found, even though distinct values for the hard-water effect could not be determined for all sites involved. Unfortunately, no live specimens could be found to resolve this problem. Therefore, archaeological samples of known context provide the most reliable basis for interpretation.

In conclusion this study shows that shells of *A. uropigimelana* and *T. palustris*, heated or unheated, are a valuable tool for evaluating chronologies. The drop in marine reservoir effect ΔR of the shells mirrors local changes in ocean circulation and upwelling and is directly linked to changes in climate and sea level during the Holocene. On a regional as well as global scale it coincides with significant changes in other paleoclimate archives. Regarding the pilot study on the terrestrial hardwater effect of *Z. insularis* and *M. tuberculata*, however, promising new results for some locations are presented. As expected, it varies with lithology, but still needs to be verified by known age samples before being used in this region.

In brief, the results of this thesis show that marine reservoir effects are not only dependent on location but also vary through time and by species. Whilst this has been demonstrated here for the Southeastern part of the Arabian Peninsula, similar variations in time and species are likely to also occur in other regions of the globe.

To establish reliable radiocarbon chronologies using shells, the reservoir effect has to be determined considering all of these factors. Whilst time consuming, and in part challenging, this approach, offers numerous possibilities for evaluating environmental data from a single material.

Table of Contents

List of figures

List of Tables

1 Introduction

Background

Radiocarbon dating, on both organic (bone collagen, wood, charcoal, etc.) and inorganic (shells, secondary carbonates, stalagmites, corals, etc.) material, is often applied for archaeological or geochronological research worldwide. In Arabia, due to the arid environment, organic material suitable for radiocarbon dating is hardly preserved. Shells are investigated in Arabia only if no other material suitable for either luminescence dating or radiocarbon dating can be found. They are not regarded as an archive themselves.

When used for radiocarbon dating, shells often show a higher age than their calendar age, this is termed the reservoir age R(t). In relation to the marine calibration curve (with 405 ± 22 years offset to the atmospheric curve) it is referred to as reservoir effect ΔR (Stuiver et al. 1986, Ascough et al. 2005) and can be calculated as ΔR = R(t) – 405 years in a first approach. So far, in chronologies on the Arabian peninsula, scientists used values from the literature (Southon et al. 2002, Dutta 2008) that had been determined from live-collected specimen (pre-bomb period) taken from museum collections. Their apparent ages differed significantly by up to 400 years (Southon et al. 2002), therefore a mean value is usually taken. In areas of upwelling, radiocarbon depleted waters are brought to the surface resulting in apparent older ages. Areas of downwelling transport atmospheric carbon into the deep sea resulting in younger ages than expected for marine organisms.

Archaeologists found that reservoir ages and reservoir effects differ between coastal sites in Oman and the United Arab Emirates (Uerpmann 1990, Charpentier et al. 2000, Staubwasser et al. 2002, Saliege 2005, Zazzo et al. 2012, Berger et al. 2013). No systematic investigation regarding shell species nor local differences or temporal variations has been conducted for shells in Arabia so far. Studies trying to tackle these questions have never resulted in species-specific ΔR and results are still given as average values, even when samples are taken from different layers and hence representative of temporal sequences (Zazzo et al. 2012, Zazzo et al. 2016).

Reservoir effects for mixed shell data varied drastically between locations at the Atlantic coast of Portugal and Spain, but decreased constantly from 4700 ^{14}C yrs BP (ΔR 527 ± 54 yrs) to 2400 ^{14}C yrs BP (ΔR -120 ± 41 yrs) (Martins and Soares 2013). However, at American coasts, it is already common to determine a species-specific reservoir effect (Alves et al. 2015, Alves et al. 2015, Alves et al. 2016, Hadden and Cherkinsky 2017, Paterne et al. 2018), although some authors still determine a mean value irrespective of species (Diaz et al. 2016). Shells of different species from the Gulf of California yielded ΔR values of several hundred years (357 – 397 at 4880 cal BP; 296 – 486 yrs at 2750 cal BP and 417 – 427 yrs around 1983 cal BP), showing no distinct pattern of decrease or increase (Dettman et al. 2015). Shells of family *Mytillidae* at the Patagonian coast (Argentina) show a rather low reservoir effect (less than -100 yrs) over the time interval 5300 to 700 ^{14}C yrs BP (Favier Dubois and Jull 2017). This can be explained by oceanic downwelling. In Oceania, a species-specific reservoir effect from archaeological

specimens of *Anadara spp*. shells (dated to 2000 – 2500 ^{14}C yrs BP) yielded reservoir effects in the range of ca. 17 to -117 yrs with *Anadara granosa* slightly younger than *Anadara antiquata* (Petchey et al. 2013).

Apart from Zazzo et al. (2016) for Ras al-Hamra, Oman, no study has determined the species-specific reservoir effect from shells of a well-defined period for the Oman and United Arab Emirates (UAE) region. Zazzo and co-workers found ΔR for *Anadara antiquata* to range between 99 and 207 years for ages between 6425 to 5760 BP but did not differentiate between the sediment/shell layers involved within this period. Another limitation is that most studies are based on live collected specimens from museum collections. The combined analysis of modern and past reservoir effects, i.e. considering temporal variabilities, is widely absent in the literature and non - systematic applications in archaeology are common. A proper determination and usage of a species-specific reservoir effect, however, is essential to use shell dating for precise chronologies. If the reservoir effect is not determined for the species used and the period of interest, this increases the uncertainty of dating and can lead to erroneous interpretation.

The prior goal of this study was a systematic approach to determine and use species-specific reservoir effects with local dependencies and temporal variation in SE Arabia. Due to the scarceness of datable organic material such as collagen, the frequently found shells offer the opportunity to set-up an alternative radiocarbon chronology in as far as the reservoir effect can be determined accurately. Shells were used by humans as food resource as well as jewelry and are omnipresent in and around excavations, especially at coastal sites. Kalba in the Emirate Sharjah, United Arab Emirates (UAE), was chosen as the main location for this study because of its archeologically well-documented excavations from the Neolithic and Bronze Age (Phillips and Mosseri-Marlio 2002, Eddisford and Phillips 2009). Moreover, this site offers the opportunity to detect the interference of upwelling in the Gulf of Oman (GO) and outflow of more saline water via the Strait of Hormuz from the Arabian Gulf (AG) over the past millennia (Johns et al. 2000, Dalongeville and Sanlaville 2005).

The Gulf of Oman is the northern extension of the Arabian Sea (AS). Upwelling in the Arabian Sea shows a seasonal pattern (Staubwasser et al. 2002, Thamban et al. 2007, Singh et al. 2011, Enzel et al. 2015, Lokier et al. 2017). It is stronger during summer monsoon, when the wind turns southeast. When upwelling in the AS is reduced, this means less admixture of depleted radiocarbon from deep ocean waters in the coastal zone and a reduction of ΔR for marine organisms (Staubwasser et al. 2002). The AG should show a reduced ΔR, because deep water is lacking and exchange with the atmosphere strong. But ΔR is influenced from discharge of carbonate-rich river water and fossil groundwater as well as carbonate-rich sediment. Outflow from the AG affects ΔR at Kalba, but weakens towards the south such as in the Muscat region, where other studies on reservoir effects of shells had been done (Zazzo et al. 2012, Zazzo et al. 2016). Hence different ΔR values by several hundred years are found for Kalba (this study) and Muscat (both *Anadara spp*.) or Suwayh (*Amiantis umbonella*) (Charpentier et al. 2000, Zazzo et al. 2012, Zazzo et al. 2016). The outflow rate from the AG depends on sea level and wind strength. Beach records show that sea level was highest around 6000 BP and dropped with occasional short pulses of sea-level rise until it reached present-day sea level after ca.1500 BP (Bernier et al. 1995, Lambeck 1996). This reduced inflow into the AS over time.

The terrestrial equivalent of the reservoir effect is the hardwater effect, which is caused by uptake of dead carbon from limestones or carbonate-bearing rocks by organisms or via groundwater. The hardwater effect has not been investigated in Arabia until now, although the contrasting lithology of limestone areas and carbonate-free ophiolites offers a suitable regional case study. Some studies on radiocarbon dating of landsnails in combination with stable isotopes are reported e.g. from North America and Israel (Goodfriend and Stipp 1983, Goodfriend 1987, Goodfriend 1990, Goodfriend 1992, Goodfriend et al. 1999, Pigati et al. 2010, Rech et al. 2016). These studies found a strong correlation between the lithology involved and the snails collected. The stable isotope $\delta^{13}C$ provided some hints regarding the amount of limestone incorporated, but without proper knowledge of diet and habitat, the data cannot be used properly.

The linkage of human migration and settlement development as well as terrestrial climate archives provides additional information to interpret the measured reservoir effects. In Arabia, a significant reduction in the amount of settlements is recorded between Neolithic and Bronze Age – the so-called "Dark Millenium" from the 4th millennium BC to 1300 BC (Uerpmann 2003). In the early Holocene, the monsoon strengthened due to a northward shift of the intertropical convergence zone (ITCZ) (Fleitmann et al. 2007). A more humid climate lasted until the Neolithic with a savanna-type vegetation and beneficial environments for grazing cattle (Parker et al. 2006, Jennings et al. 2015, Preston et al. 2015). At this time settlement density along the coast was highest. After Neolithic time, the movement of the ITCZ to south of the Arabian coast led to reduced rainfall and aridification. Settlements were abandoned, paleolakes disappeared and vegetation became desert-type (Parker et al. 2006, Matter et al. 2015). This climatic transition is best documented in stalagmites. At Hoti cave, northern Oman, stalagmites ceased to grow around 3000 BP. Qunf cave on the other hand, which is situated further south, contains stalagmites that grew undisturbed from the Neolithic to the Bronze Age, but their $\delta^{18}O$ records also point to increasing aridity or decreasing rainfall (Fleitmann et al. 2007, Fleitmann et al. 2011, Van Rampelbergh et al. 2013).

To use shells as environmental archives, periods of shell growth and response time to environmental changes has to be investigated. In particular, little is known about lifespans. Biological studies focus on reproduction cycles and the occurrence of different species. For those shells used in this thesis, only the *Arcidae* family member *Anadara senilis* has been investigated using sclerochronology and stable isotopes (Azzoug et al. 2012). So far, *Anadara uropigimelana* has not been studied for habitat and diet, but a similar lifestyle can be assumed (Yoloye 1975, Richardson 1987, Debenay et al. 1994, Azzoug et al. 2012). For *Terebralia palustris*, shell growth had been investigated worldwide with respect to diet and preferred habitat, but it has not used for environmental reconstruction (Slim et al. 1997, Fratini et al. 2008, Reid et al. 2008, Penha-Lopes et al. 2009).

As the environment and diet are mirrored in the ^{14}C data of the shells, the stable isotopes are the most important tool to evaluate these influences. So far, only few studies combine both, often to monitor freshwater pulses in estuaries (Webb 2007, Butler et al. 2009, Hadden et al. 2018).

Aims:

This thesis aims at a systematic approach to

a) *derive the reservoir ages and reservoir effects of the abundant shells associated with the archaeological sites of SE Arabia*;

b) *confirm or refute the stability of the reservoir effects in the Neolithic and the Bronze Age*;

c) *find out whether the chosen shell species react fast enough to their environment and hence provide information about environmental conditions*;

d) *investigate influences of human shell processing on measurement results (especially heating)*.

e) *attempt to evaluate hardwater effects in terrestrial shells, depending on underlying geology*;

f) *link the data on shells to other archives and prove that they can be regarded as an archive themselves;*

g) *provide advice on how shells can be used to serve as chronological tools;*

Research strategy:

I had the opportunity to sample marine shells of *Anadara uropigimelana* and *Terebralia palustris* twice, in 2013 and 2015. Sampling of shells was done at archaeological sites of different age in the Emirate Sharjah and included adjacent coastal sites to get modern reference material. One or more co-authors accompanied me on most of the sampling campaigns and discussed the archeological and regional context with me in order to develop a sampling strategy. Although the focus was laid on the reservoir effect of marine shells from shell middens around Kalba, findings of terrestrial gastropod shells at different archaeological excavations and surroundings led us to extend the study on the hardwater effect of these shells and test the dependency on rock types. The landsnails *Zootecus insularis* and the freshwater gastropods *Melanoides tuberculata* could frequently be found and were collected over a wide area of the Hadjar Mountains. The selected marine and terrestrial species differ in habitat and diet and allow for the derivation of species-specific reservoir and hardwater effects.

The systematic approach in this thesis started with fundamental information about the parameters involved. Two marine molluscan species represent different habitats and diets, but live close to each other and both near or in a mangrove forest. This raises the question whether the reservoir effect differs between the two species. The next step requires the temporal variation of the reservoir effect to be tested. If it varies, it must be explained by considering regional palaeoenvironmental information.

To better understand the reservoir effect data, including possible variations and to be able to interpret the information stored in the shell, information is needed on their habitat, lifespan, as well as dietary preferences. Therefore, I pursued a sclerochronological approach to the ontogenetic age of the shell and the variability in stable isotopes over time (Fig.1). $\delta^{18}O$ especially provides information about seasonal growth of the shell, i.e. constant throughout the year or ceasing during certain months. The age can be derived from number of seasons as well as temperature range of the estuary. $\delta^{13}C$ can point to several sources, i.e. diet and water. As a result, the identification of specific sources is difficult to assess

(McConnaughey and Gillikin 2008, Butler et al. 2011). Here, ^{14}C measurement from the same sample position yields important additional constraints (Fig.1). Shell ^{14}C has its origin mainly in water dissolved inorganic carbon (DIC).

In archaeological context, some shells had been heated before consumption. Such shells cannot be distinguished with certainty from non-heated ones during collection in the field. This raises the question as to whether the reservoir effect and stable isotope signatures are affected during the heating process. Heating of shells can be identified via deviating microstructures and shell mineralogy. Hereby, Raman spectroscopy (aragonite vs. calcite) and SEM can be used. In order to interpret mineralogical transformation processes, heating mechanisms have to be considered as given in ethnological publications (Fig.1)

For the hardwater effect, terrestrial snails and freshwater snails should be from contrasting lithologies with respect to carbonate content (Fig. 1). We collected the gastropod shells in active wadis within dry river beds. The sampling context and the fragile nature of terrestrial snail shells suggests they are modern specimens. Nevertheless, we cannot exclude reworking from river banks and full, or in parts, a real radiocarbon age. Unfortunately, we could not find live specimens to absolutely be clear about the time of death. Some shells are recovered from archaeological context, which allows cross correlation with other chronological data.

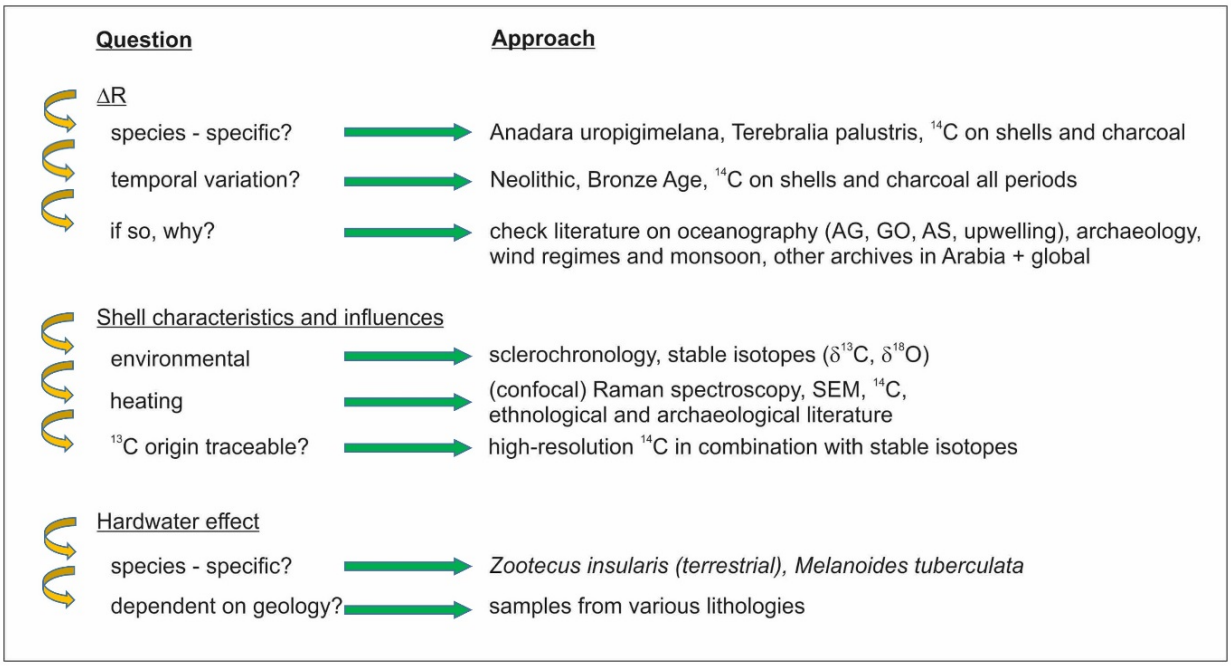

Fig.1 Flowchart to visualize the questions addressed in this work and the approach used to answer them.

Outline of the chapters to follow

The chapters of this thesis address the given study aims. In chapter 2 some background information regarding the regional setting with respect to geology, ocean circulation patterns of Arabian Gulf and Gulf of Oman are given together with an overview over the archaeological and environmental aspects between Neolithic and Iron Age.

Chapter 3 deals with the methods applied in this study. As the focus lies on radiocarbon dating of shells, I review radiocarbon dating and especially the reservoir effect. Shells are used with respect to different kinds of information stored in the shell material, therefore in chapter three an overview is given about the shell species used and the methods applied.

The published results are presented in chapter 4. Here, chapter 4.1 describes the starting point, such as the suitability of shell species, sclerochronology and stable isotopes, together with first reservoir ages from the Neolithic (paper published in Radiocarbon). In chapter 4.2 we present the species-specific and time-dependent reservoir effects in relation to environmental conditions derived from other published studies on climate proxies such as stalagmites, paleolakes etc. (paper published in Quaternary Geochronology). Radiocarbon measurements in high resolution along single shells are introduced in chapter 4.3 (publication accepted, Nuclear Instruments and Methods B) and show the limits of suitable sample sizes or measurement techniques. Because a large quantity of shells had been heated after foraging, effects of heating on the shell microstructures, mineralogy, chapter 4.4, and possible changes in radiocarbon, chapter 4.5, are presented (both papers Journal of Archaeological Science: Reports). Finally, the influence of geology on radiocarbon of terrestrial and freshwater shells is investigated in chapter 4.5 (publication under review, Journal of Arid Environment). In these chapters, the different contributions by the authors involved are noted at the beginning of the chapter, as well as the complete citation.

Chapter 5 – Discussion – considers the results and discusses them in the context of other literature on environment. A critical review on the tests is given with some suggestions on improvements.

Finally, chapter 6 – conclusions - summarizes the results and links them to the study aim, together with some aspects of future work building on the results.

Note that the publication of chapter 4.5 is still under review. It is possible that the final publication is slightly different from the text presented here, depending on the reviewers' comments.

2 Regional Settings

2.1 Study Area

The United Arab Emirates (UAE) are located in the south-eastern corner of the Arabian Peninsula and span the coasts of both the Arabian Gulf (AG) and Gulf of Oman (Fig. 2.1.1). In the eastern part of the UAE the landscape is dominated by the Hajar Mountains; dunes of the Rub al-Khali dominate the landscape to the west of the country where it borders the Arabian Gulf. Today the UAE have an arid landscape and the oldest continuous settlements usually lie along the coasts. However, the climate of this region has varied substantially in the past; evidence of ancient lakes lie beneath the dunes of the Rub al-Khali sand sea, indicating much wetter environments than those that prevail today (Parker et al. 2006, Matter et al. 2015).

Selection of study sites

Kalba was chosen as the key location for this study because it provides a lagoon with a mangrove forest, covering the complete period of interest starting from the mid Holocene to the Bronze Age. The area occupies a narrow corridor between the ocean and Hajar Mountains (Fig. 2.1.1), and traces of humans are found from at least since the Neolithic. South of the city of Kalba lies the lagoon and mangrove forest of Khor Kalba, which marks the border with Oman and which has provided an important resource for food and wood. The maximum extent of the lagoon and its mangrove forest (in ancient times) is now marked by a sabkha (salt flat (Al-Farraj 2005)) with several shell middens from the Neolithic. A settlement dating to the Bronze Age lies at the northwest boundary of the modern city of Kalba. For comparison to the lagoonal settings and the radiocarbon involved, mangroves of the Arabian Gulf were sampled. The modern mangrove at Ajman was planted 10 years ago on the remains of an ancient forest (Fig. 2.1.1). Here, both trees (woody materials) and sediments could be sampled. Umm al-Quwain lagoon and mangrove forest, also at the Arabian Gulf and north of Ajman, were also tested to take a look at radiocarbon content and reservoir age in the water.

The Hajar Mountains, the center of our study on geology and terrestrial gastropods, trend parallel to the Gulf of Oman (Fig. 2.1.1). Here, sites were sampled at different geological settings. Locations in the Dibba fracture zone (al-Hala, Gubh, Tawian Dam) are characterized by deepwater sedimentary rocks and turbiditic limestones, metamorphic rocks towards the south, as well as platform carbonates at the northern boundary. To the south, one site, Masafi, covers an outcrop of metamorphic rocks of the Dibba zone in the ophiolite region, whereas Wadi to Esfai, Shawkah, Wadi Hilo completely lie in regions of ophiolitic rocks, here as harzburgite, and local outcrops of underlying sedimentary sequences. Jebel Faya and Jebel Buhais are situated at the western boundary of the Hajar Mountains as part of the Tertiary thrust belt. Wadi Hilo, Kalba, Jebel Faya are all known for their archaeological sites.

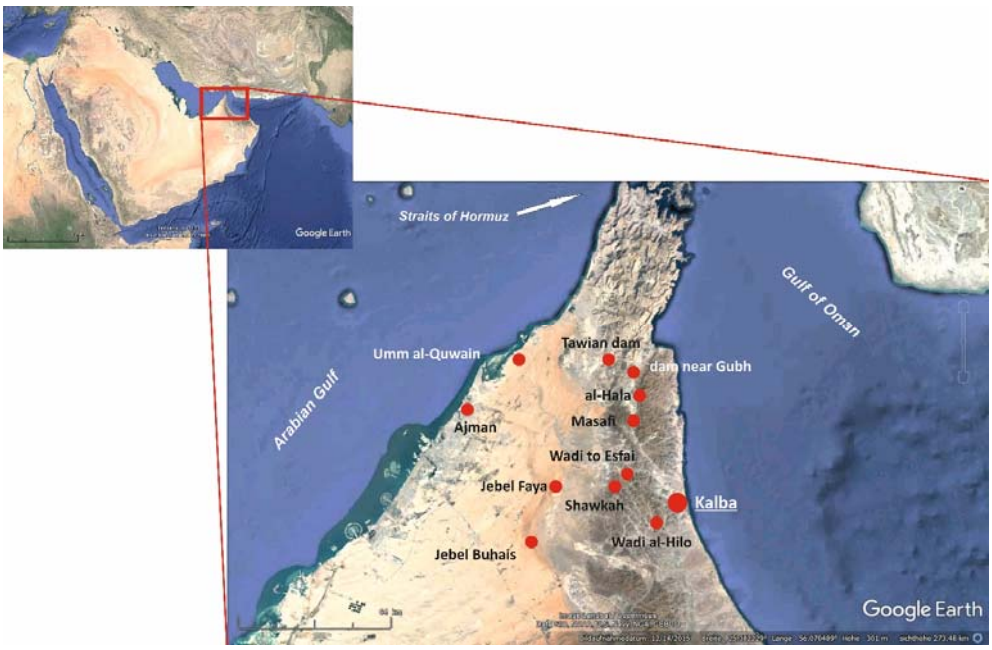

Fig. 2.1.1 Map of Arabia with locations mentioned in the texts marked in the excerpt. Maps modified from Google Earth.

2.2 Geology

The geology of the UAE can be subdivided into the thrust belt of the Hajar Mountains in the east and the foreland platform to the west. The thrust belt was formed in the upper Cretaceous by subduction of a part of the Neotethys Ocean floor. Today, subduction of the Eurasian Plate is ongoing, forming the Zagros belt along the Arabian Gulf west of the Straits of Hormuz, and the Makran Subduction Zone in the Oman Sea, east of the Straits of Hormuz. As a result of foreland bulging, the Arabian Plate is uplifting south of the Dibba Zone (Glennie 1992).

Southeast Arabia is characterized by five major tectono-sedimentary sequences: 1) pre-Permian (lower autochthonous, according to Glennie (2005)), 2) The Hajar Supergroup (upper autochthonous), 3) Allochthonous Sequence (Hawasina sediments and Semail ophiolite), 4) the Aruma Group, and 5) Tertiary Cover (Al-lazki et al. 2002). The autochthonous platform sequence is still in place whereas the overthrusted allochthonous sequence has been transferred from an oceanic realm in the east. These groups, autochthonous as well as allochthonous, were originally deposited side by side. The autochthonous group in the west represents the Mesozoic Neothetyan Arabian Shelf with shallow marine conditions and sediments deposited on continental crust (Hawasina Complex, 270 – 70 Ma) (Glennie 1992). In the east, deep pelagic sediments dominated which were deposited on Neothetyan oceanic crust between 105 – 70 Ma ago (Fig. 2.2.1 B). The Late Cretaceous process of thrusting began around 95 Ma and lasted until the early Tertiary as can be seen by Tertiary folds for example at Jebel Faya (Searle et al. 1983)(Fig. 2.2.1 C, D). The sedimentary rocks (Hawasina complex and others, see Fig. 2.2.1 A, D) were obducted by the oceanic crust (Semail ophiolith).

From Fig. 2.2.1 C, it can be derived that the ophiolite was emplaced onto the Arabian Platform from the east-southeast with the Dibba Zone as the northern boundary. The limestone-dominated autochthonous sequence of the Musandam Peninsula was deposited along the former southern margins of

the Neo-Tethys Ocean. These shelf carbonates can best be viewed in and north of the Dibba Zone, where they are not covered by the Semail Nappe (Fig. 2.2.1 C). They unconformably overlie a sequence of lower Palaeozoic sedimentary rocks. In the United Arab Emirates (UAE), the lower Palaeozoic are rocks only exposed in a limited region of the south-western Dibba Zone. To the west of the Hajar Mountains, Tertiary and Quaternary deposits dominate the landscape.

Autochtonous Sequence:

The autochthonous ("in place") sequence ranges from Precambrian (~ 850 Ma) to Cretaceous (142 – 65 Ma) in age. It encompasses crystalline basement (Fig. 2.2.1 A), overlain by lower and upper autochthonous carbonate rocks (Hajar Supergroup) and a neo-autochthonous Cenozoic sequence (Searle et al. 1983, Mattern and Scharf 2017). The basement (Fig. 2.2.1 A), the lower autochthonous carbonate, is made from highly deformed, metamorphosed sedimentary rocks (including gneiss and micaceous schist), formed by continental accretion during the Late Precambrian to Palaeozoic (600 – 300 Ma) (Glennie 2005), and intruded by igneous rocks such as dolerites, granodiorites and granites (Searle et al. 1983, Glennie 1992). These Late Precambrian meta-sedimentary rocks are dominated by siliciclastics and carbonates (Glennie 2005).

The overlying Hajar Supergroup (the upper autochthonous) comprises a continuous 3-km-thick sequence of sedimentary rocks, of mid- or Late Permian basal ages to mid-Cretaceous age at the top (Fig. 2.2.1 B, C) (Kusky et al. 2005). These rocks form a passive margin sequence for the Neo-Tethys Ocean, mostly made up of a carbonate platform sequence (Mattern and Scharf 2017) with fossiliferous marine limestone, dolostones and marls. The Hajar Supergroup comprises several formations such as the Rus Al Jibal Group, Elphinstone Group, Musandam Group and Thamama Group (Fig. 2.2.1 A). The Hajar Supergroup forms most of the rocks that can be found on the Musandam Peninsula (Fig. 2.2.1 C).

Disconnected from the early autochthonous sequences by the allochthonous sequence and a sediment gap, the neo-autochthonous sediments consists of shallow-marine limestones from the Maastrichtian to early Tertiary and overlies all other units (Searle et al. 1983). In the west, the Musandam Peninsula is overlapped by Tertiary shallow marine deposits and Holocene fluviatile and eolian deposits of the neo-autochthonous (Searle et al. 1983).

Allochthonous sequence:

The main autochthonous sequence of the Hajar Supergroup is overthrusted by four allochthonous ("out of place") sequences which are from lowest to uppermost: (1) Sumeini Group, (2) Hawasina Complex, (3) Haybi Complex and (4) Semail Ophiolite. Their palaeogeographic arrangement can be seen in Fig. 2.2.1 B and generally correspond to increasing distance to the shelf and depth. The Sumeini Group, Hawasina Complex, and Haybi Complex contain the sedimentary rocks of the Neo-Tethys Ocean, whereas the uppermost Semail Ophiolite represents the oceanic crust coming from the deepest and most distal part of the ocean basin (Fig. 2.2.1) (Mattern and Scharf 2017).

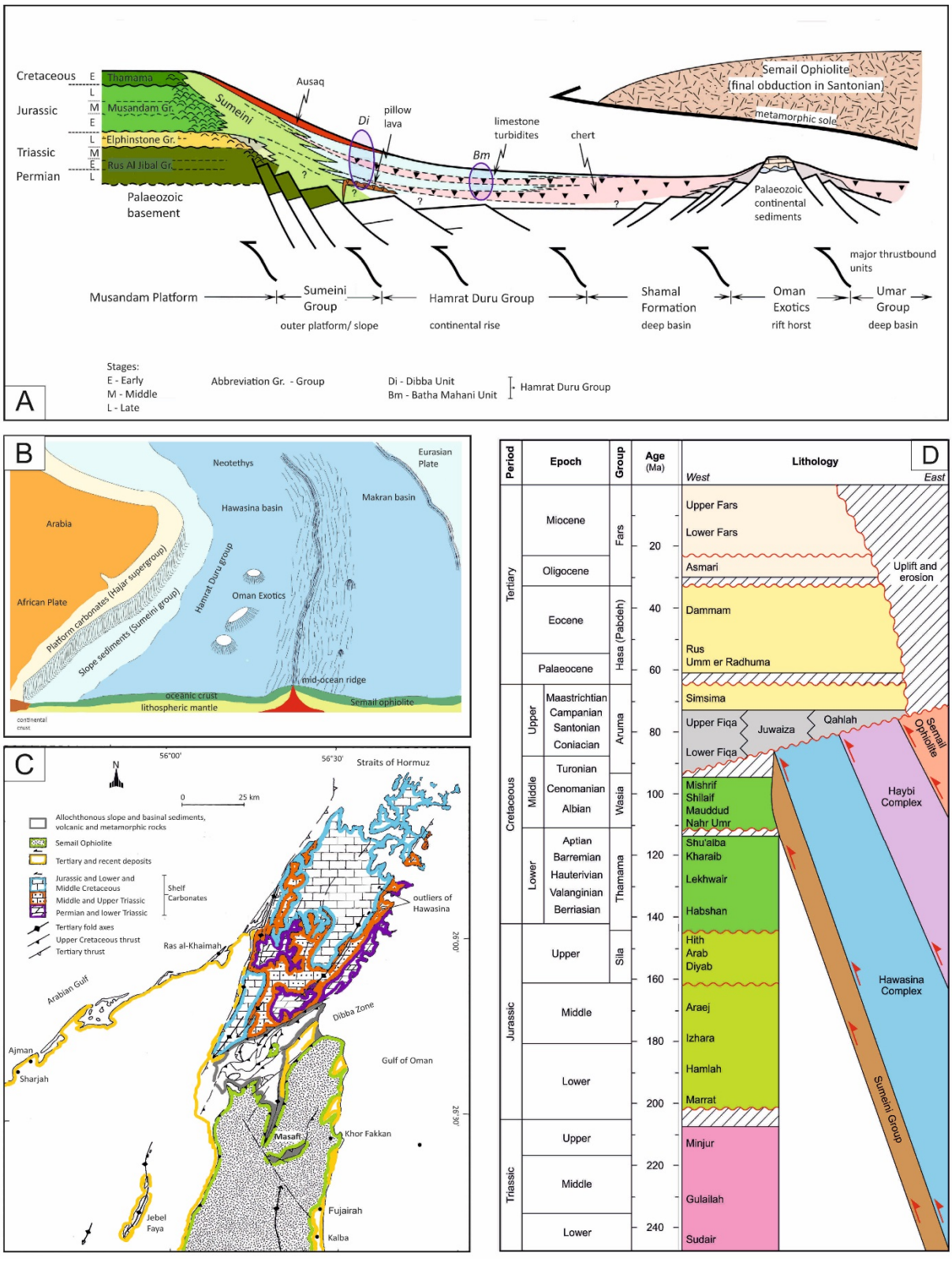

Fig. 2.2.1 Geology of Arabia. Part A: stacking order and complexes before thrust over (modified from Cooper et al, 2016). Part B: Overview of lithology before thrustover, modified and re-drawn from (Hoffmann et al. 2016). Part C: geological map of different outcrops representing different epochs of formation and replacement (modified from Searle 1983). Part D: Timing of thrustover of different formations (redrawn from Ali and Watts, 2009).

The Sumeini Group shows mostly turbiditic sediments accumulated proximally along the continental slope (Fig. 2.2.1 A, B, D). The Hawasina Complex (Fig. 2.2.1 B, D) is dominated by more distal turbiditic calcarenites (calcareous sandstones) (Wohlwend et al. 2017). During obduction, the Hawasina Complex began to form as a complex accretionary wedge (Glennie 1992, Ali and Watts 2009, Cooper et al. 2014). This caused multiple repetitions of Permian or Triassic rocks at the base and Cenomanian rocks at the top (Wohlwend et al. 2017). Moreover, other characteristic seafloor lithologies such as mid-ocean ridge basalts and seamount basalts were incorporated (Fig. 2.2.1). Similarly, distal sediments from the deeper part of the oceanic basin were thrust on top of the Hawasina complex, where they form the Haybi Complex. It is composed of calcareous grainstone turbidites capped by siliceous radiolarian cherts (Hamrat Duru group, Dibba Formation, Dhera Formation). Some large isolated carbonate blocks are incorporated in the Hyabi Complex that date to Permian and Late Triassic. In particular, some are outcropping in the Dibba Zone. These “Oman Exotics” are tectonic units bounded by shear surfaces. The Oman Exotic of Jebel Qamar at the western end of the Dibba Zone is considered a tilted block of the Oman margin incorporated into the Hawasina nappes during obduction of the ophiolite (Pillevuit et al. 1997). Sediments of the Oman Exotics date to the Ordovician to Lower Carboniferous indicating a close relation to the continental crust of the Arabian shield (Pillevuit et al. 1997). Presumably, they were mid-ocean horst structures and relicts from opening of the Neo-Tethys Ocean (Fig. 2.2.1 A). The Semail Ophiolite is the uppermost thrust unit and has the widest distribution of all allochthonous units (Fig. 2.2.1 A - D). Originally part of the Neo – Tethys ocean floor, it shows the characteristics of ocean lithosphere, comprising mantle peridotites and harzburgites (ultramafic rocks) at the base, overlain by crustal gabbros and sheeted dykes (dolerites) as feeders to extrusive basaltic pillow lavas (Glennie 1992, Cooper et al. 2014).

2.3 Climate – Present and Past

Climatic conditions today

Today´s climate is considered to undergo fast changes at the global scale, and the climate of SE Arabia is no exception. The climate of the UAE is described as semi-desert to desert with low precipitation and high potential evapo-transpiration including a mean temperature of more than 18 °C (Kömüşcü 2017). Generally, the country can be divided into three climatic zones: the coastal sites along the Arabian Gulf and the Gulf of Oman, the central desert zones (extending also to the south), and the Hajar Mountains. Studies covering the last 2 – 3 decades found a significant warming trend in the mean annual temperatures (AlSarmi and Washington 2011, Kömüşcü 2017). Warming varied between 0.3 and 2.8 °C per location, with the higher values measured at coastal stations. The precipitation shows a less distinct pattern, with a relative constant, but reduced precipitation between 2002 -2008 (AlSarmi and Washington 2011). Winter lasts from November to March with temperatures usually above 6 °C. Summer months extend from April to September and are usually very dry and hot. Temperatures at coastal cities can reach 48 -50 °C with a humidity of up to 90 % (Kömüşcü 2017). Land-sea breeze circulation from the western and eastern sides strongly affects the weather. Here, the local wind patterns are influenced by the Hajar Mountains that also play an important role in the distribution of

rainfall. Rainfall occurs from west to east with tropical monsoon systems prevailing during the summer and frontal systems in winter (Kömüşcü 2017). Annual rainfall is heaviest during winter months and can reach up to 110 mm (mean value), decreasing from north to south. February and March are the months with the heaviest rainfall (Kömüşcü 2017).

Winds systems

The climatic conditions at the UAE are controlled by semi-permanent subtropical high pressure cells that cause stable and dry weather. Semi-permanent troughs of low pressure over the Arabian Gulf also influence the climate here. The summer and winter monsoon over Asia, including annual reversal of trans-equatorial air stream at the surface and the upper troposphere, plays a major role in the environmental conditions (Fig. 2.3.1.) The main effects are surface transition from high pressure (winter) to low pressure (summer) (Kömüşcü 2017). In the upper troposphere, a change from a winter-time subtropical westerly jet stream to a tropical easterly jet in the summer can be recognized. During spring and summer, winds from the northwest are strongest. These westerlies, of which Shamal is the strongest, are funneled into the Arabian Gulf between the mountains of Turkey and Iran on one side and the Saudi Arabian plain on the other side (Fig. 2.3.1). Shamal can last for several days with reduced strength during night and can reach velocities sufficient to produce wind waves of 3-4 m in height. It also can transport significant dust. It is strongest during summer because of the quasi-permanent high-pressure cell over Saudi Arabia and the summer Asian low to the northwest. This leads to a gradient between the two systems and a persistent northwesterly wind over the Arabian Gulf (de Villiers 2010).

In winter, the Shamal transports colder air from the north by passing mid latitude lows before it meets the high pressure rise of the ensuing anticyclone. This passage of mid-latitude lows, in combination with upper air troughs, is an important rain producer. The anticyclone, however, is a separate cell of the anticyclone that rests over Asia (de Villiers 2010). Its southern part is associated with an easterly flow over the Arabian Sea that forms the winter north-east monsoon, which transports rain to east Africa's near equatorial latitudes. Over the Arabian Sea, the easterly flow crosses the equator into the Indian Ocean where it becomes westerly. Here it converges with air from the southern hemisphere in a low pressure zone at the Intertropical Convergence Zone (ITCZ) (de Villiers 2010). The Intertropical Convergence Zone (ITCZ) is an area where wind systems of the northern and southern hemispheres merge. It is a trough or cyclone coupled to high surface temperatures. With differing ability of land and sea to heat or cool, the position of the ITCZ is determined by the partition of the two. Land has a lesser thermal capacity and therefore shows faster cooling or heating than the ocean. Consequently, the air cools quicker in winter over land and heats faster in summer there. These different alterations cause an anticyclone – cyclone system where the pressure differences are compensated by the winds from high pressure to low pressure areas. This is the driver of the monsoon systems (Lendt 2000).

In the transition from winter to summer circulation, the anticyclone weakens, mean sea level pressure drops, the north-east monsoon becomes weaker and its flow more disordered. At the same time, the northwesterly winds weaken, too, and are shifted slightly to the north (Fig 2.3-1). The final change from winter to summer circulation takes place within a few weeks in May to June (de Villiers 2010). By July, the anticyclone is completely replaced by an area of low pressure. The near-equatorial trough

moves significantly to the north transporting air from the South Indian Ocean sub-tropical high pressure cell to the Asian low (de Villiers 2010). The result is a strong south-west monsoon over the northern Indian Ocean and Arabian Sea as well as southern Arabia. A low level jet stream associated with the southwest monsoon, the Findlater Jet, blocks any dust transported from the Arabian Peninsula into the Arabian Sea (Balakrishnan Nair 2006). The position of the summer low, however, results in a northerly to north-westerly wind over most of Arabia. In short, during January, there is a surface northeast monsoon flow heading to the southern hemisphere with a compensating south to north air flow and westerly stream. In July, this setting is reversed to a surface southwest monsoon flow to the northern hemisphere, with a compensating north to south flow and tropical easterly jet higher in the atmosphere. The change from summer to winter circulation takes place over a few weeks between October and November. Cooling of the land causes more stable air in the lower part of the atmosphere, whereas the upper part becomes more unstable when cold air invades from the north behind the westerly troughs (de Villiers 2010).

In summary, the wind systems are the same today as in the past, only their strength and/or coverage has changed. This may be related to the shifting of the ITCZ to some extent, as will be described more closely in the following chapters.

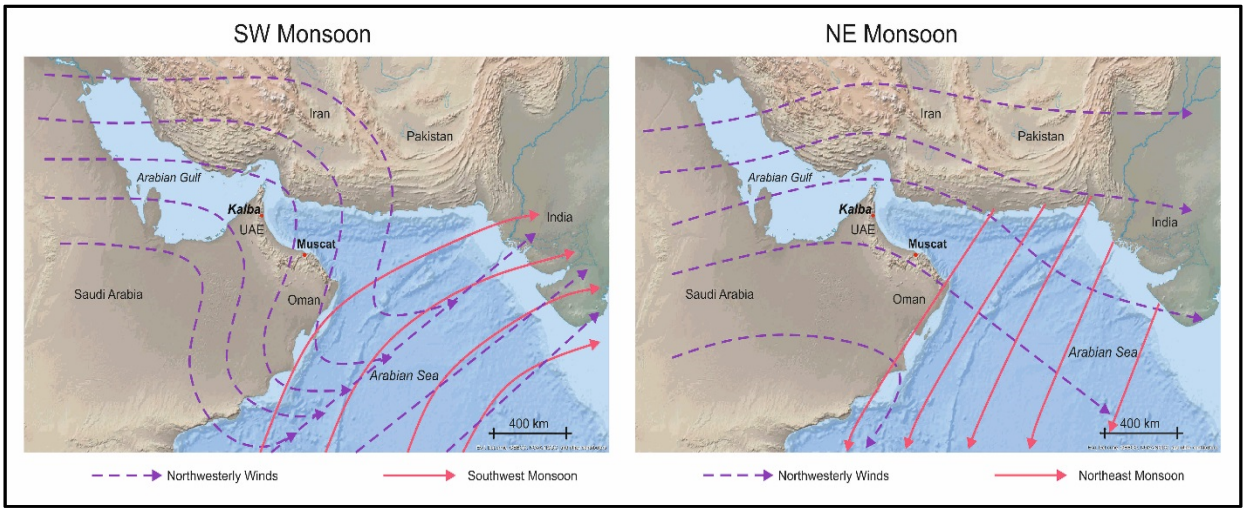

Fig. 2.3.1 Seasonal wind systems responsible for rainfall and ocean circulation patterns (modified on the basis of Balakrishnan Nair, 2006)

Reconstruction of past climates and environmental conditions - proxies

To reconstruct environmental conditions of the past, several proxies or archives are used. The marine foraminifera (*Globigerina spp.)* are already described in the section about upwelling of the Arabian Sea and provide information about nutrients through their variety of species, as well as amount of foraminifera per species present in the sedimentary records. They serve as indicators for upwelling conditions. In addition, $\delta^{18}O$ of foraminifera can be a tracer to monitor river discharge, such as Indus river discharge into the Arabian Sea (Staubwasser et al. 2002). In the context of marine sediment cores, it is also important to determine lithogenic carbonate. This is achieved by subtraction the biogenic opal

and marine carbonates from the bulk sediment. From $\delta^{18}O$ of lithogenic and biogenic component, mixing ratios and accumulation rates can be determined (Sirocko et al. 1991).

Regarding water budget and sediment availability, paleolakes and their sedimentary records are a valuable archive, together with marine sediment cores. Pollen of several plant species as well as phytoliths are used to derive whether C3 plants (savannah grassland with woods, plants at higher latitudes) or C4 plants (grassland, corn, other tropical to subtropical species) are dominant. Elemental cations and ratios are used to derive aeolian (allogenic) or fluvial (authigenic) input of sediment into the lake system. Here, the aeolian input is characterized by titanium, aluminium, iron and potassium, whereas the fluvial intake of sediment is reflected by the elements strontium, sodium and magnesium (Parker et al. 2006). Sodium and potassium are often investigated as ratios, where low Na:K ratios point to humid phases and high values reflect increased aridity and salinity and consequently increased halite concentrations. Low Na:K ratios in lakes are associated with increasing Ti values, and are thus interpreted as indicative of reducing lake levels due to increasing aridity and a relatively increased aeolian input (Parker et al. 2006).

Aluminium in marine cores reflects the continental contribution to ocean sediments (Balakrishnan Nair 2006). Iron is an important proxy as it is needed for phytoplankton growth and can reduce atmospheric carbon dioxide (Balakrishnan Nair 2006). Some elements, like calcium, show both components. Total organic carbon (TOC) serves as a monitor for biological activity. Mass specific mineral magnetic susceptibility can also help to determine environmental conditions. High mineral magnetic values for example point to high levels of magnetic material in lakes, which is related to increased influx of aeolian material from surrounding dune fields. This is usually interpreted as phase of increased aridity, vegetation loss and landscape instability (Parker et al. 2006). Magnesium shows terrigenous as well as marine origin. In marine conditions, it is basically part of calcite and considered biogenic. To determine the terrigenous origin, calcite can be dissolved in the sample of interest. Quartz and dolomite serve as proxies for dust transport from the land into e.g. the Arabia Sea (Khan 1997). Their abundance is correlated with the magnetic susceptibility.

Dust grain size distribution allows for reconstructing wind strength and is also correlated to *G. bulloides* (Khan 1997). Proxies for terrestrial input are closely linked to Westerlies because they are responsible for the transport of dust particles and aerosols from land into lake and water systems and dolomite-bearing Mesozoic strata are exposed only in northern Arabia (Balakrishnan Nair 2006). Titanium is linked to heavy minerals, such as rutile, and is also linked to grain sizes and strong winds (Balakrishnan Nair 2006). The allogenic markers are more important for our data because from the Arabian Peninsula, little to no fluvial input is expected.

With respect to terrestrial records, speleothems provide the highest spatio-temporal resolution to detect variabilities of rainfall from monsoon or other wind regimes as e.g. Westerlies. The Oxygen ($\delta^{18}O$) data of stalagmites reflects variations in the amount of rainfall and indicates a reduction in rainfall when the data is shifted to more positive values (Fleitmann et al. 2007). Also a hiatus in growth over certain periods points to a lack of water availability.

Radiocarbon dating of groundwater aquifers supports the findings of paleolake and stalagmite records of a moist phase in the early to mid-Holocene (Wood and Imes 2003). In addition, data on chemical

composition as well as isotopes ($\delta^{18}O$, $\delta^{2}H$, etc.) can contribute understanding the origin of precipitation and evaporation, to name but a few possibilities (Michelsen et al. 2015). However, this has not yet been done for the UAE. Here, $\delta^{13}C$ is used to monitor the origin and changes in water of aquifers, together with changing sedimentary and vegetation regimes to determine mixing ratios or dissolution of limestone.

Past Climate

With climate conditions varying between Mediterranean climate and Indian Ocean Monsoon, it can be deduced that the climate in Arabia has not always been as dry as today. Zones that are now arid must have been significantly more humid in past times (Parker et al. 2006, Bretzke et al. 2013). During the early to mid-Holocene, the South Asian summer monsoon was more intense than today (Staubwasser et al. 2002). The initial onset of climate change occured around 14300 ^{14}C yrs BP, documented in a decrease in dolomite input into the Arabian Sea due to changes in atmospheric circulation (Staubwasser et al. 2002). The sea level was approximately 110 m below today´s level and yet to transgress into the Arabian Gulf (AG) (Lambeck 1996, Parker et al. 2018). A major transition between glacial phase and Holocene occurs around 13060 ^{14}C yrs BP when a simultaneous sharp drop in $\delta^{18}O$ occurs with an increase in dolomite and carbonate input in sediment cores of the Arabian Sea (Staubwasser et al. 2002).

During the early to middle Holocene (Fig. 2.5.1), there is evidence that the Inter Tropical Convergence Zone (ITCZ) had moved further north leading to a northward movement of the Indian Ocean Monsoon (IOM). As a consequence, summer rainfall increased. This period is usually referred to as the “Holocene Moist Phase” (Parker et al. 2006). This humid interval, assigned to an intensification of the summer monsoon, occurred in two steps. The first at ~ 9900 – 8600 cal BP when no dolomite input could be found in the marine sedimentary records. Groundwater levels increased by up to 10 m on mainland and up to 25m on coastal aquifers (Engelhardt et al. 2013). The second is in the mid Holocene, where a return of dolomite input after 7300 ^{14}C yrs BP and an increase in dust flux after 4800 ^{14}C yrs BP was interpreted as increased aridity of the mainland (Staubwasser et al. 2002). Both effects are also visible in the records at Hoti Cave, North Oman, and at a later stage also at Qunf Cave, South Oman.

At Hoti, the dry period starts around 6600 BP with a total stop in speleothem growth at around 5200 BP. The pollen and phytolith records in the sediments of Awafi lake, for example, show C3 vegetation during the early to mid-Holocene (8.5 – 5.9 ka), representative of the Holocene moist phase as similarly seen in the stalagmite records. The lake records show a sharp decrease in lake level at 5900 cal BP, pointing to increased aridity coinciding with Bond 4 event (higher SST in the North Atlantic but also in the Arabian Sea) (Parker et al. 2006). In the following period, vegetation changed to C4 grassland types at 5.9 – 4.5 ka, with marls and sand. This is interpreted as a change in water supply from the now weak summer monsoon to the Westerly winds (strongest during winter months) as the main source of precipitation (Parker et al. 2004, Parker et al. 2006). This led to a reduction in lake levels. Above, only sand accumulation is found (Parker et al. 2006) pointing to an aridification of the area. Elementary records of the lake sediments provide additional information, e.g. higher dolomite values point to increased

terrigenous input, higher Titanium values can be linked to higher detrital input, to name but a few (Parker et al. 2016). The paleolake records of Awafi Lake, but also Wahalah lake, both in UAE, show an abrupt start of the arid phase which corroborates those data from the marine records (dust input). Around 4.3 and 3.9 ka, the lakes were completely dry.

Along the coast, the occurrence and extent of mangrove forests can be used to gain insight into estuarine systems and freshwater input. A larger extent in mangrove forests can be reconstructed from the maximum extent of contemporary sabkhas. Before 7.5 ka, the marine transgression prohibited a wider spread of the mangrove forests, however ideal conditions for mangroves occurred between 6.8 to 6.4 ka when sea levels became more stable (Berger et al. 2013). Well-defined mangrove development occurs during stable phases after a sea-level rise, roughly every 500 years, with the optimum conditions just after the marine transgression (Berger et al. 2013).

Relative sea-level rose until it reached the present sea level shortly before 6 ka; the highest sea level was around 2 m higher than today and decreased until it reached present day level again (Lambeck 1996, Dalongeville and Sanlaville 2005, Berger et al. 2013). With respect to groundwater, shallow aquifers were affected more intensely by climate changes than deeper aquifers. Between 10,000 and 3,000 years BP, groundwater was stored whereas after 3,000 BP natural depletion occurred and still continues today (Engelhardt et al. 2013). Radiocarbon dating of the aquifer near Abu Dhabi led to the interpretation that the aquifer was recharged permanently until about 6000 to 5500 yrs BP. Since then the water level in the aquifer dropped until the present level (Wood and Imes 2003).

2.4 Oceans

Situated between the shallow, highly saline waters of the Arabian Gulf (AG), and the deep Arabian Sea (AS), the Gulf of Oman (GO) represents a unique and complex hydrological system. The Arabian Gulf and the Gulf of Oman are connected through the Straits of Hormuz. Ocean circulations and wind regimes are closely linked and vary seasonally. Because of the diverging characteristics of the AG and GO/AS, both are described separately below.

Arabian Gulf (AG) and Straits of Hormuz

The semi – enclosed Arabian Gulf is nearly 1000 km long, has a maximum width of c. 370 km and a mean depth of 36 m (Kämpf and Sadrinasab 2005). The shallowest regions (<20 m) can be found along the coast of the United Arab Emirates (UAE), around Bahrain and at the head of the Gulf. The deeper regions of the Gulf are situated along the Iranian coast to the Straits of Hormuz, which ultimately connects the AG to the Indian Ocean (Kämpf and Sadrinasab 2005). (Kämpf and Sadrinasab 2005). The AG receives its freshwater from the Shatt al-Arab, fed by the Euphrates, Tigris and Karun Rivers, which have catchment headwaters in the Iranian mountains. The evaporation rate of ca. 2m/yr per unit surface area is higher than the inflow of water to the Gulf (Johns et al. 2000, Kämpf and Sadrinasab 2005). This high evaporation, influenced by the flat Gulf morphology, leads to increased salinity (30 – 42 psu,

which corresponds to ca. 4 %), depending on season and measurement depth (Michael Reynolds 1993) and an increase in water density (Kämpf and Sadrinasab 2005).

High salinity and carbon content are also evidenced by the precipitation of gypsum crystal evaporites along the exposed coastline (Omer 2010). However, the salinity also shows strong seasonal variations with a pronounced summer salinity front probably due to increased Indian Ocean Sea Water (IOSW) inflow that strengthens in late spring and summer in conjunction with a maximum outflow of dense bottom waters through the Straits of Hormuz. In this time, the wind stress generates southeast flowing surface currents (Hosseinibalam et al. 2011). In summer, a sharp seasonal thermocline develops due to a large amount of heat input and inhibits mixing between surface and bottom layers (Sultan and Elghribi 1996). In the winter season, the front retreats closer to the Straits of Hormuz leaving the Gulf surface waters saltier than during summer (Kämpf and Sadrinasab 2005).

Marine inflow over the Straits of Hormuz occurs at the surface, whereas outflow from the AG occurs along the seafloor (Johns et al. 2000, Kämpf and Sadrinasab 2005). Thermohaline flows dominate the circulation at nearly all parts of the AG. In winter and spring, wind stress reinforces thermohaline circulation of deep outflow, whereas in summer and autumn, wind stress acts in opposition to the thermohaline forcing. This results in a bottom inflow of the Gulf of Oman waters into the AG (Hosseinibalam et al. 2011).

Gulf of Oman and Arabian Sea

The Gulf of Oman as a northern component of the Arabian Sea shows a significantly different distribution pattern and origin of its water column. With the limiting influence of the landmass in the north, and the seasonality of the wind systems, the ocean circulation, too, changes seasonally and therefore causes seasonal modification in the biogeochemical processes (Lendt 2000). From the AG, a thermohaline front emerges into the GO and travels to the south along the coast (Pous et al. 2004). This highly saline, warm water mixes slowly with the surrounding GO waters and is measurable as a tongue-like structure traveling between the warm, light surface waters and the cold bottom waters until it is completely mixed by the location of Ras al-Hadd. The thermohaline structure is permanently reduced between Straits of Hormuz and Ras al-Hadd. In addition, the dense water also moves further away from the shoreline (Pous et al. 2004).

Thermocline waters from the AS mainly originate south of the southern subtropical front at 40 – 45°. The ocean circulation transports the waters along the Somali coast towards the coast of Oman (Somali Jet), depending on wind direction and strength (Thamban et al. 2007). The seasonal pattern is driven by changing wind regimes (see chapter 4.2, Fig. 4.2.2, and paragraph on upwelling below). In winter, the Northwesterly Shamal dominates, affecting transport of AS surface water from the Arabian Sea to the AG along the northern (Iranian) coast (Piontkovski et al. 2012). The summer Southwest Monsoon winds shift the balance between Arabian Sea inflow and Arabian Gulf outflow towards the Arabian Gulf; the inflow is forced along the Iranian coast (Bernier et al. 1995). This outflow increases the proportion of Indian Ocean Surface Waters (IOSW) inflow into the Gulf influencing the formation of the

Iranian Coast Jet (ICJ). This circulation breaks down in autumn and winter resulting in mesoscale eddies. In November, the Northeast wind (winter monsoon) becomes dominant, causing a reversal of ocean circulation in the northern Arabian Sea. A southward current is generated along the coast of the UAE and Oman (Johns et al. 2000). The northern Gulf of Oman experiences constant upwelling along the coast of Pakistan, but is variable along the Iranian coast (Johns et al. 2000).

A significant feature to note is the Ras al-Hadd jet that occurs off the coast of Oman, at the confluence of the southern ocean waters and the Gulf of Oman/Arabian Gulf waters. It also shows a seasonal pattern driven by the winds (Böhm et al. 1999) and mixes the dense Arabian Gulf waters with the colder waters of the Arabian Sea to a depth of several hundred meters.

Upwelling in the Arabian Sea: causes and changes during the Holocene

Upwelling describes the situation where cold, nutrient-rich waters from the deep sea are brought to the surface by ocean currents and prevailing wind regimes. The sea surface temperature (SST) is reduced by 4 – 5 °C (Smitha et al. 2014). Nutrient-rich waters fuel phytoplankton blooms, here along the coast of Somalia and Oman (Singh et al. 2011). The regularly alternating monsoon winds are the driving force behind all processes of production and resultant biological productivity in the AS (Thamban et al. 2007). The southwestern winds of the summer monsoon (June – September) especially affect the AS circulation, and cause an upwelling in the western AS (Staubwasser et al. 2002, Gupta et al. 2003, Thamban et al. 2007). In contrast, the winter monsoon largely suppresses upwelling in the western and northern parts of the AS, but leads to a moderate upwelling off Central India (Singh et al. 2011). The northeasterly winds over the northern AS cool and evaporate the sea surface, causing a surface convection and a deepening of the mixed layer (Staubwasser et al. 2002).

The archives used to derive changes in productivity or ocean currents, as well as the correlated wind regimes are sediment records from the AS. These sedimentary records are dominated by biogenic carbonates compared to lithogenic inputs. Planktonic foraminifera are especially responsive to changes in upwelling and thus track the seasonal changes very well (Gupta et al. 2003, Singh et al. 2011). Here, *Globigerina bulloides* (entrophic waters) and *G. ruber* (oligotrophic waters, surface-dwelling) are the most prominent proxies for upwelling and vertical mixing of the water column, e.g. a ration of *G. bulloides* to *G. ruber* of < 1 is interpreted as vertical mixing and/or weak upwelling, whereas values > 1 point to moderate upwelling (Singh et al. 2011). Around 4200 BP, at a time when a significant global change is reported, the Indian summer monsoon was reportedly weak, resulting in an intensified oxygen minimum zone (OMZ) and a decrease in species diversity (Das et al. 2017). Another weak summer monsoon and hence reduced upwelling, is reported for around 5600 yrs BP, 3500 yrs BP and 1500 yrs BP (Thamban et al. 2007). The upwelling conditions decreased during the late Holocene between 6000 -2000 years with only few distinct events in between (Gupta et al. 2003).

2.5 Archaeology

In the Emirate Sharjah, the first proof of human existence can be found at Jebel Faya, dated at around 127 to 95 ka ago (Armitage et al. 2011). Separated by a sterile layer of sand, another layer with finds was dated to between 38 to 10 ka. It is thus believed to be one possible route of anatomically modern humans (AMH) on their way out of Africa (Armitage et al. 2011). However, traces of AMH are found in larger amounts as late as the Paleolithic and Neolithic times. In addition, mtDNA evidence from modern populations, as described in al-Abri et al. (2012), suggests that distinct population movements from the North (Near East) to South Arabia had occurred between 13 ka and 12ka BP (Al-Abri et al. 2012).

The humid conditions of the early Holocene made it easier for people to inhabit this area. At Wadi Wutayya at the coast of Oman, several fireplaces had been dated to the late tenth, early ninth millennium BC (Uerpmann 1992). This coastal environment is a perfect refuge for human settlement and it is assumed that, with the onset of the Holocene Moist Phase, groups from these areas started to re-occupy the inland zones. In archaeological terms, this period spanning the early to mid-Holocene is described as Arabian Bifacial Tradition, named after finely pressure-flaked bifacial stone tools (Phillips and Mosseri-Marlio 2002). By the sixth millennium BC, a transition towards nomadic herding with sheep and goats had taken place, whose wild forerunners did not originate from south-east Arabia but from the neighboring countries to the north. Painted pottery of Ubaid type, imported from Mesopotamia and Iran, has been found at many coastal sites indicating the existence of contacts between these regions (Uerpmann and Uerpmann 1996, Beech et al. 2005).

Towards the end of the fourth millennium (3100 – 3000 BC) the number of settlements increased (Fig. 2.5.1). For the first time, collective burials in above-ground circular tombs are built from unworked stone, ranging from 7 – 12 m in diameter. These are found for example at Jebel al-Emalah and Jebel Hafit (Frifelt 1971) and are named after the place where they had been identified (Hafit-type). However, during this period, decorated pottery (Jamdat Nasr vessels) and bone or ivory beads identical to those found in Iran and Mesopotamia have been found and are interpreted as active trading connections between these areas. At both Jebel al-Emalah and Jebel Hafit, evidence for later re-use of the tombs, probably during the third until the first millennia, has been found. In the case of Jebel Hafit this continued until the sixth century AD.

At the beginning of the Bronze Age, a major change in the organization and importance of external trade can be seen (Phillips and Mosseri-Marlio 2002). Signs of copper smelting and production from the Bronze Age period have been found at Wadi Hilo. Here a complete workshop including a massive copper ingot were excavated (Kutterer 2013).To date, there is not much information about these people as their tombs were often robbed, already in antiquity.

During the mid to late third millennium, co-occurring with a reduced but slowly increasing number of settlements, the date palm (*Phoenix dactylifera*) was cultivated, along with cereals, vegetables and fruit in the shadow of the palms. Gardens, watered by wells, came into practice and laid the basis for oasis-like living with sheep, goat and cattle, characteristic of the wadi and piedmont settlements of the region. Fortifications and towers of the Umm an-Nar period (2500 – 2000 BC) date to the same time

and were built as the settlers felt they should protect their investment in land, water and natural resources. Fortresses of this period were found at Hili 8, Tell Abraq, and Kalba. The tombs of the Umm an-Nar period are circular faced with finely-masoned ashlar blocks, ranging from 4 – 12 m in diameter. Rectangular chambers are also found occasionally (Blau and Beech 1999). The tombs also show different structures inside, with variable configurations of crosswalls for example. In contrast to the Hafit-tombs, several hundred individuals were buried in these tombs, along with grave goods such as grave furniture like soft-stone vessels, locally manufactured ceramics and also imported pottery. Additionally, copper-bronze weaponry was found, as well as jewellery with beads and exotic items as ivory combs. These tombs, too, were often robbed already in antiquity.

The early and middle second millennium (2000 – 1200 BC) shows a significantly reduced amount of archaeological settlements (Fig. 2.5.1) which led to its description as the "dark millennium" (Uerpmann 2003) . With the domestication of camel sometime during the second millennium, a reversion to full nomadism might have taken place. This period is called "Wadi-Suq" after a site in Oman. Among the few settlements from the Wadi-Suq period are Tell Abraq (Magee et al. 2017) and Kalba 4 (Carter 1997, Eddisford and Phillips 2009). Nevertheless, during this period another change in material culture had taken place. The collective tombs of the Wadi-Suq period consist of unworked boulders and pebbles and are oval in contrast to the round Umm an-Nar tombs. The simplest kind of tomb of this period (Shimal-type) is around 30 m long and about 2 m wide. This period is known for its extensive use of copper in crafting.

During the late second to late first millennium (1200 – 300 BC, Iron Age), the number of settlements increased when compared to the "Dark Millenium" (Fig. 2.5.1). The domestication of the camel was finally well-established and offered possibilities for transport and trade over long distances (Magee 2007). The discovery of how to use sub-surface irrigation (Falaj-systems) allowed extensive irrigation of gardens and cultivable land and may also have been responsible for a significant increase in settlements across southeast Arabia (Magee et al. 2017). Evidence from excavations at Shimal, Tell Abraq, al-Hamryiah and Kalba shows that shellfish, sheep, goat and cattle were the main food resources (Magee et al. 2017). Moreover, apart from the date palm during the early Iron Age I period (1200 – 1000 BC), domesticated wheat and barley were cultivated (Boivin and Fuller 2009). Pottery seems very coarse in general during this time. A bivalve (*Marcia spp*.) was found with some remains of a cuprous pigment that might have been used as eye make-up.

The period between 1000 – 600 BC is referred to as the classic Iron Age period or Iron Age II. The extensive use of Falaj systems and an increased number of archaeological sites is assigned to this period (Händel 2014).

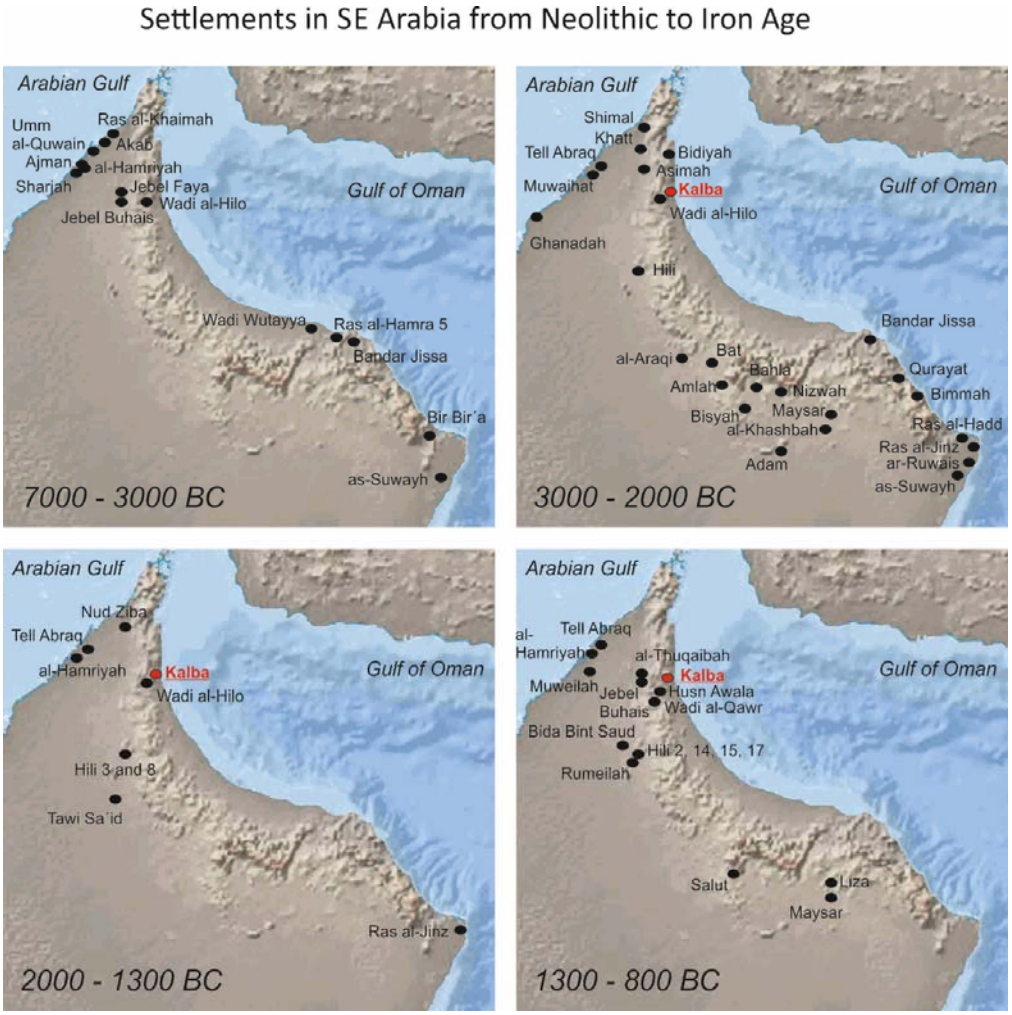

Fig. 2.5.1 Main settlements in SE Arabia between Neolithic and Iron Age. Only settlements are included, no tombs or graveyards without settlements.

2.6 Archaeology and environmental evolution of Kalba

Archaeology of Kalba:

Kalba is situated in an area with manifold settings. To the north gravel plains can be found extending towards the wadi beds further inland. The plains is covered by different tree species, mainly acacias. Finer sediments are carried to the plain, especially by the large Wadi Ham. Here the level of freshwater is closer to the surface and in combination with the fine sediment, thus provided good conditions for agriculture by well irrigation (Eddisford and Phillips 2009). Along the coastal regime, a formerly extensive mangrove forest allowed harvesting of marine food and wood.

Traces of human occupation can be found since at least the Neolithic. Although no settlement structures from this period have been detected, the presence of humans can be deduced from the many shell middens surrounding the contemporary mangrove forest. Within the oldest shell midden, hereafter referred to as KK1, bifacial stone tools have been found which are indicative of the 5th millennium BC (Phillips and Mosseri-Marlio 2002). Some of the shell middens date to the Bronze and Iron Age and can be found closer to the shore (Eddisford and Phillips 2009) which indicates a retreat of the mangrove forest between Neolithic, Bronze Age and Iron Age. Burials in this area date from Early to Middle

Bronze Age. So far, no burials for Late Bronze Age or Iron Age have been found, but a cemetery dates to the 1st to 3rd century AD (Phillips and Mosseri-Marlio 2002).

An important addition to the economy of Kalba was the introduction of agriculture, especially the date palm. Investigations also showed that the copper found and exploited in the Hajar Mountains caused significant copper poisoning in sheep and goats. Similarly high chromium and zinc concentratrions have been found in animal bones and might be responsible for some unexpected deaths (Phillips and Mosseri-Marlio 2002).

The mangrove forest remained a fundamental resource throughout the periods (Phillips and Mosseri-Marlio 2002). These possibilities allowed a larger community to permanently settle in this enclave. Site KK4, around 2 km from the shoreline and north of the sabkha, was built on during the Bronze Age. Several superimposed building phases could be detected, centered around a tower comparable to the one at Hili 8. This tower was later replaced by a mud-brick tower (Carter 1997). Another major building phase might have taken place before the Iron Age (Phillips and Mosseri-Marlio 2002).

Even though K4 was a larger settlement, it is possible that this was not the only occupational site. Several campsites for pastoralists or other specialists might have been associated with it (Phillips and Mosseri-Marlio 2002).

Marine conditions at Kalba

The oceanography near Kalba is influenced by the shallow, flat Arabian Gulf (AG) which connects with the Gulf of Oman (GO) at the Straits of Hormuz. At the location of the UAE coast, the Gulf of Oman is relatively shallow, deepening off the coast especially south of Muscat in Oman.

The marine hydrology at Kalba is highly seasonal. In summer, marine surface water originates from the Arabian Sea to the south. This ocean current transports upwelling waters that are depleted in radiocarbon. The nutrient-rich waters derive from the southwest Indian Ocean and are driven into the Arabian Sea by the Somali Jet that follows the coast of Oman and is strongest between May and October. Intensity varies in accordance with duration and strength of the SW Monsoon (Johns et al. 2003). During the second half of the year in winter, marine dynamics are dominated by deep water outflow from the Arabian Gulf (Lambeck 1996, Johns et al. 2000, Kämpf and Sadrinasab 2005). This water is still more depleted in radiocarbon, is enriched in limestone source sediments and input of dissolved inorganic carbon from coral reef rocks, e.g. near Qatar. Consequently, it yields an older reservoir age. This warm, dense and saline AG outflow forms a coastal current along the western GO, to Ras al-Hadd at the edge of the Arabian Sea (Johns et al. 2000), where the warm current meets the cold, upwelling waters of the southwest Arabian Sea.

The mangrove forest at Kalba had its largest extend during the mid-Holocene, represented by the shell midden KK1 and successively moved towards its modern position further away from the Hajar Mountains since then. The remaining sabkha contains some shell middens with the younger ones dating to the Bronze and Iron Age periods (Phillips and Mosseri-Marlio 2002). The reduced extent of the mangrove forest over time is certainly the result of increased sedimentary input to the lagoonal system, coupled to a lowered sea level.

3 Methods

3.1 Radiocarbon Dating and Reservoir Effect

Radiocarbon Dating

In 1960, Willard Libby was awarded the Nobel Prize in Chemistry for his work on the method of radiocarbon dating 15 years earlier (Olsson 2009, Jull et al. 2018). For radiocarbon dating, three carbon isotopes are of importance, of which two are stable and one radioactive. The occurrence of these isotopes differs significantly: ^{12}C (98,89 %), ^{13}C (1,11 %) and ^{14}C (10^{-10} %), of which ^{14}C is the only radioactive one and hence can be used for dating purposes. Traditionally, a half-life of 5568 years is used with 1950 as reference date, as it was first determined, however, the true half-life of radiocarbon is 5730 years (Godwin 1962, Bronk Ramsey 2008). The exponential radioactive decay law describes that after one half-life, in our case 5730 years, half the amount of the original material is decayed. After another 5730 years, half of the remaining amount is also decayed, and so on. In general it can be said that after 8-10 half-lives there is hardly enough ^{14}C left to be detected. For ^{14}C, this covers a range of approximately 50,000 years (Bronk Ramsey 2008). Therefore, all kinds of material that contain carbon and are younger than 50,000 years can theoretically be dated using radiocarbon.

Measurement techniques are aimed at either directly counting the radioactive β - decay, or attempting to measure all three isotopes with a mass-spectrometer (Olsson 2009). Because of the large difference in abundance between ^{12}C and ^{14}C (amount $^{12}C = 10^{12} * {}^{14}C$), this can only be achieved with an accelerator mass spectrometer (AMS) (Synal and Wacker 2010). The smallest system at the time of writing is the MICADAS system (Mini CArbon DAting System), developed by the ETH Zurich (Synal et al. 2007, Schulze-König et al. 2010, Kromer et al. 2013). This system is rather compact, measuring 2.5 m x 3.5 m in size, which makes it suitable for smaller rooms, compared to the space required for larger systems.

Although with AMS systems all three isotopes ^{12}C, ^{13}C and ^{14}C are measured, the ^{13}C measurement only serves to correct for fractionation occurring during the measurement. Usually $\delta^{13}C$ serves to identify characteristic materials, but not when it comes from an AMS measurement (Santos 2007). For interpretation, $\delta^{13}C$ needs to be measured using an Isotope ratio mass spectrometer (IRMS). Fractionation during measurement is usually corrected (Bronk Ramsey 2008, Olsson 2009).

The result of a radiocarbon measurement is the so-called radiocarbon age. This expression is misleading, because radiocarbon ages are not true calendar ages. Even in the early years it was established that the radiocarbon ages calculated from the radioactive decay law did not always fit to the data of known-age samples (Bronk Ramsey 2008). The results need to be calibrated to convert the measurement results into years BC/AD or years BP. Two calibration curves for the pre-bomb era are being used: one for the atmospheric records (IntCal) and one representing marine data (MarineCal). Since the calibration curve shows variability and plateau regions, reflecting changes in ^{14}C production, measurements with small error still can result in larger age ranges when the data lies on a plateau. The most prominent plateau regions are the so-called Hallstadt-Plateau (800 – 400 BC) or the Maunder Minimum

("Little Ice Age"), which is immediately followed by the Suess Effect to build a plateau between 1650 and 1950 AD (Eddy 1976, Jacobsson et al. 2017). This means that measurements, even with small measurement error, coinciding with a plateau always give the calibrated age of the whole plateau region. With the nuclear tests starting in the late 1950s, the amount of ^{14}C in the atmosphere increased dramatically. Atmospheric CO_2 measurements by several laboratories monitor changes in the atmospheric inventory since then led to the bomb calibration curve (http://calib.org/CALIBomb/).

Calibrated results must be marked as cal BC, cal AD, cal BP, whereas ^{14}C yrs BP always denote uncalibrated years. The recommendation for publishing radiocarbon dates is to give the uncalibrated, fractionation corrected data $F^{14}C$ (unit ^{14}C yrs BP or just "BP"), plus the calibrated ages with information on calibration software, calibration dataset, reservoir effects if used, plus the labcode of the laboratory that did the ^{14}C measurement (in this case MAMS for Mannheim, P for Jena, UCIAMS for Irvine). It should be self-evident to also note on which material the age was determined (charcoal, bone, etc.). Post-bomb data is in this case presented as $F^{14}C$, or if corrected for the year of sample growth, it is reported as $\Delta^{14}C$ (Reimer 2004). Throughout this thesis all data is calibrated using Oxcal 4.2 (https://c14.arch.ox.ac.uk/oxcal.html) with the IntCal13 or the Marine13 dataset respectively (Reimer et al. 2013). Uncalibrated data is always given as "^{14}C yrs BP" in this thesis.

To properly interpret radiocarbon ages, the carbon cycle should be taken into account (Fig. 3.1.1). Radiocarbon (^{14}C) is produced in the atmosphere when cosmic radiation (solar wind, galactic and extragalactic radiation) enters the stratosphere and reacts with its gaseous components. This collision results in cascade-like shower of particles of which also neutrons emerge. These neutrons react with Nitrogen to build Carbon-14 (^{14}C) under emission of a proton. The so produced ^{14}C reacts with the Oxygen in the atmosphere to build CO_2 and enters the Earth´s dynamic carbon cycle (Bronk Ramsey 2008). The CO_2 can enter several reservoirs, the most prominent being atmosphere, terrestrial and marine reservoirs. Diverse reservoirs can store varying amounts of carbon for different periods of time (Fig. 3.1.1). The exchange between atmosphere and biosphere or surface waters is rather quick, taking several years to decades (Bronk Ramsey 2008). The exchange with rather inactive reservoirs like carbonates in limestone, carbon in frozen sediment, biomass in coastal wetlands, can be very slow resulting in long storage times (Fig. 3.1.1). These long storage and exchange times result in a decrease of ^{14}C concentrations because of radioactive decay during these periods. This depletion with respect to atmospheric concentrations is described as reservoir effect and will be discussed in chapter 3.1.2. Terrestrial reservoirs like plants incorporate the carbon rather quickly through photosynthesis, which is then taken up by animals and humans through food. This short exchange rate is the reason why plants and biosphere show atmospheric values as can be seen in Fig. 3.1.1 (Bronk Ramsey 2008, Olsson 2009).

The longest storage time in an active reservoir (up to 1000 - 1500 years) occurs in the deep sea (Bronk Ramsey 2008). The marine reservoir can also store the largest amount of carbon with more than 90% (Fig. 3.1.1). This large storage volume of carbon in the oceans also acts as a buffer which dampens larger fluctuations in terrestrial carbon (Broecker et al. 1960, Bronk Ramsey 2008). The different reservoirs also differ when it comes to the exchange rate between them (Fig. 3.1.1).

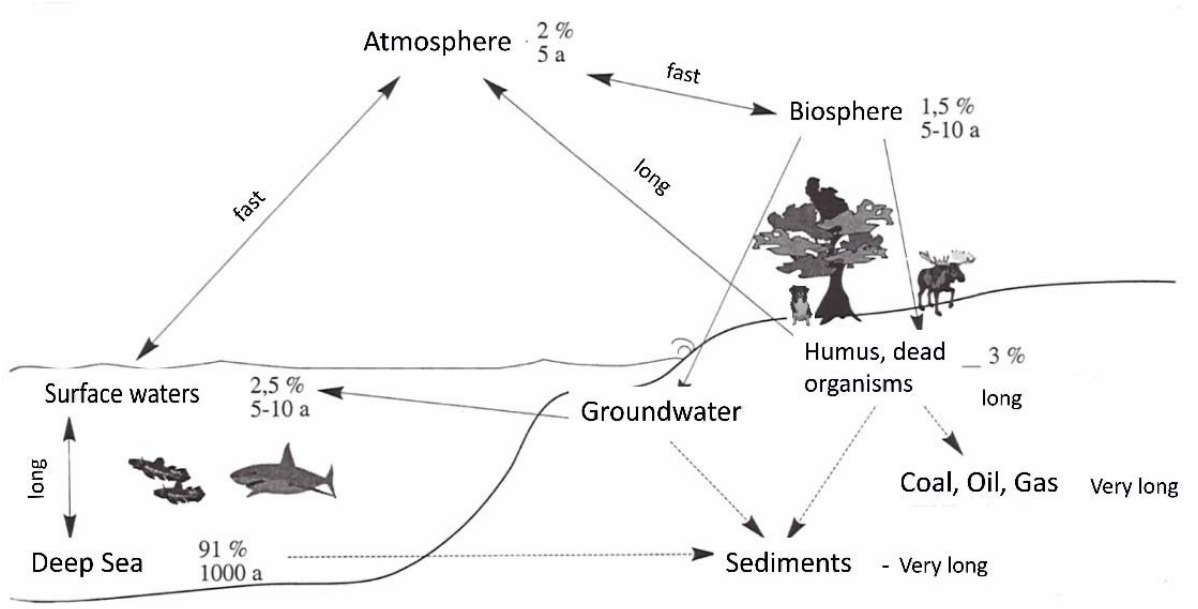

Fig. 3.1.1: Reservoirs for ^{14}C storage including exchange and storage times. Translated and modified from (Wagner 1995).

Reservoir Effect

In the paragraph above the different storage times and stored amounts of carbon are already described. The marine system, however, also requires attention with respect to this thesis. The marine reservoir effect is a consequence of the possibility for oceans to store carbon over very long periods, up to 1500 years (Dutta 2008). Surface waters exchange carbon with the atmosphere (Fig. 3.1.2). Depending on ocean circulation, this carbon can be transported into deep sea waters where it remains for a long time until is it brought up again in areas of upwelling ocean waters as in the Arabian Sea (Fig. 3.1.2). During transport in the deep sea, the radioactive ^{14}C decays and is not replaced by fresh ^{14}C as is the case within surface waters. Hence, the deep ocean waters are depleted in radiocarbon (Broecker et al. 1960). In areas of upwelling ocean circulation, this depleted or "old" water is transported back near the surface where it can be incorporated by organisms living in this environment, e.g. shells, corals, fish and algae (Fig. 3.1.2). As mentioned before, in areas of down welling ocean circulation, fresh radiocarbon is transported into deeper waters and hence in organisms living in this area the reservoir effect is less pronounced as in areas of upwelling ocean circulation. To take this into account, a marine calibration curve was set up using a mean reservoir age of 405 ± 22 years with respect to atmospheric ^{14}C valid globally (Dutta 2008, Zazzo et al. 2012, Reimer et al. 2013). This allows a rough calibration of marine data in general. Nevertheless, with respect to upwelling and down welling areas, this value can differ significantly depending on locality (Taylor and Berger 1967). Therefore, an additional value has to be added or subtracted to the marine calibration curve – the local marine reservoir effect or ΔR (Stuiver et al. 1986, Stuiver and Braziunas 1993). In some publications, it is also referred to as MRE (Ascough et al. 2005, Ascough 2009, Zazzo et al. 2012). For organisms that are still older than the marine age of 405 years, this value is positive and has to be added, for organisms younger than the 405 years it is negative and needs to be subtracted.

The *reservoir age* R(t) is calculated as the shift in years between the marine and the terrestrial sample. The *reservoir effect* ΔR can then be calculated by calibrating both marine and terrestrial sample, with the atmospheric curve and subtracting the 405 ± 22 years from the marine curve (Ulm 2002, Petchey 2008). A more effective way of calculating the reservoir effect is modelling a possible reservoir effect range in Oxcal (Zazzo et al. 2016). In addition, this procedure helps to identify possible outliers to the model and allows a decision to be made of the reliability of the model by a parameter "A" that should be at least 60%. Adjustments to the model, like narrower reservoir effect ranges, are easily done and help to improve the output (Zazzo et al. 2016). An example of this model is given in Chapter 4.2.

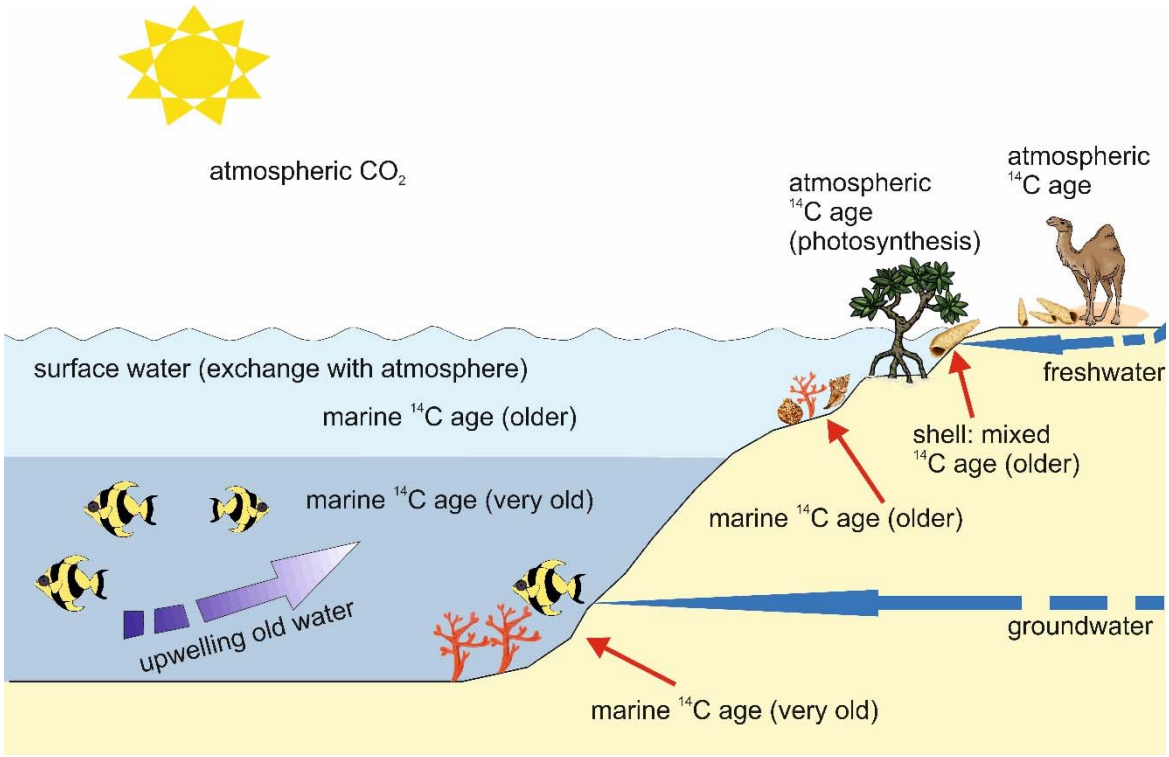

Fig. 3.1.2: Illustration of the reservoir effect: the ocean and the organisms (plants, animals) in it seem older than their calendar age. Contemporaneous terrestrial/atmospheric material is used to derive this shift in age. The shells in this thesis covered the habitat of mixed reservoir age (Terebralia palustris), marine ^{14}C age ("older", Anadara uropigimelana) and atmospheric ^{14}C age (Zootecus insularis for terrestrial, Melanoides tuberculata representing freshwater).

However, this local reservoir effect varies for different organisms. As marine organisms usually feed from other organisms or plants, it is not only the water that contributes to the species-specific local reservoir effect (Culleton et al. 2006). Plants that are completely submerged would show the signal of the water, but plants where most of the material is above the water would incorporate atmospheric CO_2 during photosynthesis and hence show a dominant, if not completely terrestrial $^{14}C/^{12}C$ ratio (Lindauer et al. 2016). In addition, organisms, like the gastropod *Terebralia palustris*, have a marine habitat but a terrestrial diet and hence a mixed reservoir effect is to be expected, as illustrated in figure 3.1.1 (note: the shells in the picture are not the shells species used in this thesis, they only serve to

outline the different habitats and diets). In addition, figure 3.1.1 tries to show the influence of groundwater and freshwater input to the nearshore zone, including mangrove forests. Chapter 4.1 introduces an example for this regarding the mangrove forests along the coast of the Arabian Gulf and the Gulf of Oman.

It should be mentioned, however, that since the nuclear bomb tests the amount of ^{14}C in the atmosphere has doubled. The ocean, being able to store large amounts of carbon, collected major parts of it and therefore marine organisms, even in upwelling areas, show a reduced or no reservoir age nowadays compared to pre-bomb periods (Jenkins 2010). This can also be seen from the atmospheric bomb calibration curve. The Southern Hemisphere shows a less pronounced bomb signal which is due to the fact that the Southern Hemisphere is dominated by oceans that take up the carbon (Hua and Barbetti 2004). This study also measured water samples in the lagoons of Ajman (Arabian Gulf) and Kalba (Gulf of Oman). Both samples yielded data with modern signal, but still the Arabian Gulf is shifted towards slightly older age. To be statistically significant, several samples, preferably monthly collection, should be measured. The lower $F^{14}C$ value points to older age in this case. When calibrated, the water from Kalba seems to have a calendar age 1956-1957 AD, whereas Umm al-Qwain calibrates to 1955-1956 AD (calibrated with Calibomb, http://calib.org/CALIBomb/ using the bomb NH3 zone). The samples in Table 3.1.1 were collected in December 2013.

Table 3.1.1: Water samples from Umm al-Qwain lagoon and Kalba lagoon. The stable isotope values are determined using an IRMS (University Mainz).

Labcode	Sample	$F^{14}C$	±	$\delta^{13}C$	±	$\delta^{18}O$	±
P 13268	Kalba (Lagoon)	1.0251	0.0040	-1.1	0.02	2.1	0.02
P 13269	Umm al-Qwain (Lagoon)	1.0110	0.0034	-1.0	0.02	3.2	0.03

Hardwater Effect:

The terrestrial version of the marine reservoir effect is called hardwater effect. Because here limestone or other carbonate reservoirs with ages in geological timescales can be responsible for depletion in ^{14}C, the hardwater effect can be significantly larger than the marine reservoir effect.

Sample Preparation and Measurement

The sample preparation for radiocarbon dating aims at removing any contaminants accumulated over time and possibly added to the sample during handling. For charcoal, ash, sediment and plant fragment samples a standard so-called ABA (acid base acid) treatment was applied. This includes an acid step (Hydrochloric acid, HCl) at 60°C to remove calcium carbonates, a base step (Sodiumhydroxid, NaOH) at room temperature to remove humic acids, and a second acid step at 60°C. The second step using

acid is needed because NaOH collects carbon dioxide (CO_2) from the air which represents a modern contamination (Lindauer et al. 2016, Lindauer et al. 2017). Because this CO_2 attaches to the surface, it is easily removed by the acid step. Between the steps that were usually applied for one hour each and afterwards, the sample is washed with ultrapure water. Ash samples were floated prior to the ABA treatment to collect the lighter ashy material that settles above the heavier sand grains. The general procedure does not vary between different laboratories, although the concentration of the chemicals, temperature and timing of preparation might differ slightly. Details of the procedures used by the laboratories involved can be found in chapter 4.2.

For shells, the pretreatment includes removal of sand by washing followed by etching of the outer, probably contaminated part of the shell using diluted acid, in our case 1% HCl, before rinsing with ultrapure water. This step usually removes 20-50 % of the shell depending on its thickness (Lindauer and Kromer 2013).

After pretreatment, the samples need to be reduced to elementary carbon. For the charcoal, ash, sediment or plant fragment samples this is achieved by combusting them in an elemental analyzer (Fig. 3.1.3 A) to gaseous CO_2 and transferring them into a glass tube (reactor) of a graphitization unit (Fig. 3.1.3 B, C). In Mannheim, two graphitization systems are available: a semi-automated self-built system (Fig. 3.1.3 B), which works with transferring CO_2 using liquid nitrogen and facilitates the graphitization of 10 samples. The second graphitization system is the automated AGE III system (IONPLUS, CH) with 7 reactors (Fig. 3.1.3 C). This system uses a zeolith to collect the CO_2 (Wacker et al. 2010). The system might have some minor memory effect. The carbonate handling system (CHS, IONPLUS), also referred to as autosampler system is attached to the AGE III graphitization (Fig. 3.1.3 D). In the reactor iron, powder is present and hydrogen gas is added. At a temperature of around 580°C (depending on laboratory, see chapter 4.2. for details depending on laboratory involved) iron acts as a catalyst to reduce CO_2 to C while the oxygen molecule reacts with hydrogen to water which is frozen out in a cooling finger (Lindauer and Kromer 2013).

Shells on the other hand, are graphitized without combustion. Here the CO_2 is hydrolyzed chemically by adding 1 ml 85% Phosphoric acid at a temperature of 70°C (Fig. 3.1.3 D). The aragonite or calcite reacts with the acid and CO_2 evaporates as gas which is transferred into a reactor using a helium flow (Wacker et al. 2013). The subsequent graphitization procedure is then the same as for the other sample materials.

The samples are then pressed into a target and measured in an AMS system. The following AMS systems were used to measure the samples of this study: the ^{14}C laboratory at CEZ Archaeometry gGmbH, Mannheim, Germany (Kromer et al. 2013), the system at the ^{14}C laboratory of the Max-Planck-Institute for Biogeochemistry in Jena, Germany (Steinhof et al. 2004, Steinhof 2016) and the ^{14}C laboratory at the University of Irvine, California, USA (Santos 2007, Beverly et al. 2010). Detailed descriptions of all three AMS systems can be found in chapter 4.2.

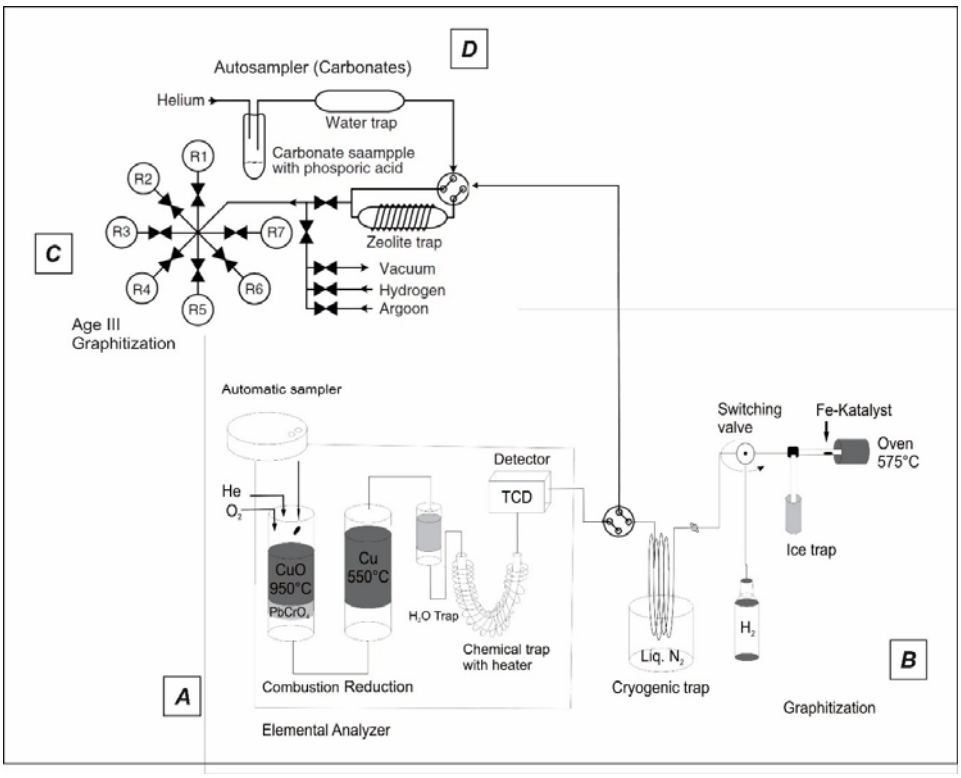

Fig. 3.1.3 Graphitization as applied in the Mannheim laboratory (Curt-Engelhorn Centre Archaeometry). Part A denotes the Elemental Analyzer, thereafter EA, (MicroCube, Elementar) where samples (charcoal, sediment, etc.) are combusted and the gases separated in the trap. When the CO_2 gas exits the EA it can either be caught in the Mannheim graphitization system, MAG, (selfbuilt, semiautomatic) denoted with "B" or be transferred to the AGE III (IONPLUS) graphitzation system that can be operated automatically. Carbonate samples (shells, stalagmites, etc.) are hydrolyzed in the Carbonate Handling System (CHS; IONPLUS), schematized in part D, which uses an autosampler system which then transfers the CO_2 gas to the AGE III system for graphitization. AGE III and CHS system are modified from Wacker et al. (2013), the EA and MAG are modified from (Lindauer and Kromer 2013).

3.2 Shells as Environmental Archives

Malacology

Malacological studies deal with selection of shells, both marine and terrestrial (Fig. 3.2.1). Those that were the most abundant ones found at the archaeological sites in Kalba were chosen, namely from the marine environment the mangrove gastropod *Terebralia palustris* and the bivalve *Anadara uropigimelana.* From the terrestrial environment the landsnail *Zootecus insularis* and the freshwater snail *Melanoides tuberculata* were collected. For some tests we also included shells of species *Periglypta reticulata* (Fig. 4.1.2, Fig. 4.1.5) in our study, a bivalve with similar habitat and diet as *A. uropigimelana* (described in chapter 4.1).

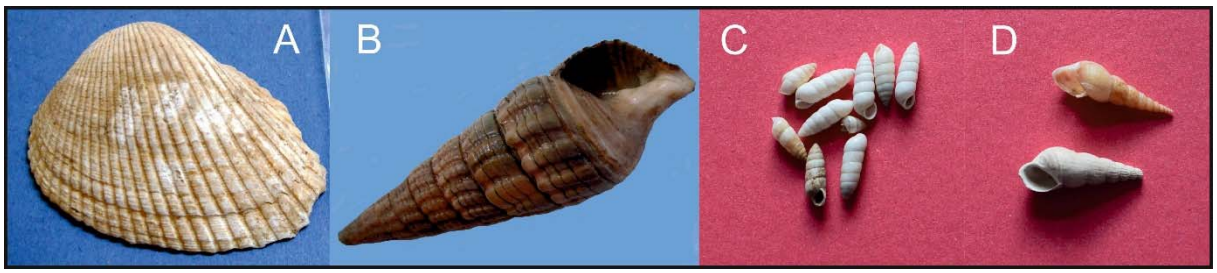

Fig. 3.2.1: Shells used in this study: A – *Anadara uropigimelana*, B – *Terebralia palustris*, C – *Zootecus insularis*, D – *Melanoides tuberculata*.

Anadara uropigimelana:

The bivalve *Anadara uropigimelana* (Fig. 3.2.1 A), family Arcidae, lives in the intertidal mudflats of lagoons and estuaries from Africa through Indian Ocean and Pacific (Tebano and Paulay 2000). It can tolerate temperatures of 15 – 32 °C and withstand large salinity fluctuations (Azzoug et al. 2012). The species is said to be rather stationary (Murray-Wallace et al. 2000). Shells of species *A. uropigimelana* are so-called filter feeders, feeding from algae and other small marine organisms (Azzoug et al. 2012, Petchey et al. 2013). It is well suited for environmental analyses because it accumulates aragonite depending mainly on tides and environmental conditions. Azzoug et al. (2012) found that in *Anadara senilis* shells the juvenile growth lines are more discernible that those in the adult part of the shell. The same was found in the *Anadara uropigimelana* shells discussed here, as can be seen in Chapter 4.1. Analyses on *Anadara senilis* have shown that the first deep external growth ring (or growth line when cut) appeared when the molluscs were around 20 months old, at an umbo-pallial-length of around 16 mm (Debenay et al. 1994). This strong first line also occurs in *Anadara uropigimelana* shells at around the same length and probably roughly the same age. The results on growth lines and stable isotopes are found in chapter 4.1 (Fig. 4.1.4).

In addition to its fast response to changes in environmental conditions the lifespan of *A. uropigimelana* with up to 45 years makes it interesting for environmental research (Petchey and Clark 2011). In Kalba, this species can be found since the Neolithic, although in period 1 of the shell midden KK1 only a few specimens were found, which might be interpreted as the time the shell started to settle in this lagoon or the time when people started foraging it, or both. When the shell material is heated, it transforms the mineral phase from aragonite to the more stable calcite, whereas the radiocarbon measurement is not affected, as described in more detail in chapter 4.4.

Terebralia palustris:

This gastropod of the family Potamidae is also known as “mud whelk” (Fig. 3.2.1 B, Fig. 4.1.2). It mainly lives in and around mangrove forests, but occasionally can be found outside of and further away (Feulner 2000). It feeds mainly from leaf litter of the mangroves. However, it is also described as an omnivorous species because it also occasionally feeds on detritus, mangrove propagules, carrion, organic sediment particles as well as benthic diatoms and bacteria (Penha-Lopes et al. 2009). Younger and older individuals are living separately including different dietary habits due to anatomical differences. The younger specimen are detrivorous or deposit feeders, whereas the older specimen prefer

fallen mangrove leaves, propagules and fruit (Penha-Lopes et al. 2009). The juvenile *T. palustris* seems to be colonizing in small creeks and large pools at the seaward front of the mangrove forest until they mature and move towards the interior, landward part of the forest (Feulner 2000, Pape et al. 2008). This change in habitat and diet is also reflected in a decrease in $\delta^{13}C$ with increasing size of the individuum (Penha-Lopes et al. 2009). The number of juvenile *T. palustris* is inversely correlated to the salinity of the water, which might be the reason why it meanwhile died out in the Arabian Gulf. The exact timing of the loss of *T. palustris* to coastal sites along the AG is currently unknown. The lifespan of this species is currently unknown. Reaching adult age takes several years, but growth is relatively rapid. They can reach a length of 40 mm within 3 years. (Feulner 2000). With a total length of up to over 100 mm it can be deduced that their lifespan might well be up to ten years or even more depending on habitat and environmental conditions. *T. palustris* is active both at low and high tide, but seems to avoid the most extreme zones of the habitat, that is driest landward and most exposed seaward zones (Pape et al. 2008). This molluscan species, is also aragonitic and transforms to calcite during heating. Here, like with *A. uropigimelana* shells, the heating does not affect the radiocarbon measurement (chapter 4.4).

When sampling for radiocarbon, care must be taken not to sample the small tip, which represents the juvenile phase in an offshore setting.

Zootecus insularis:

Zootecus insularis (Fig. 3.2.1 C) is a widespread landsnail that can be found in Arabia as well as in Africa. The lifespan is unknown but is expected to be rather short due to its limited size of 1 – 1.5 cm (Neubert 1998, Neubert 2003). The preferred habitat is described slightly different by some authors. According to the description of (Feulner and Green 2003), *Z. insularis* is widespread among the Hajar Mountains and the adjacent gravel plains which could be constrained in this work. In Musandam, it is said to be occurring at heights from wadi level to around 1600 m. In places showing cultivation, today as well as in the past, it also is present. According to Feulner and Green (2003), it often emerges from silty soils among rocks and vegetation of hills and mountains. On gravel plains and terraces it is found in silty patches, especially near *Euphorbia larica.* Empty shells are usually white and opaque. Live shells are rather pale buff coloured and slightly glossy (Feulner and Green 2003). In addition it seems that *Z. insularis* usually occurs in large numbers (Girod and Balzarini 2017).

Melanoides tuberculata:

This freshwater snail (Fig. 3.2.1 D) can often be found in Arabia as well as in Africa. As with *Z. insularis*, the lifespan of *M. tuberculata* should not be more than a few years. It easily adapts to the environment and can even be found in deltas. Usually it is associated with environments of low salinity (0,2 – 3 ‰) but can tolerate salinities of up to 23 ‰ (ca.2 %) (Plaziat and Younis 2005). The preferred habitat of *M. tuberculata* is the subaquatic soft bottom. Empty shells have the tendency to float and accumulate on lake shores (Plaziat and Younis 2005). One study found the snails associated with aquatic and subaquatic plants, up to 2 m deep, in a littoral habitat which provided shelter from wave action (Leng et al.

1999). Depending on environmental conditions, the lifespan and life history varies. In Lake Chad, *Melanoides tuberculata* reaches maturity within 5 months, but few specimens lived for more than one season. In Hong Kong and Malaysia on the other hand lifespans of up to 2 – 3 years have been reported (Leng et al. 1999).

Sclerochronology and Stable Isotopes

Mollusc shells are high-resolution and temporally aligned geochemical records of the past that, depending on the biomineralization rate, are able to monitor environmental conditions by incorporating trace elements in the skeleton (Jones et al. 1989, Schöne 2008). Environmental changes are mirrored in the shell carbonate as variable growth lines (comparable to tree rings) and differing chemical properties (Füllenbach et al. 2015, Marali et al. 2017). On timescales ranging from ultradian (less than 24 hours) to annual timescales molluscs stop growing shell material regularly. During times without growth no environmental condition is recorded. This happens during spawning and when environmental conditions drop beyond physiological tolerance of the animal, e.g. too high salinity, extreme temperature changes, to name but a few effects. These tolerances and periods of slow or no growth are genetically determined and species-specific (Schöne 2008). Retardations in growth make the environmental record of a shell incomplete and biased towards the physiological optimum of the animal. In addition, duration of the growing season and overall growth rate decrease with increasing age of mollusc (Schöne 2008), which is referred to as an ontogenetic trend (Fig. 3.2.2). Knowledge of these conditions for the shells of interest and their physiology hence is crucial when using them for palaeoenvironmental reconstruction.

Growth Lines

Changes in physio-chemical environment are recorded in shell material in the form of variable growth rates and geochemical properties (Schöne and Surge 2012). Growth lines are found along the shell, but also in the umbo. As mentioned, shell growth periodically decelerates and even ceases at certain times although environmental conditions still remain acceptable for shell growth. Decelerated growth results in the formation of growth lines comparable to tree rings and are visible in the shell material (Fig. 3.2.2). These growth lines can occur as daily growth lines and annual growth lines. The carbonate material accumulated between the growth lines is called growth increment. Growth increments and growth lines allow to assign calendar ages or times to each shell (Schöne 2008). In intertidal habitats, where *A. uropigimelana* and *T. palustris* are found, shell growth of bivalves only occurs during high tides. When the bivalve is exposed during low tide the animal is forced to keep the bivalves tightly closed and the mantle drawn back far into the shell. As now the shell growth ceases, a growth line is formed and the record of environmental conditions halted (Schöne 2008). Daily growth lines can occur on several timescales: circadian (solar day with approx. 24 hours), circalunidian (lunar day with approx. 24,8 hours) and circatidal (semidiurnal or 12.4 hours) (Schöne 2008, Schöne and Surge 2012). Circadian growth patterns usually occur in subtidal bivalves. Intertidal growth patterns are circatidal, however,

the intertidal zone is also subdivided in three groups. In low intertidal settings the time available for shell growth is longer than the semidiurnal 12.4 hours as the shell is under water for a correspondingly longer period. In mid-intertidal settings the shells only record environmental conditions for around 12.4 hours (lunar day), whereas in high-intertidal settings the shells are exposed to air for more than 12.4 hours and therefore record environmental conditions for a shorter period of the day.

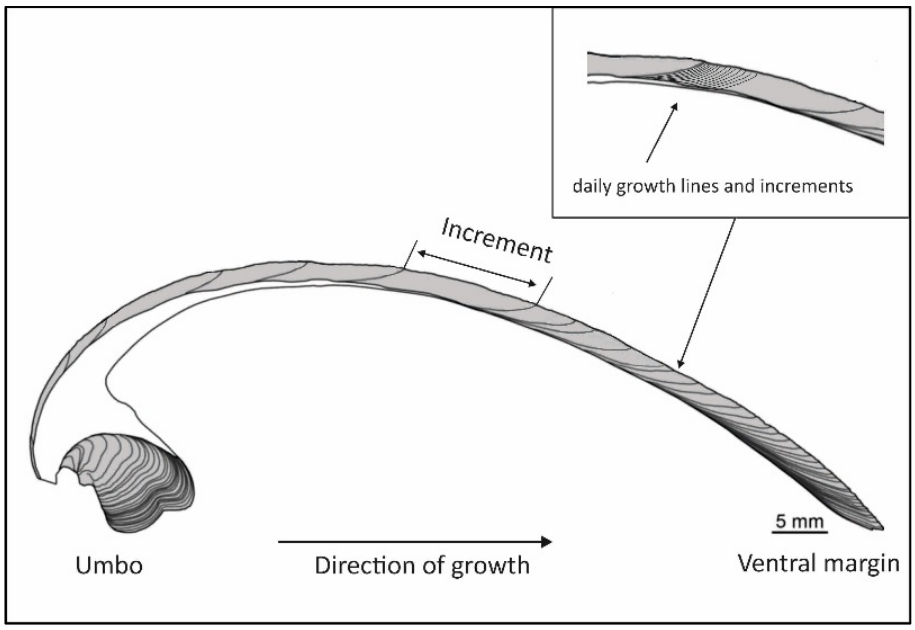

Fig. 3.2.2: Growth lines in bivalves. The ontogenetic trend is visible as narrower lines towards the ventral margin. A photo of growth lines, including daily growth lines, can be seen in chapter 4.1 (Fig. 4.1.5). Modified from (Marali et al. 2017)

The pronounced annual growth lines can be used to infer the age of the mollusc, if they are not only controlled by environmental conditions (like water temperature) alone, but also by endogenous factors (for example regular spawning periods). Some species cease to grow during a certain season, probably due to elevated water temperatures that exceed the species-specific temperature threshold. Strong environmental changes, like El Nino events, can also be seen in shells as strong growth marks (Rollins et al. 1987, Rollins et al. 1990) that seem to be out-of-band.

To measure the growth lines, shells are cut along their growth axis. The 3 mm thick slices are then polished (Fig. 3.2.2). One slice is then etched with Mutvei´s solution for growth line analysis whereas another slice can be used for stable isotopes, as described in the next Chapter 3.2.2.

To visualize growth lines more clearly, the organic material within the increments is etched away by Mutvei´s solution (Schöne et al. 2005). The additional effect is the blue colouring of the remaining carbonaceous skeleton. (Schöne et al. 2005, Lindauer et al. 2016, Schöne et al. 2017). This makes it easy to count annual or even daily growth lines, as can be seen in chapter 4.1 (Fig. 4.1.5).

Stable Isotopes $\delta^{13}C$ and $\delta^{18}O$

Stable isotopes $\delta^{13}C$ and $\delta^{18}O$ are usually measured along the shells growth direction and monitor changes throughout the lifetime of the molluscan species (Fig. 4.1.4, Fig. 4.1.6).

$\delta^{13}C$:

Carbon isotope $\delta^{13}C$ values are higher than for terrestrial material, because plants preferentially take up the light ^{12}C isotope during photosynthesis and therefore the heavier ^{13}C isotope remains in the water (Schöne and Surge 2012). The main origin of $\delta^{13}C$ in the shell is dissolved inorganic carbon (DIC) in the water. To a minor extent, metabolic CO_2 is also incorporated into the shell (McConnaughey and Gillikin 2008). Particularly for species with a shorter lifetime, there might be a trend towards increasing amount of respiratory CO_2 with increasing age. This would be seen in more negative $\delta^{13}C$ values at older age of the mollusc (McConnaughey and Gillikin 2008, Schöne and Surge 2012). However, the absence of a single origin makes it difficult to interpret the $\delta^{13}C$ data. In this case the shells discussed here have the additional parameter of an estuary with seasonal freshwater input after strong rain events, which then carries the $\delta^{13}C$ of freshwater and mixes with the ocean water. Fluvial DIC can be isotopically lighter due to input of CO_2 derived from decomposition of terrestrial plants (McConnaughey and Gillikin 2008). In estuaries, $\delta^{13}C$ of DIC decreases because salinity and alkalinity increase with increasing terrestrial influence (Khim et al. 2003).

$\delta^{18}O$:

Fortunately metabolic effects do not influence $\delta^{18}O$ in the shell material. Almost all shells precipitate their oxygen in equilibrium with the oxygen isotope composition of the ambient water (Khim et al. 2003, Schöne et al. 2005). Therefore, $\delta^{18}O$ in shells is a good tracer for temperature and geochemical changes of the water. When the temperature is known, $\delta^{18}O$ can also be used to derive the salinity variation over a certain period (Schöne and Surge 2012). In addition with growth patterns, $\delta^{18}O$ can be used to derive the timing and periodicity of shell growth (Schöne and Surge 2012). As different species prefer different conditions the information of $\delta^{18}O$ and growth lines can be used to derive the species - specific temperature range of the preferred environmental condition.

In general it can be said that a change of 1 ‰ in $\delta^{18}O$ corresponds to a change in 3-4 °C in temperature (Leng 2006). It should be kept in mind that a change towards more positive $\delta^{18}O$ values refers to a change towards colder temperature and vice versa (Schöne and Surge 2012). Seasonal freshwater input with its own $\delta^{18}O$ signature will also be visible depending on the amount of water and limestone content brought into the system (Khim et al. 2003). For speleothems, highly negative $\delta^{18}O$ values do not reflect the temperature during deposition, but rather reflect isotope depletion of rainfall and groundwater (Burns et al. 2001). According to Burns et al. (2001), the most likely source of depleted rainfall is the Indian Ocean summer monsoon. Here, the depletion in $\delta^{18}O$ is caused by strong convection associated with monsoonal circulation. The speleothem fluid inclusions indicate a predominantely westerly winter source of rainfall from the mid Holocene onwards (Parker et al. 2016).

4 Results and Publications

4.1 Investigating the Local Reservoir Age and Stable Isotopes of Shells from SE Arabia

Susanne Lindauer[1,2], Soraya Marali[3], Bernd R Schöne[3], Hans-Peter Uerpmann[4], Bernd Kromer[1], Matthias Hinderer[2]

[1]Curt-Engelhorn-Zentrum Archaeometry gGmbH, Klaus-Tschira-Archaeometry-Centre, C4, 8, 68159 Mannheim, Germany.
[2]Institute of Applied Geosciences, Technical University Darmstadt, Schnittspahnstr. 9, 64287 Darmstadt, Germany.
[3]Institute of Geosciences, University of Mainz, Joh.-J.-Becherweg 21, 55128 Mainz, Germany.
[4]Center for Scientific Archaeology, Eberhard-Karls-University Tübingen, Rümelinstraße 23, 72070 Tübingen, Germany.

Contributions: SL, MH, BRS designed the study; SL, HPU, MH collected the samples; SL, SM, BRS took the stable isotope samples; SL, BK did the ^{14}C measurments; SL wrote the paper with contributions from SM and BRSr
Citation: Lindauer, S., Marali, S., Schöne, B.R., Uerpmann, H.-P., Kromer, B., Hinderer, M., 2016. Investigating the Local Reservoir Age and Stable Isotopes of Shells from Southeast Arabia*. Radiocarbon* **59***,* 355-372*.*

4.1.1 Abstract

We recently started a systematic approach to determine the reservoir age in southeast Arabia and its dependence on mollusc species and their environment. This part of the study concentrates on local reservoir age and stable isotopes of the lagoonal species *Terebralia palustris* and *Anadara uropigimelana* at Khor Kalba, Oman Sea. Environmental and nutritive influences on molluscs are reflected in the radiocarbon and stable isotope signal. We found a local reservoir age of *A. uropigimelana* of about 940 years and that of *T. palustris* as 800 years. Sclerochronological analyses yielded information about seasonality of growth and death in *A. uropigimelana*. The modern shell of *Periglypta reticulata* shares food resources and habitat with *A. uropigimelana*, of which we did not find a modern specimen. It provided information on response to changes in temperature in the lagoonal system needed for suitability as reflecting climatic conditions. We were interested in carbon pathways of the mangrove in Kalba and a mangrove planted anew on a former mangrove sediment in Ajman. Being an obvious source of charcoal and food of *T. palustris* makes this information necessary. Further analyses will be performed to interpret changes in reservoir age in complex lagoonal systems as reaction to environmental variability

Keywords: ^{14}C, reservoir effect, mangroves, T. palustris, A. uropigimelana, P. reticulata, stable isotopes, sclerochronology, United Arab Emirates, Oman Sea.

4.1.2 Introduction

The coastal areas of southeast Arabia (see map, Fig. 4.1.1) have been inhabited by humans for thousands of years and represent a possible way “out of Africa” for *Homo sapiens* (Armitage et al. 2011). Due to the arid climate prevailing there since the middle Holocene, establishing accurate chronologies based on radiocarbon dating can be very challenging. Charcoal can sometimes be found as distinct

fragments, but often as part of an ashy sediment layer. Organic material like bone collagen, wood, or seed are often badly preserved if available at all. Inorganic material like bone apatite can easily exchange carbon with its surrounding. Recently, Antoine Zazzo and colleagues (Zazzo et al. 2013, Zazzo 2014) published promising results by using bone apatite. Unfortunately, at our sites no bone material was found in the same context.

The most widespread marine material found at excavations along the coasts are shells, often accumulated to shell middens of up to several meters height. The shells commonly show an older age as indicated by archaeology or ^{14}C dating from contemporaneous terrestrial organic materials, which is known as the reservoir age, or R(t) (Dutta 2008). In the course of establishing a calibration curve for the ocean environment, several reservoir ages have been determined using specimens from museum collections, collected alive (i.e. during the pre-bomb era). For the Indian Ocean, to which our study area belongs, local reservoir ages for several areas in the Arabian Sea were determined, ranging from 486 years in Dohar, Qatar, to 501 years in Muscat, Oman (Southon et al. 2002) in comparison to values of 441 years in the Arabian Gulf and 583 years along the Gulf of Oman (Dutta 2008). In Ra´s al-Hamra, Oman, Zazzo and colleagues determined a reservoir age of 568 ± 56 ^{14}C yr for the 5th millennium BC (Zazzo et al. 2012) and 645 ± 40 years for the 4th millennium BC (Zazzo et al. 2016) .

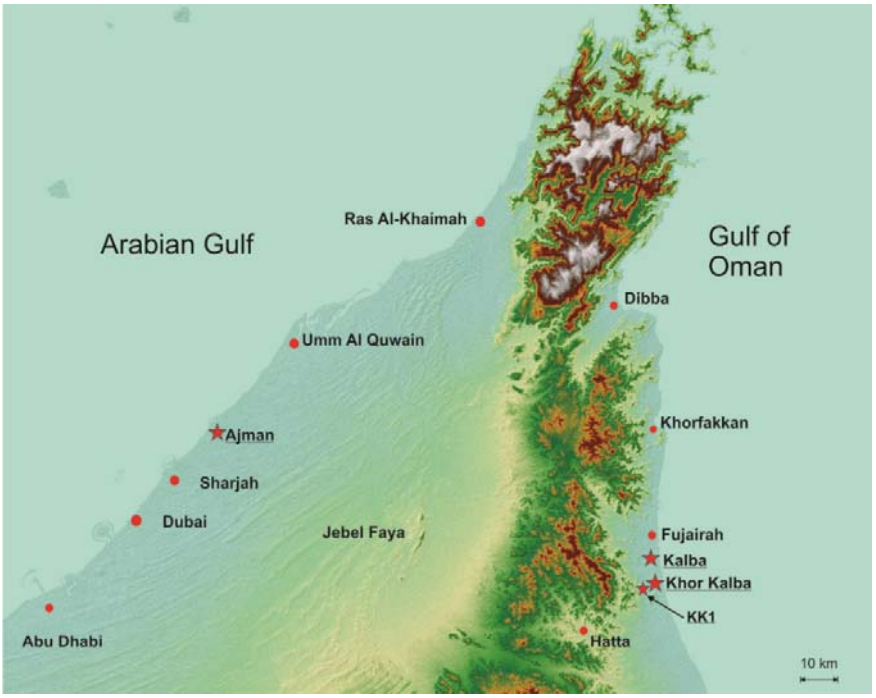

Fig. 4.1.1 Map of South-East Arabia (United Arab Emirates). Sites mentioned in this publication are marked with a star and the text underlined.

The reservoir age can be variable over time and differ among species and localities (Culleton et al. 2006). In Culleton´s study, stable isotopes were used to trace influences of upwelling water as, for example, more intense upwelling is accompanied by higher $\delta^{18}O$ values. These changes in stable isotopes reflect changes in environmental conditions like marine or terrestrial input. These changes are also mirrored in changes in the local reservoir ages. For the Arabian Peninsula, a systematic approach to understand the differences in reservoir ages has so far not been established for different species over different periods of time. Nevertheless, interesting and important work has been done on shells

and mangroves with respect to archaeology and paleoclimate in Oman (Berger et al. 2005, Berger et al. 2013). In this article, we approach our research on the Gulf of Oman as a combination of stable isotope analyses, $\delta^{13}C$ and $\delta^{18}O$, to look for seasonal behavior in the shells as well as seawater or terrestrial input that will also influence the reservoir effect directly.

The article will take a closer look at two of the most abundant species in archaeological sites, the bivalve mollusc *Anadara uropigimelana* and the gastropod *Terebralia palustris*. Due to the differences of the molluscan lifestyle, we would expect minor differences in the reservoir age between *A. uropigimelana* and *T. palustris* from the same site. For example, *T. palustris* feeds on leaves, whereas *A. uropigimelana* feeds on plankton; hence, we would expect the *Terebralia sp*. to show a lower reservoir age than *Anadara sp.* due to the enhanced terrestrial signal in the food resource. However, owing to the upwelling of deep water in the Arabian Sea (Gulf of Oman), we expect a shift in reservoir age at the eastern coast of the Arabian Peninsula towards older ages. The two mollusc species live in or near mangroves, places that were preferred environments for humans from where they gained most of their marine food. At first, we will concentrate on the Gulf of Oman, especially the region of Kalba, to study whether the shells usually found by archaeologists can also be used to for dating by tracing the reservoir age of (1) species and (2) seawater signature over time. Modern tree and sediment samples from Kalba and Ajman (Arabian Gulf) help to understand these complex systems and allow to trace back these patterns into the archaeological and paleoenvironmental context.

Localities

Kalba

Kalba is located in the Emirate Sharjah at the northern coast of the Gulf of Oman where the Hajar Mountains approach the coast (see Fig. 4.1.1). Along the coast, mangroves are accompanied by *sabkhas* (coastal salt flats, former mangrove sediment) followed by gravel plains as well as wadi beds further inland (Phillips and Mosseri-Marlio 2002). Khor Kalba is the name of the region with few distinct settlement structures close to the sabkha and mangrove. The city Kalba itself lies north of the mangrove area (cf. Fig. 4.1.1). Today, the large sabkha points to a more inland position – or an even wider extend - of the mangrove in earlier times (Phillips and Mosseri-Marlio 2002).

The oldest known shell midden of Kalba is situated along a hillslope of the Hajar Mountains at the western edge of the sabkha. During the excavations of Carl Phillips, this shell midden was referred to as KK1 (Khor Kalba site 1, Fig. 4.1.1 and Fig. 4.1.7), which is the name we will use herein for consistency. The first hint towards a Neolithic age was derived from the bifacial stone tools found in the midden. These are indicative for the 5th millennium BC (Phillips and Mosseri-Marlio 2002). No archaeological settlement in the form of building remains has been found for this cultural period. One possible interpretation is that the midden represents a specialized area where molluscs were extracted, maybe also consumed, or packed for transport. The shell deposits of KK1 themselves are densely packed, covering a depth of roughly 50 cm. The majority of shells belong to the gastropod *T. palustris* and the oyster *Saccostraea cucullata* along with several specimens of the bivalve *Anadara* sp.

The mangrove forest at Khor Kalba, with *Avicenna marina* as dominant tree species, is today a protected natural area (Fig. 4.1.2d).

Ajman

Ajman lies north of Dubai and Sharjah at the coast of the Arabian Gulf. Today, a small mangrove and a lagoon are present. The environment around Ajman is arid with sand dunes in the outermost part of the Rub al-Khali. In contrast to Kalba, the mountains are more than 50 km away (cf. Fig. 4.1.1). This has a direct influence on the freshwater input, with the input being lower in this area. The mangrove forest in Ajman was planted artificially around 10 yr ago most probably on a former mangrove sediment from ancient times. We chose to sample this mangrove only to gain insight into possible shifts in ^{14}C age due to carbon pathways in the mangrove tree itself, here *Avicenna marina*, owing to the old sediment. Near Ajman, no settlement structure from the Neolithic with shell layers was accessible at the time of sampling.

Shells

The gastropod, *Terebralia palustris* (cf. Fig. 4.1.2a) inhabits muddy sites of mangroves. Hence, it is also called a mud whelk or mud creeper. Its lifespan is currently unknown. The juvenile *T. palustris* spends its youth on the seaward front of the forests and moves deeper into the mangrove approximately at the age of four. It will thus have slightly different ^{14}C signals (more depleted) as a young snail compared to adult snails. Therefore, no juvenile specimens are typically found in shell middens near mangroves (Pape et al. 2008). In addition, *T. palustris* changes its feeding habits during ontogeny. As a juvenile, it eats mud and fallen leaf debris, whereas the adult snail grazes on fallen leaves.

The bivalve *Anadara uropigimelana* (Fig. 4.1.2b) lives in intertidal mudflats of lagoons and estuaries and reaches a lifespan of up to 45 yr (Petchey and Clark 2011). It can withstand large salinity fluctuations and lives at temperatures ranging between 15 and 32 °C. The shell material is aragonite. *A. uropigimelana* is a surface deposit feeder and occurs throughout the Indian Ocean region (Tebano and Paulay 2000, Azzoug et al. 2012, Petchey et al. 2013). It buries itself in the sand up to a depth of 20 cm.

Fig. 4.1.2 Shell specimens from Khor Kalba referred to in this publication: (a) Terebralia palustris, (b) Anadara uropigimelana, (c) Periglypta reticulata. (d) Khor Kalba mangrove.

The bivalve *Perigplypta reticulata* (see Fig. 4.1.2c) can often be found in tropical environments such as the Indo-Pacific. It burrows in sand and mud of intertidal zones, but can also be found in sublittoral zones. It is a suspension feeder that subsists on planktonic algae and organic matter (Bieler et al. 2004). So far, no sclerochronological analyses have been performed on *P. reticulata,* but it has a lifestyle and feeding habits similar to that of *Anadara sp*. We used *P. reticulata* to monitor the influence of the environment on shell growth because we did not find a life specimen of *A. uropigimelana*. It also allowed us to derive the sea surface temperature range for the mangrove at Khor Kalba.

Sclerochronology

Bivalves and gastropods grow by periodically accreting carbonate at all shell margins. This results in distinct shell growth patterns consisting of growth lines and growth increments. Growth lines are formed during periods of slow growth, whereas growth increments represent periods of fast growth. Growth patterns can be used as an internal calendar to temporally align the growth record.

In intertidal settings, molluscs form growth patterns that closely reflect the tidal regime (Evans, 1972; House and Farrow, 1968; Ohno, 1986; Schöne, 2008). Growth lines are formed during low tide and growth increments during high tide. In semidiurnal tide regimes, a couplet of two (circatidal) increments and lines is thus developed, whereas in diurnal tidal regimes only one pair of a (circlunidian) increment and line is formed. During spring tides, the growth lines are more sharply delimited and more distinctly developed than during neap tides. This results in a distinct fortnightly (ca.14-daily) growth pattern with bundles of ca.13.5 (perigee fortnight cycle: new to full moon) and 15.5 (apogee fortnight cycle: full moon to new moon) circalunidian increments and lines, and 27 to 31 circatidal increments and lines (Hallmann et al., 2009). Note that the circatidal lines are typical much more pronounced than the semidiurnal growth patterns. Aside from tide-controlled growth patterns, there is also an annual slowdown of shell growth resulting in the formation of annual growth lines. Azzoug et al. (2012) (Azzoug et al. 2012) hypothesize that their formation in *Anadara* sp. is controlled by harsh seasonal environmental conditions or the reproduction cycle.

Although some information is available on the food resources of the studied mollusc species and their interaction with the environment (Patel et al. 1978, Debenay et al. 1994, Azzoug et al. 2012), little is known about their growth histories. Azzoug et al. (2012) studied growth patterns and stable isotopes of *Anadara* sp. from Senegal to quantitatively estimate the duration of rainy and dry seasons and examine the possibility of using large fossil shell accumulations for studies of the long-term variability of the West African Monsoon seasonality. This formed the basis of our analysis of the same genus from the United Arab Emirates. For example, an increase in upwelling of seawater is accompanied by an increase in $\delta^{18}O$ because colder deep water mixes with surface water. Estuarine inlets are more influenced by terrestrial runoff where streams are depleted in $\delta^{13}C$ by 5-10 ‰ compared to mean ocean water. Freshwater inputs lower both $\delta^{13}C$ and $\delta^{18}O$ (Culleton et al. 2006). These effects should also be mirrored as small changes in the local reservoir effect and provide information on the sources of these changes.

4.1.3 Material and Methods

Sampling strategy

As the mangrove in Kalba (Fig. 4.1.2d) existed for several thousand years and survived many generations of trees, it is an ideal sampling site for our study. To determine the reservoir age of *A. uropigimelana* and *T. palustris,* we sampled a shell midden (KK1) at Khor Kalba, Gulf of Oman (Fig. 4.1.1 and Table 4.1.1). We used a trench from an earlier excavation with a distinct ash layer close to the bottom (see Fig. 4.1.7). As it was not clear at the beginning whether all the shells would give the same age or whether age differences existed following the stratigraphic order, we sampled several shell layers (Table 4.1.1). We expected to find two distinct age ranges around 4000 BC for the shell midden KK1 based on the excavation of Phillips and Mosseri-Marlio (2002). Unfortunately, the ash layer contained only tinsels of charcoal in a sandy matrix instead of distinct charcoal fragments. Being close to the mangrove, it seemed obvious that one source of wood might be the mangrove itself. The dominant mangrove tree in Kalba today is *Avicenna marina*. When we derive a reservoir effect for the shells from paired terrestrial-marine samples, we must be sure to understand the terrestrial samples as well. With the hypothesis that the main source of the carbon in the ash is burnt mangrove tree, we sampled modern leaves and branches together with the first few cm of sediment in the Mangrove at Kalba (protected area, see Fig. 4.1.2 d and Table 4.1.2). Even without measuring the sediment with respect to its compounds it allows an interpretation of the data of the trees. Understanding this system is crucial not only to characterize the signal of the ash in case it was mainly wood from *Avicenna sp*., but also because the leaves provide a food resource for the molluscs. If the tree incorporates old carbon from the sediment in significant amounts, its terrestrial signal is in fact a mixed signal and could not be used for determining a reservoir effect.

Table 4.1.1 Samples taken at Khor Kalba shell midden KK1.

Labcode	Sample name	Site	Material	Remarks
MAMS 22875	KSM BL Ash	Kalba KK1	Ashy sediment	Ash layer
MAMS 22876	KSM BL Terebralia	Kalba KK1	Shell marine	In ash layer
MAMS 22877	KSM UBL Terebralia	Kalba KK1	Shell marine	Below ash
MAMS 22878	KSM UBL Anadara	Kalba KK1	Shell marine	Below ash
MAMS 22879	KSM OBL Terebralia	Kalba KK1	Shell marine	Above ash
MAMS 22880	KSM OBL Anadara 1	Kalba KK1	Shell marine	Above ash
MAMS 22867	KSM OBL Anadara 2	Kalba KK1	Shell marine	Above ash
MAMS 22884	KSM 10-15 Terebralia	Kalba KK1	Shell marine	10-15cm from surface
MAMS 22885	KSM 10-15 Anadara	Kalba KK1	Shell marine	10-15cm from surface
MAMS 22882	KSM GOF Terebralia	Kalba KK1	Shell marine	Just below surface
MAMS 22883	KSM GOF Anadara	Kalba KK1	Shell marine	Just below surface

We also sampled the mangrove at Ajman, Arabian Gulf (Fig. 4.1.1, Table 4.1.2). However, as the mangrove at Ajman was planted 10 years ago on the sediment of a former mangrove sabkha, we used it to trace carbon pathways in the mangrove tree that might influence molluscan specimen using mangrove leaves as food resource.

Shells have been successfully used as tracers of environmental and climate changes (Rollins et al. 1990, Schöne et al. 2005, Wanamaker Jr et al. 2011, Azzoug et al. 2012, Marali and Schöne 2015). Therefore we took a closer look at *A. uropigimelana* shells and the single specimen of *P. reticulata* in order to analyze their potential use as environmental recorders for the lagoonal setting. *P. reticulata* was chosen as no modern *A. uropigimelana*. could be found. In this study, *T. palustris* was not used for the sclerochronological analysis part, but will be studied in the near future. The reservoir effect is a mirror for environmental influences and these are recorded in the shell. Knowledge about how fast a mollusc reacts to its environment and at what time it builds the shell (throughout the year at the same rate or rather seasonal), and hence records the changes, is important to know if we want to use it later as a paleoclimate indicator (not in this paper).

Table 4.1.2 Samples taken at the mangroves of Ajman (Arabian Gulf) and Khor Kalba (Gulf of Oman).

Labcode	Sample name	Site	Material
MAMS 21281	AM1 leaf	Ajman mangrove	Leaf
MAMS 21282	AM2 branch	Ajman mangrove	Wood
MAMS 21283	AM3 sediment	Ajman mangrove	Sediment
MAMS 21270	KNR1 leaf	Kalba mangrove	Leaf
MAMS 21271	KNR2 branch	Kalba mangrove	Wood
MAMS 21274	KNR3 sediment	Kalba mangrove	Sediment
MAMS 22868	KS M1 Periglypta	Kalba mangrove entrance	Shell marine

Sclerochronology of *Anadara sp.* and *Periglypta sp.*

To prepare the bivalve specimens for sclerochronological analyses, i.e., growth pattern and stable isotope analyses ($\delta^{13}C$ and $\delta^{18}O$), the shells are mounted to a Plexiglas block with a quick-drying plastic welder. Two ca. 3 mm-thick sections were cut from within each shell along the axis of maximum growth perpendicular to the annual growth line using a Buehler Isomet 1000 low-speed precision saw equipped with a 0.4 mm-thick diamond wafering blade. Then, the sections were mounted on glass slides, ground with SiC (800 and 1200 grit), and polished with Al_2O_3 powder (1 µm). Between each step, the sections were ultrasonically rinsed (Schöne et al. 2011). One of the two (air-dried) sections was used to study annual growth patterns. For this purpose, the polished section was immersed in Mutvei´s solution for 20 min at 37 – 40 °C (Schöne et al. 2005), then rinsed with demineralized water and air-dried. Mutvei´s solution facilitates the recognition of shell growth patterns as it stains growth lines dark blue and produces a three dimensional relief of etch-resistant growth lines and deeply etched growth increments. The growth patterns were then viewed under a reflected-light stereomicroscope (Leica Wild M2C) and digitized with a Nikon Coolpix 995 camera. Increment widths were measured using the software Panopea (©Schöne and Peinl).

To determine the possible relationship between shell growth rate and increment width of the *A. uropigimelana* and *P. reticulata,* inherent age-related growth trends were first mathematically eliminated. This was accomplished by fitting an polynome function to the growth curve and computing dimensionless growth indices (Schöne and Surge 2012) by calculating the ratio of the measured versus predicted

growth value at each year. Subsequently, these values were standardized in order to directly compare relative growth increment time-series of different individuals with each other or with environmental variables.

The other polished shell section (second slice of the valve) of the *A. uropigimelana* specimen was first inspected via Raman spectrometry to determine the $CaCO_3$ polymorph. Raman measurements were done at the Institute of Geosciences at the University of Mainz (Horiba Jobin Yvon LabRam 800 spectrometer equipped with Olympus BX41 optical microscope); for further details see (Milano et al. 2015). Then, powder samples for stable isotope analysis were drilled or milled from the shell of both species following the growth pattern by using a cylindrical diamond drill bit (1 mm diameter, Komet/Gebr. Brasseler GmbH and Co. KG model no. 835104010) mounted to a Rexim Minimo drill system. Samples (50 to 120 µg) were analyzed with a Finnigan MAT 253 continuous-flow isotope ratio mass spectrometer equipped with a Gas Bench II. Isotope values were reported relative to V-PDB and calibrated against a Carrara marble standard ($\delta^{18}O$ = -1.91 ‰; $\delta^{13}C$ = 2.01 ‰). The precision error based on repeated measurements of the standards is better than ± 0.07 ‰ for $\delta^{18}O$ and better than ± 0.05 ‰ for $\delta^{13}C$. For more details of the measurement procedure, see (Füllenbach et al. 2015).

First, we sampled the shells by drilling holes in the outer shell layer at nearly equidistant intervals. To obtain a higher resolved isotope time-series, a 4 mm portion of the *A. uropigimelana* shell was micro-milled in steps of ca. 100 µm parallel to the growth lines (Fig. 4.1.4). These samples were used to determine $\delta^{18}O$ and $\delta^{13}C$ values. Shell growth patterns were used to temporally contextualize the isotope data, i.e. to assign seasonal dates to the sampled shell portions. Because of the lack of modern *Anadara sp.* during our sampling campaign, we chose to use another bivalve, *P. reticulata*, to trace changes in environment, here water temperature reflected in the $\delta^{18}O$ signal, in this estuarine habitat as well as response time of the shell species. Being similar to *Anadara sp*. in food resource and habitat, this allows to draw some conclusions for both species.

Preparation of radiocarbon samples and the reservoir effect

Samples for radiocarbon dating were prepared at the Klaus-Tschira-Archaeometry Centre, Mannheim. To determine the ^{14}C data close to the time when the molluscs died, if possible the most recently formed shell material was used, i.e. the ventral margin in the case of the bivalves and the aperture or last visible whorl in the case of the gastropods. From the ventral margin, small chips were taken and surface contamination, such as sedimentary calcium carbonate removed by etching the fragments in 1 % HCl in an ultrasonic bath for 1 min. All information on the concentration of the chemicals used here refers to vol % if not mentioned otherwise. The ultrasonic bath provides a soft mechanical treatment during the etching process. Next, the fragments were rinsed in distilled water and dried.

We determined the local reservoir age for the Khor Kalba mollusc samples (*A. uropigimelana* and *T. palustris*) from the shell midden as paired samples in connection with the ash layer (containing about 5% C) in which they were embedded, which we interpret as being contemporaneous. Although ash contains a lot of siliceous material, it shows tinsels of charcoal, which we extracted by floating; hence, we are sure to be able to use it like charcoal. The ashy sediment sample, containing a large amount of carbonate, was etched with 4 % HCl (hydrochloric acid) for several hours in order to completely remove

remnants of sedimentary $CaCO_3$. When the reaction stopped, the acid was changed until no carbonate reaction was recognized. This step was undertaken at room temperature. Subsequently, the sample was treated with 0.4 % NaOH (sodium hydroxide) to remove humic acids. Finally, the sample was treated again with 4% HCl at 60 °C. The mangrove samples (leaves and branches to check for possible reservoirs effects in the tree) from Khor Kalba and Ajman, were treated with acid base acid (ABA) - 4 % HCl, 0.4 % NaOH and again 4 % HCl at 60 °C - to remove carbonates and surface contamination. The sediment samples from the mangrove soil experienced a treatment comparable to the ash sample with two steps of 4 % HCl and a step using 0.4 % NaOH in between to remove any carbonates and humic acids, respectively. Between each step and after the entire pretreatment, samples were rinsed with distilled water and finally dried at 60 °C. The terrestrial samples (ash, leaves, branches, sediments) were combusted using an elemental analyzer (Micro Cube, Elementar) as described in (Lindauer and Kromer 2013). The shell samples were converted to CO_2 using phosphoric acid in an Autosampler system at 70 °C as described in (Wacker et al. 2013) and graphitized with the AGE III system, both produced by Ionplus (Switzerland). All graphite samples were measured at the DatingMicadas in Mannheim and corrected for isotopic fractionation as described previously (Kromer et al. 2013, Lindauer and Kromer 2013).

The reservoir effect was calculated as the difference between the two archives using the software package ResAge by Guillaume Soulet (Soulet 2015) which can be downloaded as supplement to his publication.

4.1.4 Results and Discussion

Sclerochronology and stable isotopes

A. uropigimelana from shell midden KK1

The growth patterns of the *A. uropigimelana* specimen from the shell midden KK1 were difficult to determine. Immersion in Mutvei's solution only resulted in a pale blue-colored surface, so that the growth increments and lines were hard to recognize. Eventually, diagenetic overprint resulted in a loss of some organic matrices, which the dye contained in Mutvei's solution, Alcian Blue, would typically stain. However, diagenetic alteration was not more severe. As demonstrated by Raman spectrometry, the examined old shell still consists of aragonite and has not been converted into calcite (Fig. 4.1.3).

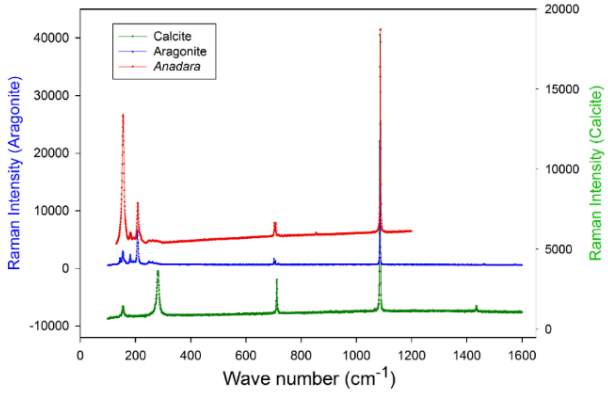

Fig. 4.1.3 Raman spectroscopy of one *A. uropigimelana specimen (top line) and the carbonate reference materials (pure calcite is the bottom line; pure aragonite is shown in between the sample and the calcite data).*

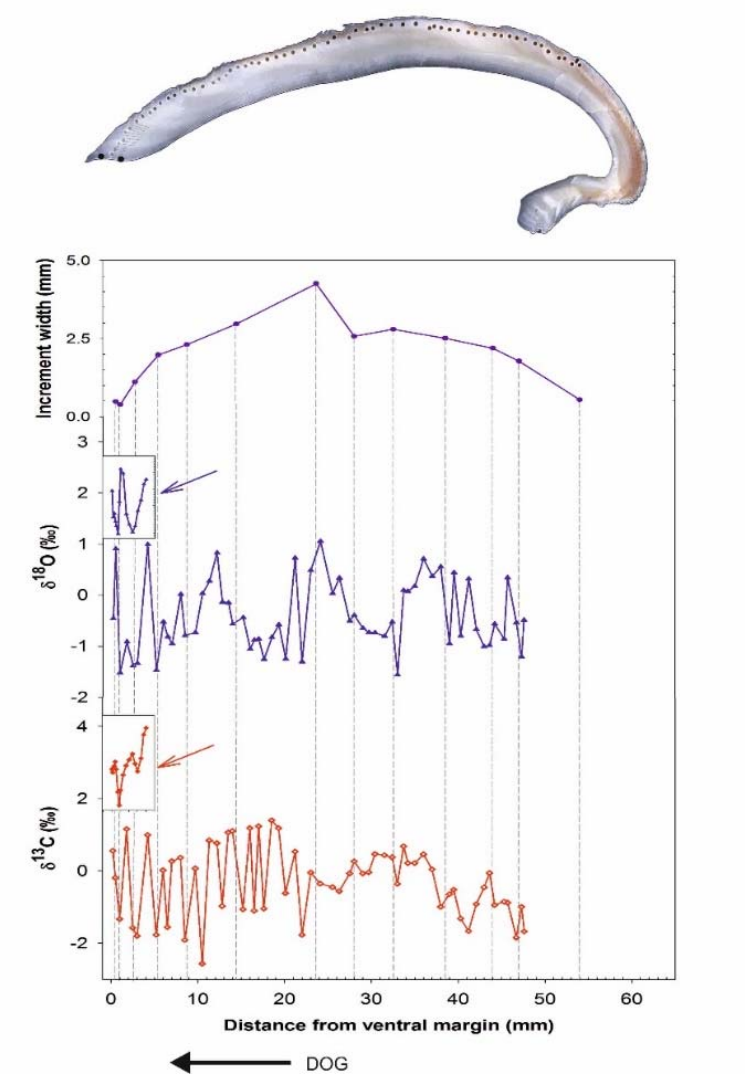

Fig. 4.1.4 Polished section of *Anadara uropigimelana* (MAMS 22867) from Khor Kalba shell midden KK1 on top. The holes originate from drilling the samples. Displayed below are the results of the growth increment width (top); $\delta^{18}O$ and $\delta^{13}C$ values from powder samples obtained via drilling are represented as triangles (middle) and diamonds (bottom), respectively. Insets display stable isotope data from milled powder samples. DOG denotes direction of growth.

Due to the difficulties with the Mutvei's solution, we chose to count only the most distinct growth lines (Fig. 4.1.4). The width of the annual increments decrease through ontogeny, representing the well-known age-trend (von Bertalanffy 1938, Jones et al. 1989, Azzoug et al. 2012, Marali and Schöne 2015). The seasonal temporal alignment of the shell record, and thus the rate of seasonal shell formation, was accomplished by comparing the $\delta^{18}O$ curve with the growth patterns. As can be seen in Fig. 4.1.4, the $\delta^{18}O$ curve (blue line) shows a clear sinusoidal shape, which can be interpreted as a seasonal temperature signal. It also shows that the growth increments not only represent annual lines, but are superimposed by distinct growth marks probably caused by changes in food resource or escape from predators (stress mark). Since shell oxygen isotope data and temperature are negatively correlated (Grossman & Ku 1986; a change in $\delta^{18}O$ by 1 ‰ corresponds to a change in water temperature of ca. 4.3 °C), more positive $\delta^{18}O$ values indicate colder water temperature and more negative $\delta^{18}O$ values warmer water. In the studied specimen, $\delta^{18}O$ values slowly increased after the annual growth line, followed by a more rapid decrease toward the following annual growth line. These findings suggest that the shell grew more rapidly during the winter season than during summer, and the annual growth line formed during the warmest season. The studied specimen died during winter.

Interpreting the $\delta^{13}C$ signal is very challenging. Besides a strong physiological control, the stable carbon isotopes reflect changes in food availability, the water dissolved inorganic carbon (DIC) signature, and freshwater input (Khim et al. 2003, Culleton et al. 2006). Generally speaking, it can be said that strong freshwater input results in a depletion of $\delta^{13}C$ due to soil processes and plant material. The signal of $\delta^{18}O$ also decreases in a similar way because of fractionation during precipitation and reduced salinity of the freshwater. For the same reasons, the apparent ^{14}C age and the local reservoir effect could increase.

The $\delta^{13}C$ signal rises slowly and oscillates around a constant value with some distinct features. Towards the ventral margin, drilling obviously cannot resolve the patterns properly in contrast to milling the sample section. The pattern of $\delta^{13}C$ resembles that of the $\delta^{18}O$ curve with respect to positions of minimal and maximal values at several points. From the wider shape of the features in both curves, it can be inferred that the *Anadara uropigimelana* specimen grew up in a more homogeneous environment and later moved closer to the mangrove with multiple changes in food resource, freshwater, and water temperature.

Periglypta reticulata and Modern Lagoonal Signal

To investigate the extend to which shells from a lagoon also reflect seasonal patterns in $\delta^{18}O$ and $\delta^{13}C$, a modern sample of *P. reticulata* from Kalba, which shows similar lifestyle and feeding behavior as *A. uropigimelana,* was analyzed. As demonstrated in Fig. 4.1.5, distinct seasonal and subseasonal growth lines and increments are developed in *P. reticulata* shells. Subseasonal growth patterns seem to be controlled by the tides because they show a recurrent pattern of ca. 13 to 15 lines and increments, possibly reflecting circlunidian growth patterns. Altogether, more than 580 microgrowth lines were counted in a shell portion that likely formed during 2 yr. This further supports the interpretation of lunar daily growth patterns.

Judging from the $\delta^{18}O$ curve, the studied shell portion was formed during a time interval of ca.2 to 3 yr (compare Fig. 4.1.6). The shell was collected in December 2013 with closed valves but without mollusc inside. When interpreting the last point of the graph in Fig. 4.1.6 as being very close to the time of death, it becomes evident that the shell died in winter. The ^{14}C measurement allows us to interpret that it died shortly before it was collected, although with a second possible result around 1956. The $\delta^{18}O$ values at the ventral margin show very high positive values, which suggest cold temperatures. Like *A. uropigimelana*, *P. reticulata* seems to grow at maximum rate during the colder months of the year (winter and spring), whereas shell formation rate is reduced during summer (minimum $\delta^{18}O$ values). Therefore the species *P. reticulata* seems to react immediately on changes in water temperature reflected in the $\delta^{18}O$ signal.

P. reticulata with a change in $\delta^{18}O$ of up to 2.5 - 3 ‰ allows us to interpret traceable environmental changes in the lagoon throughout the year reflected in water temperature changes of 12-16 °C. As mentioned earlier and quoted from Grossman & Ku (1986), a change in $\delta^{18}O$ by 1 ‰ corresponds to a change in water temperature of 4.3 °C. The $\delta^{13}C$ pattern is following a certain trend towards more negative values. There seems to be a parallel trend with $\delta^{18}O$ between samples 8 and 12 during the maximum growth period between winter and spring that points to a depletion of both signals, probably

influenced by freshwater. The parallel rise of both stable isotope signals towards positive values around sample 17 might originate from some change in the signal of the food resource as it coincides with two distinct growth marks. Thus also the $\delta^{13}C$ influences are recorded rather quickly in the shell. We see here that this estuarine habitat shows clear seasonal changes and the bivalves (*Anadara sp*. as well as *Periglypta sp.),* although they bury in the sediment, record these changes in their shell.

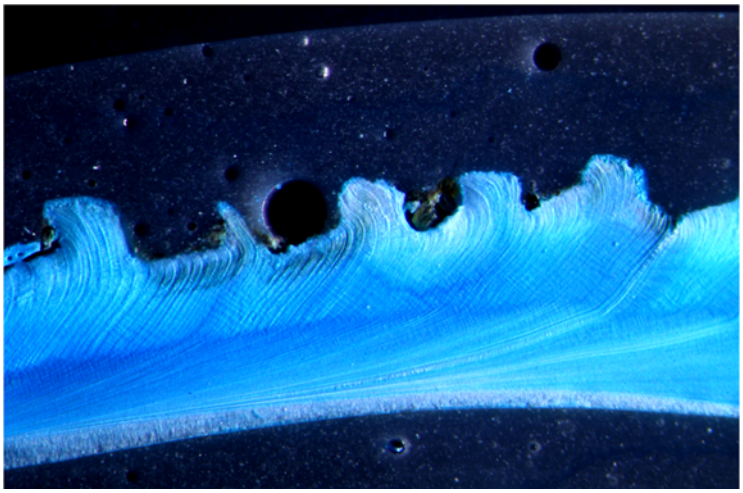

Fig. 4.1.5 Periglypta reticulata, Khor Kalba (MAMS 22868), excerpt of section etched with Mutvei´s solution for growth increment analysis.

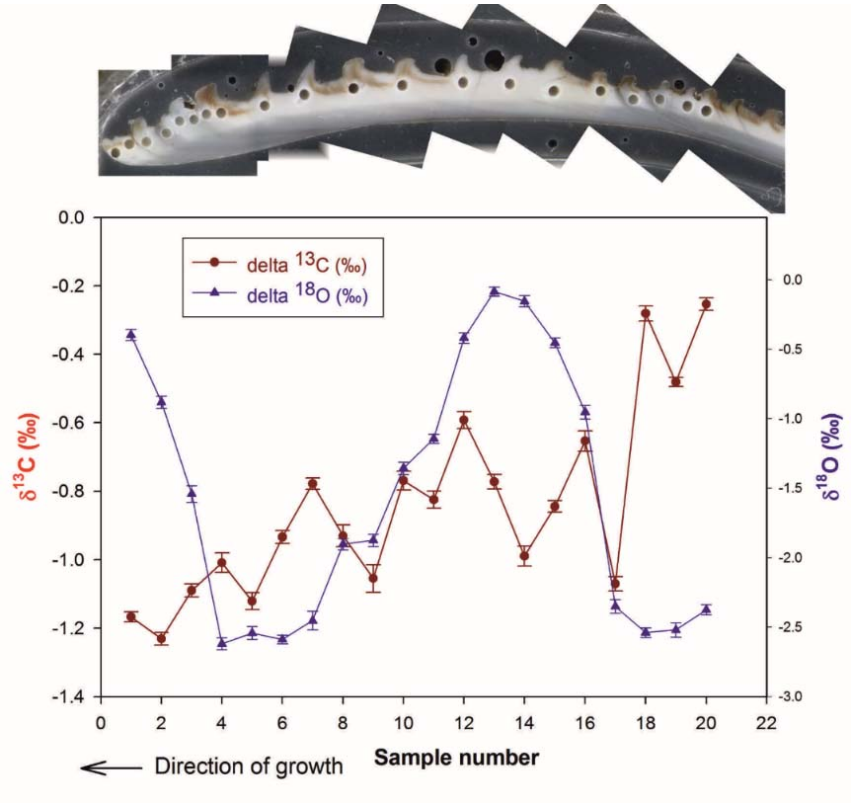

Fig. 4.1.6 $\delta^{18}O$ (triangels, sinusoidal line) and $\delta^{13}C$ (dots) measurements of *Periglypta reticulata* shell from Khor Kalba. On top the polished section with the drilled sample locations can be seen. "DOG" denotes *direction of growth*.

Radiocarbon dating and Reservoir age

For the shell midden KK1 at Kalba, we found two age groups corresponding to around 6900 BP and 6300 BP (Table 4.1.3 and Fig. 4.1.7), which point to two distinct layers of the shell midden as proposed by (Phillips and Mosseri-Marlio 2002). In order to calculate a preliminary local reservoir age for this period at Kalba, we used the samples of lowermost layer containing the ashy sediment (

Table 4.1.4). We call it preliminary as the shell midden needs further sampling of shells to establish the statistical significance.

Table 4.1.3 Results of radiocarbon measurements on the samples from the shell midden KK1, Khor Kalba. Refer to Table 4.1.1 for sample description.

Labcode	Sample Name	^{14}C (BP)	F^{14}C
MAMS 22875	KSM BL Ash	6117 ± 26	0.4670 ± 0.0015
MAMS 22876	KSM BL Ter	6911 ± 28	0.4230 ± 0.0015
MAMS 22877	KSM UBL Ter	6924 ± 27	0.4224 ± 0.0014
MAMS 22878	KSM UBL Ana	7058 ± 27	0.4153 ± 0.0014
MAMS 22879	KSM OBL Ter	6545 ± 26	0.4427 ± 0.0014
MAMS 22880	KSM OBL Ana	6273 ± 27	0.4580 ± 0.0015
MAMS 22882	KSM MuGOF Ter	6257 ± 26	0.4589 ± 0.0015
MAMS 22883	KSM MuGOF Ana	6310 ± 26	0.4559 ± 0.0015
MAMS 22884	KSM 10-15 uGOF Ter	6262 ± 26	0.4586 ± 0.0015
MAMS 22885	KSM 10-15 uGOF Ana	6272 ± 27	0.4580 ± 0.0015
MAMS 22867	KSM A2OBL Ana	6295 ± 26	0.4567 ± 0.0015

The thorough pretreatment of the ash samples resulted in a reliable age of 6117 ± 26 years BP. The program ResAge was applied to the ^{14}C data of the ash and shells collected from the same layer (see Table 4.1.1). For the two *T. palustris* specimen, we received reservoir ages of 794 and 807 yr and calculated a simple mean value of 800.5 yr for the Neolithic period at Kalba for this species, being aware of the lack of statistical significance. There seems to be a difference from the local reservoir effect of *A. uropigimelana*, which was even higher than the one for *T. palustris*, namely 941 ± 37 yr older than the contemporaneous ash. One could argue that the shell might be older because of a really older age than the charcoal in the ash, but then also the *T. palustris* of the same layer should be much older. In the lowermost layer, hardly any *Anadara sp*. were found, which we interpret as being the time when it started to settle at Khor Kalba and only few specimens were caught by fishermen. This reservoir age, too, is preliminary and needs further sampling. Although we did not use a statistically significant amount of shells per species, we can say that the local reservoir age for Kalba at this period is higher than the reservoir effects we find in the literature cited in the Introduction, and indeed differs between the species under investigation. Looking at the values in Southon et al. (2002), we see that for some species the authors find few values from the 19th century that are not too different with 786 ± 51 ^{14}C years BP (*Marcia flammea* from Muscat). The ash sample was also measured with an IRMS in Mainz to determine its δ^{13}C value. With a δ^{13}C of -25,76 ‰, we can say that the ash sample extracted consisted of charcoal from wood (mangroves lie in the range of -24-28 for leaves, see (Rodelli et al. 1984)).

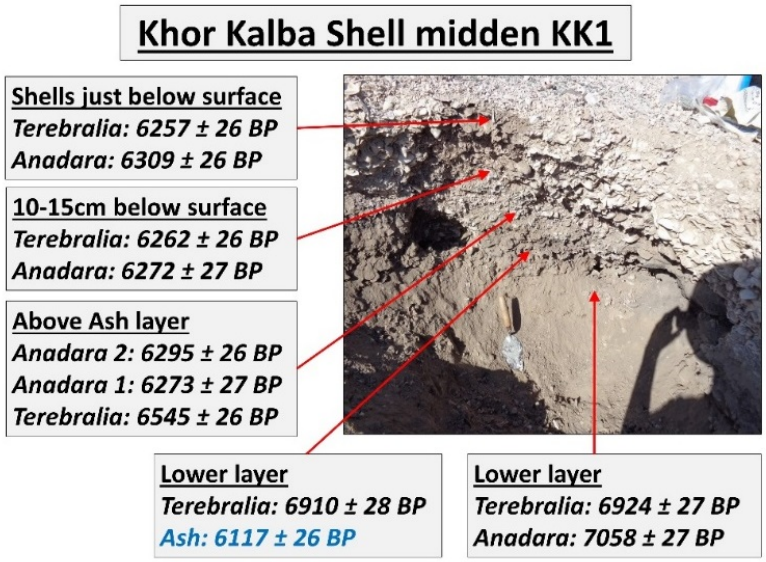

Fig. 4.1.7 Khor Kalba shell midden KK1 and uncalibrated data from radiocarbon measurements of different depth in the stratigraphy. The age of the terrestrial sample ("ash") is written in blue .

Table 4.1.4 Radiocarbon local reservoir effect of *T. palustris* (including mean value) and *A. uropigimelana* from Khor Kalba. The corresponding stratigraphy of the shell data can be seen in Fig. 4.1.7 Khor Kalba shell midden KK1 and uncalibrated data from radiocarbon measurements of different depth in the stratigraphy. The age of the terrestrial sample ("ash") is written in blue . The $\delta^{13}C$ for the ash samplecwas measured with an IRMS.

Labcode	Sample	$F^{14}C$	R(t)	R(t), mean	Remarks
MAMS 22875	KSM BL Ash	0.4670 ± 0.0015			$\delta^{13}C$=-25,76 ‰
MAMS 22876	KSM BL Ter	0.4230 ± 0.0015	794 ± 38	800.5 ± 53	Mean R(t) only on *T. palustris*, 1 σ
MAMS 22877	KSM UBL Ter	0.4224 ± 0.0014	807 ± 37		
MAMS 22878	KSM UBL Ana	0.4153 ± 0.0014	941 ± 37		

Table 4.1.5 Radiocarbon measurements of Mangrove samples from Ajman (AM), Kalba natural reservation area (KNR) and the *Periglypta reticulata* specimenl from Kalba beach.

Labcode	Sample Name	$F^{14}C$	^{14}C (BP)
MAMS 21281	AM 1 plant	1.0106 ± 0.0023	
MAMS 21282	AM2 wood	1.0128 ± 0.0023	
MAMS 21283	AM3 sed	0.7599 ± 0.0018	2205 ± 19
MAMS 21270	KNR1 leaf	1.0274 ± 0.0023	
MAMS 21271	KNR2 wood	1.0314 ± 0.0023	
MAMS 21274	KNR 3 sed	0.9255 ± 0.0021	620 ± 18
MAMS 22868	KS M1T2 *Periglypta*	1.0220 ± 0.0025	

The modern leaf, wood and sediment samples from the mangroves at Ajman and Kalba showed the contributions of atmosphere and dead carbon on the mangrove ^{14}C data (Table 4.1.5): sediments from the artificially planted mangrove at Ajman (Arabian Gulf) yield an age of 2200 yr BP, and also the branch and the attached fresh leaf were a lot older than expected resulting in a collection year of around AD 1955 instead of AD 2013. This suggests that the plants incorporated carbon from the sediment as well as from the atmosphere. The reservoir effect at Kalba is less pronounced with sediment ages of 620 yr BP. At Kalba, the mangrove itself, leaves and wood, show a shift in age of 2 yr (estimated) and point to a time of collection approximately 2011 to 2013 (Fig. 4.1.8). Here we can derive a negligible influence of sediment on which the mangrove grows. Overall, the reservoir effect on the mangrove wood itself

is insignificant for determination of the reservoir age of the shells and does allow the calibration of mangrove data as terrestrial material. Regarding the pathways, we see the fresh leaves essentially influenced by the atmosphere. For the mangrove wood, in fact the branch on which the leaf was attached, this is also true although it shows a little older age, which just reflects that it started to grow longer ago than the leaf. The crucial role of the samples from Ajman here lies in the fact that the trees were planted on a carbonaceous soil (old sabkha), which is responsible for the larger deviation from the expected result and hence a more obvious reservoir effect. We can thus say that maybe up to 1 ‰ of dead carbon (1 ‰ corresponds to ca.80 ^{14}C years) can be incorporated in the trees.

When calibrating the modern bomb radiocarbon samples to check their correspondence with the time of collection in December 2013, using the software CALIBomb (http://calib.qub.ac.uk/CALIBomb/), we only received periods corresponding to around 1955. Ingeborg Levin kindly provided us the new atmospheric radiocarbon measurements from Jungfraujoch (Switzerland) to test whether the modern samples might have corresponding intersections on the atmospheric curve. For the leaf and wood samples from Ajman, we received no intercept after 1955. However, at Kalba (Gulf of Oman) we found a corresponding intercept for leaf and wood samples as well as the *P. reticulata* shell within the last 2 yr since collection in December 2013 (Fig. 4.1.8, in addition to the intercepts around 1955). Our modern shell, *P. reticulata*, even seemed to have very little or no reservoir effect, which is rather unexpected. Of course, a second possible result occurs in the 1950s. This interpretation must be taken with caution because the atmospheric measurements were not done on the Arabian Peninsula and due to the meridional gradient the $^{14}CO_2$ level might be 1-2 ‰ higher than at the Jungfraujoch station in Switzerland (I. Levin, pers. comm.). But without any contemporary atmospheric data from this area, this allows us to at least estimate any shifts. Moreover, this species has not yet been in the focus of research with respect to sclerochronology and ^{14}C reservoir effects.

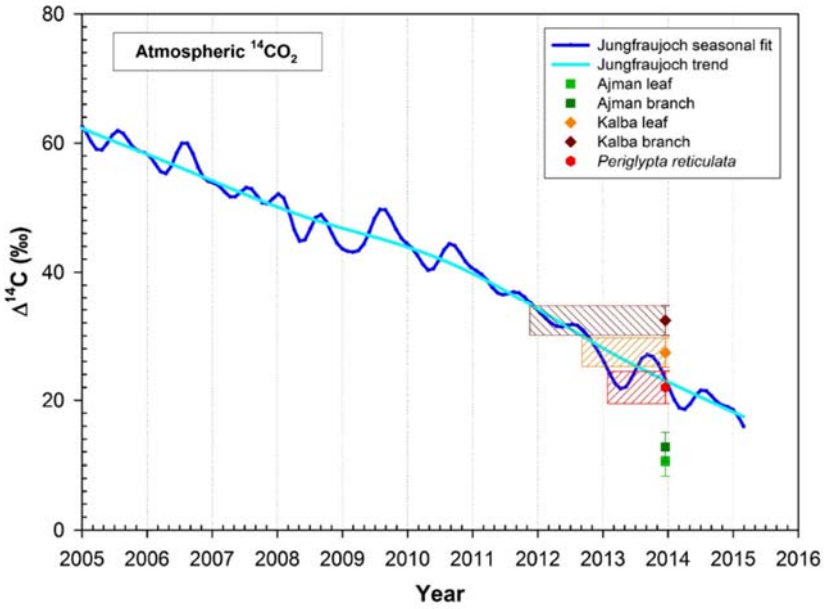

Fig. 4.1.8 Modern samples of Mangroves Ajman and Kalba (data cf. Table 4.1.5) in comparison with atmospheric data from Jungfraujoch, kindly provided by Ingeborg Levin (unpublished data).

4.1.5 Conclusions

The measurements on modern mangroves from both coastal regimes point to a minor influence of the sediment on the tree data, which is expected even when taking the atmospheric influence on leafs and aerial roots of *Avicenna marina* into account. We were able to show that both species *A. uropigimelana* and *T. palustris* are suitable for determining the local reservoir effect, and in the case of *A. uropigimelana*, to provide information on the environmental conditions in which they lived using the light stable isotopes $\delta^{13}C$ and $\delta^{18}O$. For *T. palustris,* the latter still needs to be verified for the study area. The modern sample of the mollusc *P. reticulata* was useful to calibrate the life history of this species and monitor the rate of change in water temperature of the estuarine at Khor Kalba.

Our measurements suggest a difference in reservoir age between both species of roughly 100 years with *A. uropigimelana* pointing to a higher local reservoir effect during the Neolithic period. These rather high values for the reservoir ages point to either a period of stronger upwelling of ocean water from the Arabian Sea or strong freshwater input if the freshwater feeding the mangrove should be depleted in ^{14}C, which has not been investigated so far. Our reservoir ages of 800 and 940 years are certainly higher than those derived by Zazzo et al. (2012, 2016) who quotes a mean value of 645 ± 40 yr (4^{th} millennium BC) for *Anadara antiquata* used and 568 ± 56 yrs (5^{th} millennium BC) for a mixture between several species in Ras al-Hamra, Oman, but our findings seem to be consistent with the *Marcia flammea* specimen from Muscat (786 ± 51 yr BP) quoted in Southon et al. (2002). This can be explained by the locations of the two sites. Kalba is further north towards the Strait of Hormuz where the Oman Sea tightens up, whereas in Ras al-Hamra and Muscat the Oman Sea is a lot more open and part of the Arabian Sea; hence, it might have a slightly different local circulation pattern. The difference between the species clearly reflects the differences in food resource and habitat, leaves compared to plankton and attaching to roots compared to burying in the sand. The isotope data of the prehistoric shell showed a more erratic signature of the stable isotopes than the modern specimen. This might be due to differences in oceanic circulation or terrestrial influences, but might also reflect changes in microstructures due to the age of the specimen. Additionally, the *A. uropigimelana* shell covered roughly 6 yr where the *P. reticulata* shell with the same size covered only about 2-3 yr and hence provided a higher resolution. It would be helpful to investigate the fluctuations in ^{14}C at the same positions where the stable isotope measurements had been sampled. This would help to interpret the origin of the signal, probably also for $\delta^{13}C$ and allow to deduce the possible variability of the reservoir age over the shells lifetime. Hence, archaeologists trying to interpret data on the basis of shell measurements should ensure to use a species that has been investigated with respect to this problem or discuss the data according to the aspects presented here. We need to draw our attention to changes in local reservoir age over time and monitor changes, e.g. during Bronze Age, to provide the archaeologists with the appropriate reservoir age.

The systematic approach to understanding the correlation between atmospheric and marine signal in the shells but also in their food resource and habitat turned out to be the ideal basis for determining and understanding the local reservoir age on the two species under investigation, *T. palustris* and *A. uropigimelana*. The stable isotope measurements allow to derive seasonality, changes in habitat, and

response time for environmental changes to explain changes of the reservoir age over the shells lifetime as well as changes over different periods in time. In a next step, we will extend this research to a different period that is important for the archaeologists as well (Bronze Age, Iron Age). An important topic of future work will be the stable isotope analysis on *T. palustris*, to not only to determine the lifespan of this species and to what extend it mirrors environmental changes, e.g. fluctuations of salinity, sea surface temperature ($\delta^{18}O$), or food resources ($\delta^{13}C$). This would provide necessary information for archaeologists and paleoclimatology. Being able to derive reservoir effects with the same species enables tracing environmental changes through changes in the reservoirs effects.

4.1.6 Acknowledgements

The authors would like to thank Dr. Sabah Jasim and Eisa Yousif from the Department of Antiquities Sharjah for the possibility to work in this area. We are much obliged to the Environment & Protected Areas Authority of the Government of Sharjah for admission to the protected mangrove in Khor Kalba. Dr. Ingeborg Levin, Institute for Environmental Physics, Heidelberg, kindly provided atmospheric ^{14}C data and fit. Michael Maus, Institute for Geosciences, Mainz, was a great help in running the stable isotope measurements. We are very grateful to Dr. Tobias Häger, Dr. Amy Prendergast and Stefania Milano, Institute for Geosciences, Mainz, for performing the Raman spectrometry. ^{14}C and stable isotope measurements were financed by Deutsche Forschungsgemeinschaft (DFG HI 643/23). Moreover, we would like to thank the two reviewers for their help with improving the manuscript.

4.1.7 References

Armitage, S. J., S. A. Jasim, A. E. Marks, A. G. Parker, V. I. Usik and H.-P. Uerpmann (2011). The Southern Route 'Out of Africa': Evidence for an Early Expansion of Modern Humans into Arabia. Science 331(6016): 453-456.

Azzoug, M., M. Carré and A. J. Schauer (2012). Reconstructing the duration of the West African Monsoon season from growth patterns and isotopic signals of shells of Anadara senilis (Saloum Delta, Senegal). Palaeogeography, Palaeoclimatology, Palaeoecology 346-347(0): 145-152.

Berger, J.-F., S. Cleuziou, G. Davtian, M. Cattani, F. Cavulli, V. Charpentier, M. Cremaschi, J. Giraud, P. Marquis, C. Martin, S. Méry, J. C. Plaziat and J. F. Saliège (2005). Évolution paléogéographique du Ja'alan (Oman) à l'Holocène moyen : impact sur l'évolution des paléomilieux littoraux et les stratégies d'adaptation des communautés humaines. Paléorient: 46-63.

Berger, J. F., V. Charpentier, R. Crassard, C. Martin, G. Davtian and J. A. López-Sáez (2013). The dynamics of mangrove ecosystems, changes in sea level and the strategies of Neolithic settlements along the coast of Oman (6000-3000 cal. BC). Journal of Archaeological Science 40: 3087-3104.

Bieler, R., I. Kappner and P. M. Mikkelsen (2004). Periglypta listeri (J. E. Gray, 1838) (Bivalvia:Veneridae) in the western Atlantic: Taxonomy,, Anatomy, Life Habits and Distribution. Malacologia 46(2): 427-458.

Culleton, B. J., D. J. Kennett, B. L. Ingram, J. M. Erlandson and J. R. Southon (2006). Intrashell Radiocarbon Variability in Marine Molluscs. Radiocarbon 48(3): 387-400.

Debenay, J. P., D. L. Tack, M. Ba and I. Sy (1994). Environmental Conditions, Growth and Production of Anadara Senilis (Linnaeus, 1758) in a Senegal Lagoon. Journal of Molluscan Studies 60(2): 113-121.

Dutta, K. (2008). Marine 14C Reservoir Age and Suess Effect in the Indian Ocean. Journal of Earth Science India I(III): 175-188.

Füllenbach, C. S., B. R. Schöne and R. Mertz-Kraus (2015). Strontium/lithium ratio in aragonitic shells of Cerastoderma edule (Bivalvia) — A new potential temperature proxy for brackish environments. Chemical Geology 417: 341-355.

Jones, D. S., M. A. Arthur and D. J. Allard (1989). Sclerochronological records of temperature and growth from shells of Mercenaria mercenaria from Narragansett Bay, Rhode Island. Marine Biology 102: 225-234.

Khim, B.-K., D. E. Krantz, L. W. Cooper and J. M. Grebmeier (2003). Seasonal discharge of estuarine freshwater to the western Chukchi Sea shelf identified in stable isotope profiles of mollusc shells. Journal of Geophysical Research: Oceans 108(C9): 3300.

Kromer, B., S. Lindauer, H.-A. Synal and L. Wacker (2013). MAMS - A new AMS facility at the Curt-Engelhorn-Centre for Achaeometry, Mannheim, Germany. Nuclear Instruments and Methods in Physics Research Section B: Beam Interactions with Materials and Atoms 294(0): 11-13.

Lindauer, S. and B. Kromer (2013). Carbonate Sample Preparation for 14C Dating Using an Elemental Analyzer. Radiocarbon 55(2-3): 364-372.

Marali, S. and B. R. Schöne (2015). Oceanographic control on shell growth of Arctica islandica (Bivalvia) in surface waters of Northeast Iceland — Implications for paleoclimate reconstructions. Palaeogeography, Palaeoclimatology, Palaeoecology 420(0): 138-149.

Milano, S., B. R. Schöne and R. Witbaard (2015). Changes of shell microstructural characteristics of Cerastoderma edule (Bivalvia) — A novel proxy for water temperature. Palaeogeography, Palaeoclimatology, Palaeoecology.

Pape, E., A. Muthumbi, C. P. Kamanu and A. Vanreusel (2008). Size-dependent distribution and feeding habits of Terebralia palustris in mangrove habitats of Gazi Bay, Kenia. Estuarine, Coastal and Shelf Science 76: 797-808.

Patel, B., S. Patel, M. C. Balani and S. Pawar (1978). Flux of certain radionuclides in the blood-clam Anadara granosa Linneaus under environmental conditions. Journal of Experimental Marine Biology and Ecology 35(2): 177-195.

Petchey, F., S. Ulm, B. David, I. McNiven, B. Asmussen, H. Tomkins, N. Dolby, K. Aplin, T. Richards, C. Rowe, M. Leavesley and H. Mandui (2013). High-resolution radiocarbon dating of marine materials in archaeological contexts: radiocarbon marine reservoir variability between Anadara, Gafrarium, Batissa, Polymesoda spp. and Echinoidea at Caution Bay, Southern Coastal Papua New Guinea. Archaeological and Anthropological Sciences 5(1): 69-80.

Petchey, F. C., Geoffrey (2011). Tongatapu hardwater: Investigation into the 14C marine reservoir offset in lagoon, reef and open ocean environments of a limestone island. Quaternary Geochronology 6: 539-549.

Phillips, C. S. and C. E. Mosseri-Marlio (2002). Sustaining Change: The Emerging Picture of the Neolithic to Iron Age Subsistence Economy at Kalba, Sharjah Emirate, UAE. Fifth International Symposium on the Archaeozoology of southwestern Asia and adjacent areas, Amman, Jordan, ARC-Publicaties Groningen.

Rodelli, M. R., J. N. Gearing, P. J. Gearing, N. Marshall and A. Sasekumar (1984). Stable isotope ratio as a tracer of mangrove carbon in Malaysian ecosystems. Oecologia 61(3): 326-333.

Rollins, H. B., D. H. Sandweiss and J. C. Rollins (1990). Molluscs and coastal archaeology; A review. Decade of North American Geology, Centennial Special Volume 4 "Archaeological Geology of North America". J. D. D. N.P. Lasca, Geological Society of America: 467-478.

Schöne, B. R., E. Dunca, J. Fiebig and M. Pfeiffer (2005). Mutvei's solution: An ideal agent for resolving microgrowth structures of biogenic carbonates. Palaeogeography, Palaeoclimatology, Palaeoecology 228(1–2): 149-166.

Schöne, B. R., J. Fiebig, M. Pfeiffer, R. Gleβ, J. Hickson, A. L. A. Johnson, W. Dreyer and W. Oschmann (2005). Climate records from a bivalved Methuselah (Arctica islandica, Mollusca; Iceland). Palaeogeography, Palaeoclimatology, Palaeoecology 228(1–2): 130-148.

Schöne, B. R. and D. M. Surge (2012). Bivalve Sclerochronology and Geochemistry. Part N (Revised), Volume 1 Mollusca 6 Bivalvia. P. A. Selden, Paleontological Institute University of Kansas: 1-24.

Schöne, B. R., A. D. Wanamaker Jr, J. Fiebig, J. Thébault and K. Kreutz (2011). Annually resolved d13Cshell chronologies of long-lived bivalve molluscs (Arctica islandica) reveal oceanic carbon dynamics in the temperate North Atlantic during recent centuries. Palaeogeography, Palaeoclimatology, Palaeoecology 302(1-2): 31-42.

Soulet, G. (2015). Methods and codes for reservoir–atmosphere 14C age offset calculations. Quaternary Geochronology 29: 97-103.

Southon, J., M. Kashgarian, M. Fontugne, B. Metivier and W. W.-S. Yim (2002). Marine Reservoir Corrections for the Indian Ocean and Southeast Asia. Radiocarbon 44(1): 167-180.

Tebano, T. and G. Paulay (2000). Variable recruitment and changing environments create a fluctuating resource: the biology of Andara uropigimelana (Bivalvia: arcidae) on Tarawa Atoll. Atoll Research Bulletin 488: 1-15.

von Bertalanffy, L. (1938). A quantitative theory of organic growth (inquiries on growth laws. II). Human Biology 10: 181-213.

Wacker, L., R. H. Fülöp, I. Hajdas, M. Molnár and J. Rethemeyer (2013). A novel approach to process carbonate samples for radiocarbon measurements with helium carrier gas. Nuclear Instruments and Methods in Physics Research Section B: Beam Interactions with Materials and Atoms 294(0): 214-217.

Wanamaker Jr, A. D., K. J. Kreutz, B. R. Schöne and D. S. Introne (2011). Gulf of Maine shells reveal changes in seawater temperature seasonality during the Medieval Climate Anomaly and the Little Ice Age. Palaeogeography, Palaeoclimatology, Palaeoecology 302(1-2): 43-51.

Zazzo, A. (2014). Bone and enamel carbonate diagenesis: A radiocarbon prospective. Palaeogeography, Palaeoclimatology, Palaeoecology 416(0): 168-178.

Zazzo, A., M. Lebon, L. Chiotti, C. Comby, E. Delqué-Kolic, R. Nespoulet and I. Reiche (2013). Can We Use Calcined Bones for Radiocarbon Dating the Paleolithic? Radiocarbon 55(2-3): 1409-1421.

Zazzo, A., O. Munoz, E. Badel, I. Béguier, F. Genchi and L. G. Marcucci (2016). A Revised Radiocarbon Chronology of the Aceramic Shell Midden of Ra's Al-Hamra 6 (Muscat, Sultanate of Oman): Implication For Occupational Sequence, Marine Reservoir Age, and Human Mobility. Radiocarbon 58(2): 383-395.

Zazzo, A., O. Munoz, J. F. Saliège and C. Moreau (2012). Variability in the marine radiocarbon reservoir effect in Muscat (Sultanate of Oman) during the 4th millennium BC: reflection of taphonomy or environment? Journal of Archaeological Science 39(7): 2559-2567.

4.2 Local Marine Reservoir Effect at Kalba (UAE) between Neolithic and Bronze Age: An Indicator of Sea Level and Climate Changes

Susanne Lindauer [a, b], Guaciara M. Santos [c], Axel Steinhof [d], Eisa Yousif [e], Carl Phillips [f], Sabah A. Jasim [e], Hans-Peter Uerpmann [g], Matthias Hinderer [b]

[a] Curt-Engelhorn-Zentrum Archaeometry, Klaus-Tschira-Archaeometry-Centre, C4, 8, 68159 Mannheim, Germany

[b] Institute of Applied Geosciences, Technical University Darmstadt, Schnittspahnstr. 9, 64287 Darmstadt, Germany

[c] Earth System Science, University of California, Irvine, B321 Croul Hall, Irvine, CA 92697-3100, USA
[d] Max-Plack Institute for Biogeochemistry, Hans-Knoll-Str. 10, 07745 Jena, Germany
[e] Directorate of Antiquities, Department of Culture & Information, Sharjah, United Arab Emirates
[f] UMR 7041, ArScAn du CNRS, Maison Rene Ginouves de l'Archeologie et de l'Ethnologie, 21 Allee de l'Universite, 92023 Nanterre cedex, France
[g] Center for Scientific Archaeology, Eberhard-Karls-University Tübingen, Rümelinstraße 23, 72070 Tübingen, Germany

Contributions: SL, MH designed the study; SL, GS, AS measured radiocarbon; SL, EY, HPU, MH collected the samples; SAJ provided the logistics in UAE; SL, GS wrote the paper.
Citation: Lindauer, S., Santos, G.M., Steinhof, A., Yousif, E., Phillips, C., Jasim, S.A., Uerpmann, H.-P., Hinderer, M., 2017. The local marine reservoir effect at Kalba (UAE) between the Neolithic and Bronze Age: An indicator of sea level and climate changes. *Quaternary Geochronology* **42***,* 105-116*.*

4.2.1 Abstract

We investigate the local marine reservoir effect at Kalba, United Arab Emirates (UAE), between the Neolithic and Bronze Age with respect to possible changes through time and mollusc species diversity. Two distinctive species living in or close proximity to the mangrove of Khor Kalba provide insights into ocean circulation patterns in this coastal environment. The species selected are the bivalve *Anadara uropigimelana*, and the gastropod *Terebralia palustris.* They have been an important local food resource for humans since at least the Neolithic. Our results show that for the Neolithic and Bronze Age, the reservoir effects ΔR are quite different for the species selected. For *A. uropigimelana* the ΔR decreases from 576 ± 90 to 112 ± 44 years, while for *T. palustris*. the reduction ranges from 389 ± 66 to -19 ± 36 years. These results are coeval with other multi-proxies (stalagmite records and sea level changes) for the middle Holocene, and suggest that the main cause of the decreasing reservoir effect is a changing – in this case declining - sea level and an increasingly drier climate.

4.2.2 Introduction:

In arid environments preservation of organic material is rather insufficient. To build reliable radiocarbon (^{14}C) chronologies all possible materials must be taken into account, including those of fossil shells originating from shallow-water coastal areas and estuaries. However, marine shells tend to be radiocarbon depleted (i.e. ^{14}C-deficient) compared to their atmospheric counterparts, creating offsets that must be accounted for in order to be properly used in chronological models. The reason for the depletion in ^{14}C of marine organisms lies in the fact that oceans can store carbon in the deep sea for up to 1000 years. Upwelling ocean circulation transports old carbon to the surface which is then incorporated by the organisms. The specific offset between coeval terrestrial-shell samples can be expressed as Marine reservoir effect ΔR or just ΔR. The effect is well described in the publications of Dutta (2008) and Southon et al. (2002). Earlier investigations in the Indian Ocean (including the Arabian Sea) concerning local marine reservoir effects observed in shells were restricted to the pre-bomb period, and to museum collections of shells collected alive mainly during the 19th century or from archaeological excavations (Southon et al. 2002, Dutta 2008, Zazzo et al. 2012). Here then a mean ΔR was determined

by using all available shells, independent of species or possible temporal variability, apart from one recent publication (Zazzo et al. 2016). For sites where all organic materials are relatively scarce this approach might be unavoidable, and for shell species sharing similar habitats and food resources, it might be even acceptable (Ascough et al. 2005).

We draw your attention to a location on the coast of the Gulf of Oman, Kalba (Fig. 4.2.1), which shows signs of human occupation since Neolithic times, as well as signs of an intact mangrove forest for about the same timespan. During archaeological excavations shell middens and settlements with shell layers were found. This allowed us to address local reservoir effects in the following three ways:

1) We investigated its dependence on shell species by analyzing, the marine bivalve *Anadara uropigimelana* and the mangrove gastropod *Terebralia palustris.* We also determined the local ΔR change over time of both species by comparing Neolithic and Bronze Age sites in Kalba.

2) These results are then discussed regarding the earlier investigations on the reservoir effect calculated for neighboring areas.

3) The long-term changes on regional climate and environmental conditions. If we see a change in ΔR over time it needs to be discussed in comparison of climate proxies of neighboring areas to be able to judge whether or not these changes are caused by climatic effects or only food resources of the shells for example. Food is an important factor of carbon storage in the shell. Hence e.g. mangroves leaves as a food resource result in a lower reservoir effect than algae. For our shells this is already discussed in Lindauer et al. (2016).

An earlier publication (Lindauer et al. 2016) explained how shells in Kalba reflect the environment they live in, and whether the species *A. uropigimelana* and *T. palustris* were suitable candidates to study ΔR in this region. Preliminary results for the shell midden KK1 during the Neolithic period showed a significant age offset compared to the contemporaneous terrestrial material, but the lack of statistical significance due to the low number of specimens of *A. uropigimelana*. called for further analysis. Moreover, the complexity of the Arabian Peninsula ecoregion, with its coastal mangroves and intricate ancient history, demanded the sampling of a younger archaeological site (e.g. K4) to help with comparisons and discussion.

With our research we intend to go one step further and take all possible ecosystem drivers (e.g. upwelling strength, sea level changes and climate, shell species and their dietary habits) into account to better understand any ΔR variability in this location. For proper ΔR interpretations and to obtain quantitative uncertainties when deriving reservoir effects from isolated locations in a specific region, shell species and ecosystem attributes are as important as the local oceanic and climatic conditions. Once we understand how those combined effects can affect ΔR, we may be able to successfully describe its temporal variation in the past.

Regional Setting and Archaeology

Kalba is an enclave in the Emirate Sharjah located on the Gulf of Oman, United Arab Emirates (UAE). Being part of the Arabian Sea (see Fig. 4.2.1), the Gulf of Oman is also known as the Oman Sea, but for

consistency with international publications we will use Gulf of Oman here. At this site, the Hajar Mountains rise steeply from the coastline. Old shell middens dating back to the Neolithic spread along the beach as shown in Fig. 4.2.2. At the south of Kalba there is a lagoon with occasional freshwater from rainfall and a mangrove forest known as Khor Kalba with an extensive sabkha surrounding the mangroves today. Here we studied the Neolithic shell midden Khor Kalba site 1 (KK1) and the Bronze Age settlement Kalba 4 (K4) further north near the modern town Kalba. In order to maintain consistency across works, we use the names of the sites as introduced by Phillips and Mosseri-Marlio (2002).

The oldest shell midden KK1 is located near the foot of a hill between the Hajar Mountains and the sabkha (supratidal salt flat). Apart from shells, bifacial stone tools were also found, indicating that the site was visited during the 5th millennium BC (Phillips and Mosseri-Marlio 2002). Other sites, such as KK2-13 are relatively younger (around 3000 yrs BP for shells, see Philips and Mosseri-Marlio (2002)) especially towards the beach line (Fig. 4.2.2). The major archaeological finds in this region, including the distinct settlements and tombs, date back to the Bronze and Iron Age period. The mound referred to as K4 has revealed several superimposed building phases as described by Phillips and Mosseri-Marlio (2002). The earliest period is associated with a circular tower structure around which, during the middle of the second millennium BC, a large mud-brick tower was built. Further construction continued during the Iron Age, including a large wall around the settlement. It is possible that the settlement was abandoned during the first millennium BC. Nevertheless, it is certain that the mangroves at Khor Kalba were already there during the Neolithic period, and most probably served as an important source of food and wood to the settlers and/or travelers (Phillips and Mosseri-Marlio 2002).

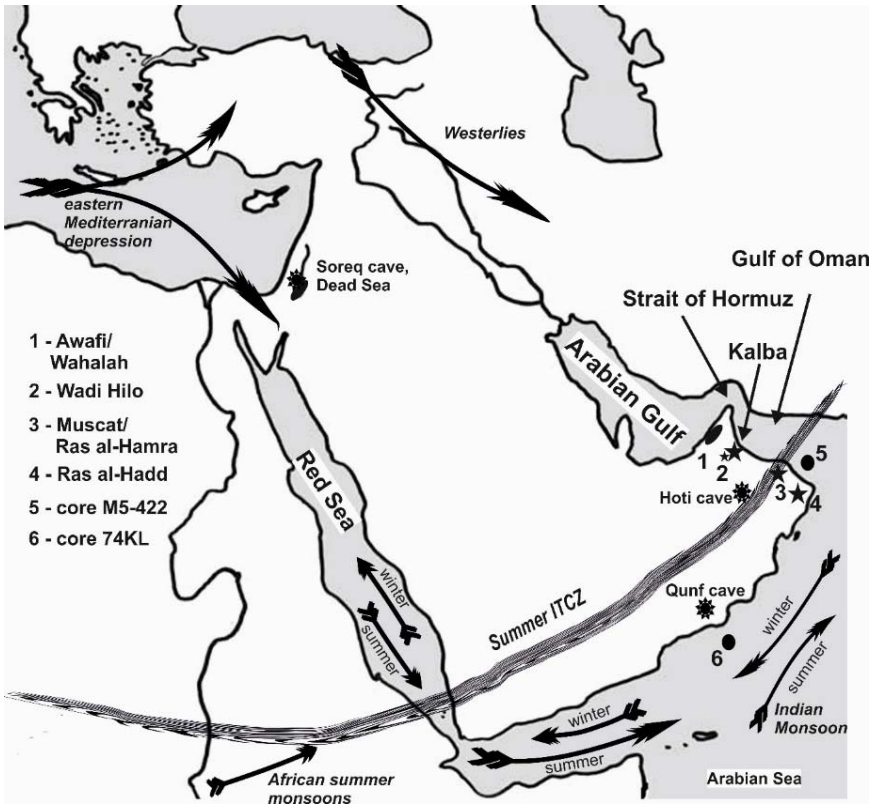

Fig. 4.2.1 Map with Kalba, UAE, in the context of the paleoclimate proxies (Soreq cave, Dead Sea, Hoti cave, Qunf cave, Awafi lake, Wahalah lake, sediment cores) that are discussed in the text. The arrows represent the dominant wind directions including seasonality that influence our area of interest.

Chronological aspects and Radiocarbon

Several methods exist today to help establish the chronology of an archaeological site or a paleoenvironment. Apart from stratigraphic and archaeological context, such as artifactual evidence for human occupation(s) (such as flint stones and pottery fragments), sediments can be dated using optically stimulated luminescence (OSL) or sedimentological methods. Certainly plenty of marine shells can be found at archaeological sites along the coast, or even inland. At the coastline, where the molluscs were harvested by humans, the remains can be found deposited as shell middens. Further inland, they appear as grave goods or undefined archaeological finds, as for example in Wadi al-Hilo around 20 km southwest of Kalba (Kutterer et al. 2012, Uerpmann et al. submitted). As already mentioned these marine shells appear to be older in ^{14}C ages compared to terrestrial materials, due to the upwelling of old carbon in this marine habitat (see Fig. 4.2.3). Therefore ΔR can vary geographically due to different upwelling intensity, changing ocean circulation patterns, sea level change or freshwater inflow to name only some important controlling factors. Hence we speculate that the marine reservoir effect in Kalba may not necessarily be constant over time. Moreover, shells apparent ages can vary due to species dietary habits (Ascough et al. 2005, Culleton et al. 2006). Different food-resources and habitats can lead to differences in the marine reservoir effect. Therefore, species special traits such as food resources and shifts over their habitat conditions, must be properly investigated.

The marine reservoir effect in the Gulf of Oman has been investigated previously by others, e.g. (Southon et al. 2002, Dutta 2008, Zazzo et al. 2012, Zazzo et al. 2016). The publications by Southon and Dutta together with their co-workers used data on shells from museum collections that were collected alive before 1945. They determined ΔR values of e.g. 163 yrs for Qatar in the Arabian Gulf and 285 years for Muscat. Zazzo (2012, 2016) found data slightly lower than the Muscat data, as will be discussed in detail in comparison with our data.

Throughout this publication uncalibrated radiocarbon ages will be cited as ^{14}C yrs BP, whereas calibrated ages will be mentioned as cal yrs BP or in case of several thousand years as ka cal BP.

Holocene climate variability

Paleoclimate investigations concerning the Holocene in South-East Arabia have been undertaken using a variety of materials: lake and dune deposits (Parker et al. 2006, Parker et al. 2006, Enzel et al. 2015, Parker et al. 2016), marine sediment records (Staubwasser et al. 2002, Leuschner and Sirocko 2003), speleothems (Fleitmann et al. 2007, Fleitmann and Matter 2009, Van Rampelbergh et al. 2013) to name but a few. The highest paleoclimatic resolution in this region is provided by the speleothem records of Hoti cave in North Oman, and Qunf Cave (South Oman). Sedimentary records from the Dead Sea further north (Migowski et al. 2006, Weninger et al. 2009), and other lake records from the Arabia also provide interesting information regarding the climatic system for this area. The marine sediment cores are less intense in signal, but nevertheless provide information about the ocean at the times of interest. There are many more paleoclimate investigations that are not mentioned but point in the same direction. We decided to compare our data with key, representative sites.

A common finding among these archives is the fact that South Arabia appeared to have been way wetter during the early Holocene (i.e. between 10 ka and 6 ka ago) than nowadays (Parker et al. 2006).

Controversies exist regarding the exact ending of this wet period. The controversy appears to be related to specific locations, as reviewed in Van Rampelbergh et al. (2013). While sedimentary records of the Arabian Sea and the speleothem records of South Oman suggest a gradual decrease in precipitation since approximately 8 ka years ago, records from Northern Oman and the United Arab Emirates (e.g. the speleothems in Hoti cave and the sedimentary records of the Rub al-Khali) indicate that the end of the wet period came rather abrupt around 6 ka. Note that among the sites studied so far, those that suggest a sudden change in wetness are nowadays outside the Intertropical Convergence Zone (ITCZ) as indicated in Fig. 4.2.1. The northernmost position of the ITCZ during summer shifted to the south of the UAE and North Oman around 6 ka ago, disconnecting these areas from monsoonal rains. This leaves winter Westerly rainfall as the main source of precipitation (Parker et al. 2006), and winds coming from the West (see Fig. 4.2.1). Soreq Cave and the Dead Sea are also influenced by these Westerly winds, which is one of the reasons why we want to compare our data also to these locations further north. The wind directions plotted in Fig. 4.2.1 show the complex patterns with seasonal change that also are reflected in the ocean circulation shown in Fig. 4.2.2.

Ocean circulation and geology

Near Kalba the seafloor is rather flat and the Gulf of Oman narrows towards the Strait of Hormuz. The water current here is complex, as it reverses direction seasonally (Fig. 4.2.2) and probably depends on the direction of the ocean currents that are described for different seasons. The water at Kalba is not only influenced by the waters of the Arabian Sea, but also by the Arabian Gulf (Johns et al. 2000, Dalongeville and Sanlaville 2005). During winter the upwelled deep waters from the Arabian Sea flows near the Kalba coastline site and over the Straits of Hormuz into the Arabian Gulf (red arrows in Fig. 4.2.2). In the summertime the outflow from the Arabian Gulf passes by Kalba hereby affecting the water mixing in the mangrove estuary (blue arrows in Fig. 4.2.2). This is in accordance with the wind directions in Fig. 4.2.1. The Arabian Gulf itself is very flat and has a high evaporation rate which increases temperature and salinity. Apart from the carbonaceous rocks and sediments the strong evaporation enhances the development of minerals including gypsum (Purser 1973).

The ocean floor in the Gulf of Oman becomes significantly steeper near Muscat and Ras al-Hadd (see Fig. 4.2.1 for locations, Fig. 4.2.2 for bathymetry). Between Kalba and Ras al-Hamra, near Muscat, the seafloor drops from several hundred to over 2000 meters. Here the denser water sinks to the bottom and away from the coast. Below Muscat and also Ras al-Hadd the waters show a stronger exchange as the Arabian Sea is wider open.

Sea level change during the Holocene has varied with a possible high stand occurring around 6 ka cal BP when the water could have been 2-3 m higher than today (Bernier et al. 1995, Lambeck 1996, Lambeck et al. 2011). This sea level height might be relative because geological evidence shows that the Arabian Plate near the Straits of Hormuz is moving north (Hoffmann et al. 2013).

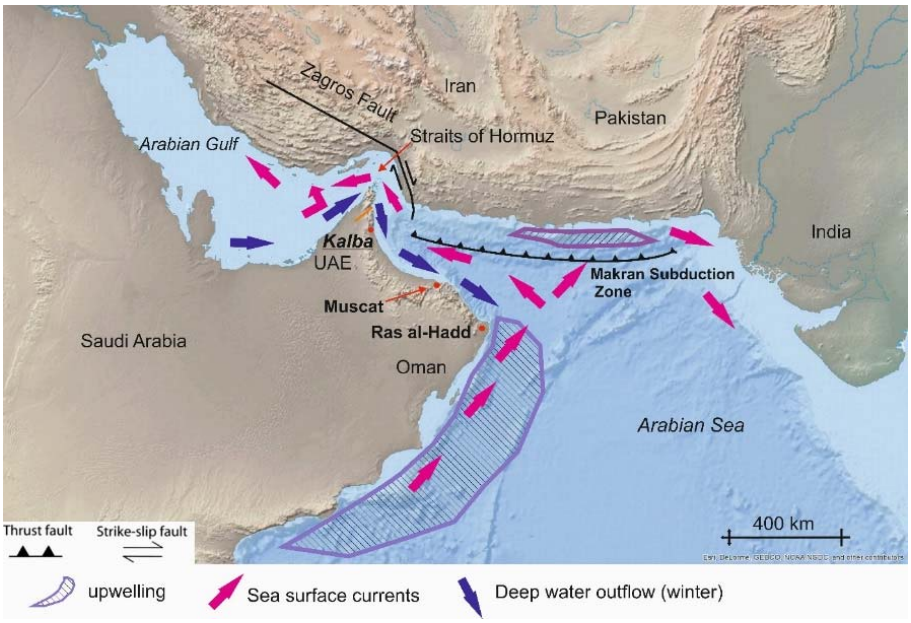

Fig. 4.2.2 Map showing bathymetric and terrestrial heights with modern seasonal ocean circulation patterns and upwelling water from Arabian Sea. The Dibba zone is marked as an orange line. Map modified after (Schneider et al. 2016) with information on upwelling from (Staubwasser et al. 2002) and seasonal flow directions from (Dalongeville and Sanlaville 2005).

Along the Straits of Hormuz the Arabian plate is subducting. The Arabian Peninsula is characterized by Ophiolite, the old Tethys Ocean floor, with local differences in mineral composition, and overlying Carbonates. Along the coastal margins fracture zones and subduction zones can be found. Strong wave events are documented in sediments found near ancient settlements and point to very active tectonics (Hoffmann et al. 2015).

4.2.3 Materials and Methods:

Site description, sample collection and rationality

Shell and ash samples from the shell midden KK1 at Khor Kalba (see Fig. 4.2.3) were taken 2013. Details of the shells midden can be found in (Phillips and Mosseri-Marlio 2002). The shell midden although quite large in extent is only about 50 cm high with respect to the shells. There is no layered structure apart from an extensive lens of ashy sediment at the bottom. Only through radiocarbon dating was it was possible to recognize two distinct periods of accumulation. The preliminary ^{14}C investigations and respective ΔR calculation regarding these samples were published (Lindauer et al. 2016). During 2015 this shell midden was re-sampled, aiming to collect a more representative population of *A. uropigimelana*. shells from the lowermost KK1 layer. This layer also contains lots of ashy sediment. Only three more *A. uropigimelana* specimens were found at the outermost edge of the ashy sediment. We also collected a second sample from the ash at the edge to verify the previous ^{14}C dating result, because the relative sampling positions was not identical (see Fig. 4.2.3). If the results for the two ash samples are different it is possible to calculate two reservoir effects for KK1 and see whether they overlap or whether they are different within errors.

The shell midden KK1 shows two distinct time ranges for the shells and the ashes. There are approximately 7000 ^{14}C yrs BP at the bottom and 6300 ^{14}C yrs BP (shell ages) immediately above until the surface of the midden (ca.50cm). Occasionally, ashy sediment age determinations can pose a problem, because this type of carbonaceous material can contain carbon from multiple sources, e.g. charcoal and/or carbon inclusions in minerals (Braadbaart et al. 2012). Therefore, measurements of δ^{13}C were used to examine the possible origin of the carbon in the ashy sediment.

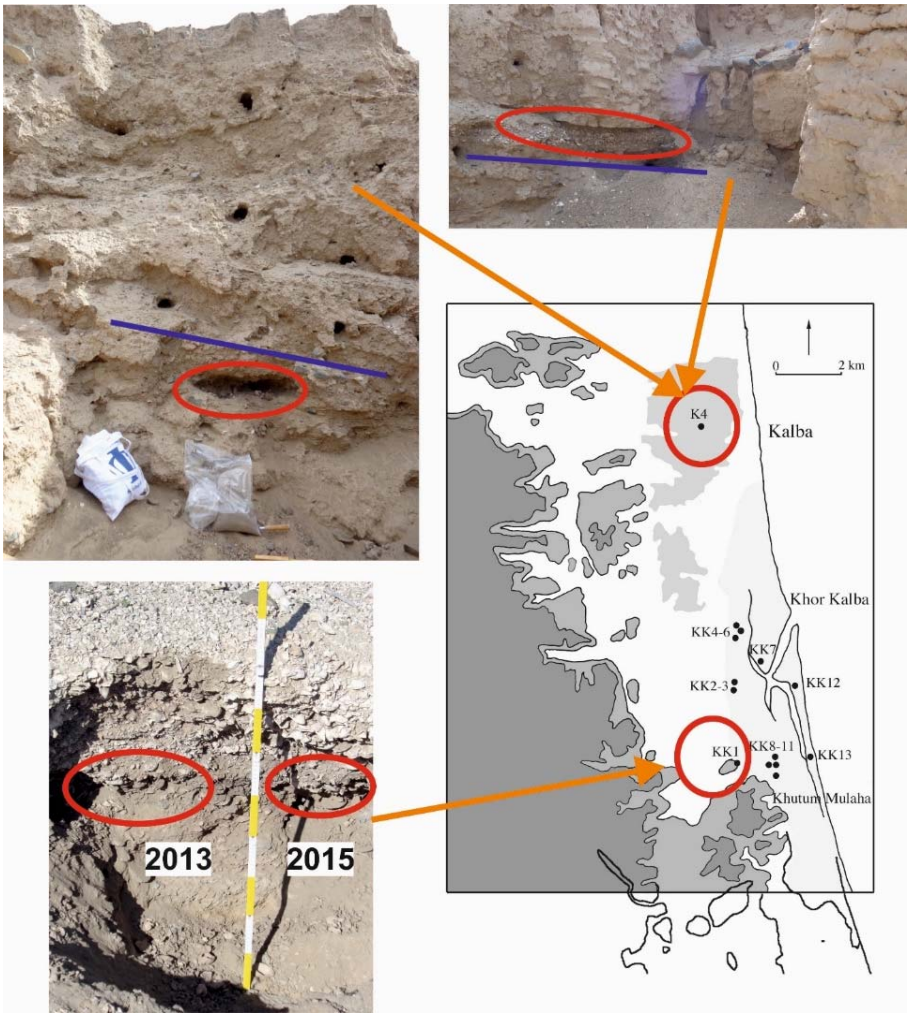

Fig. 4.2.3 The sites at Kalba studied here (red circles) include the settlement K4 and the Neolithic shell midden KK1 located at the edge of the mangrove and sabkha area. The upper left photo shows sampling of the lower layer MBZ1 (below blue line). The upper right photo depicts the shell-rich layer MBZ2 (above blue line) slightly tilted to the right at K4 site. The vertical structure visible to the right is part of the mud brick wall mentioned in the text. The bottom photo was taken in 2013 and shows part of the shell midden KK1 where the samples had been taken (red circles). The map with the locations at the right was modified from (Phillips and Mosseri-Marlio 2002), photos S. Lindauer.

In order to verify possible changes in ΔR over time, we sampled a second site in Kalba, K4 (Fig. 4.2.3). This site was once a settlement inhabited during the Bronze and Iron Age, and was excavated during the 1990s (Phillips and Mosseri-Marlio 2002). We found two layers of shells, ash, and charcoal fragments next to an Iron Age mudbrick wall. The charcoal fragments of the lower layer were in association with burnt date stones. Distinct charcoal or charred date stones are ideal terrestrial reference material for determining ΔR. As mentioned earlier, ash samples are often difficult to interpret. The lower layer (named "MBZ1" hereafter) is approximately 30 cm thick, and besides the presence of charcoal and burnt date stones, it also contains fragments and unbroken specimens of *A. uropigimelana*. and *T. palustris*. This layer is overlain by another layer extremely rich in shells, referred to as "MBZ2". This

layer is around 30-40 cm thick, and is slightly tilted towards the mud brick wall (Fig. 4.2.3). MBZ2 layer hardly contained any ash, however we managed to find half of a bivalve of *A. uropigimelana*. with a charcoal fragment embedded in it. It was not immediately clear whether the two layers MBZ1 and MBZ2 are significantly different in age even though they are clearly separated. Through ^{14}C measurements we obtained a clear picture of their time sequences.

To constrain the possible age ranges within the layers, we sampled and ^{14}C dated several specimens of both *A. uropigimelana* and *T. palustris* per site and layer (Table 4.2.1).

Table 4.2.1 List of sites in Kalba with number of samples per shell specimen and organic matter collected.

Period	Site	Layer	Year of collection	Material	No of samples
Bronze Age	K4	MBZ2	2015	*A. uropigimelana*	5
				T. palustris	4
				charcoal	1
		MBZ1		*A. uropigimelana*	5
				T. palustris	4
				charcoal	1
				charred date stone	1
Neolithic	KK1		2013	*A. uropigimelana*	2
				T. palustris	5
				ash	1
			2015	*A. uropigimelana*	3
				T. palustris	4
				ash	1

Sample pretreatment for isotopic analysis

The ^{14}C measurements were conducted in multiple laboratories, hence sample processing and subsequent analysis differed slightly among facilities. The facilities involved are the German laboratories of Curt-Engelhorn-Zentrum Archaeometry Mannheim (CEZA Mannheim ^{14}C lab; sample code *MAMS*), Max-Planck-Institute for Biogeochemistry Jena (MPI-BGC Jena; sample code *P*), and the USA facility Keck Carbon Cycle AMS (KCCAMS; sample code *UCIAMS*). Some of the major differences on sample processing and analysis are described below.

Shells were sampled at the ventricular margin to determine a date as close as possible to the time of death, being aware that due to the ontogenetic age trend in shells it is possible to sample a time span of more than one year. For analysis performed at CEZA Mannheim ^{14}C lab and MPI-BGC Jena, the outer surface contamination was removed by etching with 1% HCl and washing with Milli-Q water three times. The carbonate samples at CEZA were hydrolyzed using 96% phosphoric acid in an autosampler system by Ionplus in combination with the Age III graphitization system also by Ionplus (Wacker et al. 2013, Lindauer et al. 2016). Graphite samples were then measured by the MICADAS AMS system at the ^{14}C lab of the Klaus-Tschira-Archaeometrie-Zentrum, Mannheim (Kromer et al. 2013). In the Jena lab aragonite from shells were extracted using a headspace extraction at a special inlet to the graphitization system and measured using the 3MV Tandetron accelerator (HVEE, Amersfoort, Netherlands) at the MPI-BGC Jena (Steinhof et al. 2004). At KCCAMS carbonate fragments were physically inspected

under microscope, 30% leached and also hydrolyzed using 96% phosphoric acid in disposable blood vials (Santos et al. 2004, Santos and Xu 2016). The cryogenically clean CO_2 released was transferred to reaction volume for graphitization following established protocols (Santos 2007), and then measured at a modified NEC 0.5MV 1.5SDH-2 compact AMS system (Beverly et al. 2010).

Charcoal and charred date stone samples received the same pretreatment before being measured at CEZA Mannheim or MPI-BGC Jena. They were given an ABA treatment consisting of 4% HCl followed by 0.4% NaOH and a final HCl step. Each chemical steps had a duration of 60 minutes. While the HCl steps were done at elevated temperature (60°C), the NaOH step was carried out at room temperature. In between and after all steps the chemicals were removed with Milli-Q water. Ashy sediments were pretreated the same way as charcoal samples with the difference that the first acid step was done at room temperature as long as a reaction could be seen with renewal of acid in between, until no further reaction could be detected (Lindauer et al. 2016). Terrestrial samples were then combusted using an elemental analyzer (Elementar) and graphitized using a self-built graphitizer system that uses liquid nitrogen to fill the reactors (Lindauer and Kromer 2013). At the MPI-BGC Jena the prepared ash and charcoal samples were combusted using an elemental analyzer (NC2500, Carlo Erba, Milano, Italy) before the CO_2 gas was collected by the UGCS (Universal Gas Collection System) line including a cryogenic trap and 20 ports for graphitization reactors (Steinhof et al. 2004). At KCCAMS we also processed and measured ashy and charcoal samples using an ABA procedure with the main difference being the chemical strength applied (e.g. 1N HCl and 1N NaOH, with both digestions applied at 60°C), as it is described in (Santos and Ormsby 2013). Chemically clean organics were subjected to sealed tube combustion to produce CO_2, and thus graphitized as per carbonate samples, before ^{14}C-AMS measurements at the spectrometer (Santos and Xu 2016).

Isotopic analyses of $\delta^{13}C$ were performed from ash and ash/charcoal samples at the Earth System Science Research Center, Institute of Geosciences, University Mainz for MAMS-samples (Lindauer et al. 2016) and at the Earth System Science, University of California, Irvine, for the KCCAMS samples. Ash is normally composed of a complex matrix with microscopic sizes of charcoal fractions and carbonaceous minerals (Braadbaart et al. 2012), and therefore can present difficulties in determining their chronology. Thus, the stable isotope ratio mass spectrometer (IRMS) measurements performed here have the intent to draw information concerning the sample carbon source(s) of those materials. While some AMS instruments do provide online-$\delta^{13}C$ values, those are also a product of instrument fractionation and therefore are used solely to correct the ^{14}C data for these effects (Santos 2007, Lindauer and Kromer 2013). At KCCAMS CO_2 aliquots from pre-treated ash and ash/charcoal were recovered after combustion and measured by using a continuous flow stable isotope ratio mass spectrometer (Delta-Plus CFIRMS) interfaced with a Gasbench II (for CO_2 input). Stable isotope results are reported as values in ‰ relative to the Vienna Pee Dee Belemnite (vPDB). Total organic carbon has also been determined by using a Fision NA 1500NC elemental Analyzer from Finegan DeltaPlus IRMS. At the Institute for Geosciences in Mainz the $\delta^{13}C$ of the charcoal sample (MAMS 22875) was measured using a Flash2000 Elementar Analyzer (Thermo) with a Finnigan MAT 253 stable isotope ratio mass spectrometer. Results are reported in the same way as at KKCAMS.

Radiocarbon data are being reported as uncalibrated ages (^{14}C yrs BP) following recommended conventions for the reporting of ^{14}C (Stuvier and Polach 1977). As mentioned before calibrated ages are reported as cal BP. To calibrate the conventional ^{14}C ages we used Oxcal 4.2 with the Intcal13 dataset (Bronk Ramsey and Lee 2013, Reimer et al. 2013). The reservoir effects were modelled for each site separately (KK1 and K4). We used a phase model in Oxcal with undetermined reservoir effect ΔR, as presented in (Zazzo et al. 2016).

4.2.4 Results and Discussion:

Radiocarbon measurements and reservoir effects ΔR

The complete isotopic results are presented inTable 4.2.2. The results for the two mollusc species *A. uropigimelana* and *T. palustris* show a species-specific ΔR, as suggested by Lindauer et al. (2016) with *A. uropigimelana* showing tentatively higher reservoir effects ΔR than *T. palustris* The δ^{13}C measurements of both parts of the KK1 ash layer point to a wooden material (C3 plant) as major carbon component. Therefore, we conclude that their ^{14}C results are suitable to be used as terrestrial analogue for reservoir effect ΔR calculations. Moreover, the younger ^{14}C age range of part of the shell fragments in the KK1 shell midden suggests a second occupation period during later times which is relevant for archaeologists. Hence, we decided to calculate two reservoir effects to account for each timeframe/layer and shell species during the Neolithic.

The reservoir effect ΔR for *A. uropigimelana* declines from 576 ± 90 yrs to 200 ± 30 yrs during the Neolithic. For *T. palustris* the change in ΔR shows a reduction from 389 ± 66 yrs to 172 ± 99 yrs for the same period, e.g. between 7.0 and 6.5 ka cal BP. This corresponds to a change in reservoir effect of more than 350 yrs for *A. uropigimelana* and nearly 200 yrs for *T. palustris* within just 600 yrs (calibrated ages of terrestrial material in Table 4.2.3)

The archaeological site Kalba K4 yielded two time periods as well (3530 and 3420 ^{14}C yrs BP), both matching the Middle Bronze Age. Here we were able to measure distinct charcoal pieces (J 13304), charred date stone (J 13305), and another charcoal sample (UCIAMS171125 & -171126). As the MBZ1 and MBZ2 layers can be clearly distinguished (Fig. 4.2.2 and Fig. 4.2.3), calculating a reservoir effect for this period was much more straightforward.

The Neolithic shell midden KK1 and the sampled Middle Bronze Age archaeological site K4 are apart by nearly 3000 yrs. During this period the reservoir effect ΔR was further reduced to 105 ± 50 yrs (MBZ1) and 112 ± 44 yrs (MBZ2) for *A. uropigimelana*, and -26 ± 46 yrs (MBZ1) and -19 ± 36 yrs (MBZ2) for *T. palustris*, respectively (Table 4.2.2). We found unexpected high shell species-dependency in ΔR.

Table 4.2.2 Individual radiocarbon data on shells and contemporary terrestrial material (ash, charcoal, charred date stone) are shown, including duplicates. The ΔR values represent 2σ probability distributions. Only $\delta^{13}C$ data from IRMS measurements is given. The order of magnitude of the uncertainty of these results is of 0.1‰ based on measurements of multiple standards (e.g. ATP- Atropine, USGS 24-graphite). Samples published in (Lindauer et al 2016) can be recognized by their MAMS code as they had been renamed for consistency.

Site/Layer	Labcode	Sample ID	Material	^{14}C age (yrs BP)	$\delta^{13}C$ (‰)	%C	ΔR (yrs)
KK1	*MAMS 22875*	*KK1 2013 ash*	*Ash*	*6117 ± 26*	*-25.2*	*5.3*	
	MAMS 29217	KK1 2013 Ana2	*A. uropigimelana*	7073 ± 30			***A. uropigimelana 576 ± 90***
	MAMS 22878	KK1 2103 Ana1	*A. uropigimelana*	7058 ± 27			
	MAMS 22876	KK1 2013 Ter1	*T. palustris*	6911 ± 28			
	MAMS 22877	KK1 2013 Ter2	*T. palustris*	6924 ± 27			***T. palustris 389 ± 66***
	UCIAMS171097	KK1 2015 Ter1	*T. palustris*	6870 ± 20	-4.2		
	UCIAMS171098	KK1 2015 Ter2	*T. palustris*	6855 ± 25	-4.5		
	UCIAMS171099	KK1 2015 Ter3	*T. palustris*	6850 ± 20	-4.5		
KK1	*UCIAMS173933*	*KK1 2015 ash*	*Ash*	*5755 ± 20*	*-20.8*	*5.0*	
	UCIAMS173934	*KK1 2015 ash*	*Ash (duplicate)*	*5690 ± 20*	*-20.6*	*5.0*	
	MAMS 22867	KK1 2013 Ana3	*A. uropigimelana*	6295 ± 26			
	MAMS 22880	KK1 2013 Ana4	*A. uropigimelana*	6273 ± 27			
	MAMS 22883	KK1 2013 Ana5	*A. uropigimelana*	6310 ± 26			***A. uropigimelana 200 ± 30***
	MAMS 22885	KK1 2013 Ana6	*A. uropigimelana*	6272 ± 27			
	UCIAMS171094	KK1 2015 Ana1	*A. uropigimelana*	6305 ± 15	-2.4		
	UCIAMS171095	KK1 2015 Ana2	*A. uropigimelana*	6300 ± 20	-1.4		
	UCIAMS171096	KK1 2015 Ana3	*A. uropigimelana*	6295 ± 20	-0.9		
	P 14279	KK1 2015 Ter1	*T. palustris*	6386 ± 28			
	MAMS 22882	KK1 2013 Ter3	*T. palustris*	6257 ± 26			***T. palustris 172 ± 99***
	MAMS 22884	KK1 2013 Ter4	*T. palustris*	6262 ± 26			
K4/MBZ1	*P13304*	*K4 MBZ1 char*	*Charcoal*	*3531 ± 40*			
	P 13305	*K4 MBZ1 DS*	*Date stone*	*3537 ± 35*			
	P 13306	K4 MBZ1 Ana1	*A. uropigimelana*	3954 ± 54			
	P 13307	K4 MBZ1 Ana2	*A. uropigimelana*	3891 ± 35			***A. uropigimelana 105 ± 50***
	P 13308	K4 MBZ1 Ana3	*A. uropigimelana*	3989 ± 38			
	P 13309	K4 MBZ1 Ana4	*A. uropigimelana*	3983 ± 40			
	P 13310	K4 MBZ1 Ana5	*A. uropigimelana*	3976 ± 50			
	P 13311	K4 MBZ1 Ter1	*T. palustris*	3958 ± 42			
	P 13312	K4 MBZ1 Ter2	*T. palustris*	4224 ± 43			
	P 13313	K4 MBZ1 Ter3	*T. palustris*	3764 ± 41			***T. palustris -26 ± 46***
	P 13314	K4 MBZ1 Ter	*T. palustris*	3732 ± 45			
	P 13315	K4 MBZ1 Ter5	*T. palustris*	3845 ± 45			
K4/MBZ2	*UCIAMS171125*	*K4 MBZ2 char*	*Charcoal*	*3425 ± 15*	*-24.0*	*61.0*	
	UCIAMS171126	*K4 MBZ2 char*	*Charcoal (duplicate)*	*3420 ± 15*	*-23.0*		
	UCIAMS171084	K4 MBZ2 Ana1	*A. uropigimelana*	3825 ± 15	-2.1		
	UCIAMS171085	K4 MBZ2 Ana2	*A. uropigimelana*	3835 ± 15	-1.2		***A. uropigimelana 112 ± 44***
	UCIAMS171086	K4 MBZ2 Ana3	*A. uropigimelana*	3830 ± 15	-1.7		
	UCIAMS171087	K4 MBZ2 Ana4	*A. uropigimelana*	3880 ± 15	-1.6		
	UCIAMS171088	K4 MBZ2 Ana5	*A. uropigimelana*	3945 ± 15	-1.4		
	UCIAMS171089	K4 MBZ2 Ter1	*T. palustris*	3690 ± 15	-3.0		
	UCIAMS171090	K4 MBZ2 Ter2	*T. palustris*	3690 ± 15	-4.8		***T. palustris -19 ± 36***
	UCIAMS171091	K4 MBZ2 Ter3	*T. palustris*	3715 ± 20	-3.4		
	UCIAMS171092	K4 MBZ2 Ter4	*T. palustris*	3790 ± 20	-3.8		

Table 4.2.3 Calibrated results of terrestrial samples from Kalba. Calibration was done using Oxcal 4.2 with the IntCal13 dataset.

Labcode	Sample ID	Material	Radiocarbon ages			
			Uncalibrated	Calibrated		
			yrs BP	cal BP (1σ)	cal BP (2σ)	mean cal BP
MAMS 22875	KK1 2013 ash	Ash	6117 ± 26	7146 - 6946	7156 - 6906	7013 ± 69
UCIAMS173933	KK1 2015 ash	Ash	5755 ± 20	6601 - 6499	6634 - 6493	6557 ± 41
UCIAMS173934	KK1 2015 ash	Ash (dup.)	5690 ± 20	6491 - 6445	6508 - 6408	6465 ± 26
P 13304	K4 MBZ1 char	Charcoal	3531 ± 40	3828 - 3714	3854 - 3644	3762 ± 51
P 13305	K4 MBZ1 DS	Date stone	3537 ± 35	3835 - 3721	3868 - 3694	3775 ± 48
UCIAMS171125	K4 MBZ2 char	Charcoal	3425 ± 15	3695 - 3641	3719 - 3632	3671 ± 28
UCIAMS171126	K4 MBZ2 char	Charcoal (dup.)	3420 ± 15	3692 - 3640	3705 - 3614	3667 ± 25

Comparison of the ΔR results with other published data

Zazzo et al. (2016) determined ΔR values based on *A. antiquata* collected at Ras al-Hamra (at the RH6 prehistorical site) located on the east coast of Oman, near Muscat (Fig. 4.2.1, Fig. 4.2.2). Assuming that shell members of the same genus share similar food resources and habitats, we compare our ΔR determinations obtained with the marine species of *A. uropigimelana* with those derived from *A. antiquata* determined in Zazzo et al. (2016). For these comparisons we use our data drawn from the shell midden KK1, e.g. the terrestrial layers collected in 2013 and 2015, which is more or less contemporary to the data at Ras al-Hamra and dated to (see Table 4.2.3) 7013 ± 69 cal BP (MAMS 22875) and 6557 ± 41 cal BP (UCIAMS173933) as well as its duplicate measurement of 6465 ± 26 cal BP (UCIAMS173934) reported in Table 4.2.3. For *A. uropigimelana* we determined a ΔR of 576 ± 90 (±2σ) and 200 ± 30 (±2σ) yrs, respectively. Zazzo et al. (2016) calculated a ΔR of 202 ± 96 (±1σ) yrs for the oldest layer (subunit SU 185, 7077 ± 49 cal BP). For the younger layer (subunit SU 117, 6675 ± 31 cal BP) the ΔR value calculated by Zazzo et al. (2016) is 144 ± 25 (±1σ) yrs. It should be noted that Zazzo et al. (2016) then used the mean ΔR of all layers they had found. For *T. palustris* a direct comparison cannot be done, because no species specific ΔR for this species was determined by Zazzo or anyone else.

While our ΔR determination overlaps within errors with Zazzo et al. (2016) for the KK1 late period, e.g. for the younger layer, the offset between the older layers is significantly different. The difference in ΔR cannot be attributed to underestimation in uncertainties, as we already report our data with ±2σ errors instead of just ± 1σ. Problems with the ^{14}C age determinations from ash samples cannot be evoked either, as our $\delta^{13}C$ values point to charred wood as the dominant carbon source in the ash sample. Furthermore, chemical extractions applied were robust and gave consistent results among duplicates (Table 4.2.2 and Table 4.2.3.). Assuming that the species-dependent variations in ΔR have been somewhat normalized when comparing results obtained with similar shell species, the distinctive ΔR variability presented here must be due to differences in climatic and oceanic conditions between Ras al-Hamra and Kalba sites at around 7000 cal BP (6100 ^{4}C yrs BP).

When we take a look at the ocean currents near Kalba and Ras al-Hamra (see "ocean circulation" and Fig. 4.2.2) we see that both locations are influenced by different ocean circulation patterns. A steep continental margin closer to the shore should favor a more intense upwelling effect near surface at Ras al-Hamra. Thus, at Ras al-Hamra site one may expect higher ΔR determinations at all times. It is possible that the outflow of the Arabian Gulf carries an increased amount of old carbon due to a higher salinity of the Arabian Gulf as an effect of higher temperature and hence higher evaporation rates. The higher salinity leads to an increased dissolution of limestone and carbon from coral reefs and carbonate sediments and hence an enrichment with old carbon. For the Arabian Gulf it was found that high salinity and temperature together with the extreme aridity have led to an extensive development of evaporate minerals like gypsum (Purser 1973) as already mentioned. In addition limestone from the subduction zone around the Straits of Hormuz might be dissolved to some extent when the water flows out. This increases the density of the water body (Purser 1973). This effect might have been stronger during the early Holocene when the sea level at around 6 ka BP was between higher than today and dropped again afterwards (Bernier et al. 1995, Lambeck 1996). As around 7 ka BP the water level was still rising, more water would flow in and out of the Arabian Gulf. If this current carries high amounts of old carbon this may explain the higher ΔR value along the coast of Kalba over the flat part of the ocean floor. The effect of the outflow at the coast near Ras al-Hamra during the same period of time might be reduced due to the drop in depth of the seafloor and therefore sinking of the denser water. These considerations account for the difference between the two locations, but do not explain the change in ΔR over time.

Sea Level and Climate Change reflected in a change of ΔR over time

The temporal change in reservoir effect at Kalba from the Neolithic to Bronze Age is significant, and most importantly very high. From this point, a question arises: Why is there a change in the order of several hundred years? A possible reason for such a dramatic offset must be a strong change in environmental conditions. From the shells ^{14}C results alone it remains unclear whether this change happened abruptly, or whether it happened gradually between the Neolithic and Bronze Age periods. Because a change in reservoir effect reflects a change in environmental conditions we need to take a closer look at the environmental or climate proxies investigated by some colleagues.

To properly evaluate this issue, we cross checked our results with those from other works on paleoclimate records in adjacent regions as can be seen in Fig. 4.2.1. In Fig. 4.2.4 we also highlight the ^{14}C ages of the terrestrial samples associated to our ΔR determinations of the shell midden KK1 and K4 sites in comparison to the data of the other proxies discussed below.

When comparing our data with stalagmite records, those of Hoti Cave are the nearest records. Others stalagmite records that give important information about the periods of interest are those of Qunf Cave (around 600 km south of Hoti), and, further North, Soreq Cave in Israel, southwest of Jerusalem. Regarding stalagmite records, a shift in $\delta^{18}O$ to more positive values is interpreted as a reduction in precipitation and hence a shift to a more arid climate (Preston et al. 2015), whereas changes in $\delta^{13}C$

reflect changes in vegetation type where an enrichment of $\delta^{13}C$ points to an increase in C_4 plants to the soil CO_2 (Bar-Matthews and Ayalon 2004).

Hoti Cave does not show a continuous record throughout the entire Holocene and shows a hiatus between 2.5-5.2 ka BP (Fleitmann et al. 2007). Drier periods were recorded for example from 7.5 to 7.2 ka cal BP and from 6.5 to 6.3 ka cal BP, and were less distinct from 5.9 to 5.3 ka BP. This shift in $\delta^{18}O$ is interpreted as a southward retreat of the ITCZ (Intertropical convergence zone) and the monsoon rain, followed by a replacement from the southern to a northern moisture source as well as a change in the seasonality of precipitation from summer to winter precipitation (Fleitmann et al. 2007). This coincides with our change in reservoir effect at the shell midden site and its continued influence until at least the duration of the Kalba K4 settlement, as can be seen in Fig. 4.2.4.

Qunf Cave however, further south of Kalba, still appeared to be under the influence of the ITCZ after 6.3 ka cal BP. Its $\delta^{18}O$ signature gradually decreased about 2‰ between 9 ka and 3 ka cal BP. For Qunf Cave climate conditions were different than for Hoti and hence also for Kalba as the monsoon influenced this cave throughout the Holocene bringing enough rain to support it with drip water for the stalagmite growth and therefore Qunf cave can only give a rough estimate to the environmental conditions influencing the northern region, but shows stronger changes parallel to our shell midden data.

Soreq Cave, although being quite some distance further north of Kalba, shows significant features of its $\delta^{18}O$ and especially its $\delta^{13}C$ signatures. Between 8.5 and 7.0 ka cal BP the $\delta^{13}C$ data seems anomalously high whereas the $\delta^{18}O$ only shows a gradual increase. Apart from the strong $\delta^{13}C$ event around 8.2 ka cal BP, equivalent to the global cooling event, there are two major changes observed in the data. One is a short pulse in $\delta^{18}O$ around 5.2 ka cal BP accompanied by a decrease in $\delta^{13}C$. The second, is an increase in $\delta^{18}O$ and $\delta^{13}C$ during a period of several hundred years between 4.6 and 4.0 ka cal BP which is interpreted as an increase in C_4 vegetation by Bar-Matthews and Ayalon (2004). Anomalously high $\delta^{13}C$ values are here interpreted as increased atmospheric CO_2 signal (Bar-Matthews and Ayalon 2004). The second high $\delta^{13}C$ peak around 7ka BP coincides with our oldest shell midden data whereas the younger shell midden data lies on the plateau following this peak. The $\delta^{18}O$ data is rather unspecific at Soreq during these periods which indicates rather constant water sources (precipitation), maybe due to the Westerlies.

The Dead Sea lake level record seems to corroborate the data from Soreq Cave nearby with stronger features as in the stalagmite records. It seems that the high $\delta^{13}C$ values of Soreq Cave here are contemporary with a drop in water level of the Dead Sea. We have a slow water level rise starting around 6-7 ka cal BP and a final significant rise in lake level just around our K4 MBZ data until about 3500 ka cal BP (Fig. 4.2.4), followed by a drastic drop in lake level at the Dead Sea. This supports our finds that our changes in reservoir effect are local but may be linked to changing climates on a larger scale.

The increasing aridity visualized in the hiatus of Hoti can also be seen in the drying out of paleolake sites such as Awafi and Wahalah in the UAE (Fig. 4.2.1) as well as the correlated dune development of the Rub al-Khali. Awafi lake shows a reduced detrital sediment input in the period between 7.6 and 6.4 ka cal BP, which is less pronounced in Wahalah lake further southwest (Parker et al. 2016). But both show a significant increase in detrital flux after this time reflected in an increase in the Titanium signal. Here Wahalah lake shows an earlier Titanium and detrital flux signal around 5.9 to 5.2 ka cal BP than

Awafi which shows a slow increase between 6.0 and 5.4 ka cal BP followed by a sudden increase until 5.0 ka cal BP (Parker et al. 2016). Both lakes show only minor differences which can be attributed to local effects, but are consistent in the overall pattern, reflecting a change in precipitation as a consequence of a disconnection from the southerly summer rainfall and an increase in sedimentation due to the following increased aridity of the area. This is well in accordance with the interpretation from the stalagmite records and marks the beginning of a landscape reconfiguration (Parker et al. 2016). The deposition of Aeolian sand in Awafi around 4 ka cal BP marks the period of total desiccation. Changes around 4 ka cal BP can be found in several of the paleoclimate records throughout the Arabian Peninsula (Arz et al. 2006, Parker et al. 2016), but also in other regions influenced by the monsoon (Staubwasser et al. 2003, Parker et al. 2016). The periods mentioned above (5.9 ka, 4.3-3.9 ka) are amongst the periods correlated with rapid climate change and characterized by reduced temperature, increased aridity, major changes in atmospheric circulation and monsoon activity as identified by several scientists (Mayewski et al. 2004, Parker et al. 2016). These climatic effects and the increase in aridity can also be seen in the marine records that have been analyzed by several authors and might be mirrored in a decrease of local marine reservoir effect ΔR.

The marine records as investigated by (Sirocko et al. 1993, Staubwasser et al. 2002) show increased Fe (iron) values at times of greater Aeolian input. The signal is less distinct, e.g. in core 74KL Arabian Sea, or in core M5 422 from the Gulf of Oman, and times of increased input can be clearly distinguished and correspond to times of changes in the lake records as well as the stalagmite data (Parker et al. 2016). As the Arabian Sea sediment cores show less distinct features we can only use the overall patterns that can be distinguished, but they also support our finds of a reduction in reservoir effect due to a change in ocean water. The increased input from aeolian sediment reflects a drier environment (more sediment available due to increased aridity) and possibly also a reduced sea level, especially in the Arabian Gulf, which might be partially due to a lack of freshwater input.

At first sight, the younger ash data from the shell midden KK1 (5755 ± 20 yrs BP; UCIAMS173933) for which we derived a ΔR (*A. uropigimelana*) of 200 ± 30 (±2σ) years and 172 ± 99 for *T. palustris* seems to fit perfectly with the $\delta^{18}O$ drop in Hoti Cave. The larger ΔR of 576 ± 90 (±2σ) and 389 ± 66 yrs for *A. uropigimelana* and *T. palustris* respectively at 6117 ± 26 yrs BP (MAMS 22875) seems to coincide with a drop in $\delta^{13}C$ at Soreq cave in Jerusalem, Israel, pointing to a wet period contemporaneous with a higher sea level at the Arabian Gulf as we had discussed in section “comparison of ΔR results”. This seems to be a rather wide spread than just a local phenomenon.

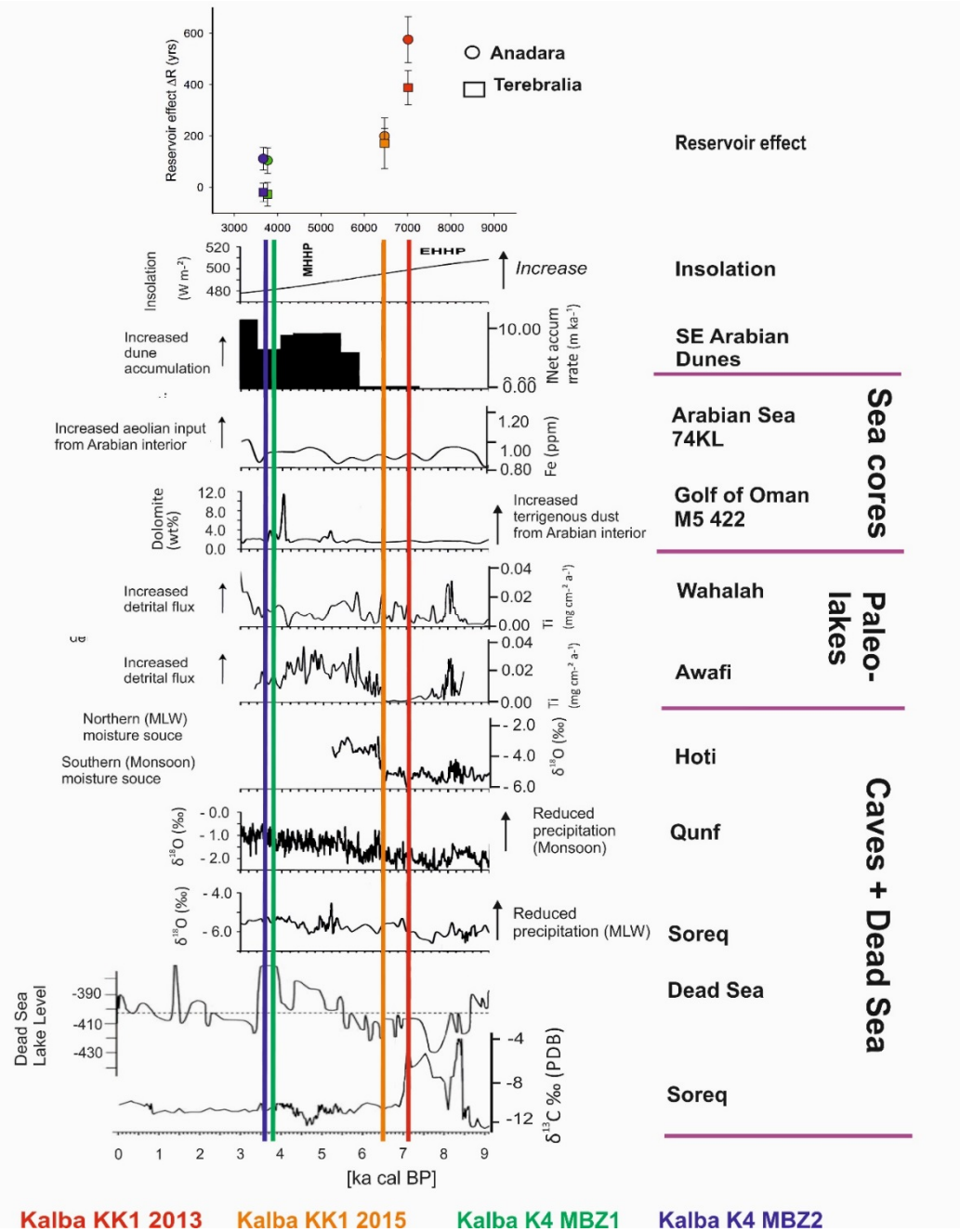

Fig. 4.2.4 Comparison of climate proxies, here stalagmites of Oman (Hoti Cave, Qunf Cave) and the Dead Sea lake level, plus Soreq cave in Israel as well as paleolakes in the UAE and sediment cores from the Arabian Sea with calculated reservoir effects. Combined and modified from (Parker et al. 2016) and (Weninger et al. 2009). The periods represented by our data are also shown as colored solid lines and labeled accordingly. Additionally the species specific reservoir effects are plotted on top for comparison.

Local effects also contribute to the way the environmental signal is stored in the proxies of interest. Coastal morphology not only is influenced by marine events, but also by the way sediments, marine as well as aeolian or fluvial, are accumulated in estuarine basins. (Al-Farraj 2005) explains the development of sabkhas and estuarine environments in the light of coastal events, sea level change, and terrestrial sediment transport culminating in supratidal salty, dry sabkha, where once mangrove forest was found. This must also be kept in mind for interpretation of the development of the lagoon in Kalba, which also includes a large sabkha up to the shell midden KK1 that lies around 2 m higher than the sea

level today. Mangrove habitats over time have been investigated by (Berger et al. 2013) for the coast of Oman. The authors here describe several phases of mangrove development in Oman during the Holocene with respect to sea level and human settlements. During a phase between 5500-4800 cal BC (around 6.1 ka ^{14}C yrs BP), which is comparable to phase one at the shell midden KK1, they describe a sea level similar to today This also marks a phase of reduced sea level rise after deglaciation.

The next phase, 4800-4400 cal BC (around 5.8 ka ^{14}C yrs BP) is described as optimum for mangrove development around the complete Arabian Sea documented in the amount of shells found in the archaeological sites pointing to extensive exploitation and interpreted as correlated to a higher sea level along the coasts of Oman, followed by a phase of fluctuations in sea level between 4400-3900 cal BC, around 5.5 ka ^{14}C yrs BP, (Berger et al. 2013). This phase points to a decrease of spread of mangroves due to a decrease in sea level recorded in the Arabian Gulf and the Arabian Sea accompanied by an abrupt climate change recorded in the Hoti Cave stalagmites. Besides the reduction in terrestrial freshwater input due to reduced precipitation would have an important effect on this ecosystem. Towards the end of this period the sea level rises again, but only for a short period of time, followed by a drop in sea level and a further decrease of mangroves. The next period between 3800-3500 cal BC (around 5.4 ka ^{14}C yrs BP) is described as a second optimum for mangrove development (Berger et al. 2013) with a high sea level in the Arabian Gulf and the northern Gulf of Oman, although less extensive than the previous one. The next phase, 3500-3000 cal BC (ca. 5.2 ka ^{14}C yrs BP), is again described by a lack of mangrove data pointing to a decrease in mangroves and sea level as well as to an increase in aridity. Hence Berger et al (2013) interpret their data as evidence of past lagoon and mangrove extension during maximum sea level rise and high fluvial activity during the early to mid-Holocene.

The sea level itself is not only dependent on climatic conditions but also on tectonic events such as subduction. Along the Straits of Hormuz we find the Makran Subduction zone which marks the line where the Arabian plate subducts under the Eurasian plate. North of the Dibba zone the peninsula is subducting whereas south of it the Hajar mountains are rising (Hoffmann et al. 2013, Hoffmann et al. 2015). This might lead to erroneous interpretations about sea levels along the coasts of the Gulf of Oman and the Arabian Gulf. For example storm or tsunami events flood the areas of settlements and do not indicate a change in sea level, but can be linked to tsunamis, as found at Ras al-Hadd, south of Muscat (Hoffmann et al. 2015). Here a flooding event took place at around 4450 ± 200 cal BP, most probably due to a tsunami caused by an earthquake along the Makran Subduction Zone. The upwelling of old ^{14}C-depleted carbon in the Arabian Sea is only of minor influence at Kalba as it mainly takes place along the southern coast of Oman or along the coast of India and Iran. Kalba is basically seasonally influenced by the outflow of Arabian Gulf deep waters (see Fig. 4.2.2), as well as from inflow from the Arabian Sea. This leads to a stronger dependence on effects of Arabian Gulf waters and their carbonate contents as discussed in section “comparison of ΔR results”. A reduced water body in the Arabian Gulf or an increase of seafloor height (probably caused by subduction of the mountainous regions of the Musandam peninsula) reduces the amount of water flowing out through the Straits of Hormuz as well as the inflow from the Gulf of Oman. A reduction of outflow probably results in less dissolved old carbon flowing past the beaches of Kalba and reducing the reservoir effect further during the MBZ compared to the Neolithic period. A reduction of Arabian Gulf water coincides also with increasing aridity

and hence reduced freshwater input from wadis after rainfall. Depending on the Geology the freshwater input can carry depleted ^{14}C waters, hence this resource needs further investigation and will therefore not be included in the discussion so far.

All the climatic information as well as tectonics and local effects lead us to the interpretation that the reduction of the ΔR over time is a reflection of the change in climate including oceanic conditions, overlapped by a species specific difference in ΔR due to food resources and habitat, as suggested by (Lindauer et al. 2016).

4.2.5 Conclusions:

Lindauer et al. (2016) had already shown that shell species under investigation are influenced by dietary habits as well as environmental conditions, which can impact local ΔR determinations. Here, we go a step further and correlate local ΔR determinations to paleoproxy data, allowing us to better interpret our change in reservoir effect as a reflection of the climate changes with a reduction of in ΔR due to decreasing sea level and increasing sedimentation rate in the lagoon close to Kalba. The two opposing factors would affect the mangrove and eventually its local environment, as described by (Al-Farraj 2005). In this extended research we are able to extend the species specific dependency of the reservoir effect also to younger timescales. Although the difference decreases between Neolithic and Bronze Age it remains significant which can be explained by the influences of habitat and food resource. Especially *A. uropigimelana* drops dramatically in ΔR which could reflect the decrease of old carbon in the ocean water. *T. palustris* on the other hand is strongly influenced by atmospheric carbon due to its feeding on mangrove leaf litter, whereas *A. uropigimelana* is a filter feeder strongly dependent on marine carbon sources.

At Kalba, paired terrestrial/shell ^{14}C data of bivalve *Anadara uropigimelana* and gastropod *Terebralia palustris* show species-specific local reservoir effects with consistently higher values derived from *Anadara uropigimelana*. In addition, we could show that the reservoir effect from both species decreases significantly between Neolithic and Middle Bronze Age. Once our Neolithic ΔR determinations were compared with those further south in Oman, we observed significant differences. Our ΔR values are at least 100 years higher, which can be explained by local ocean circulation patterns and lagoon shoreline development.

Regarding other paleoclimate proxies in the vicinity of the studied area, our data fits well with changes observed in stalagmite records and paleolakes as well as sediment cores from the Arabian Sea. While for the Neolithic period ΔR assessment yield us values of 576 ± 90 years for *A.uropigimelana* and 389 ± 66 years for *T. palustris*, respectively, a decrease to 112 ± 44 and -19 ± 36 years were observed from the same species during the Bronze Age. The discontinuity of our data from 7 ka cal BP to 3 ka cal BP can be regarded as a result of all the climate events that took place during this period, and which are reflected in the data of paleoproxies discussed here. Nevertheless, it appears that those same climatic and sea level changes are mirrored in the reservoir effect changes we observed in our ^{14}C shells over time. Species specific differences remain significant over time although with a decreasing tendency

probably due to stronger changes of carbon content in food resources and habitat for *A. uropigimelana* than for *T. palustris*

The mangrove of Khor Kalba shows exceptionally well how the marine and the terrestrial influences on an estuarine system overlap and take action. We see the results in the reservoir effects of the different shell species, reflecting different pathways of influence through food resource and habitat and including minor, hence local, as well as major climatic influences to describe the situation over a certain period of time.

Acknowledgements:

Bastian Schneider kindly provided help with the map including bathymetric and elevation data. We thank the German Research Foundation for partly funding the radiocarbon age determinations (HI 643/19-1). Adrian Parker helped a lot with improving the manuscript. We are grateful to Gösta Hoffmann for reviewing the manuscript.

4.2.6 References:

Al-Farraj, A. (2005). An evolutionary model for sabkha development on the north coast of the UAE. *Journal of Arid Environments* 63: 740-755.

Arz, H. W., F. Lamy and J. Pätzold (2006). A pronounced dry event recorded around 4.2 ka in brine sediments from the northern Red Sea. *Quaternary Research* 66(3): 432-441.

Ascough, P. L., G. T. Cook, A. J. Dugmore, E. M. Scott and S. T. Freeman (2005). Influence of Mollusc Species on Marine ΔR Determinations. *Radiocarbon* 47(3): 433-440.

Bar-Matthews, M. and A. Ayalon (2004). Speleothems as palaeoclimate indicators, a case study from Soreq Cave located in the Eastern Mediterranean Region, Israel. Past climate variability through Europe and Africa, Springer**:** 363-391.

Berger, J. F., V. Charpentier, R. Crassard, C. Martin, G. Davtian and J. A. López-Sáez (2013). The dynamics of mangrove ecosystems, changes in sea level and the strategies of Neolithic settlements along the coast of Oman (6000-3000 cal. BC). *Journal of Archaeological Science* 40: 3087-3104.

Bernier, P., R. Dalongeville, B. Dupuis and V. de Medwecki (1995). Holocene shoreline variations in the Persian Gulf: Example of the Umm al-Qowayn lagoon (UAE). *Quaternary International* 29–30: 95-103.

Beverly, R. K., W. Beaumont, D. Tauz, K. M. Ormsby, K. F. Von Reden, G. M. Santos and J. R. Southon (2010). The Keck Carbon Cycle AMS Laboratory, University of California, Irvine: status report. *Radiocarbon* 52(2): 301-309.

Braadbaart, F., I. Poole, H. D. J. Huisman and B. van Os (2012). Fuel, Fire and Heat: an experimental approach to highlight the potential of studying ash and char remains from archaeological contexts. *Journal of Archaeological Science* 39(4): 836-847.

Bronk Ramsey, C. and S. Lee (2013). Recent and Planned Developments of the Program OxCal.

Culleton, B. J., D. J. Kennett, B. L. Ingram, J. M. Erlandson and J. R. Southon (2006). Intrashell Radiocarbon Variability in Marine Molluscs. *Radiocarbon* 48(3): 387-400.

Dalongeville, R. and P. Sanlaville (2005). L'évolution des espaces littoraux du golfe Persique et du golfe d'Oman depuis la phase finale de la transgression post-glaciaire. *Paléorient* 31(1): 9-26.

Dutta, K. (2008). Marine ^{14}C Reservoir Age and Suess Effect in the Indian Ocean. *Journal of Earth Science India* I(III): 175-188.

Enzel, Y., Y. Kushnir and J. Quade (2015). The middle Holocene climatic records from Arabia: Reassessing lacustrine environments, shift of ITCZ in Arabian Sea, and impacts of the southwest Indian and African monsoons. *Global and Planetary Change* 129: 69-91.

Fleitmann, D., S. J. Burns, A. Mangini, M. Mudelsee, J. Kramers, I. Villa, U. Neff, A. A. Al-Subbary, A. Buettner, D. Hippler and A. Matter (2007). Holocene ITCZ and Indian monsoon dynamics recorded in stalagmites from Oman and Yemen (Socotra). *Quaternary Science Reviews* 26(1â€“2): 170-188.

Fleitmann, D. and A. Matter (2009). The speleothem record of climate variability in Southern Arabia. *Comptes Rendus Geoscience* 341(8-9): 633-642.

Hoffmann, G., C. Grützner, K. Reicherter and F. Preusser (2015). Geo-archaeological evidence for a Holocene extreme flooding event within the Arabian Sea (Ras al Hadd, Oman). *Quaternary Science Reviews* 113: 123-133.

Hoffmann, G., M. Rupprechter and C. Mayrhofer (2013). Review of the long-term coastal evolution of North Oman: subsidence versus uplift [Review der langfristigen Küstenentwicklung Nordomans - Senkung und Hebung]. *Zeitschrift der Deutschen Gesellschaft für Geowissenschaften* 164(2): 237-252.

Johns, W. E., G. A. Jacobs, J. C. Kindle, S. P. Murray and M. Carron (2000). Arabian marginal seas and gulfs. Technical Report 2000-01, University of Miami RSMAS**:** 60.

Kromer, B., S. Lindauer, H.-A. Synal and L. Wacker (2013). MAMS - A new AMS facility at the Curt-Engelhorn-Centre for Achaeometry, Mannheim, Germany. *Nuclear Instruments and Methods in Physics Research Section B: Beam Interactions with Materials and Atoms* 294(0): 11-13.

Kutterer, A. U., S. Doppler, M. Uerpmann and H.-P. Uerpmann (2012). Neolithic cremation in south-east Arabia: archaeological and anthropological observations at FAY- NE10 in the Emirate of Sharjah (UAE). Arabian Archaeology & Epigraphy, Wiley-Blackwell. **23:** 125-144.

Lambeck, K. (1996). Shoreline reconstructions for the Persian Gulf since the last glacial maximum. *Earth and Planetary Science Letters* 142(1â€“2): 43-57.

Lambeck, K., A. Purcell, N. C. Flemming, C. Vita-Finzi, A. M. Alsharekh and G. N. Bailey (2011). Sea level and shoreline reconstructions for the Red Sea: isostatic and tectonic considerations and implications for hominin migration out of Africa. *Quaternary Science Reviews* 30(25–26): 3542-3574.

Leuschner, D. C. and F. Sirocko (2003). Orbital insolation forcing of the Indian Monsoon â€“ a motor for global climate changes? *Palaeogeography, Palaeoclimatology, Palaeoecology* 197(1â€“2): 83-95.

Lindauer, S. and B. Kromer (2013). Carbonate Sample Preparation for ^{14}C Dating Using an Elemental Analyzer. *Radiocarbon* 55(2-3): 364-372.

Lindauer, S., S. Marali, B. R. Schöne, H.-P. Uerpmann, B. Kromer and M. Hinderer (2016). Investigating the Local Reservoir Age and Stable Isotopes of Shells from Southeast Arabia. *Radiocarbon* 59(2): 355-372.

Mayewski, P. A., E. E. Rohling, J. Curt Stager, W. Karlén, K. A. Maasch, L. David Meeker, E. A. Meyerson, F. Gasse, S. van Kreveld, K. Holmgren, J. Lee-Thorp, G. Rosqvist, F. Rack, M. Staubwasser, R. R. Schneider and E. J. Steig (2004). Holocene climate variability. *Quaternary Research* 62(3): 243-255.

Migowski, C., M. Stein, S. Prasad, J. F. W. Negendank and A. Agnon (2006). Holocene Climate Variability and Cultural Evolution in the Near East from the Dead Sea Sedimentary Record. *Quaternary Research* 66(3): 421-431.

Parker, A., C. Davies and T. Wilkinson (2006a). The early to mid-Holocene moist period in Arabia: some recent evidence from lacustrine sequences in eastern and south-western Arabia. *Proceedings of the Seminar for Arabian Studies* 36: 243-255.

Parker, A. G., A. S. Goudie, S. Stokes, K. White, M. J. Hodson, M. Manning and D. Kennet (2006b). A record of Holocene climate change from lake geochemical analyses in southeastern Arabia. *Quaternary Research* 66: 465-476.

Parker, A. G., G. W. Preston, A. Parton, H. Walkington, P. E. Jardine, M. J. Leng and M. J. Hodson (2016). Low-latitude Holocene hydroclimate derived from lake sediment flux and geochemistry. *Journal of Quaternary Science* 31(4): 286-299.

Phillips, C. S. and C. E. Mosseri-Marlio (2002). Sustaining Change: The Emerging Picture of the Neolithic to Iron Age Subsistence Economy at Kalba, Sharjah Emirate, UAE. Fifth International Symposium on the Archaeozoology of southwestern Asia and adjacent areas, Amman, Jordan, ARC-Publicaties Groningen.

Preston, G. W., D. S. G. Thomas, A. S. Goudie, O. A. C. Atkinson, M. J. Leng, M. J. Hodson, H. Walkington, V. Charpentier, S. Méry, F. Borgi and A. G. Parker (2015). A multi-proxy analysis of the Holocene humid phase from the United Arab Emirates and its implications for southeast Arabia's Neolithic populations. *Quaternary International* 382: 277-292.

Purser, B. H. (1973). The Persian Gulf : Holocene carbonate sedimentation and diagenesis in a shallow epicontinental sea / edited by B.H. Purser. Berlin, Springer-Verlag.

Reimer, P. J., E. Bard, A. Bayliss, J. W. Beck, P. G. Blackwell, C. Bronk Ramsey, C. E. Buck, H. Cheng, R. L. Edwards, M. Friedrich, P. M. Grootes, T. P. Guilderson, H. Haflidason, I. Hajdas, C. Hatté, T. J. Heaton, D. L. Hoffmann, A. G. Hogg, K. A. Hughen, K. F. Kaiser, B. Kromer, S. W. Manning, M. Niu, R. W. Reimer, D. A. Richards, E. M. Scott, J. R. Southon, R. A. Staff, C. S. M. Turney and J. van der Plicht (2013). IntCal13 and Marine13 Radiocarbon Age Calibration Curves 0–50,000 Years cal BP.

Santos, G. M. and K. Ormsby (2013). Behavioral Variability in ABA Chemical Pretreatment Close to the 14C Age Limit. *Radiocarbon* 55(2-3): 534-544.

Santos, G. M., J. R. Southon, K. C. Druffel-Rodriguez, S. Griffin and M. Mazon (2004). Magnesium perchlorate as an alternative water trap in AMS graphite sample preparation: a report on sample preparation at KCCAMS at the University of California, Irvine. *radiocarbon46* 1(165-173).

Santos, G. M. and X. Xu (2016). Bag of Tricks: A Set of Techniques and other Resources to Help 14C Laboratory Setup, Sample Processing, and Beyond. *Radiocarbon* FirstView: 1-17.

Santos, G. M. M., R B; Southon, J R; Griffin, S; Hinger, E; Zhang, D. (2007). AMS 14C Sample Preparation at the KCCAMS/UCI Facility: Status Report and Performance of Small Samples. *Radiocarbon* 49(2): 255-269.

Schneider, B., G. Hoffmann and K. Reicherter (2016). Scenario-based tsunami risk assessment using a static flooding approach and high-resolution digital elevation data: An example from Muscat in Oman. *Global and Planetary Change* 139: 183-194.

Sirocko, F., M. Sarnthein, H. Erlenkeuser and e. al. (1993). Century scale events in monsoonal climate over the past 24,000 years. *Nature* 364: 322-324.

Southon, J., M. Kashgarian, M. Fontugne, B. Metivier and W. W.-S. Yim (2002). Marine Reservoir Corrections for the Indian Ocean and Southeast Asia. *Radiocarbon* 44(1): 167-180.

Staubwasser, M., F. Sirocko, P. M. Grootes and H. Erlenkeuser (2002). South Asian monsoon climate change and radiocarbon in the Arabian Sea during early and middle Holocene. *Paleoceanography* 17(4): 1063.

Staubwasser, M., F. Sirocko, P. M. Grootes and M. Segl (2003). Climate change at the 4.2 ka BP termination of the Indus valley civilization and Holocene south Asian monsoon variability. *Geophysical Research Letters* 30(8): n/a-n/a.

Steinhof, A., G. Adamiec, G. Gleixner, G. J. van Klinken and T. Wagner (2004). The New 14C Analysis Laboratory in Jena, Germany. *Radiocarbon* 46(1): 51-58.

Uerpmann, H.-P., M. Uerpmann, M. Hinderer, S. Lindauer, C. Neureiter, R. Ghukasyan, S. Kesejyan and A. Petrosyan (submitted). HLO1-South: An Early Neolithic Site in the Wadi al-Hilo (Sharjah, UAE). *Arabian Archaeology and Epigraphy*.

Van Rampelbergh, M., D. Fleitmann, S. Verheyden, H. Cheng, L. Edwards, P. De Geest, D. De Vleeschouwer, S. J. Burns, A. Matter, P. Claeys and E. Keppens (2013). Mid- to late Holocene Indian

Ocean Monsoon variability recorded in four speleothems from Socotra Island, Yemen. *Quaternary Science Reviews* 65: 129-142.

Wacker, L., R. H. Fülöp, I. Hajdas, M. Molnár and J. Rethemeyer (2013). A novel approach to process carbonate samples for radiocarbon measurements with helium carrier gas. *Nuclear Instruments and Methods in Physics Research Section B: Beam Interactions with Materials and Atoms* 294(0): 214-217.

Weninger, B., L. Clare, E. Rohling, O. Bar-Yosef, U. Boehner, M. Budja, M. Bundschuh, A. Feurdean, H. G. Gebe, O. Joeris, J. Lindstaedter, P. Mayewski, T. Muehlenbruch, A. Reingruber, G. Rollefson, D. Schyle, L. Thissen, H. Todorova and C. Zielhofer (2009). The impact of rapid climate change on prehistoric societies during the Holocene in the Eastern Mediterranean. *Documenta Praehistorica* 36: 7-59.

Zazzo, A., O. Munoz, E. Badel, I. Béguier, F. Genchi and L. G. Marcucci (2016). A Revised Radiocarbon Chronology of the Aceramic Shell Midden of Ra's Al-Hamra 6 (Muscat, Sultanate of Oman): Implication For Occupational Sequence, Marine Reservoir Age, and Human Mobility. *Radiocarbon* 58(2): 383-395.

Zazzo, A., O. Munoz, J. F. Saliège and C. Moreau (2012). Variability in the marine radiocarbon reservoir effect in Muscat (Sultanate of Oman) during the 4th millennium BC: reflection of taphonomy or environment? *Journal of Archaeological Science* 39(7): 2559-2567.

4.3 Highly Resolved Radiocarbon Measurements on Shells from Kalba, UAE, using Carbonate Handling System and Gas Ion Source with MICADAS

Susanne Lindauer [a,b], Ronny Friedrich [a], Robin van Gyseghem [a], Bernd R. Schöne [c], Matthias Hinderer [b]

[a] Curt-Engelhorn-Center Archaeometry, C4, 8, 68159 Mannheim, Germany

[b] Institute of Applied Geosciences, Technical University Darmstadt, Schnittspahnstr. 9, 64287 Darmstadt, Germany

[c] Institute of Geosciences, University of Mainz, Joh.-J.-Becherweg 21, 55128 Mainz, Germany.

Contributions: SL collected the samples, drilles the subsamples, designed the study and wrote the paper, RvG and SL prepared the samples and standardsfor measurement,BRS adviced the drilling and provided sample containers and drills, MH supervised the study, RF tuned the AMS and helped with the measurements and calculations of cross-contamination.

Citation: Lindauer, S., Friedrich, R., van Gyseghem, R., Schöne, B.R., Hinderer, M., 2018a. Highly-resolved radiocarbon measurements on shells from Kalba, UAE, using carbonate handling system and gas ion source with MICADAS. *Nuclear Instruments and Methods in Physics Research Section B: Beam Interactions with Materials and Atoms* in press.

4.3.1 Abstract:

The Mini Carbon Dating System (MICADAS) represents a flexible AMS system for measuring radiocarbon samples either in the form of graphite or CO_2 gas. We used the possibility to attach a carbonate handling system (CHS) to the gas ion source (GIS) to measure smaller amounts of carbonates (< 500 µg) than is usually required for graphite samples (1 mg). We determined a blank correction for different sample sizes ($F^{14}C$ ranging from ~ 0.0045 to ~ 0.017) from graphs. The use of OXA II as solid target and as gas fed through the GIS is presented. Cross-contamination is detected to be in the range of ~6%, but depends on the sample size and ^{14}C content of the previous sample. Our system delivers reliable data

for sample sizes down to 30 µg C when enough blanks (here > 3) are used to clean the system. We tested the CHS-GIS combination on heated and unheated archaeological shells of *Anadara uropigimelana* from Kalba, Sharjah Emirate, United Arab Emirates (UAE). Even though the amount of carbon in the samples was small (4 – 22 µg C) the performance of the CO_2 dating system permits the comparison of trends in the ^{14}C data to stable isotope measurements ($\delta^{18}O$ and $\delta^{13}C$). With 10 – 20 µg C, however, our sample sizes were too small, suffering from cross-contamination and elevated blanks, and our blank samples prior to the small samples were not enough. Hence, an interpretation in combination with the stable isotope data was not possible beyond comparison of trends.

Keywords: Radiocarbon, Gas Ion Source, Carbonate Handling System, AMS, Shells, Stable Isotopes.

4.3.2 Introduction:

Mollusc shells are often used for radiocarbon dating, especially to answer archaeological questions regarding chronologies when no organic material is preserved (Uerpmann 1990, Biagi 1994, Magee et al. 2009). Interdisciplinary studies have revealed that shells can also contribute to modern climate studies and serve as paleoclimate archives (Boivin and Fuller 2009, Butler et al. 2010, Azzoug et al. 2012, Hallmann et al. 2013, Lindauer et al. 2017). In this context, sclerochronolgy including shell growth patterns, element analyses and stable isotopes provides an important tool to gain information about life history of the animal and environmental conditions that occurred during its lifetime such as salinity, freshwater inflow, changes in temperature of the seawater, and food resources to name but a few (Shirai et al. 2014, Lindauer et al. 2016, Colonese et al. 2017, Prendergast et al. 2017).

Combining radiocarbon, sclerochronology and stable isotope data, sheds light on local environmental effects and changes in these over time. The change in $\delta^{18}O$ for example often shows a periodicity which reflects seasonal changes in temperature and salinity over the lifespan of the mollusc (Lindauer et al. 2016). A change of 1‰ in $\delta^{18}O$ corresponds to a temperature change of ca. 4°C (Leng 2006, Leng and Lewis 2016). Therefore, knowing the seasonal and inter-annual amplitudes of environmental variables allows us to derive a temperature range for the site. The $\delta^{13}C$ signal on the other hand depends on different sources including food resources and changes in water composition. Freshwater input can change the $\delta^{13}C$ significantly if the freshwater carries a lot of carbonate, e.g., when it flows through limestone-rich areas and manages to dissolve some of the limestone (Ascough 2010, Keaveney and Reimer 2012). Hence the interpretation of this signal is not straightforward as it might overlap with different or changing food resources at the same time. As most of the carbon responsible for the $\delta^{13}C$ should have the same origin as ^{14}C in the shell, measuring radiocarbon along the shell might help to better interpret $\delta^{13}C$ data. The same origin here can represent different influences on the respective signal. For example, old carbon brought in from limestone, possibly dissolved in freshwater, will shift $\delta^{13}C$ towards more positive values, but at the same time will be depleted in radiocarbon, hence shifting the signal towards older ages. In other studies, an enrichment in $\delta^{13}C$ in algae and cyanobacteria - a food resource for molluscs - during summer months compared to winter months has been reported (Ng et al. 2007).

Measuring radiocarbon along the growth axis of the shell was done for three purposes: a) to take a closer look at whether we can measure samples of 20 µg C or less and will the measurement still yield reliable results suitable for interpretation; b) to determine the blank level and cross-contamination effects in the CHS-GIS combination; c) as an application to determine the variation and amplitude of ^{14}C throughout the lifespan of *Anadara uropigimelana.* from this lagoon (here Kalba, UAE) and to investigate whether highly resolved measurements can clarify the origin of the $\delta^{13}C$ signal of samples in this area.

4.3.3 MICADAS, Gas Ion Source (GIS) and Carbonate Handling System (CHS)

The MICADAS AMS system, installed at Curt-Engelhorn-Centre for Archaeometry (CEZA) since 2009, is described in detail by several authors (Synal et al. 2007, Schulze-König et al. 2010, Kromer et al. 2013). The hybrid Cs sputter source facilitates the measurement of both graphite targets and gaseous CO_2 samples (Fahrni et al. 2013, Wacker et al. 2013). Gaseous measurements are performed by means of the gas interface (GIS) at CEZA since 2014. Detailed information about the MICADAS gas ion source in general is described in (Fahrni et al. 2013). For samples measured as graphite (typically 1 mg C) the measurement time per target varies from 30 to 60 minutes depending on the required precision. The ^{12}C current is measured at the low energy end and usually reaches around 35-50 µA for graphite measurements.

The GIS can be coupled to several CO_2 sources including an elemental analyzer (EA), a carbonate handling system (CHS), a cracker for the direct analysis of gas ampoules, as well as the possibility to attach an isotope ratio mass spectrometer (IRMS) (Wacker et al. 2013, Bard et al. 2015, McIntyre et al. 2016). The GIS using the cracker system was successfully applied at CEZA for small amounts of CO_2 (down to 3 µg C) extracted from ice cores (Hoffmann et al. 2017). In their publication, Hoffmann and co-workers found that the efficiency and therefore the counting statistics strongly depend on the CO_2 mass flow to the surface of the titanium target. This can be adjusted by regulating the pressure of the syringe and the amount of CO_2 in the helium flow at a certain Cesium temperature (usually around 160-170 °C for GIS measurement). A mixture of 2.7 - 4% CO_2 in Helium at a syringe pressure between 1600 to 1800 mbar seems to be ideal for measurements with the MICADAS. This results in a ^{12}C current of 8-12 µA at the low energy side of the accelerator. Blank values from a CO2 gas tank were noted as $F^{14}C$ (0.0081 ± 0.0027), which corresponds to 36,000 to 42,000 years BP. More information about the performance of the cracker has already been reported by Hoffmann et al. (2017).

In this study we have used the CHS system for the carbonates connected to the GIS which allowed us to also produce a mixture of 4% CO_2 in helium and regulate the flow during measurement. Further information about the MICADAS gas ion source in general is described in detail in (Fahrni et al. 2013). MICADAS was tuned with Oxalic acid (OXA II) before and after measurements. First, solid targets were used for OXA II, for the magazine with only IAEA-C1 and IAEA-C2 samples for blank assessment and cross-contamination. At a later stage, OXA II as gas was used and also fed through the GIS. Routinely, we analyze the measurements using the analytical software Bats (Wacker et al. 2010). Data is calibrated in Oxcal 4.2 using IntCal13 (Ramsey 1995, Bronk Ramsey and Lee 2013, Reimer et al. 2013)

4.3.4 Sample material and methods

Shells and stable isotopes

We used two shells of the bivalve species *Anadara uropigimelana* from Kalba (UAE). One was recovered from a Neolithic shell midden near the modern mangrove. The second was collected from a shell layer (Bronze Age, BZ) at the archaeological site of Kalba, further north of the mangrove area. Archaeological layers and sites are described in (Lindauer et al. 2017). The shell from the Bronze Age layer showed signs of heating and is discussed in detail elsewhere (Lindauer et al. 2018).

For analysis, shells were cut along the axis of maximum growth and 3 mm-thick slices were mounted on plexiglas blocks with a plastic welder. Powder samples for stable isotope and radiocarbon analysis were drilled using a diamond-coated drill bit (1mm diameter) mounted on a Rexim Minimo drill system as described by (Lindauer et al 2016). For ^{14}C measurements, samples of 4 – 22 µg C (shell carbonate powder weight of 60 - 264 µg) were hydrolyzed using 0.5 ml of 85 % phosphoric acid at 70 °C in an autosampler CHS (Carbonate Handling System, IONPLUS AG), then transferred to the GIS (IONPLUS AG) using helium as carrier gas and fed as a 4 % CO_2-in-Helium gas mixture into the MICADAS system through a capillary. Stable isotopes of carbon and oxygen were measured with a Finnigan MAT 253 continuous-flow IRMS at the Institute of Geosciences, University of Mainz (Lindauer et al. 2016). Results were reported relative to V-PDB and calibrated against an in-house Carrara marble standard ($\delta^{18}O$ = –1.91 ‰; $\delta^{13}C$ = +2.01 ‰). The external reproducibility (accuracy), based on repeated measurements of NBS-19, equals ± 0.04 ‰ for $\delta^{18}O$ and ± 0.03 ‰ for $\delta^{13}C$.

The same cross-sectioned shell slices that had been used for stable isotope analyses were subsequently used for radiocarbon dating. For sampling, we closely followed the shape of the growth lines to reduce time-averaging and tried to sample parallel to the stable isotope drill holes to recover the same information stored in the shell. Because the samples were taken from the inner part of the shell no further pretreatment was applied to the samples.

Blank IAEA-C1 and standard IAEA-C2

IAEA-C1 (marble) and IAEA-C2 (travertine) are provided by the International Atomic Energy Agency (IAEA) and have consensus values of $F^{14}C$ = (0.00 ± 0.0002) and (0.4114 ± 0.0003), respectively (Rozanski et al. 1992).

Here, IAEA-C1 is used as blank for background determination of the sample preparation system (CHS and GIS) as well as detection of cross-contamination effects. Blank sample weights varied from 10 to 150 µg C. The measurements routinely started with a larger sample to be able to adjust the GIS in terms of mass flow if necessary. Measurements of IAEA-C1 and IAEA-C2 were used to check for cross-contamination and dependence on sample size. Both, IAEA-C1 (marble) and IAEA-C2 (travertine) were hydrolyzed and measured in the same way as the samples to be dated.

4.3.5 Results and Discussion:

Blank IAEA-C1 and standard IAEA-C2

We measured a complete magazine of IAEA-C1 to determine blank values and IAEA-C2 to yield information about cross-contamination. This magazine, unlike the magazines with dating samples, was measured using OXA II in gaseous form fed through the GIS like the samples themselves which resulted in elevated blank values. The results of the IAEA-C1 measured show that samples with larger weights yield lower $F^{14}C$ values and therefore lower background (Fig. 4.3.1). In particular, blank-sample weights around 10 µg C show an elevated background. 20 µg C samples returned a lower background, but still not always sufficiently consistent for reliable results. Blank sample weights of 50 µg C and more showed reliably low $F^{14}C$.

To account for the contamination of a previous sample, we measured IAEA-C2 with $F^{14}C \approx (0.4114 \pm 0.0003)$. We do not derive a constant contamination as the cross-contamination depends on the size of the sample/blank of interest and the sample measured right before. The cross-contamination mainly originates from the system (CHS + GIS with trap and capillary). For different sample sizes the contamination will be different because the syringe collecting the sample from the trap will be drawn back differently for different sample amounts and hence host different amounts of C. The cross contamination of the previous sample is less significant for sample sizes larger than 50 µg C. For smaller samples the contamination can contribute several permil depending on the modern carbon content of the previous sample. In our case, after an IAEA-C2 measurement with 20 µg C, the following IAEA-C1 measurement was increased by $F^{14}C \approx 0.0255$ in addition to the normal background value of $F^{14}C \sim 0.0045$. Salazar and co-workers investigated cross-contamination for their MICADAS system at Bern and provided helpful advice about how to account for this effect (Salazar et al. 2015). When using the mathematics described there we can derive a cross-contamination of for example ~1 µg C from the previously measured IAEA-C2 to obtain a $F^{14}C$ of 0.03 for a 20 µg C IAEA-C1 blank sample. This emphasizes how sensitive the system is to cross contamination. This corresponds to a contamination of ~ 6 % of the previous sample. We can conclude that our system has a background for standard samples of around $F^{14}C \sim 0.0045$ when using the lowest measured value. Using a 95% confidence interval, the blank values from magazine MA171213G result in a background of $F^{14}C$ 0.0040 ± 0.0012 ($r^2 = 0.804$). For samples of 20 µg C and 10 µg C, blanks values of $F^{14}C \sim 0.014$ and ~ $F^{14}C$ 0.017, respectively, seem to be achievable (Fig. 4.3.1). Hence samples with $F^{14}C$ in this range or below need to be measured with larger sample sizes.

There seems to be a "cleaning effect" at the beginning and maybe some kind of memory effect on the trap. Blank (IAEA-C1) and IAEA-C2 were usually measured as the first samples extracted (after several oxalic acid on graphite targets for tuning). With respect to cleaning and cross-contamination, figure Fig. 4.3.1 can be interpreted to suggest that three IAEA-C1 samples of sizes above 50 µg C are enough to clean the system and erase cross-contamination effects. For samples of around 20 µg C, the system yielded not only elevated backgrounds, but, as expected, larger measurement errors. In this range, three to four blank samples would lead to reliable ages in a clean system. Samples of roughly 10 µg C or below need a thorough cleaning of the system and a well-defined blank assessment. But here, the measurement error is so high due to poor counting statistics (few data points) that data in this sample

size is not reliable, especially when the sample is low in $F^{14}C$. Modern samples might yield enough ^{14}C to still facilitate good measurement statistics and hence less cross-contamination effects. This still needs to be tested in our case.

Another source of contamination is the septum of the vials. It can be damaged by the syringe used to extract the CO_2 gas from the CHS. Occasionally, the syringe shaves off pieces from the septum if it is slightly bent. Depending on the extent of the damage from shaving, atmospheric CO_2 might enter the vial and contaminate the sample CO_2. Apart from this, the syringe gets clogged and the flow reduced or even blocked. However, the sample is not lost and can then still be measured anew after the syringe is cleaned.

As mentioned above, we noticed elevated blank values in magazine MA171213G (December 2017) compared to the IAEA-C1 measurements from previous magazines (July/August 2017, Fig. 4.3.3). One reason is that, starting in December 2017, we used Oxa II gas from a bottle which then, too, had to go through the capillary and led to elevated $F^{14}C$. We also used blank CO_2 gas after the Oxa II gas that subsequently showed a higher value at the beginning with a decrease in $F^{14}C$ after several samples. Unfortunately, we had measured an OXA II instead of a blank before the IAEA-C1 for tuning and monitoring purposes. The advantage of the OXA II gas is that it can easily be adjusted to different sample sizes without previous graphitization and target pressing. The disadvantage is that it contaminates the GIS significantly and requires several blanks afterwards to clean the system.

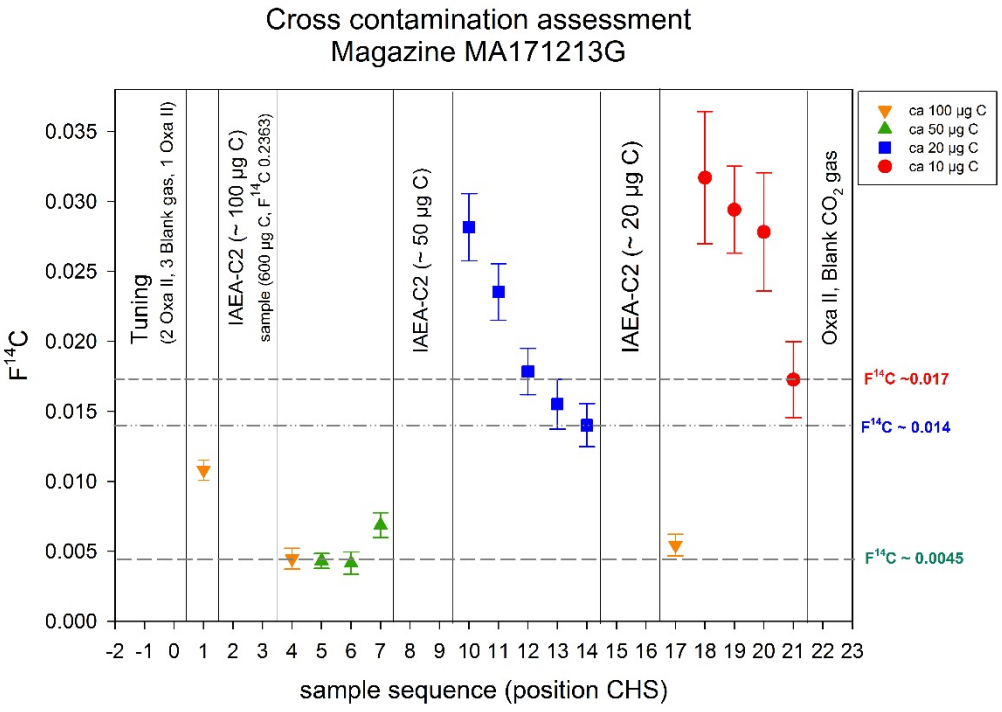

Fig. 4.3.1 IAEA C1 measurements for different sample weights from Magazine MA171213G with respect to measurement sequence (CHS position) and Carbon content (µg C). Dashed lines denote the minimum $F^{14}C$ achieved per µg C range.

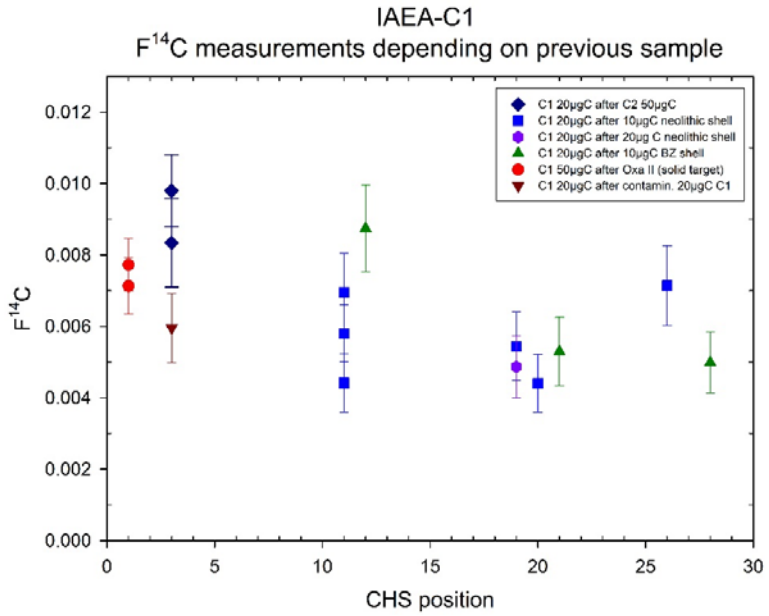

Fig. 4.3.2 Measurements of IAEA-C1 of 20 µg C and 50 µg C depending on previous sample and with respect to CHS position.

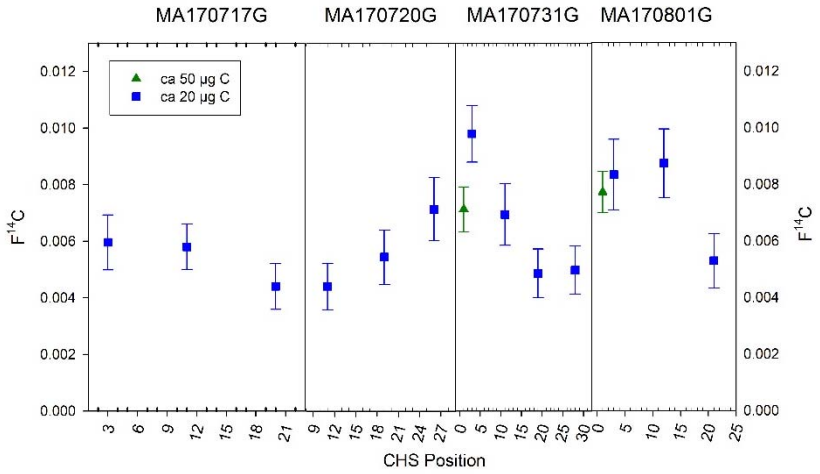

Fig. 4.3.3 IAEA-C1 measurements of magazines with shell samples. Blue circles refer to IAEA-C1 sample sizes of around 20 µg C, green triangles represent IAEA-C1 sample sizes of around 50 µg C.

To clean the system, the blank CO_2 gas is ideal because the measurement can start with a standard sample size and reduce the amount of carbon (C) subsequently to the same amount as IAEA-C1 and dating samples. The blank CO_2 gas yielded values of as low as $F^{14}C$ 0.002. Therefore, in the future it should be possible to decrease our background to a level of around $F^{14}C$ ~ 0.003. In case of problems with the syringe, this will help to analyze the data with a reliable background of the same size if the IAEA-C1 measurement fails or not enough IAEA-C1 samples were hydrolyzed.

The blank IAEA-C1 measurements done with the shell samples varied between sample sizes of 20 µg C and 50 µg C. As can be derived from figureFig. 4.3.3, the results are indistinguishable so all of them were used as blanks to analyze the shell measurements.

Shell radiocarbon data in comparison to stable isotope results

Although the bivalves lived in a lagoon where the stable isotope data of the shells can be subject to large variations due to marine as well as terrestrial and freshwater input, $\delta^{18}O$ time-series show a distinct seasonality reflecting seasonal changes in water temperature. This seasonality is less clearly seen in the $\delta^{13}C$ data, because carbon can have several origins apart from dissolved inorganic carbon (DIC) in water or carbon from food resources. The two shells had been dated for another study in order to determine their reservoir effect (both shells). The second shell from the Bronze Age was also investigated with respect to effects of heating (Lindauer et al. 2017, Lindauer et al. 2018). The results can be seen in Table 4.3.1.

Table 4.3.1 Radiocarbon (AMS) ages of the shells determined from the last formed portions of the shell (ventral margin) as reported in (Lindauer et al. 2017)

Labcode	**Sample ID**	**Period**	**^{14}C age**		**$F^{14}C$**	
			yrs BP	**±**		**±**
MAMS 22867	KK1 2013 Ana 3	Neolithic	6295	26	0,4567	0,0015
P 13306	K4 MBZ Ana1	Middle Bronze Age	3954	54	0,6157	0,0033

<u>*Anadara uropigimelana* from Neolithic shell midden Kalba KK1</u>

This shell (MAMS 22867) was sampled for stable isotopes with high resolution (62 samples) to obtain seasonal environmental information. Measurements of $\delta^{18}O$ and $\delta^{13}C$ were performed on the same sub-sample. The sampling positions (Fig. 4.3.4) were chosen at nearly equidistant intervals. Toward the ventral margin (right edge of the shell in Fig. 4.3.4), the shell was considerably harder than near the umbo (juvenile part, left portion of the shell in Fig. 4.3.4). Shells accumulate less material with age – the so–called ontogenetic trend – which is reflected in narrower growth lines and must be taken into account when sampling for seasonality (Schöne et al. 2005, Schöne 2008).

For radiocarbon dating, 62 samples were drilled within the same growth line/increment as the stable isotope samples (Fig. 4.3.4). Sample weights for the radiocarbon samples ranged from 10 to 20 µg C.

Shell data was blank corrected using the IAEA-C1 blank measurements of the respective magazines, as discussed in the previous paragraph. The shell had already been dated and with the blank correction the data fits the previous result (Table 4.3.1).

The $\delta^{18}O$ shows a sinusoidal shape which can be interpreted as seasonal temperature signal. The shell grew more rapidly during winter season until summer and accumulated less aragonite during and after the summer months (Fig. 4.3.5). The $\delta^{13}C$ signal, on the other hand, rises and oscillates around a constant value. Both signals are similar with respect to positions of minimal and maximal values at certain points (Fig. 4.3.5 sample numbers 3, 15, 30, 46 and 56 for example). It seems that in the juvenile phase and younger adulthood the specimen grew in a rather homogeneous environment and later moved

towards the mangrove forest with more variation in food resources, occasional freshwater input (sample No 34, 46) and changing water temperature (Lindauer et al. 2016). Sudden changes of $\delta^{18}O$ and $\delta^{13}C$ in the same direction are usually interpreted as freshwater input. If this interpretation holds true, ^{14}C values could also be lower and return higher ages. Geologically, the Hajar Mountains in this region (Kalba) consist mainly of ophiolites which does not contain significant amounts of limestone. Carbonates could only be washed into the lagoon from the adjacent sabkha during flash floods. Here then, the ^{14}C content would drop to lower values, reflecting older ages. In figure 5, this might be visible at sample positions 5 and 46. The ontogenetic trend is visible as variation with less distinct features towards the ventral margin (higher sample numbers) (Fig. 4.3.5.)

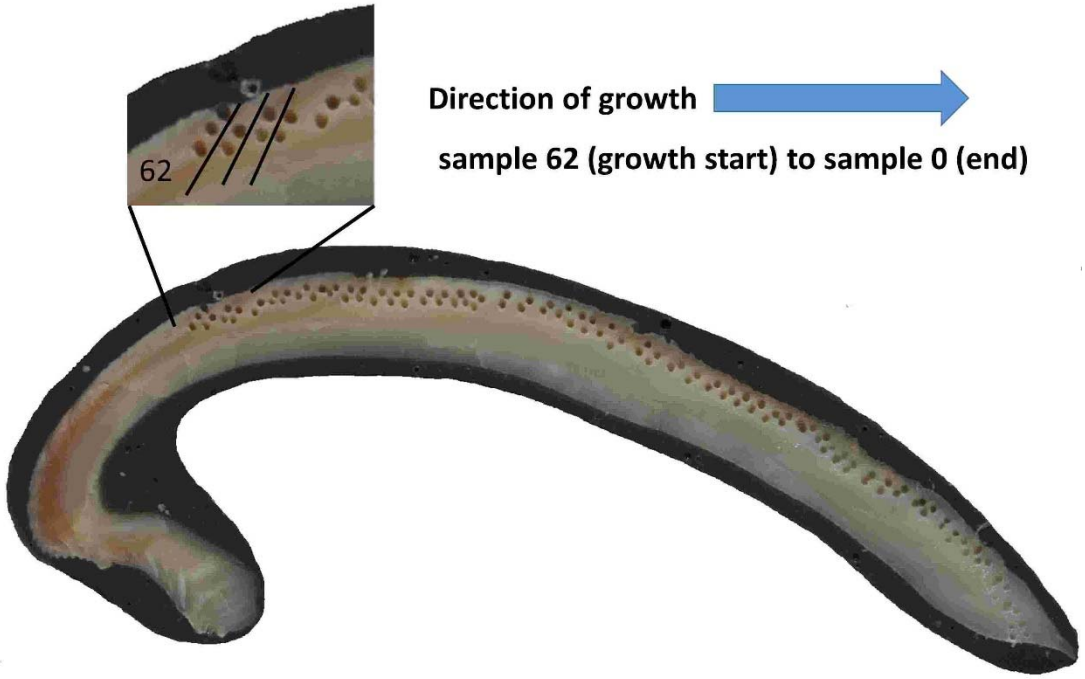

Fig. 4.3.4 *Anadara uropigimelana*. from Neolithic shell midden Kalba KK1. Samples for stable isotopes are on the outer rim of the shell, ^{14}C samples further inside and slightly shifted to remain within the same growth line. The inlet shows the last samples which are at the beginning of the growth of the shell.

The general pattern of the $F^{14}C$ data, which can only be interpreted carefully due to the large errors and cross contamination of some samples, seems to follow the trend of the $\delta^{13}C$ measurements. Furthermore, it is known that a change in ocean circulation occurred roughly every 6 months with an outflow of radiocarbon-depleted water from the Arabian Gulf (see Lindauer et al., 2017). Interpreting only the trends, this seasonality seems to be reflected in the seasonality of the $F^{14}C$ and the $\delta^{13}C$ data (Fig. 4.3.5).

What is also interesting is the large ^{14}C variation within the shell. Even when taking into account the rather large errors due to few measurements because of small sample size, a clear pattern is apparent that shows a non-uniform spread of ages throughout the shell. This range is higher in the young portion of the shell, but the mean $F^{14}C$ seems to decrease slightly during the lifespan of the shell.

We should keep in mind, that data of samples less than 30 µg C with a cross-contamination as in our system are not reliable enough for a detailed interpretation of the values measured. We discussed the data in spite of its lack of reliability to show how the data could be used a) with increased sample size and hence reliability and b) interpreting the trends alone.

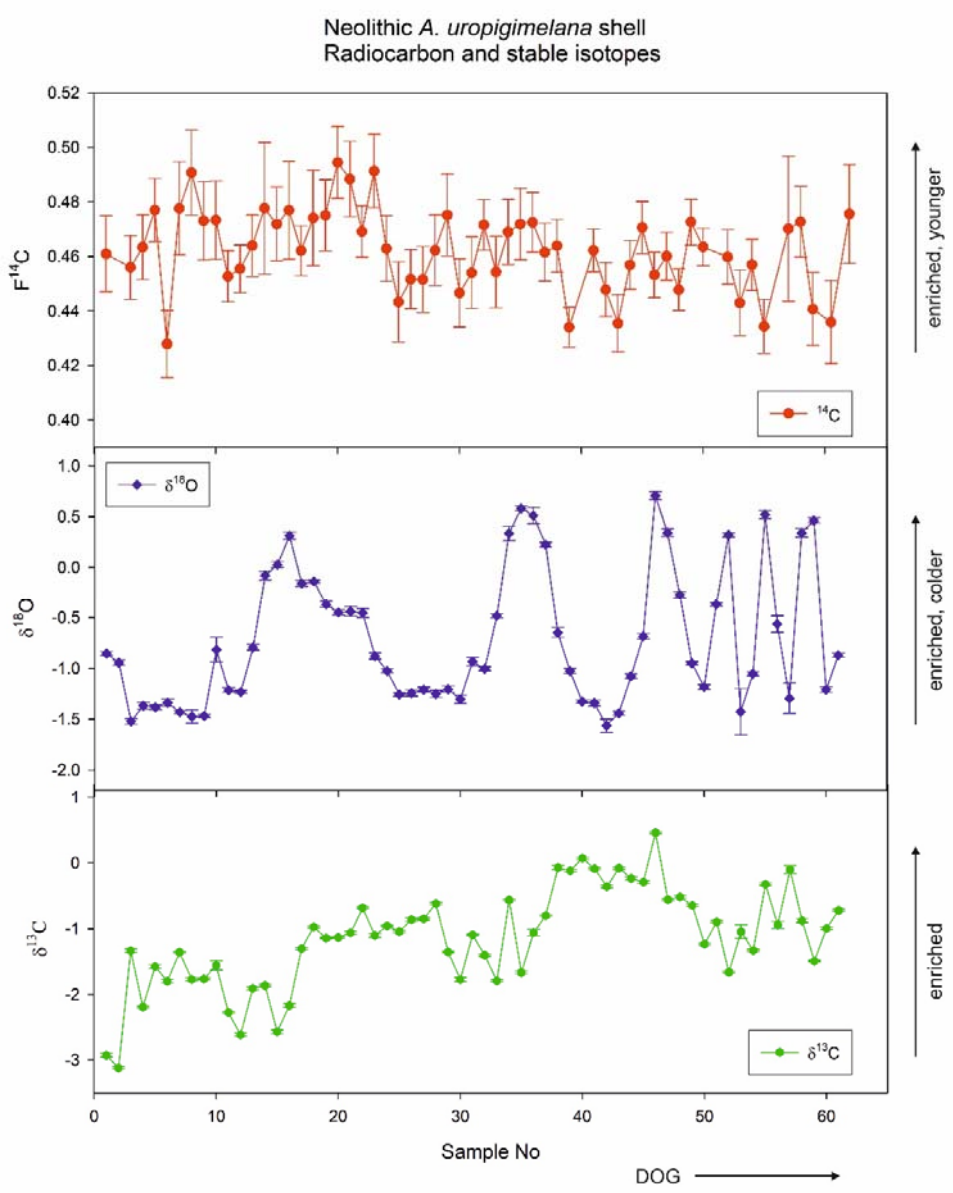

Fig. 4.3.5 Stable isotope values ($\delta^{18}O$, $\delta^{13}C$, both in ‰ V-PDB) and radiocarbon data for *Anadara uropigimelana* from the Neolithic shell midden, Kalba KK1. DOG denotes the "direction of growth" of the shell, from umbo to ventral margin. Sample NO refers to numbering in Fig. 4.3.4.

Bronze Age Anadara uropigimelana from Kalba K4 archaeological site

This shell shows signs of being heated. This leads to a change in microstructure as described by (Milano et al. 2016). In another study on this and other shells of the same species, it could be shown that the radiocarbon age is not influenced by the heating process (Lindauer et al. 2018). In this case, the shell was heated, or burnt, rather quickly, with fire lasting only a few minutes (Meehan 1982). This time

span is too short to incorporate significant amounts of CO_2 from the atmosphere or the fuel used. Other cooking or heating methods also show that the heating is usually done within minutes (Meehan 1977, Meehan 1982).

Darker areas of the shell (possible those receiving stronger heat) were harder to sample than lighter regions (see Fig. 4.3.6). This shell was originally only sampled for stable isotopes and a thermal influence not visible from the outside. Therefore, only 17 samples were taken for light stable isotope analysis because heated shells are not very useful for paleoclimate analyses as a systematic shift of the $\delta^{18}O$ data is very likely (Milano et al. 2016). Because of the shift in $\delta^{18}O$ in heated shells, samples were only taken to monitor trends in $\delta^{18}O$ and $\delta^{13}C$ and to test the robustness of the ^{14}C measurement within a heated specimen. Here we used the isotope data to determine the seasonality. In the previous study (Lindauer et al. 2018) it was found that this shell specimen shows zones of incomplete transition of aragonite into calcite. Nevertheless, even though radiocarbon measurements on heated *A. uropigimelana* are reliable, we wished to test whether the trends from the stable isotopes are also visible in ^{14}C of a burnt shell with transition zones of aragonite and calcite. In portions of shell formed during the organism's youth, samples were taken at coarser resolution than from portions formed later in its lifetime, near the ventral margin (see Fig. 4.3.6) to account for the ontogenetic trend. Sampling in towards the ventral margin was easier than at the hardened, completely heated part towards the umbo. This trend was found to be opposite to the unheated specimen, reflecting the progress of heat along the shell.

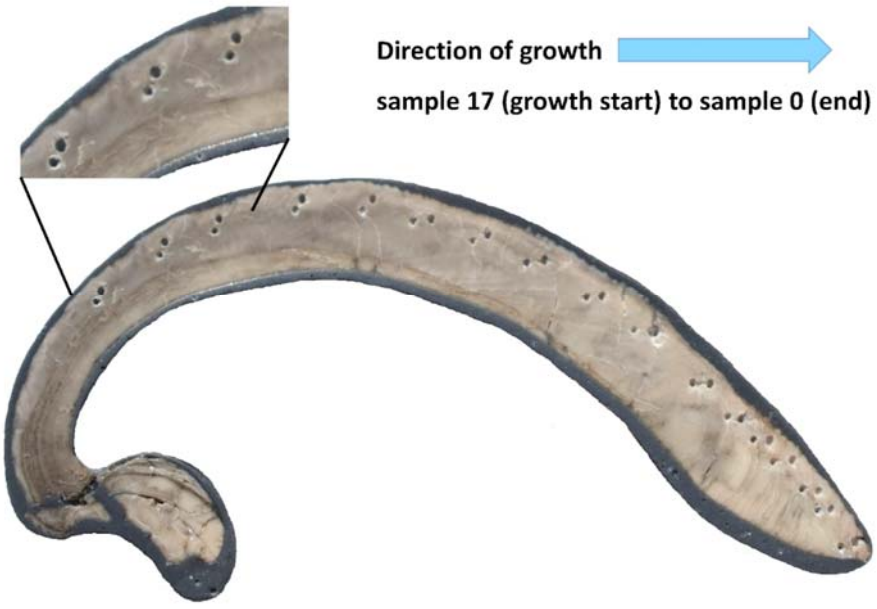

Fig. 4.3.6 *A. uropigimelana* from Bronze Age settlement Kalba K4. Samples for stable isotopes were taken from the outer portion of the outer shell layer, those for ^{14}C analyses came from further inside of the shell. The inlet shows sample spots near the umbo, i.e., at shell portions that formed during youth of the bivalve. The differential heating can be seen as a change from dark grey (higher temperature) to light grey (lower temperature).

In this case, as before, we used IAEA-C1 blanks of the respective magazines for blank correction as they were of approximately the same mass as the samples. The shell had already been dated and with the blank correction the data fits the previous results (Table 4.3.1).

Despite the lower sample resolution, it was still possible to identify the seasonality in the $\delta^{18}O$ data and estimate that the bivalve reached an age of ~ 4 years. However, the $\delta^{13}C$ data did not reflect seasonal variations which might be associated with the polymorphic transformation (change from aragonite to calcite) during the heating process. One radiocarbon sample was lost (no 17) during processing and thus, interpolated in the graph (Fig. 4.3.7). Although less emphasized, $\delta^{13}C$ variations show some peculiarities. If lower values reflect freshwater influence or changing ocean circulation patterns, as in the case of the neolithic specimen, such events occurred at least three times during lifetime of this Bronze Age specimen (measurement numbers 14-13, 10, 6-7), also implying a depletion in radiocarbon from a possible limestone enrichment of the freshwater or the seasonal outflow of ^{14}C-depleted waters from the Arabian Gulf.

The variation in ^{14}C data seems less pronounced than in the Neolithic shell discussed in the previous section. However, sampling resolution was a lot lower than in the Neolithic shell, and the actual spread of the data may thus been higher than observed. In addition, only two samples obtained a carbon content of around 20 µg C, whereas the rest yielded 11 µg C or less. The low sample weight was a result of the heating process and the subsequent difficulties in drilling the material. Closer to the thoroughly burnt umbo the sampling by drilling was a lot harder than towards the ventral margin where parts of the shell still showed signs of aragonite although the microstructures had already lost their characteristic pattern (see Lindauer et al., 2018).This leads to enlarged errors of the single measurement due to low counting statistics. To corroborate the findings, a higher resolution sampling would be required in combination with a sample size of at least 50 µg C for reliable interpretations. Here, too, as in the case of the Neolithic specimen, a detailed analysis with respect to paleoclimate investigations does not make sense and only trends can be read from the data.

Our results show that the combination of CHS and GIS (both IONPLUS) provides a suitable combination for reliable gas measurements of carbonates in the small sample range of down to 30 µg C. Problems in handling the CHS-GIS combination are mainly due to the syringe that extracts the CO_2 out of the sample vial of the CHS. As soon as unexpected low values occur (apart from the Helium flux dropping significantly) the CHS gas flow is blocked or strongly reduced and the syringe needs to be cleaned which prevents fully automated measurements of this combination. Before measuring samples, a thorough blank correction and cross-contamination needs to be determined. Valuable advice of how to achieve this is given in (Santos et al. 2007, Salazar et al. 2015, Tuna et al. 2018). We found a nominal blank of our CHS-GIS combination to be $F^{14}C$ 0.0040 ± 0.0012 (LSQ Fit with r^2 = 0.804, 95% confidence interval). The error of the ^{14}C measurement is significantly higher compared to graphite measurements with typical errors of 20-30 years in the age range investigated with the shells used.

When comparing the data from the Neolithic shell and the Bronze Age shell we suggest a slightly adjusted sampling strategy of sampling with lower resolution than for the Neolithic shell, only using data points near growth lines or in between aiming at a resolution of 6 months to one year. Too much data does not facilitate the overall interpretation as can be seen in Fig. 4.3.5.

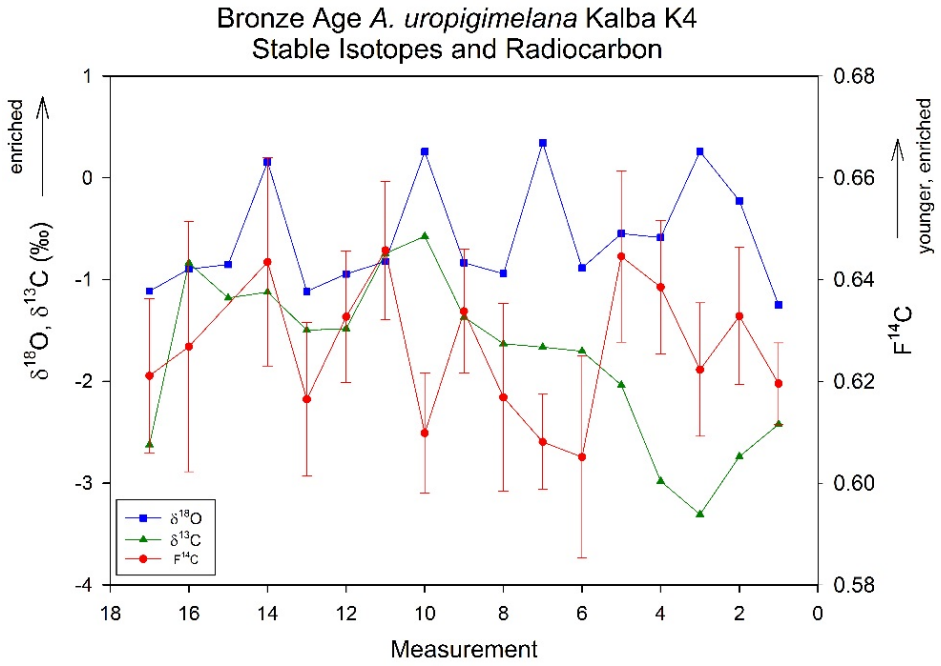

Fig. 4.3.7 Stable isotope ($\delta^{18}O$, $\delta^{13}C$, both in ‰ V-PDB, on the left y-axis) and radiocarbon data (uncorrected $F^{14}C$ on the right y-axis) for *A. uropigimelana* from the Bronze Age settlement, Kalba K4. DOG denotes the "direction of growth" of the shell from umbo to ventral margin.

In spite of the large measurement errors, we see a large range of $F^{14}C$ throughout the shell that is very likely influenced by environmental radiocarbon sources including habitat and food. However, a result of the measurements is the large amplitude of data within a single shell although with large errors. This at least helps to answer the question of the best sampling strategy for shells using standard sample sizes. To smooth out the seasonal variations in ^{14}C data, the best strategy is to sample several seasons for one ^{14}C sample. For molluscs with a lifespan of less than 20 years or so, the error can be neglected when it comes to dating of archaeological shells. For some older-growing species such as *Arctica islandica* that can reach lifespans of over 500 years, samples from the ventral margin can only be used to determine the time of death.

At the beginning of the measurements, at least three blanks of the same sample size as the samples of interest should be measured to clean the system. Due to a possible cross-contamination visible in the C1 data, samples of similar age ranges should be measured in a row to reduce this effect. If OXA II measurements are included in between the sample measurements it is necessary to measure at least two blank samples after the OXA II. Clearly the best way to handle a variety of samples is a large amount of blank measurements of varying sample size to account for any of the aforementioned effects.

Regarding our data, the ideal way to analyze the samples is to measure IAEA-C1 as blank sample with various weights then analyze the samples with the blanks of similar weights.

4.3.6 Conclusions:

This study demonstrates that high-resolution radiocarbon measurements can provide important insights into sources of carbon during shell growth only if the sample size is big enough to eliminate cross-contamination effects. Samples close to the measurement background suffer from cross-contamination. In our case a cross-contamination of ~6 % was found for the first IAEA-C1 after a larger IAEA-C2. The cross contamination, however, is size dependent – on both, contaminant as well as sample – and depends strongly on the amount of ^{14}C of the contaminating sample. We determined our background for samples of approx. 50 µg C to $F^{14}C$ 0.0045 graphically (lowest value measured) and $F^{14}C$ 0.0040 ± 0.0012 using a least squares fit with 95% confidence interval. Using the blank CO_2 gas and thorough cleaning, it should be possible to decrease the background to below $F^{14}C$ ~ 0.003.

Samples should contain at least 30 µg C to yield reliable results and counting statistics to erase cross-contamination effects. In the case of the Neolithic shell sample, an increased sample size with respect to µg C would help to find out about changing ocean circulations reflected in higher $\delta^{18}O$ and depleted ^{14}C data. With an ideal sampling resolution, lower than the one used, it is possible to infer these influences.

Heating of the shells does not allow to interpret the $\delta^{18}O$ regarding water temperature or salinity, but it still allows to derive seasonal variations and does not influence the radiocarbon age. The radiocarbon signal seems to be shifted in comparison with the stable isotope signals which might be the result of metabolic processes. However, in general it follows the seasonality of the $\delta^{18}O$. Within a single shell, radiocarbon ages varied significantly which allowed us to derive a better sampling strategy for samples with standard sizes measured as solid targets.

In conclusion, the method presented here may not be applied as a routine for dating shells, but it provides valuable information to understand estuarine or lagoonal environments if the sample size is chosen accordingly. This method is time-consuming regarding the sampling as well as the measurements and is therefore quite costly. To be able to use it for paleoenvironmental research, sample sizes need to contain at least 30 µg C and be cross-contamination and blank corrected.

Acknowledgements:

We thank the German Research Foundation for funding the stable isotope measurements (HI 643/19-1). We would like to thank Michael Maus for providing help with the stable isotope measurements. Sven Wiegand from CEZA is gratefully acknowledged for providing help regarding the financial part of the radiocarbon measurements. Soraya Marali helped a lot with cutting and polishing the shells.

We would like to thank Sabah A. Jasim and Eisa Yousif from the Directorate of Antiquities, Sharjah, for their support on site and fruitful discussions. SL would like to thank Dr. David Hindle for his help to improve the language in the manuscript.

Last but not least, the authors would like to thank two anonymous reviewers that took a lot of effort to help improve the manuscript.

4.3.7 References:

Ascough, P. L. e. a. (2010). Temporal and Spatial Variations in Freshwater 14C Reservoir Effects: Lake Myvatn, Northern Iceland. *Radiocarbon* 52(2-3): 1098-1112.

Azzoug, M., et al. (2012). Reconstructing the duration of the West African Monsoon season from growth patterns and isotopic signals of shells of Anadara senilis (Saloum Delta, Senegal). *Palaeogeography, Palaeoclimatology, Palaeoecology* 346-347(0): 145-152.

Bard, E., et al. (2015). AixMICADAS, the accelerator mass spectrometer dedicated to 14 C recently installed in Aix-en-Provence, France. *Nuclear Instruments and Methods in Physics Research Section B: Beam Interactions with Materials and Atoms* 361(0): 80-86.

Biagi, P. (1994). A radiocarbon chronology for the aceramic shell-middens of coastal Oman. *Arabian Archaeology and Epigraphy* 5(1): 17-31.

Boivin, N. and D. Fuller (2009). Shell Middens, Ships and Seeds: Exploring Coastal Subsistence, Maritime Trade and the Dispersal of Domesticates in and Around the Ancient Arabian Peninsula. *Journal of World Prehistory* 22(2): 113-180.

Bronk Ramsey, C. and S. Lee (2013). Recent and Planned Developments of the Program OxCal.

Butler, P. G., et al. (2010). Marine climate in the Irish Sea: analysis of a 489-year marine master chronology derived from growth increments in the shell of the clam Arctica islandica. *Quaternary Science Reviews* 29(13–14): 1614-1632.

Colonese, A. C., et al. (2017). Shell sclerochronology and stable isotopes of the bivalve Anomalocardia flexuosa (Linnaeus, 1767) from southern Brazil: Implications for environmental and archaeological studies. *Palaeogeography, Palaeoclimatology, Palaeoecology* 484: 7-21.

Fahrni, S. M., et al. (2013). Improving a gas ion source for 14C AMS. *Nuclear Instruments and Methods in Physics Research Section B: Beam Interactions with Materials and Atoms* 294(0): 320-327.

Hallmann, N., et al. (2013). Holocene climate and seasonality of shell collection at the Dundas Islands Group, northern British Columbia, Canada—A bivalve sclerochronological approach. *Palaeogeography, Palaeoclimatology, Palaeoecology* 373(0): 163-172.

Hoffmann, H., et al. (2017). Status report: Implementation of gas measurements at the MAMS 14C AMS facility in Mannheim, Germany. *Nuclear Instruments and Methods in Physics Research Section B: Beam Interactions with Materials and Atoms* 410(Supplement C): 184-187.

Keaveney, E. M. and P. J. Reimer (2012). Understanding the variability in freshwater radiocarbon reservoir offsets: a cautionary tale. *Journal of Archaeological Science* 39(5): 1306-1316.

Kromer, B., et al. (2013). MAMS - A new AMS facility at the Curt-Engelhorn-Centre for Achaeometry, Mannheim, Germany. *Nuclear Instruments and Methods in Physics Research Section B: Beam Interactions with Materials and Atoms* 294(0): 11-13.

Leng, M. J. (2006). Isotopes in Palaeoenvironmental Research, Springer Netherlands.

Leng, M. J. and J. P. Lewis (2016). Oxygen isotopes in Molluscan shell: Applications in environmental archaeology. *Environmental Archaeology* 21(3): 295-306.

Lindauer, S., et al. (2016). Investigating the Local Reservoir Age and Stable Isotopes of Shells from Southeast Arabia. *Radiocarbon* 59(2): 355-372.

Lindauer, S., et al. (2018). Heating mollusc shells - A radiocarbon and microstructure perspective from archaeological shells recovered from Kalba, Sharjah Emirate, UAE. *Journal of Archaeological Science: Reports* 21: 528-537.

Lindauer, S., et al. (2017). The local marine reservoir effect at Kalba (UAE) between the Neolithic and Bronze Age: An indicator of sea level and climate changes. *Quaternary Geochronology* 42(Supplement C): 105-116.

Magee, P., et al. (2009). Multi-disciplinary research on the past human ecology of the east Arabian coast: excavations at Hamriya and Tell Abraq (Emirate of Sharjah, United Arab Emirates). *Arabian Archaeology & Epigraphy* 20: 18-29.

McIntyre, C. P., et al. (2016). Online 13C and 14C Gas Measurements by EA-IRMS–AMS at ETH Zürich. *Radiocarbon*: 1-11.

Meehan, B. (1977). Hunters by the seashore. *Journal of Human Evolution* 6(4): 363-370.

Meehan, B. (1982). Shell Bed to Shell Midden. Canberra, Australian Institute of Aboriginal Studies.

Milano, S., et al. (2016). Effects of cooking on mollusk shell structure and chemistry: Implications for archeology and paleoenvironmental reconstruction. *Journal of Archaeological Science: Reports* 7: 14-26.

Ng, J. S. S., et al. (2007). The effects of acidification on the stable isotope signatures of marine algae and molluscs. *Marine Chemistry* 103(1–2): 97-102.

Prendergast, A. L., et al. New research on the development of high-resolution palaeoenvironmental proxies from geochemical properties of biogenic carbonates. *Palaeogeography, Palaeoclimatology, Palaeoecology*.

Ramsey, C. B. (1995). Radiocarbon calibration and analysis of stratigraphy; the OxCal program. *Radiocarbon* 37(2): 425-430.

Reimer, P. J., et al. (2013). IntCal13 and Marine13 Radiocarbon Age Calibration Curves 0–50,000 Years cal BP. *Radiocarbon* 55(4): 1869-1887.

Rozanski, K., et al. (1992). The IAEA 14C Intercomparison Exercise 1990. *Radiocarbon* 34(3): 506-519.

Salazar, G., et al. (2015). Development of a method for fast and automatic radiocarbon measurement of aerosol samples by online coupling of an elemental analyzer with a MICADAS AMS. *Nuclear Instruments and Methods in Physics Research Section B: Beam Interactions with Materials and Atoms* 361: 163-167.

Santos, G. M., et al. (2007). Ultra small-mass AMS 14C sample preparation and analyses at KCCAMS/UCI Facility. *Nuclear Instruments and Methods in Physics Research Section B: Beam Interactions with Materials and Atoms* 259(1): 293-302.

Schöne, B. R. (2008). The curse of physiology—challenges and opportunities in the interpretation of geochemical data from mollusk shells. *Geo-Marine Letters* 28(5): 269-285.

Schöne, B. R., et al. (2005). Climate records from a bivalved Methuselah (Arctica islandica, Mollusca; Iceland). *Palaeogeography, Palaeoclimatology, Palaeoecology* 228(1–2): 130-148.

Schulze-König, T., et al. (2010). BioMICADAS: Compact next generation AMS system for pharmaceutical science. *Nuclear Instruments and Methods in Physics Research Section B: Beam Interactions with Materials and Atoms* 268(7-8): 891-894.

Shirai, K., et al. (2014). Assessment of the mechanism of elemental incorporation into bivalve shells (Arctica islandica) based on elemental distribution at the microstructural scale. *Geochimica et Cosmochimica Acta* 126(0): 307-320.

Synal, H.-A., et al. (2007). MICADAS: A new compact radiocarbon AMS system. *Nuclear Instruments and Methods in Physics Research Section B: Beam Interactions with Materials and Atoms* 259: 7-13.

Tuna, T., et al. (2018). Development of small CO2 gas measurements with AixMICADAS. *Nuclear Instruments and Methods in Physics Research Section B: Beam Interactions with Materials and Atoms*.

Uerpmann, H.-P. (1990). Radiocarbon Dating of shell middens in the Sultanate of Oman. *PACT* 29(IV.5): 335-347.

Wacker, L., et al. (2010). Bats: A new tool for AMS data reduction. *Nuclear Instruments and Methods in Physics Research Section B: Beam Interactions with Materials and Atoms* 268(7-8): 976-979.

Wacker, L., et al. (2013). A versatile gas interface for routine radiocarbon analysis with a gas ion source. *Nuclear Instruments and Methods in Physics Research Section B: Beam Interactions with Materials and Atoms* 294(0): 315-319.

Wacker, L., et al. (2013). Towards radiocarbon dating of single foraminifera with a gas ion source. *Nuclear Instruments and Methods in Physics Research Section B: Beam Interactions with Materials and Atoms* 294(0): 307-310.

4.4 Mollusc Carbonate Thermal Behaviour and its Implications in understanding prehistoric fire events in shell middens

Stefania Milano [a,b], Susanne Lindauer [c], Amy L. Prendergast [d], Evan A. Hill [e], Chris O. Hunt [f],

Graeme Barker [g], Bernd R. Schöne [b]

[a] Department of Human Evolution, Max Planck Institute for Evolutionary Anthropology, Deutscher Platz 6, 04103 Leipzig, Germany

[b] Institute of Geosciences, University of Mainz, Joh.-J.-Becherweg 21, 55128 Mainz, Germany

[c] Curt-Engelhorn-Zentrum Archaeometry gGmbH, Klaus-Tschira-Archaeometry-Centre, C4, 8, 68159 Mannheim, Germany

[d] School of Geography, University of Melbourne, 221 Bouverie St, Carlton 3053, VIC, Australia

[e] School of Natural and Built Environment, Queens University Belfast, Elmwood Ave, Belfast BT9 6AY, United Kingdom

[f] School of Natural Sciences and Psychology, Liverpool John Moores University, Byrom Street, Liverpool, United Kingdom

[g] McDonald Institute for Archaeological Research, University of Cambridge, Downing St, Cambridge CB2 3ER, United Kingdom

Contributions: ALP sample collection and project elaboration, SM, SL, ALP designed this study; SM did the Raman and SEM measurements; SL, EH collected the samples and produced the radiocarbon data; SM, SL, ALP, EH, GB, CoH wrote the paper.

Citation: Milano, S., Lindauer, S., Prendergast, A.L., Hill, E.A., Hunt, C.O., Barker, G., Schöne, B.R., 2018. Mollusk carbonate thermal behaviour and its implications in understanding prehistoric fire events in shell middens. *Journal of Archaeological Science: Reports* **20**, 443-457.

4.4.1 Abstract:

Archaeological shell middens are particularly important for reconstructing prehistoric human subsistence strategies. However, very little is known about shellfish processing, especially when related to the use of fire for dietary and disposal purposes. To shed light on prehistoric food processing techniques, and experimental study was undertaken on modern gastropod shells (*Phorcus lineatus*). The shells were exposed to high temperatures (200–700 °C) to investigate subsequent mineralogy and macro- and microstructural changes. Afterwards, the three-pronged approach was applied to archaeological shells from Haua Fteah cave, Libya (*Phorcus turbinatus*) and from shell midden sites in the United Arab Emirates (*Anadara uropigimelana* and *Terebralia palustris*) to determine exposure temperatures. Results indicated that shells from the Haua Fteah were exposed to high temperatures (600–700 °C) during the Mesolithic period (ca. 12.7–9 ka), whereas specimens from the Neolithic period (ca. 8.5–5.4 ka) were mainly exposed to lower temperatures (300–500 °C). The thermally-induced changes in *A. uropigimelana* and *T. palustris* shells from the South East Arabian archaeological sites were similar to those seen in *Phorcus spp*. suggesting a broad applicability of the experimental results at an interspecific level. Although heat significantly altered the appearance and mineralogy of the shells, ^{14}C AMS ages obtained on burnt shells fit within the expected age ranges for their associated archaeological contexts, indicating that robust radiocarbon ages may still be obtained from burnt shells. Our study indicates that the combination of microstructural and mineralogical observations can provide important information to infer shellfish processing strategies in prehistoric cultures and their change through time.

4.4.2 Introduction

Shells grow incrementally throughout the lifetime of molluscs and function as protection and support structures. Shells also serve as excellent palaeoenvironmental archives (i.e. Jones, 1983; Schöne et al., 2004; Butler et al., 2013), because they faithfully record the physical and chemical conditions of their ambient environment and temporal changes to these. Such information is stored in the form of geochemical and structural properties (Epstein et al., 1953; Goodwin et al., 2001; Schöne, 2008). Sclerochronology is the research field that studies the temporal context of shell chemical composition (i.e. stable isotopes and trace elements) and physical accretionary patterns to produce extremely highly resolved palaeoenvironmental reconstructions (Schöne et al., 2005; Miyaji et al., 2007; Milano et al., 2017; Oschmann, 2009). For example, shell oxygen isotope content (δ18Oshell) is routinely used as paleothermometer (Schöne et al., 2005; Ferguson et al., 2011; Prendergast et al., 2013; Prendergast and Schöne, 2017). A rapidly growing interest in the research field of sclerochronology supports the spread of its methodologies and approaches to different disciplines such as archaeology and environmental biomonitoring (Mannino and Thomas, 2002; Andrus, 2011; Steinhardt et al., 2016; Schöne and Krause, 2016). The analysis of mollusc shell material is especially relevant within the framework of prehistoric archaeology. Shellfish have been an important dietary component since the emergence of anatomically modern humans (ca.300,000 yrsr ago; de Lumley, 1966), due to their easy accessibility,

reliable availability throughout the year and source of proteins and micronutrients essential for physical development (Erlandson, 2001; Broadhurst et al., 2002; Marean et al., 2007; Fa, 2008). The application of sclerochronology substantially broadens the potential use of mollusc shells in archaeology. Besides being suitable palaeoenvironmental archives, the shells become a key tool for understanding the response of human behaviour to climatic changes. For instance, δ^{18}Oshell is used to constrain the season of mollusc collection (Mannino et al., 2007; Burchell et al., 2013; Prendergast et al., 2016). In turn, seasonality provides information on the seasonal mobility of hunter-gatherer societies and helps to identify whether sites were permanently or ephemerally occupied (Shackleton, 1973; Mannino and Thomas, 2002; Eerkens et al., 2013). However, the processes related to mollusc preparation, consumption and disposal are still largely unknown (Milano et al., 2016). In some cases, it has been observed a modification of the shell structure by removal of the gastropod apex with stone tool, thorn or canine tip to allow the mollusc to be sucked out (Girod, 2011). As for bivalves, the shells were sometimes scarred or wholesale smashed (Hammond, 2014). Evidence of pyrotechnology associated with mollusc shell middens suggests that a certain degree of heat exposure may have been involved in some cases (Erlandson et al., 1999; Berna and Goldberg, 2008; Taylor et al., 2011). However, few studies have addressed the reconstruction of such processes in the framework of prehistoric marine resource exploitation (Andrus and Crowe, 2002; Aldeias et al., 2016; Milano et al., 2016) and this study will be the first instance where this has been carried out. The present study builds upon previous work by Milano et al. (2016) who found that significant structural and chemical changes occurred in modern mollusc shells when they were heated at ≥ 300 °C for 20 min or more. Here, we investigate the effects of a shorter heat exposure (5 min), since shellfish are generally thought to be processed for short periods of time. To achieve this aim, modern *Phorcus lineatus* are used as a calibration tool to understand the response to thermal treatments at the macro-, microstructural and geochemical level. These findings are then applied to archaeological specimens from the Haua Fteah, eastern Libya (*Phorcus turbinatus*) to test whether high temperatures exposure can be detected in archaeological shells of the same genus using the three-pronged approach developed in the experimental phase. Archaeological specimens from the United Arab Emirates (*Anadara uropigimelana* and *Terebralia palustris*) are used to understand the efficacy of this three-pronged approach on a broader scale to other mollusc species. Furthermore, given the importance of shells for radiocarbon dating coastal sites and the abundance of burnt shells in middens (Douka et al., 2014; Lindauer et al., 2016), we present preliminary results on the influence of thermal alterations on shell radiocarbon dating results.

4.4.3 Materials and methods

A total of 41 shells were analysed (Table 4.4.1). Fifteen live-collected shells of *P. lineatus* were used for the experimental phase. The archaeological material consisted of eighteen specimens of *P. turbinatus* selected from key occupation contexts in the Mesolithic and Neolithic layers from the Haua Fteah cave in Libya, as well as six specimens of *A. uropigimelana* and two specimens of *T. palustris* from shell midden sites near Kalba in the United Arab Emirates (Fig. 4.4.1).

Table 4.4.1 List of studied specimens and details on their provenance.

ID	Species	Provenance	Period
A001	*P. lineatus*	Portugal	Modern
A001_M	*P. lineatus*	Portugal	Modern
A001_MR	*P. lineatus*	Portugal	Modern
A200	*P. lineatus*	Portugal	Modern
A200_M	*P. lineatus*	Portugal	Modern
A300	*P. lineatus*	Portugal	Modern
A300_M	*P. lineatus*	Portugal	Modern
A400	*P. lineatus*	Portugal	Modern
A400_M	*P. lineatus*	Portugal	Modern
A500	*P. lineatus*	Portugal	Modern
A500_M	*P. lineatus*	Portugal	Modern
A600	*P. lineatus*	Portugal	Modern
A600_M	*P. lineatus*	Portugal	Modern
A700	*P. lineatus*	Portugal	Modern
A700_M	*P. lineatus*	Portugal	Modern
M006_1	*P. turbinatus*	Haua Fteah, [illegible]	Capsian
M006_2	*P. turbinatus*	Haua Fteah, [illegible]	Capsian
M005_1	*P. turbinatus*	Haua Fteah, [illegible]	Capsian
M005_2	*P. turbinatus*	Haua Fteah, [illegible]	Capsian
M002_1	*P. turbinatus*	Haua Fteah, [illegible]	Capsian
M002_2	*P. turbinatus*	Haua Fteah, [illegible]	Capsian
M002_3	*P. turbinatus*	Haua Fteah, [illegible]	Capsian
U747_1	*P. turbinatus*	Haua Fteah, [illegible]	Neolithic
U747_2	*P. turbinatus*	Haua Fteah, [illegible]	Neolithic
U747_3	*P. turbinatus*	Haua Fteah, [illegible]	Neolithic
U743_1	*P. turbinatus*	Haua Fteah, [illegible]	Neolithic
U743_2	*P. turbinatus*	Haua Fteah, [illegible]	Neolithic
U743_3	*P. turbinatus*	Haua Fteah, [illegible]	Neolithic
U743_4	*P. turbinatus*	Haua Fteah, [illegible]	Neolithic
U742_1	*P. turbinatus*	Haua Fteah, [illegible]	Neolithic
U742_2	*P. turbinatus*	Haua Fteah, [illegible]	Neolithic
U742_3	*P. turbinatus*	Haua Fteah, [illegible]	Neolithic
U742_4	*P. turbinatus*	Haua Fteah, [illegible]	Neolithic
K4 SL Ana3	*A. uropigimelana*	Oman Sea	Bronze [illegible]
K4 SL GA1	*A. uropigimelana*	Oman Sea	Bronze [illegible]
K4 BZ GT1	*T. palustris*	Oman Sea	Bronze [illegible]
K4 BZ UGT1	*T. palustris*	Oman Sea	Bronze [illegible]
KSM UBL [illegible]	*A. uropigimelana*	Oman Sea	Neolithic
KS Ana 1	*A. uropigimelana*	Oman Sea	Neolithic
KK1 Ana3	*A. uropigimelana*	Oman Sea	Neolithic
KK1 Ana4	*A. uropigimelana*	Oman Sea	Neolithic

Shell material: *P. lineatus and P. turbinatus*

Phorcus spp. are rocky shore gastropods living in the intertidal zone along the Mediterranean (*P. turbinatus*: Menzies et al., 1992; Schembri et al., 2005; Mannino et al., 2008; Prendergast et al., 2013) and Eastern North Atlantic coasts (*P. lineatus*: Kendall, 1987; Donald et al., 2012; Gutiérrez-Zugasti et al., 2015). Both species are sensitive to seasonal environmental changes, specifically water temperature fluctuations.

Furthermore, they are extremely abundant in prehistoric sites of this region (Mannino and Thomas, 2001; Colonese et al., 2011; Hunt et al., 2011; Bosch et al., 2015; Gutiérrez-Zugasti et al., 2015). Therefore, many previous studies have used their geochemical data for palaaeoenvironmental reconstructions (Mannino et al., 2003; Colonese et al., 2009; Prendergast et al., 2016). In the present study, *P. lineatus* (previously known as *Osilinus lineatus* and *Monodonta lineata*) was selected as a modern reference and P. turbinatus (previously known as *Osilinus turbinatus*, *Monodonta turbinate* and *Trochocochlea turbinata*) for the archaeological case study. Despite being two distinct species, they share similar shell shape, size and the same microstructural organization and mineralogy and they live within the same microenvironments on the Mediterranean and Atlantic coasts. Their shell consists of two aragonitic layers with specific organizations.

The outer shell layer (oSL) is arranged in spherulitic prismatic microstructures whereas the inner shell layer (iSL) consists of nacre (Mannino et al., 2008; Milano et al., 2016). The minor phenotypic and taxonomically relevant differences between the two species in shell colouration and aperture size likely do not influence the structural behavior of the shell in reaction to thermal stress.

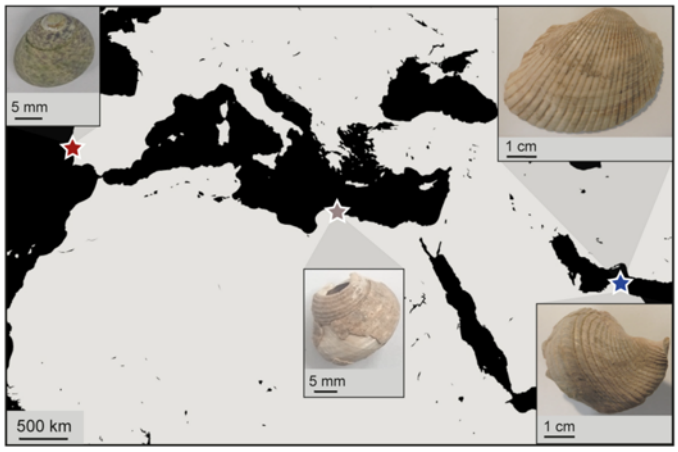

Fig. 4.4.1 Map showing the localities encompassed in the study. Red star: Praia do Tamariz, Portugal, where the modern Phorcus lineatus were collected. Grey star: Haua Fteah cave, Libya, where the archaeological Phorcus turbinatus were excavated. Blue star: sites in the UEA from which the archaeological remains of *Anadara uropigimelana* and *Terebralia palustris* were excavated. (For interpretation of the references to colour in this figure legend, the reader is referred to the web version of this article.)

Shell material: *A. uropigimelana and T. palustris*

A. uropigimelana and *T. palustris* inhabit tropical mudflats. *A. uropigimelana* is a bivalve of the Arcidae family (ark clams), which is widely distributed in East Africa and the Central Pacific. It lives in shallow waters (1–8 m) in association with seagrass beds and can reach 45 years of age (Tebano and Paulay, 2001; Petchey et al., 2013). *T. palustris*, also known as mud whelk, is one of the largest gastropods of mangrove-dominated habitats in the Pacific Ocean (Plaziat, 1984; Houbrick, 1991; Carlen and Olafsson, 2002). It is typically found in the intertidal zone and its lifespan is currently unknown. Possibly the adult size is reached after about four years, when it moves from offshore environments into the mangrove settings (Nishihira et al., 2002). Both species are very abundant in the prehistoric record in the Arabian Sea region (Biagi et al., 1984; Beech and Kallweit, 2001; Gardner, 2005; Lindauer et al., 2017). The shell of *A. uropigimelana* is entirely aragonitic and consists of three layers. The oSL is organized in branching crossed-lamellar structures, the middle shell layer (mSL) is formed of linear-crossed lamellae and the

iSL is characterized by irregular complex-crossed lamellae. Likewise, the shell of *T. palustris* is aragonite and is organized in simple-crossed lamellar (oSL and iSL) and linear-crossed lamellar microstructures (mSL). The terminology follows the author's observations and the description from Carter et al. (2012).

Modern and archaeological settings

Modern specimens of *P. lineatus* were collected from Praia do Tamariz, Portugal (38.7036°N, −9.4038°E) on 10 August 2016. The shells were gathered from a rocky portion in the mid-intertidal zone just outside the estuary of the Tajo River on the Atlantic coast (Fig. 4.4.1). To minimize the effects of ontogeny on the stable isotope results, shells with similar sizes were selected. Maximum shell height ranged between 12 and 14.3mm and the maximum shell width ranged between 13.3. and 15.7 mm. This size class represents the average shell size of *P. lineatus* adult population in the region (da Costa, 2015). Immediately after collection, the specimens were frozen for about one hour and subsequently the soft tissues were removed. The archaeological remains of *P. turbinatus* were collected from the Haua Fteah cave, Libya (Fig. 4.4.1). The Haua Fteah cave was first excavated in 1951–1955 by Charles McBurney, who cut a 14 m-deep stepped trench from the level of the present cave floor, exposing a deep sequence of occupation dating from the last intergacial to the Holocene (McBurney, 1967). New excavations (ERC:TRANSNAP) coordinated by Prof. Graeme Barker between 2008 and 2015 reopened the McBurney trench and cut an overlapping series of small trenches down its southern face (Barker et al., 2010, Barker et al., 2012; Farr et al., 2014). Eleven of the eighteen specimens used in this study were from Trench U, a small (0.75m×1 m) cutting in the upper 2m of the sediments which exposed occupation levels of Neolithic character and age. The Neolithic phase in the cave has a modelled age of ca. 8.5–5.4 cal. BP (Douka et al., 2014). These shells were excavated in 2012 from contexts 742, 743 and 747. These sediments, especially context 747, were associated with evidence of extensive burning in form of frequent charcoal, visibly charred animal bone and shell, and lithic artefacts with thermoclastic fractures. Seven specimens were selected from Trench M, a 2m×1m trench cut down the same side of the McBurney trench at ca. 2–8m depth. The specimens were excavated in 2009 and 2010 from contexts 10,002, 10,005 and 10,006, which have been dated to the Early Holocene and can be ascribed to the Mesolithic Capsian phase of occupation defined by McBurney (1967). The sediments were similar in character to those of Trench U in terms of their plentiful evidence for firing events. The archaeological remains of *A. uropigimelana* and *T. palustris* were excavated from open sites on the Gulf of Oman coast in the United Arab Emirates (Fig. 4.4.1). Specimen KS Ana1, KSM UBL Ana2, KK1 Ana3 and KK1 Ana4 came from the shell midden KK1 situated near the mangroves at Kalba, along the northern coast of the Gulf of Oman (Lindauer et al., 2016). Specimen KS Ana1 was found on the beach nearby and it yielded a radiocarbon age of 7328–7113 cal. BP. It may have remained in the mangrove sediments or in the sabkha (salt flat) since Neolithic times or perhaps washed out recently from an archaeological midden where it was found on the beach. This would also explain its good preservation. The shell midden KK1 is at the outermost edge of the sabkha of the mangrove at Kalba and contains only material from the Neolithic, in two distinct phases. These are reflected in the shell ^{14}C ages that range from ca. 7146 – 6946 cal. BP at the base to ca. 6600–6450 cal. BP at the surface (1σ). Specimens K4 SL

Ana3, K4 SL GA1, K4 BZ GT1 and K4 BZ UGT1 were excavated from site Kalba K4, lying close to the modern town of Kalba north of a mangrove area. This site has evidence of settlement structures that can be ascribed to the Bronze Age and Iron Age. Two distinct layers (MBZ 1 and MBZ 2) situated close to an Iron Age mudbrick wall contain a large amount of shells, both burnt and unburnt, together with charcoal fragments. The lower layer (MBZ1) contained fewer shells than the immediately overlying layer MBZ2. Both layers are around 30 cm thick. Dating measurements show that both layers can be ascribed to the Middle Bronze Age (Lindauer et al., 2017). The shells of the lower MBZ1 have a mean age of ca. 3882–3727 cal. BP and the upper MBZ2 shells of ca. 3695–3641 cal. BP. The results are in accordance with the archaeological data from previous excavations (Phillips and Mosseri-Marlio, 2002).

Experimental design

The experiment on modern shells followed a similar protocol to that described by Milano et al. (2016). However, in this case the shells were exposed to different temperatures for 5 min. The choice of this duration was twofold: (1) to identify potential changes in shell behaviour after short (5 min) heat exposure as compared with the medium (20 min) and long (60 min) heat exposures that were tested in the previous study (Milano et al., 2016) and (2) to attempt to reconstruct the temperatures at which archaeological shellfish were processed. Sparse ethnographic observations (e.g. Meehan, 1977, 1982) as well as modern traditions (e.g. Smith, 1978) suggest that the bivalves are processed for only few minutes before consumption. The shells were heated at 200 °C, 300 °C, 400 °C, 500 °C, 600 °C and 700 °C in a high temperature tube furnace. Specimens were placed in the furnace when the desired temperature was stabilized to ensure the reproducibility of the experiment and to minimize the noise deriving by temperature fluctuations. In order to record potential weight loss, each shell was weighted before and after the roasting experiment to the nearest 1 mg.

Shell preparation

To study the specimens, modern and archaeological shells were fully embedded in Struers EpoFix resin and air-dried for 24 h. This strategy prevented the shells from breaking during the following preparation steps. Each resin block was glued to a plexiglass cube and a low-speed precision saw (Buehler Isomet 1000) was used to cut two sections (ca. 2mm thick) perpendicular to the growth direction. One section of each specimen was glued to a microscope slide with JB KWIK epoxy resin and was later used for geochemical analyses. The other section was used for SEM observations. All shell sections were ground on a Buehler Metaserv 2000 grinder-polisher machine with silicon carbide papers of different grit sizes (P320, P600, P1200, P2500). After each grinding step, the slabs were immersed in de-ionized water and ultrasonically rinsed for 2 min. A Buehler VerduTex cloth with a 3 µm diamond suspension was used to polish the sections. The sections used for SEM analysis were etched for 5 s in 1 vol% HCl and bleached for 30 min in 6 vol% NaOCl, to remove the organic sheets masking the microstructures.

Macro-, microstructural and mineralogical analyses

Modern shells were photographed before and after the thermal treatments allowing a visual comparison at macroscopic scale. To identify thermal changes, the colouration of the shells was identified according to the Pantone colour system. The sections prepared for the SEM were analysed using a Zeiss Axio Imager.A1m stereomicroscope to record potential changes in the appearance of the two shell layers. Prior to the microstructural analysis, the samples were sputter-coated with a 2 nm-thick layer of platinum using a Leica EM ACE200 Vacuum Coater. The surface of the sections was studied with a 3rd generation LOT Quantum Design Phenom Pro desktop SEM with 10 kV accelerating voltage equipped with a backscatter electron detector. Shell mineralogy was investigated in each shell layer by using a Horiba Jobin Yvon LabRam800 spectrometer equipped with an Olympus BX41 optical microscope. The instrument employed a 532.21 nm laser wavelength, a 400 µm confocal hole, a grating with 1800 grooves/mm, an entrance slit width of 100 µm and 50× long-distance objective lens. The integration time of each scan ranged between 3 and 5 s.

Stable isotope analysis

The stable isotope composition of the modern specimens was analysed on carbonate powder sampled after heating the shells. Carbonate material was obtained from each shell by microdrilling the inner layer (nacre) with a Rexim Minimo dental drill mounted to a stereomicroscope and equipped with a conical drill bit of 300 µm in diameter (Komet/Gebr. Brasseler GmbH & Co. KG, model no. H52 104,003). A Thermo Fisher MAT 253 gas source isotope ratio mass spectrometer in continuous flow mode coupled to a GasBench II at the Institute of Geosciences, University of Mainz was used to analyse the carbonate samples by phosphoric acid digestion (70 °C for 120 min). The isotope data were calibrated against a NBS-19 calibrated Carrara marble standard ($\delta^{18}O$=−1.91‰). The average internal precision (1σ) was 0.03‰ and the external reproducibility (1σ) was 0.05‰. The $\delta^{18}O$ profiles of the heated shells were compared to the $\delta^{18}O$ profiles of the control specimens, which were not exposed to high-temperature treatments.

Radiocarbon dating

For radiocarbon dating, small chips were taken near the apex of three *P. turbinatus* specimens. In order to avoid any contamination from sedimentary calcium carbonate or a mixture of different shell layers, the external layer of the shells was physically removed. The fragments of nacre were further processed at the Curt-Engelhorn-Center for Archaeometry, Mannheim, Germany. The material was acidified in phosphoric acid at 70 °C by using an Autosampler system and measured using the MICADAS system (Kromer et al., 2013; Wacker et al., 2013). The results were calibrated with the Marine13 curve (Reimer et al., 2013) and corrected using the Mediterranean reservoir correction (ΔR) of 58 ± 85 14C years (Reimer and McCormac, 2002) using OxCal v.4.3.2.

Statistical analyses

ANOVA, Mann-Whitney and Tukey's HSD post hoc tests were performed using the software PAST to test whether the 5-min heat exposure had a significant effect on shell geochemistry as well as whether the different durations changed the oxygen isotopic signatures.

4.4.4 Results

Experimental results on the effect of roasting on the shells

At macroscopic level, the 5-minute thermal treatment caused a similar effect as reported for *P. turbinatus* in the previous experiment by Milano et al. (2016), in which shells were roasted for 20 min and 60 min. Visible alteration of the shell surface occurred at temperatures higher than 200 °C. For instance, the typical background cream colouration (Pantone: 7497C) alternated with pigmented blotches (438C) started to change at 300 °C, when the shells acquired a dark colouration with a tendency toward a brown shade (background: 7531C; blotches: 7518C). At 400 and 500 °C, the shells became grey (background: 404C; blotches: 417C) and the outer shell layer started to detach. At 600 °C, the colouration only slightly changed (background: 416C; blotches: 417C) and the material brittleness increased, whereas at 700 °C, the colouration turned into a cream-white tone (background and blotches: 401C; Fig. 4.4.2A). Furthermore, the heat exposure induced a 14 to 25% weight loss, with a greater loss at higher temperatures (Fig. 4.4.2B).

At the microstructural level, roasting at 200 °C did not cause any visible change of the shell microstructure. First-order and second-order prisms (oSL) and platelets (iSL) of the heated samples did not appreciably differ from those of unheated samples. At 300 °C, the oSL did not show any visible alteration whereas the nacre platelets became slightly porous with nanometer sized holes appearing on their surfaces (Fig. 4.4.2C–D). At 400 °C, the single second-order prisms of the oSL were still recognizable. However, sheets of organic material emerged between the first-order prisms partially covering the shell surface. The platelets of the nacre started to fuse and large cracks developed on the surface. After heating at 500 °C, the oSL underwent a significant transformation with the formation of new irregular-shaped units surrounded by organic sheets. Meanwhile, the iSL surface was partially covered by organic matter which emerged from the inter-lamellar voids that formed at 400 °C (Fig. 4.4.2C–D). The appearance of the oSL at 600 °C is very similar to the previous treatment (500 °C) with an enhanced presence of organic material. The platelets of the nacre showed a higher degree of fusion in every direction with large quantities of organics in between them. At 700 °C, the surface of the biomineral units of the oSL units became more compact with a decrease in porosity. At the same time, the agglomeration of the iSL platelets led to the formation of new boundaries delineating larger and irregular units (Fig. 4.4.2C–D). The shell mineralogy was also affected by heat (Fig. 4.4.2C–D). Originally, the shells were fully aragonitic as indicated by Raman peaks at 152 cm−1,180 cm−1, 207 cm−1,707 cm−1and 1086 cm−1. The transition from aragonite into calcite started at 400 °C in the oSL and is indicated by an extra peak at 281 cm−1 (Fig. 4.4.2C). At this temperature, however, the iSL was still completely aragonitic. At 500 °C, both layers were transformed into calcite with peaks at 153 cm−1, 281 cm−1, 713 cm−1 and 1086 cm−1. Similar to our previous results (Milano et al., 2016), the shell

oxygen isotope composition changed in response to the heat treatment. The $\delta^{18}O_{shell}$ values of the control sample ranged between −1.0 and +1.0‰. The oxygen isotope range is more negative than the range obtained by the control shells used in Milano et al. (2016). This offset reflects the difference of the local environments.

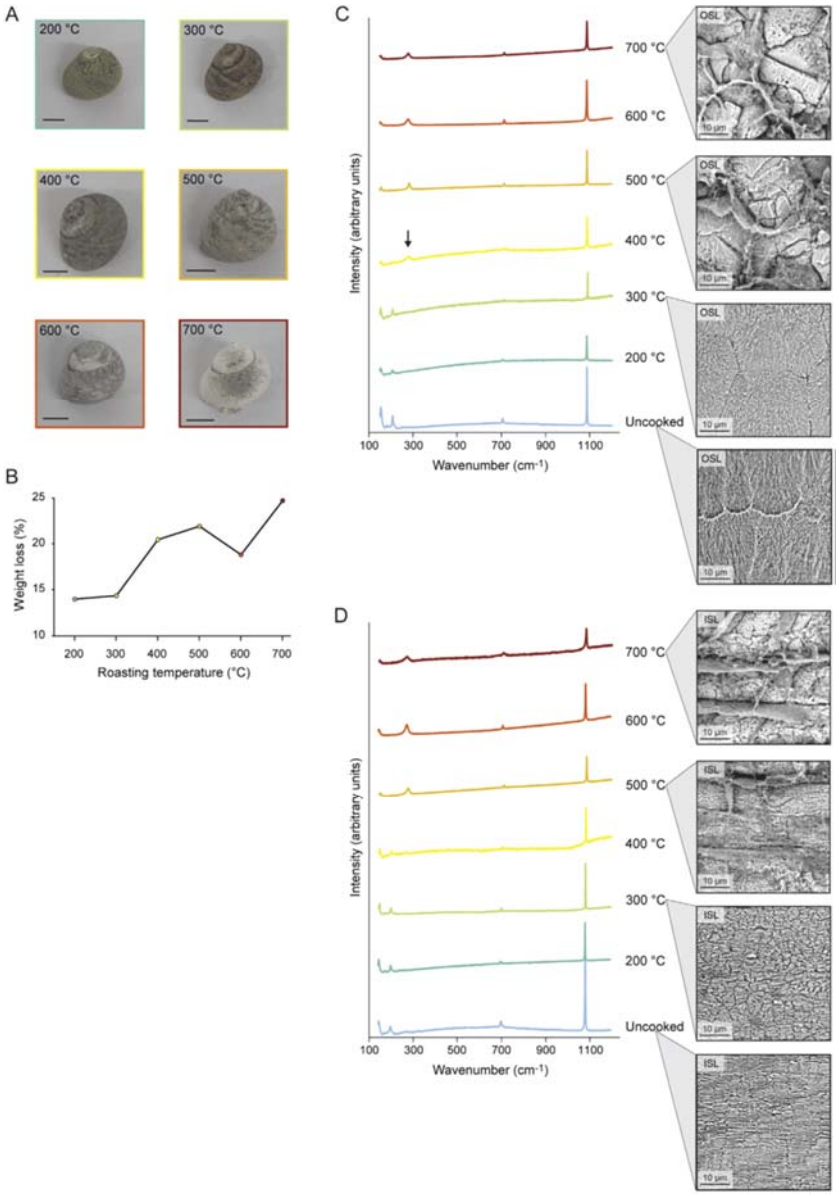

Fig. 4.4.2 Effects of the 5-min heating experiment on P. lineatus shell. (A) Overall shell appearance after the thermal exposure at different temperatures. Scale bars=5 mm. (B) Shell weight loss in response to heat. (C) Effect of heat on the outer shell layer (OSL) mineralogy and microstructures. The black arrow shows the extra peak in the 400 °C Raman spectrum indicating the transition phase from aragonite into calcite. (D) Thermal response of the inner shell layer (ISL) mineralogy and microstructures.

The shells from Portugal used in the present study were collected from an area characterized by much larger freshwater input, and hence lower $\delta^{18}O_{shell}$ values, than the specimens from Libya used in Milano et al. (2016). The oxygen isotope composition of shells processed at 200 °C and 300 °C for 5 mins ranged between −0.5 and +0.7‰ (Fig. 4.4.3A). According to the Mann- Whitney U-test there is no statistical difference between these heated samples and the control shells ($p > 0.05$; Fig. 4.4.3B). The effect of the shell exposure at 400 °C could not be tested, because the nacre layer was too thin to obtain sufficient carbonate powder. As expected, higher temperatures (500–700 °C) had a significant influence on $\delta^{18}O_{shell}$. Average values were offset by −1.5‰ ± 0.2 with respect to the average values of the control

material. Minimum and maximum values were offset by −0.8‰ ± 0.1 and−0.8‰ ± 0.7, respectively (Fig. 4.4.3A). The oxygen isotopic composition of the shells heated over 500 °C was statistically different from the lower temperature treatments and the control conditions (Mann-Whitney test $p < 0.05$; Fig. 4.4.3B). A comparison between the current data and the results published in Milano et al. (2016) was used to determine the influence of the duration of the heating process on the shell. The offsets of the $\delta^{18}O_{shell}$ values from the respective control values were calculated for the three duration treatments (5, 20 and 60 min). The offsets of minimum, average and maximum $\delta^{18}O_{shell}$ values were statistically similar among all treatment durations (ANOVA $p > 0.05$).

Archaeological shells: Structural and mineralogical organization

The *P. turbinatus* specimens from the Haua Fteah presented interindividual differences in their appearance at macroscopic scale (Fig. 4.4.4). All of the Mesolithic specimens (Trench M) showed a homogenous dark grey surface with areas of partial detachment of the oSL (i.e. M002_1 in Fig. 4.4.4D). The nacre was less uniform and lighter grey in colour. In general, these shells looked similar to those of the experiment roasted at 600 °C (Fig. 4.4.2A). Two specimens from the Neolithic context 747 (U747_1 and U747_2) were lighter grey and looked similar to shells heated at 500 °C. The third specimen from this layer (U747_3) showed an iridescent iSL and an overall colouration likely related to lower heating temperatures (i.e., 300 °C). All four Neolithic *P. turbinatus* specimens from context 743 were light brown in colour and showed iridescent nacre (i.e. U743_3 in Fig. 4.4.4B). The same applied to the two shells from context 742 (U742_2 and U742_4; Fig. 4.4.4A), whereas U742_1 and U742_3 were grey as if subjected to higher temperatures (Fig. 4.4.4C). In good agreement with the observations of the macro appearance of the shells, microstructures varied greatly between individuals. The prisms in the oSLs of the Mesolithic specimens from were replaced by porous irregular units and the nacre platelets were fused together into larger agglomerates (Fig. 4.4.4D). The integral microstructural reorganization and the subsequent absence of any of original secondary prisms (oSL) and platelets (iSL) recall the structural arrangement of the modern samples exposed to high temperatures (600 °C; Table 2). A similar architecture was observed in the Neolithic specimens U747_1, U747_2 and U742_3. On the other hand, all shells from context 743 and specimens U747_3 and U742_4 showed well-defined prismatic structures in the oSL and slightly porous platelets in the iSL, which looked similar to the experimental shells heated at 300 °C (Fig. 4.4.4B). Shell U742_1 represented the only case identifiable as processed at a temperature of ca. 500 °C (Table 4.4.2). The prisms of the oSL appeared to have undergone major fusion at 400 °C (Fig. 4.4.4C). However, the single elongated prisms were still partially visible and they were not completely transformed as in the case of the material burned at 600 °C. A similar pattern was observed in the nacre, where the agglomerations of platelets started to define new structural units (Fig. 4.4.4C). The microstructures of specimen U742_2 were perfectly preserved and did not show any sign of thermal alteration (Fig. 4.4.4A, Table 4.4.2). According to Raman spectroscopy, seven shells were entirely aragonitic and eleven were calcitic (Fig. 4.4.5). All Mesolithic specimens and four of the Neolithic specimens consisted of calcite (Fig. 4.4.5A), whereas the remaining specimens from Trench U were aragonitic (Fig. 4.4.5B). No transition phase was detected and the two shell layers always shared the same mineralogy. Based on the results presented above, the calcitic shells were categorized as having been exposed to temperatures in excess of 500 °C (Table 4.4.2). Similar to the *P.*

turbinatus, some archaeological specimens of *A. uropigimelana* and *T. palustris* from the United Arab Emirates sites displayed an altered overall appearance (Fig. 4.4.6). Shells K4 SL Ana3, KSM UBL Ana2, KK1 Ana3 and KK1 Ana4 showed the characteristic homogenous creamy colour of unaltered *A. uropigimelana* (Fig. 4.4.6A). A slightly darker shade, especially on the inner shell surface, was visible in KK1 Ana4. Two shells, KS Ana1 and K4 SL GA1, showed a grey shell surface. The first was characterized by a light tone, whereas the latter was darker with shaded areas on the inner shell surface clearly indicating heat exposure (Fig. 4.4.6A). In the case of *T. palustris*, one specimen (K4 BZ UGT 1) had its surface colouration preserved, whereas a second specimen (K4 BZ GT 1) was very dark (Fig. 4.4.6B).

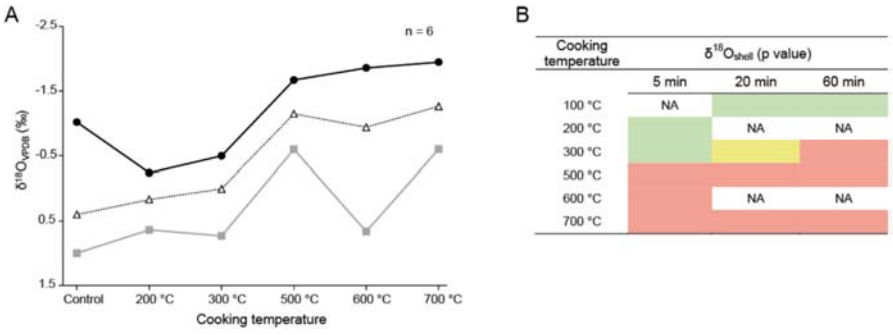

Fig. 4.4.3 Thermal behaviour of shell oxygen isotopes. (A) Oxygen isotope composition after roasting at the different temperatures. Grey squares = maximum $\delta^{18}O_{shell}$; open triangles=average $\delta^{18}O_{shell}$; black circles = minimum $\delta^{18}O_{shell}$. (B) The table refers to the different cooking durations tested in the present study and the previous study by Milano et al. (2016). Green cells indicate statistical similarity between isotope values of the heated and control shells ($p > 0.05$). Red cells indicate statistical difference ($p < 0.05$). The yellow cell relates to a disagreement in the case of the specimen roasted at 300 °C for 20 min. Its isotopic signature was statistically similar to the one of the control shell but different to the second control sample. (For interpretation of the references to colour in this figure legend, the reader is referred to the web version of this article.)

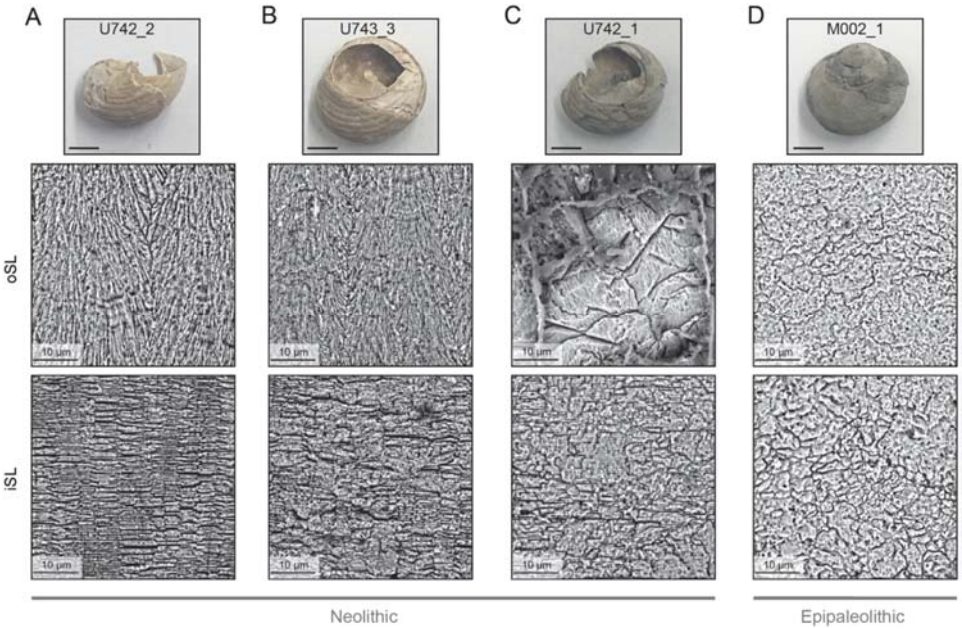

Fig. 4.4.4 Macroscopic appearance and microstructural organization of *P. turbinatus* shells from (A–C) Neolithic contexts and (D) Mesolithic contexts in the Haua Fteah cave. The first row of SEM images refers to the prismatic microstructures of the OSL. The second row displays the nacre platelets of the ISL. The visible changes in structural organization denote possible exposure to heating processes. Scale bars if not otherwise indicated = 5 mm.

Shell ID	Reconstructed cooking temperature		
	Macroscale appearance	Microstructures	Mineralogy
M006_1	600 °C	600 °C	≥ 500 °C
M006_2	600 °C	600 °C	≥ 500 °C
M005_1	600 °C	600 °C	≥ 500 °C
M005_2	600 °C	600 °C	≥ 500 °C
M002_1	600 °C	700 °C	≥ 500 °C
M002_2	600 °C	600 °C	≥ 500 °C
M002_3	600 °C	700 °C	≥ 500 °C
U747_1	500 °C	600 °C	≥ 500 °C
U747_2	500 °C	600 °C	≥ 500 °C
U747_3	500 °C	300 °C	< 500 °C
U743_1	300 °C	300 °C	< 500 °C
U743_2	300 °C	300 °C	< 500 °C
U743_3	300 °C	300 °C	< 500 °C
U743_4	300 °C	300 °C	< 500 °C
U742_1	400 °C	500 °C	≥ 500 °C
U742_2	Not cooked	Not cooked	< 500 °C
U742_3	500 °C	600 °C	≥ 500 °C
U742_4	500 °C	300 °C	< 500 °C

Table 4.4.2 Reconstruction of shell exposure temperature by using shell overall appearance, microstructures and mineralogy as proxies in archaeological specimens of *P. turbinatus*.

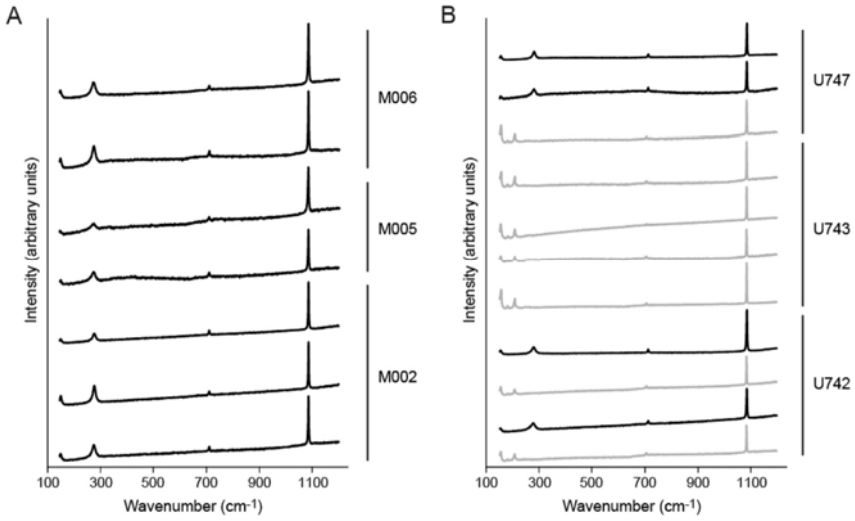

Fig. 4.4.5 Raman spectra of *P. turbinatus* ISLs from (A) Neolithic contexts and (B) Mesolithic contexts in the Haua Fteah cave. All Mesolithic specimens and four Neolithic specimens were calcitic (black lines); the rest of the Neolithic specimens were aragonitic (grey lines).

The well-preserved *A. uropigimelana* specimens K4 SL Ana3, KSM UBL Ana2, KS Ana1, KK1 Ana3 and KK1 Ana4 showed well-defined crossed-lamellar structures in the oSL, linear-crossed lamellae in the mSL and irregular complex-crossed lamellae in the iSL. The excellent preservation state was also corroborated by the presence of organic microtubules across the shell layers (Fig. 4.4.6A). Conversely, shell K4 SL GA1 displayed altered microstructures. The first order lamellae of the oSL and mSL were still visible, whereas the morphometric characteristics of the third order lamellae were changed. The units were fused together in large agglomerates with new boundaries (Fig. 4.4.6A). These features recall the oSL of *Phorcus spp*. heated at 600 °C. In the iSL, the lamellae lost their individuality and elongated shape, forming compact clusters of material separated by organic sheets and cracks (Fig. 4.4.6A). The *T. palustris* specimen K4 BZ UGT 1 showed the typical simple and linear-crossed lamellar

microstructures (Fig. 4.4.6B), whereas in specimen K4 BZ GT 1 lamellar biomineral units were transformed into large irregular-shaped assemblages in the oSL and iSL. In the mSL, small granular carbonate units with well-defined boundaries prevailed (Fig. 4.4.6B). Such alteration was likely related to high temperatures (≥ 500 °C). However, in this case an accurate estimate of the processing temperature cannot be provided based on the microstructures, because no such architecture was previously observed in the mSL. Typical aragonite Raman spectra occurred in all but two *A. uropigimelana* and *T. palustris* specimens. The mineralogy of K4 SL GA1 and K4 BZ GT 1 was entirely calcitic (

Radiocarbon dating of *P. turbinatus* from Haua Fteah

Specimen U742_2, with no sign of heat exposure (Fig. 4.4.4A), was dated to 7184 ± 21 ^{14}C years BP calibrated to 7772–7438 cal. BP (2σ). Specimen U742_1, with signs of high temperature exposure (Fig. 4.4.4C), was dated to 7300 ± 21 ^{14}C years BP calibrated to 7901–7556 cal. BP. both these dates fit with existing ^{14}C dates for context U742. Specimen U742_3 (Fig. 4.4.4), with burning marks, was dated to 6378 ± 21 ^{14}C years BP calibrated to 7002–6558 cal. BP. These dates fit with the current chronostratraphic understanding of Context U743, which is paired with U742 stratigraphically (Fig. 4.4.8). Associated ^{14}C radiocarbon ages are available from other materials dated in Trench U are also included in this study for comparative purposes (Table 4.4.3). The relatively broad spread of dates from U742 fits sedimentological model for this part of the Haua Fteah deposition sequence and all sit within the existing age range for these context. Context U742 is one of a group of chronologically identical contexts (with U743, U744, U746 and U747) that form a cross section of a debris flow that contains archaeological material that can be attributed to the Neolithic.

4.4.5 Discussion

A comparative approach to thermal-induced diagenesis in biogenic carbonates

Diagenesis encompasses all physical and chemical processes occurring to the tissues after the death of the animal. The present study focuses exclusively on thermally-induced diagenesis associated with heat exposure. High temperatures accelerate a process that naturally would require thousands of years. When dealing with archaeological remains it is important to differentiate between the two types of diagenetic processes to ensure a correct interpretation of the results. In order to do so, the whole shell assemblage needs to be taken into consideration. Specimens from a certain archaeological layer are subjected to similar environmental conditions after burial (i.e. depth, sediment composition and soil pH). Therefore they are likely to share similar preservation conditions. The overall preservation state indicates whether natural diagenesis altered the shells or not. Any deviation from the average preservation state is likely related to different processes. In our case, shells without evidence of burning are generally well-preserved suggesting that natural diagenesis did not occur (Prendergast et al., 2016). Any altered shell is likely to be related to heat-induced diagenesis. Although this approach allows a reasonable distinction between natural and artificial diagenesis, further studies on naturally-altered shell material are needed to characterize the structural and mineralogical key features relative

to this type of diagenesis. As previously demonstrated by Milano et al. (2016), the macroscopic and microscopic appearance of *Phorcus spp*. shells gradually altered as the processing temperatures increased. Although the thermal exposure time was reduced to 5 min in the present study, similar mineralogical and geochemical changes were observed. The only exception is the temperature at which the aragonite-to-calcite transformation of the oSL occurred, i.e., 400 °C in the present study and 300 °C in Milano et al. (2016). Based on this discrepancy, we suggest that the duration of the thermal exposure may play a role in the development rate of such taphonomic processes. However, time is only of secondary importance in comparison to the actual processing temperature. In good agreement with the most of our results, Aldeias et al. (2016) demonstrated that the mineralogy of *Cerastoderma edule* and *Scrobicularia plana* shells showed no differences after roasting for 5 and 20 min. In abiogenic and biogenic minerals, the aragonite-to-calcite and microstructural transformations have been previously observed to occur very rapidly at critical temperatures around 400 °C and 500 °C, respectively (Lécuyer, 1996; Koga et al., 2013). As a consequence, it will most likely be impossible to reconstruct the processing duration based on the analysis of archaeological shells, but it is possible to reconstruct the temperatures at which they were exposed. Consequently, it may be possible to postulate the type of fire or fuel that created those temperatures.

P. lineatus shells lost weight after roasting, especially at temperatures above 300 °C (21.5% weight loss). Heat-induced weight losses have previously been reported from biogenic and abiogenic minerals (Yoshioka and Kitano, 1985; Balmain et al., 1999; Bourrat et al., 2007). Thermal exposure induces a three-step release of water and organic content. At first, the endothermic reaction provokes dehydration through evaporation of the water incorporated in the mineral phase (Yoshioka and Kitano, 1985; Perić et al., 1996; Huang and Li, 2009). Then, at temperatures between 250 °C and 450 °C, the organic matter in the shell starts to degrade (Bourrat et al., 2007; Huang and Li, 2009). In *Phorcus spp*., this temperature range conforms to the appearance of large organic sheets partially masking the carbonate microstructures (Fig. 4.4.2). The degradation intensifies at higher temperatures (> 500 °C) and is associated with weight losses up to 50% (Balmain et al., 1999; Zolotoyabko and Pokroy, 2007; Huang and Li, 2009; Villagran et al., 2011). In the present study, temperature was increased stepwise by 100 °C steps to systematically investigate structural and mineralogical changes of the shells. The outer shell layer of *P. lineatus* started to transform from aragonite to calcite at 400 °C. This process was completed at 500 °C. In the case of the nacre, no such broad transition phase was detected. Conversion to calcite took place at 500 °C, at which point the iSL was entirely calcitic. According to previous studies, however, polymorphic transition of mollusc shells already started at temperatures of 250–350 °C, and conversion to calcite was completed between 400 °C and 500 °C (Lécuyer, 1996; Maritan et al., 2007; Aldeias et al., 2016). Conversion temperatures seem to vary between species. As shown by Aldeias et al. (2016), the mineralogy of *C. edule* and S. plana reacts differently to heating. In *C. edule* polymorphic conversion occurs between 250 and 500 °C, whereas in *S. plana* the transformation only starts at 350 °C and is completed at 400 °C. The observed differences in polymorphic conversion temperatures may be explained by specific structural properties of the materials.

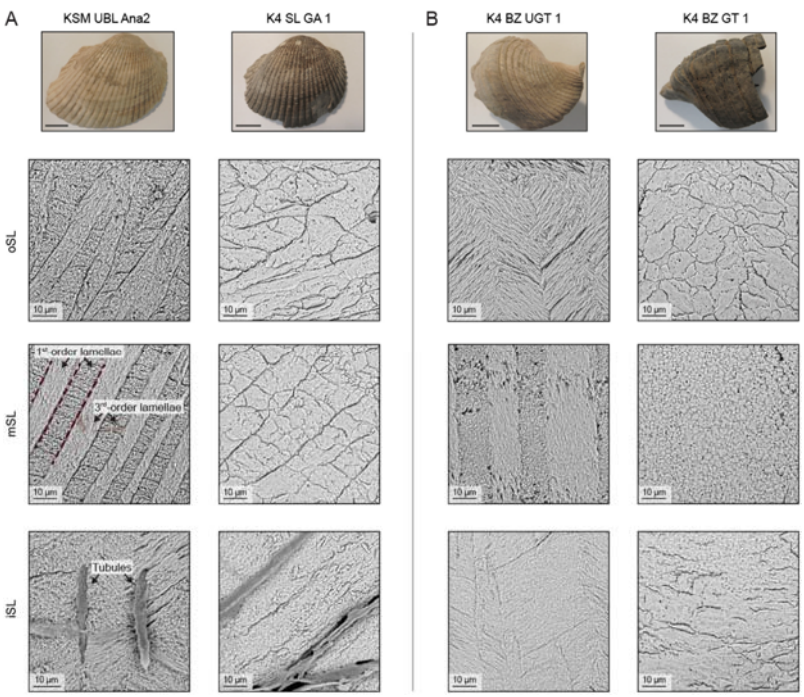

Fig. 4.4.6 Macroscopic appearance and microstructural organization of the archaeological shells from the United Arab Emirates. (A) Whole shell and SEM images of two *A. uropigimelana* specimens. Shell KSM UBL Ana2 showed the typical microstructural architecture of the species. Highlights on the SEM images indicate the first and third order units of the crossed-lamellar structures as well as the organic microtubules perforating the shell material. Specimen K4 SL GA 1 shows the alteration of the overall colour and microstructures, possible related to heat treatment. (B) Whole shell and SEM images of two *T. palustris* specimens with regular (K4 BZ UGT 1) and altered microstructures and appearance (K4 BZ UGT 1). Scale bars if not otherwise indicated = 1 cm.

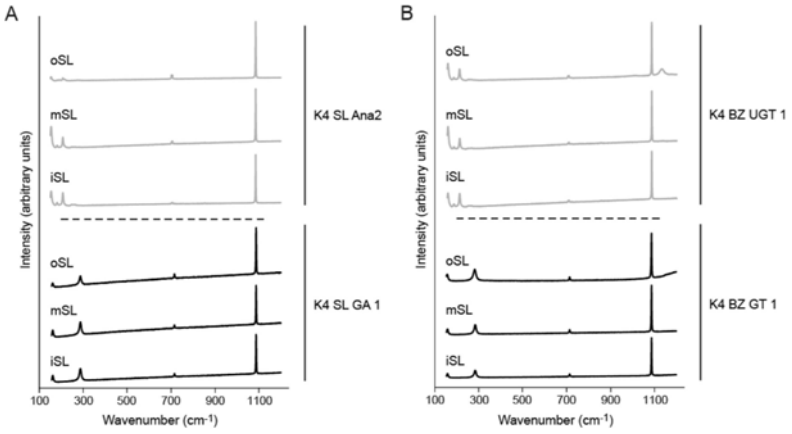

Fig. 4.4.7 Raman spectra of (A) *A. uropigimelana* and (B) *T. palustris* from the United Arab Emirates archaeological sites. Specimens K4 SL Ana2 and K4 BZ UGT 1 preserve their aragonitic OSL, MSL and ISL (grey lines). Specimens K4 SL GA 1 and K4 BZ GT 1 display calcite in all shell layers (black lines).

Crystal morphology and crystallography were previously identified as potential factors controlling mineralogical transformations (Koga et al., 2013). In abiotic systems, aragonite crystals split and released water trapped within them. Furthermore, calcite nucleation occurs preferably along mineral cracks and twin boundaries (Bischoff and Fyfe, 1968; Liu and Yund, 1993). For these reasons, crystal characteristics and positions of boundaries influence the conversion reaction (Koga et al., 2013). The architectural diversity among mollusc species and shell layers may be the origin of the variable reaction of different biominerals to thermal stress (Kobayashi and Samata, 2006). Aragonitic mineral units tend to lose density and acquire nanopores on their surfaces, while a network of cracks forms in the material (Perdikouri et al., 2011; Villagran et al., 2011; Gomez-Villalba et al., 2012). These features were also observed in the present study in *P. lineatus* specimens roasted at 400 °C, i.e., before full conversion into calcite.

Table 4.4.3 Trench U (Haua Fteah) ^{14}C dates

Sample ID	Lab Code	Material	Age (^{14}C years)	±	Age (cal BP) (unmodelled)	Age (cal BP) (modelled)
U742_1	MAMS 30538	*P. Turbinatus*	7300	21	7901–7556 *[1]	7869–7560 *[1]
U742_2	MAMS 30539	*P. Turbinatus*	7184	21	7772–7438 *[1]	7747–7461 *[1]
U742_3	MAMS 30540	*P. Turbinatus*	6378	21	7002–6558 *[1]	6978–6610 *[1]
ARO747UG	OxA-27,391	*P. Turbinatus*	8171	37	8891–8381 *[1]	8776–8385 *[1]
ARO747UC	OxA-27,490	*P. Turbinatus*	7447	35	8024–7652 *[1]	8008–7675 *[1]
742 < 5982 > /118C	UBA-28873	charcoal	6965	39	7551–7405	7551–7405
743 < 5984 > /119C	UBA-28874	charcoal	6291	50	6883–6627	6880–6630
746 < 88 > / A	UBA-25915	*H. Melanostoma*	8670	39	8930–8534 *[2]	8840–8531 *[2]
743 < 83 >	UBA-25912	*H. Melanostoma*	7732	37	7850–7590 *[2]	7840–7605 *[2]

Symbol *[1] indicates dates corrected using reservoir offset of 58 ± 85 14C years (Reimer and McCormac, 2002).

Symbol *[2] indicates dates corrected using reservoir offset of 476 ± 48 14C years (Hill et al., 2017).

Given the complexity in the thermal behaviour of biogenic materials, the three-pronged approach of mineralogical, macro- and microscopic observations is essential to better understand the thermally-induced diagenetic processes. The identification of specific changes in the shell can be used as indicator of shell processing temperatures, although possibly with some differences from species to species.

Implications of heat exposure for palaeoenvironmental reconstructions

Heat exposure can induce an exchange of oxygen isotopes with the surrounding environment, drastically altering initial shell isotopic composition (Andrus and Crowe, 2002; Milano et al., 2016). Temperatures higher than 300 °C are observed to cause a significant decrease in $\delta^{18}O_{shell}$ (Milano et al., 2016). Our results are in good agreement with the previous findings suggesting that the use of burnt mollusc shells may have important implications for palaaeoenvironmental reconstructions. A decrease in $\delta^{18}O_{shell}$ translates into an overestimation of the reconstructed water temperature, which can jeopardize the reliability of related reconstructions. Furthermore, burning at high temperatures can influence the results of palaeoseasonality studies by incorrectly estimating the season(s) of mollusc collection, which in turn may affect the interpretation of hunter-gatherer mobility and settlement use. It is recommended to discard shells with signs of thermal exposure for isotopic analyses. However, it has to be noted that not all heating intensities imply isotopic alteration. Low temperatures (< 300 °C) do not induce significant changes in the $\delta^{18}O_{shell}$. Shells exposed to such temperatures can still be used to accurately estimate palaeotemperatures. However, a careful analysis is needed to differentiate between the different heat exposures and to ensure an optimal sample selection for isotopic studies. It is also advisable to avoid any form of pre-treatment involving heating, which was commonly adopted in the past as method for organic matter removal (Mook, 1971).

Prehistoric fire events and shell middens

Different types of fire events can be associated to shell middens, according to their nature and use. The first evidence for controlled fire is dated to around 300,000–250,000 years ago and it is related to a change in hominin habits, especially concerning diet (James et al., 1989; Shahack-Gross et al., 2014;

Gowlett, 2016). Among the main benefits of using fire for dietary purposes are the maximization of energy gain and food digestibility and the development of social abilities such as storing, sharing and processing food (Ragir, 2000; Wrangham and Conklin-Brittain, 2003; Wrangham, 2009; Wrangham and Carmody, 2010). Several ethnographic studies suggest that cooking may play an important role in shellfish consumption (Percy, 1608; Meehan, 1977, 1982). Cooking is generally known to facilitate the extraction of the edible portion. In fact, the heat weakens the muscle attachment of the molluscs causing the valves to open (bivalves) and the flesh to detach more easily. In Australia and North America molluscs were placed over or underneath fire, coals or hot stones (Kroeber and Barrett, 1960; Beaglehole, 1974; Bailey, 1977). In other cases, they were cooked in earth ovens (Meehan, 1982; Waselkov, 1987; Thoms, 2008). Additionally, steaming was adopted as an alternative technique by some ethnic groups such as the Maori in New Zealand and the Quileute and the Tlingit in the Pacific Northwest (Best, 1924; Reagan, 1934; Newton and Moss, 1984). Generally, the cooking processes were rather fast, possibly lasting only a few minutes (Meehan, 1977; Thoms, 2008). After being cooked, mollusc soft tissues were sometimes dried or smoked to enable storage for longer periods of time and for trading purposes (Greengo, 1952; Moss, 1993). In addition to food preparation, fire could have being used for trash disposal (Ford, 1989). Ethnographic observations by Meehan (1982) describe occasional burning of food debris by igniting grass on top of large mounds of disposed shells. However, in other cases, the shells were arranged in heaps and covered with sand, without involving any fire (Bird and Bliege Bird, 1997). Alternatively, Mougne et al. (2014) suggested the shell refuses to be directly thrown into a fire. To contextualize our results in the light of the ethnographic records, the experimental work by Aldeias et al. (2016) simulating different firing techniques offers a valuable source of information. The authors showed that when a fire was set on top or underneath a pile of shells, there was a great degree of heterogeneity in the shell mineralogical response. The heat diffusion affected differently the single specimens according to their position in respect to the heat source, resulting in a mixture of aragonitic and calcitic shells. Our results indicate that the distribution of specific burning-related features is generally shared among the specimens of the same layer suggesting a homogenous exposure to heat. An exception to this trend is represented by the shells from the Neolithic layer U742, which will be discussed further below. Such uniform heat exposure likely implies heating of relatively small quantities of shells with a similar position in respect to the fire whereas large amounts of material, characteristic of disposal mounds, would induce a significant spatial heat gradient and diverse thermal response. Furthermore, concerning the food disposal by throwing the shells into the fire, this involves direct contact with extreme temperatures. Under these circumstances, the shells would become extremely brittle and prone to a rapid disintegration with limited chances of fossil 'survival' (Milano et al., 2016). In this perspective, our data conform better with firing events associated to food processing rather than food disposal. However, further analysis on additional material is needed before unequivocally discriminate between the two different types of fire. Estimation of shellfish heating temperatures from the Haua Fteah suggests a clear distinction between the two archaeological contexts studied here. The seven Mesolithic shells all appear to have been exposed to temperatures between 600 and 700 °C. These temperatures can be reached when the shellfish are situated in close proximity to the heat source without being directly in contact with it. Temperatures between 633 and 781 °C were recorded when experimentally roasting the molluscs on a surface with fuel and fire on top of them (Aldeias et

al., 2016). Such temperatures fit well with our observations on the shell remains. However, it has to be considered that roasting temperatures also largely depend on the type of fuel used. In the experiments by Aldeias et al. (2016), pine wood and pine needles were adopted, whereas grass material is known to burn at lower temperatures (max. 430 °C; Wolf et al., 2013). In the light of these observations and our own results, shellfish during the Mesolithic phase at the Haua Fteah were probably processed underneath woody fires. In contrast, the Neolithic shells from the Haua Fteah layers U747 and U743 have features pointing to lower temperature exposure: ca. 71% were heated at temperatures around 300 °C. The drastic increase in remains exposed to lower temperatures in the Neolithic phase can be explained by changes in the shellfish processing. A potential interpretation is related to the appearance of the first pottery during the Neolithic, which could have been used to prepare shellfish (McBurney, 1967; Douka et al., 2014; Prendergast et al., 2016). Although the use of vessels for processing marine resources has not been yet attested around the Mediterranean during the Neolithic (Debono and Craig, 2014), it has been previously observed in other regions (Craig et al., 2011; Taché and Craig, 2015). An experiment conducted by Maggetti et al. (2011) showed that clay pots exposed to fire can reach temperatures of around 300 °C after ca. 10 min, supporting our observations in the shells of layers U747 and U743. A second interpretation of the lower temperature exposure during the Neolithic encompasses similar heating processes with the adoption of substantially different types of fuel. As mentioned above, the usage of grasses as fuel could explain the lower burning temperatures experienced by the Neolithic shells. As an exception to the general trend observed in the results, the shells from unit U742 present heterogeneous burning features related to temperatures from 300 °C to 600 °C, with one shell without any burning sign. On the basis of our observations two hypotheses can be discussed. Different burning degrees may indicate the presence of a thermal gradient related with the use of fire for disposal purposes. Alternatively, the shell may reveal changes in cooking processes in relation to the type of fuel used and/or cooking vessels adoption. In the case of the archaeological samples from the United Arab Emirates, both species showed evidences related to heating at 500–600 °C. Archaeological sites in this area dated to the late Bronze Age or Classic Wadi Suq period (2000–1500 BCE) are characterized by a large amount of pottery remains such as beakers and spouted globular jars (Carter, 1997). In this region, food processing with pots seems to have appeared during the Bronze Age, whereas roasting on fire was the preferred method in earlier times (Händel, 2013). However, the small sample size considered in the present study does not allow us a more precise interpretation. In order to better understand the evolution of shellfish processing in the area, additional specimens are needed. Together with intentional fires, natural burning events can occur in shell middens. A distinction between intentional and unintentional firing events can hardly be determined on the basis of shell thermal response. However, as in the case of disposal by directly throwing the shells into fire, long-lasting uncontrolled fires would lead to the complete disappearance of the shell remains within the midden. In our case, the preservation of large fragments and whole shells suggests that the heat exposure was likely not related to long-lasting natural fires. However, rapid fires cannot fully be discharge as potential burning sources.

Heat exposure and radiocarbon dating robustness

Previous studies on shell-tempered pottery showed that these materials provide consistent ^{14}CAMS dates (Rick and Lowery, 2013). To obtain resistant ceramics, shell-tempered pottery is typically fired at 300–600 °C and - after cooling - fired again to 500–600 °C (Kingery et al., 1976; Herbert, 2008). Such temperatures do not seem to affect radiocarbon ages on the shell inclusions, which fit well with dates from charcoal and bone fragments of the same context (Rick and Lowery, 2013). Shells analysed in the present study did not differ from already available ages of the same stratigraphic context. According to the structural and mineralogical analyses, two of the samples were burned at 500 °C and 600 °C, whereas the third one was not burned. The relatively homogeneous AMS dates suggest that heating does not affect radiocarbon ages, even when polymorphic transformation has occurred. This may be due to the fact that the extremely small quantity of carbon remaining in the material (ca 0.1 wt%) is still enough to allow AMS dating (Lanting et al., 2001). Furthermore, physical alterations of the biomineral such as structural unit enlargement and recrystallization seem to provide a barrier protecting the remaining carbon (van Strydonck et al., 2005).

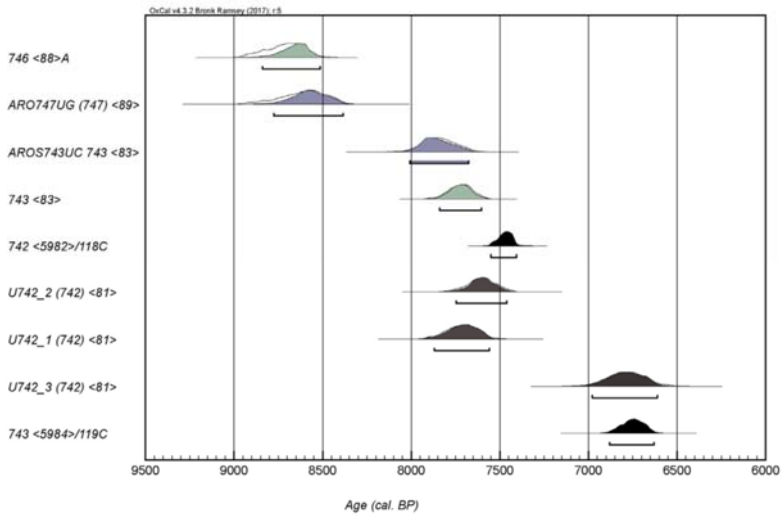

Fig. 4.4.8 Distribution of calibrated ^{14}C dates of Haua Fteah Trench U. Colour-coding corresponds to the different materials used in the dating. Green = *H. melanostoma* shells; blue = well-preserved *P. turbinatus*; grey = *P. turbinatus* from this study; black=charcoal.

Methods to identify thermal exposure on shell remains

Our results show that the overall appearance of shells alone is an insufficient approach to identify heating-related changes (Milano et al., 2016). Although useful in cases of exposure to high temperatures with evident burning marks, examination by the naked eye has important limitations when it comes to lower temperatures. For instance, based on the outer shell layer, specimen U742_2 seemed to have been exposed to 300 °C. However, according to more detailed analysis using SEM it turned out to be untreated. The analysis of the mineralogical response to heat is valuable when combined with other methods. However, it may prove ambiguous when used alone. The archaeological material analysed for this study did not show any carbonate polymorph transition phase. Therefore, Raman spectroscopy could only help to distinguish between temperatures below and above 500 °C. Our current and previous results indicate that a combined approach of optical microscopy, SEM and Raman spectroscopy is the most suitable solution to identify alterations related to shellfish processing. The combined use to these techniques will provide more robust data on heating exposure, whether the aim of

the research is to preclude heated shells for palaeotemperature reconstructions (Milano et al., 2016) or to examine the food processing in more detail. Although the experimental phase was specifically designed for *Phorcus spp*., the observations showed similarities with the thermal behavior of *A. uropigimelana* and *T. palustris*. Such analogy in the responses to heat suggests that temperature estimation can be achieved among different mollusc species even without a specific foregoing experimental phase. Results of our findings can be used to answer a broad spectrum of different questions in the framework of shell midden research and shell-tempered pottery studies. Further studies on calcite mollusc shells are needed to complement the existing data on aragonite shells. This will improve the understanding of the biomineralized tissue thermal response in the case of a more stable calcium carbonate phase. Although the methodology developed offers a powerful toolbox to reconstruct shell thermal exposure, care must be paid when interpreting the results in the archaeological context. As discussed, the preservation conditions of the shells (i.e., entire shells/small fragments; homogenous/ heterogeneous burning features) can offer insights into the type of fire event. However, these parameters cannot resolve with certainty the exact nature of the fire (intentional/natural; cooking-related/disposal- related). Furthermore, it is important to mention that, given the irreversible nature of the structural and mineralogical thermal response, multiple burning events cannot be discerned. As for any study on burnt remains, the signature preserved is related to the highest temperature experienced by the shell material.

4.4.6 Conclusions

The experimental component of this study has confirmed that shellfish processing methods encompassing temperatures greater than or equal to 300 °C do significantly alter mollusc shell material, but that the duration of the heating does not appear to significantly affect the behaviour of the shell to thermal treatment. According to these findings, structural and chemical changes occur as soon as the shell is exposed to high temperatures. The results also confirm that using burnt shells for palaeoenvironmental reconstructions can produce incorrect temperature estimations and affect the interpretation of environmental and human-related conditions. One proviso to these findings is that the experiments were conducted on fresh shell from which the flesh had been removed when the live molluscs were collected, and further experimental work is needed to establish what impact the presence of body fluids might have on the results. However, burned shells remain a valuable source of information. The experimental changes observed in the modern shells at macro-, microstructural and mineralogical scales have allowed us to determine a set of criteria to detect heating temperatures that can easily be applied to archaeological shells. Analysis of archaeological shells of *P. turbinatus* from the Haua Fteah cave in coastal northeast Libya revealed that during the Mesolithic the shells were uniformly exposed to high temperatures (shells in close proximity to the heat source) whereas during the Neolithic lower temperatures were recorded. Although, the use of fire for non-dietary purposes cannot be completely ruled out, the trend in our results can be interpreted as a temporal change in shellfish preparation. Analysis of archaeological shells of *A. uropigimelana* and *T. palustris* from Neolithic and Bronze Age shell midden sites on the coast of the United Arab Emirates found that some specimens did not show any evidence of burning while others showed indications of high-temperature exposure. Although

burning affected the shell structure and mineralogy, it does not appear to have a significant influence on radiocarbon ages suggesting the possibility of using burnt remains for dating purposes. The fact that the thermal reaction of different species is similar provides confidence in applying the techniques outlined in this study at an interspecific level.

Acknowledgements

The authors thank Michael Maus and Dr. Tobias Häger for helping during isotope analysis and Raman measurements and Dr. Lucy Farr for selecting the shells from the Haua Fteah assemblage. Funding for this study was kindly provided by the EU within the framework (FP7) of the Marie Curie International Training Network ARAMACC (604802) to SM and by the Alexander von Humboldt Postdoctoral Fellowship (1151310) and McKenzie Postdoctoral Fellowship to AP. The Haua Fteah excavations were undertaken with the permission of the Libyan Department of Antiquities and with funding to GB from the Society for Libyan Studies and from the European Research Council (Advanced Investigator Grant 230421), whose support is also gratefully acknowledged. The three anonymous reviewers are thanked for their constructive comments on the manuscript.

Appendix A.

Supplementary data Supplementary data to this article can be found online at https://doi.org/10.1016/j.jasrep.2018.05.027.

4.4.7 References

Aldeias, V., Gur-Arieh, S., Maria, R., Monteiro, P., Cura, P., 2016. Shell we cook it? An experimental approach to the microarchaeological record of shellfish roasting. Archaeol. Anthropol. Sci. http://dx.doi.org/10.1007/s12520-016-0413-1.

Andrus, C.F.T., 2011. Shell midden sclerochronology. Quat. Sci. Rev. 30, 2892–2905. http://dx.doi.org/10.1016/j.quascirev.2011.07.016.

Andrus, C.F.T., Crowe, D.E., 2002. Alteration of otolith aragonite: effects of prehistoric cooking methods on otolith chemistry. J. Archaeol. Sci. 29, 291–299. http://dx.doi. org/10.1006/jasc.2001.0694.

Bailey, G.N., 1977. Shell mounds, shell middens, and raised beaches in the Cape York Peninsula. Man 11, 132–143.

Balmain, J., Hannoyer, B., Lopez, E., 1999. Fourier transform infrared spectroscopy (FTIR) and XRD analyses of mineral and organic matrix during heating of mother of pearl (nacre) from the shell of the mollusc Pinctada maxima. J. Biomed. Mater. Res. 48, 749–754. http://dx.doi.org/10.1002/(SICI)1097-4636(1999)48.

Barker, G., Antoniadou, A., Armitage, S., Brooks, I., Candy, I., Connell, K., Douka, K., Drake, N., Farr, L., Hill, E., Hunt, C., Inglis, R., Jones, S., Lane, C., Lucarini, G., Meneeley, J., Morales, J., Mutri, G., Prendergast, A.L., Rabett, R., Reade, H., Reynolds, T., Russell, N., Simpson, D., Smith, B., Stimpson, C., Twati, M., White, K., 2010. The Cyrenaican Prehistory Project 2010: the fourth season of investigations of the

Haua Fteah cave and its landscape, and further results from the 2007-2009 fieldwork. Libyan Stud. http://dx.doi.org/10.1017/S0263718900004519.

Barker, G., Bennett, P., Farr, L., Hill, E., Hunt, C., Lucarini, G., Morales, J., Mutri, G., Prendergast, A.L., Pryor, A., Rabett, R., Reynolds, T., Spry-Marques, P., Twati, M., 2012. The Cyrenaican Prehistory Project 2012: the fifth season of investigations of the Haua Fteah cave. Libyan Stud. 43, 115–136. http://dx.doi.org/10.1017/ S026371890000008X.

Beaglehole, J.C. (Ed.), 1974. The Journals of Captain James Cook on his Voyages of Discovery: The Voyage of the Endeavor, 1768–1771. Hakluyt Society, Cambridge.

Beech, M., Kallweit, H., 2001. A note on the archaeological and environmental remains from site JH57, a 5th–4th millennium BC shell midden in Jazirat al-Hamra, Ra's al-Khaimah. Tribulus 11, 17–20.

Berna, F., Goldberg, P., 2008. Assessing Paleolithic pyrotechnology and associated hominin behaviour in Israel. Isr. J. Earth Sci. 56, 107–121. http://dx.doi.org/10.1560/ IJES.56.2-4.107.

Best, E., 1924. The Maori. vol. 2 Wellington.

Biagi, P., Torke, W., Tosi, M., Uerpmann, H., 1984. Qurum: a case study of coastal archaeology in Northern Oman. Coast. Archaeol. 16, 43–61.

Bird, D.W., Bliege Bird, R.L., 1997. Contemporary shellfish gathering strategies among the Meriam of the Torres Strait Islands, Australia: testing predictions of a central place foraging model. J. Archaeol. Sci. 24, 39–63. http://dx.doi.org/10.1006/jasc. 1995.0095.

Bischoff, J.L., Fyfe, W.S., 1968. Catalysis, inhibition, and the calcite-aragonite problem: I. The calcite-aragonite transformation. Am. J. Sci. http://dx.doi.org/10.2475/ajs.266. 2.80.

Bosch, M.D., Wesselingh, F.P., Mannino, M.A., 2015. The Ksâr'Akil (Lebanon) mollusc assemblage: Zooarchaeological and taphonomic investigations. Quat. Int. 390, 85–101. http://dx.doi.org/10.1016/j.quaint.2015.07.004.

Bourrat, X., Francke, L., Lopez, E., Rousseau, M., Stempfle, P., Angellier, M., Alberic, P., 2007. Nacre biocrystal thermal behaviour. Spec. Publ. R. Soc. Chem. 9, 1205–1208. http://dx.doi.org/10.1039/b709388h.

Broadhurst, C.L., Wang, Y., Crawford, M.A., Cunnane, S.C., Parkington, J.E., Schmidt, W.F., 2002. Brain-specific lipids from marine, lacustrine, or terrestrial food resources: potential impact on early African Homo sapiens. Comp. Biochem. Physiol. B Biochem. Mol. Biol. 131, 653–673. http://dx.doi.org/10.1016/S1096-4959(02)00002-7.

Burchell, M., Cannon, A., Hallmann, N., Schwarcz, H.P., Schöne, B.R., 2013. Refining estimates for the season of shellfish collection on the Pacific Northwest coast: applying high-resolution stable oxygen isotope analysis and sclerochronology. Archaeometry 55, 258–276. http://dx.doi.org/10.1111/j.1475-4754.2012.00684.x.

Butler, P.G., Wanamaker, A.D., Scourse, J.D., Richardson, C.A., Reynolds, D.J., 2013.

Variability of marine climate on the North Icelandic Shelf in a 1357-year proxy archive based on growth increments in the bivalve Arctica Islandica. Palaeogeogr. Palaeoclimatol. Palaeoecol. 373, 141–151. http://dx.doi.org/10.1016/j.palaeo.2012. 01.016.

Carlen, A., Olafsson, E., 2002. The effects of the gastropod Terebralia palustris on infaunal communities in a tropical tidal mud-flat in East Africa. Wetl. Ecol. Manag. 10, 303–311.

Carter, R., 1997. The Wadi Suq period in south-east Arabia: a reappraisal in the light of excavations at Kalba, UAE. Proc. Semin. Arab. Stud. 27, 87–98.

Carter, J.G., Harries, P.J., Malchus, N., Sartori, A.F., Anderson, L.C., Bieler, R., Bogan, A.E., Coan, E.V., Cope, J.C.W., Cragg, S.M., Garcia-March, J.R., Hylleberg, J., Kelley, P., Kleemann, K., Kriz, J., Mcroberts, C., Mikkelsen, P.M., Pojeta, J.J., Temkin, I., Yancey, T., Zieritz, A., 2012. Illustrated glossary of the bivalvia. Treatise Online 1, 209.

Colonese, A.C., Troelstra, S., Ziveri, P., Martini, F., Lo Vetro, D., Tommasini, S., 2009. Mesolithic shellfish exploitation in SW Italy: seasonal evidence from the oxygen isotopic composition of Osilinus turbinatus shells. J. Archaeol. Sci. 36, 1935–1944. http://dx.doi.org/10.1016/j.jas.2009.04.021.

Colonese, A.C., Mannino, M.A., Bar-Yosef Mayer, D.E., Fa, D.A., Finlayson, J.C., Lubell, D., Stiner, M.C., 2011. Marine mollusc exploitation in Mediterranean prehistory: an overview. Quat. Int. 239, 86–103. http://dx.doi.org/10.1016/j.quaint.2010.09.001.

Craig, O.E., Steele, V.L., Fischer, A., Hartz, S., Andersen, S.H., Donohoe, P., Glykou, A., Saul, H., Jones, M.D., Koch, E., Heron, C.P., 2011. Ancient lipids reveal continuity in culinary practices across the transition to agriculture in Northern Europe. Proc. Natl. Acad. Sci. U. S. A. 108, 17910–17915. http://dx.doi.org/10.1073/pnas.0913714.

Da Costa, M.A., 2015. Distribution and Shape Analysis of Phorcus lineatus and Phorcus sauciatus along the Portuguese Coast. Universidade de Lisboa.

Debono, Spiteri C., Craig, O.E., 2014. Biomolecular and isotopic characterisation of lipid residues absorbed in Impressed Wares from the Early Neolithic village of Skorba, Malta. Malta Archaeol. Rev. 14–22.

Donald, K.M., Preston, J., Williams, S.T., Reid, D.G., Winter, D., Alvarez, R., Buge, B., Hawkins, S.J., Templado, J., Spencer, H.G., 2012. Phylogenetic relationships elucidate colonization patterns in the intertidal grazers Osilinus Philippi, 1847 and Phorcus Risso, 1826 (Gastropoda: Trochidae) in the northeastern Atlantic Ocean and Mediterranean Sea. Mol. Phylogenet. Evol. 62, 35–45. http://dx.doi.org/10.1016/j. ympev.2011.09.002.

Douka, K., Jacobs, Z., Lane, C., Grün, R., Farr, L., Hunt, C., Inglis, R.H., Reynolds, T., Albert, P., Aubert, M., Cullen, V., Hill, E., Kinsley, L., Roberts, R.G., Tomlinson, E.L., Wulf, S., Barker, G., 2014. The chronostratigraphy of the Haua Fteah cave (Cyrenaica, northeast Libya). J. Hum. Evol. 66, 39–63. http://dx.doi.org/10.1016/j.jhevol.2013. 10.001.

Eerkens, J.W., Byrd, B.F., Spero, H.J., Fritschi, A.K., 2013. Stable isotope reconstructions of shellfish harvesting seasonality in an estuarine environment: implications for late Holocene San Francisco Bay settlement patterns. J. Archaeol. Sci. 40, 2014–2024. http://dx.doi.org/10.1016/j.jas.2012.12.018.

Epstein, S., Buchbaum, R., Lowenstam, H.A., Urey, H.C., 1953. Revised carbonate-water isotopic temperature scale. Bull. Geol. Soc. Am. 64, 1315–1326.

Erlandson, J.M., 2001. The archaeology of aquatic adaptations: paradigm for a new millennium. J. Archaeol. Res. 9, 287–350.

Erlandson, J.M., Rick, T.C., Vellanoweth, R.L., Kennett, D.J., 1999. Maritime subsistence at a 9300 year old shell midden on Santa Rosa Island, California. J. F. Archaeol. 26, 255–265. http://dx.doi.org/10.1179/jfa.1999.26.3.255.

Fa, D.A., 2008. Effects of tidal amplitude on intertidal resource availability and dispersal pressure in prehistoric human coastal populations: the Mediterranean-Atlantic transition. Quat. Sci. Rev. 27, 2194–2209. http://dx.doi.org/10.1016/j.quascirev.2008. 07.015.

Farr, L., Lane, R., Abdulazeez, F., Bennett, P., Holman, J., Marasi, A., Prendergast, A., Al-Zweyi, M., Barker, G., 2014. The Cyrenaican Prehistory Project 2013: the seventh season of excavations in the Haua Fteah cave. Libyan Stud. 45, 163–173.

Ferguson, J.E., Henderson, G.M., Fa, D.A., Finlayson, J.C., Charnley, N.R., 2011. Increased seasonality in the Western Mediterranean during the last glacial from limpet shell geochemistry. Earth Planet. Sci. Lett. 308, 325–333. http://dx.doi.org/ 10.1016/j.epsl.2011.05.054.

Ford, P.J., 1989. Molluscan assemblages from archaeological deposits. Geoarchaeology 4, 157–173. http://dx.doi.org/10.1002/gea.3340040205.

Gardner, A.S., 2005. Marine mollusc shells from two archaeological sites near Al Ain. Tribulus 15 (1), 9–12.

Girod, A., 2011. Land snails from Late Glacial and Early Holocene Italian sites. Quat. Int. 244, 105–116.

Gomez-Villalba, L.S., Lopez-Arce, P., Alvarez De Buergo, M., Fort, R., 2012. Atomic defects and their relationship to aragonite-calcite transformation in portlandite nanocrystal carbonation. Cryst. Growth Des. 12, 4844–4852.

Goodwin, D.H., Flessa, K.W., Schöne, B.R., Dettman, D.L., 2001. Cross-calibration of daily growth increments, stable isotope variation, and temperature in the Gulf of California bivalve mollusc Chione cortezi: implications for palaeoenvironmental analysis. PALAIOS 16, 387–398. http://dx.doi.org/10.1669/0883-1351(2001)016.

Gowlett, J.A.J., 2016. The discovery of fire by humans: a long and convoluted process. Philos. Trans. R. Soc. B Biol. Sci. 371, 20150164. http://dx.doi.org/10.1098/rstb. 2015.0164.

Greengo, R.E., 1952. Shellfish of the California Indians. Anthropol. Soc. 7, 63–114.

Gutiérrez-Zugasti, I., Garcia-Escarzaga, A., Martin-Chivelet, J., Gonzalez-Morales, M.R., 2015. Determination of sea surface temperatures using oxygen isotope ratios from Phorcus lineatus (Da Costa, 1778) in northern Spain: implications for paleoclimate and archaeological studies. The Holocene 25, 1002–1014. http://dx.doi.org/10.1177/0959683615574892.

Hammond, H., 2014. Taphonomic analysis of archaeomalacological assemblages: shell middens on the northern coast of Santa Cruz (Patagonia, Argentina). Intersecciones in Antropologia Suppl. 15 (1).

Händel, M., 2013. Al-Hamriya - Dynamik einer Muschelhaufenlandschaft in den Vereinigten Arabischen Emiraten. Archit. Aust. 77–96.

Herbert, J.M., 2008. The history and practice of shell tempering in the Middle Atlantic: a useful balance. Southeast. Archaeol. 27, 265–285.

Hill, E.A., Reimer, P.J., Hunt, C.O., Prendergast, A.L., Barker, G.W., 2017. Radiocarbon ecology of the land snail Helix melanostoma in Northeast Libya. Radiocarbon 59, 1–22. http://dx.doi.org/10.1017/RDC.2017.49.

Houbrick, R.S., 1991. Systematic review and functional morphology of the mangrove snails Terebralia and Telescopium (Potamididae; Prosobranchia). Malacologia 33, 289–338.

Huang, Z., Li, X., 2009. Nanoscale structural and mechanical characterization of heat treated nacre. Mater. Sci. Eng. C 29, 1803–1807. http://dx.doi.org/10.1016/j.msec.2009.02.007.

Hunt, C.O., Reynolds, T.G., El-Rishi, H., Buzaian, A., Hill, E., Barker, G.W., 2011. Resource pressure and environmental change on the North African littoral: Epipalaeolithic to Roman gastropods from Cyrenaica, Libya. Quat. Int. 244, 15–26. http://dx.doi.org/10.1016/j.quaint.2011.04.045.

James, S.R., Dennell, R.W., Gilbert, A.S., Lewis, H.T., Gowlett, J.A.J., Lynch, T.F., Mcgrew, W.C., Peters, C.R., Pope, G.G., Stahl, A.B., 1989. Hominid use of fire in the Lower and Middle Pleistocene: a review of the evidence. Curr. Anthropol. 30, 1–26. http://dx.doi.org/10.2307/2743299.

Jones, D.S., 1983. Sclerochronology: reading the record of the molluscan shell. Am. Sci. 71, 384–391.

Kendall, M.A., 1987. The age and structure of some northern populations of the trochid gastropod Monodonta lineata. J. Molluscan Stud. 53, 213–222.

Kingery, W.D., Bowen, H.K., Uhlmann, D.R., 1976. Introduction to Ceramics. John Willey and Sons, New York.

Kobayashi, I., Samata, T., 2006. Bivalve shell structure and organic matrix. Mater. Sci. Eng. C 26, 692–698. http://dx.doi.org/10.1016/j.msec.2005.09.101.

Koga, N., Kasahara, D., Kimura, T., 2013. Aragonite crystal growth and solid-state aragonite-calcite transformation: a physico-geometrical relationship via thermal dehydration of included water. Cryst. Growth Des. 13, 2238–2246. http://dx.doi.org/10. 1021/cg400350w.

Kroeber, A.L., Barrett, S.A., 1960. Fishing among the Indians of Northwestern California. University of California Anthropological Records.

Kromer, B., Lindauer, S., Synal, H., Wacker, L., 2013. A new AMS facility at the Curt-Engelhorn-Centre for Achaeometry, Mannheim, Germany. Nucl. Inst. Methods Phys. Res. B 294, 11–13. http://dx.doi.org/10.1016/j.nimb.2012.01.015.

Lanting, J.N., Aerts-Bijma, A.T., van der Plicht, J., 2001. Dating of cremated bones. Radiocarbon 43, 249–254. http://dx.doi.org/10.2458/azu_js_rc.v.3946.

Lécuyer, C., 1996. Effects of heating on the geochemistry of biogenic carbonates. Chem. Geol. 129, 173–183. http://dx.doi.org/10.1016/0009-2541(96)00005-8.

Lindauer, S., Marali, S., Schöne, B.R., Uerpmann, H.-P., Kromer, B., Hinderer, M., 2016. Investigating the local reservoir age and stable isotopes of shells from Southeast Arabia. Radiocarbon 355-372. http://dx.doi.org/10.1017/RDC.2016.80.

Lindauer, S., Santos, G.M., Steinhof, A., Yousif, E., Phillips, C., Jasim, S.A., Uerpmann, H.P., Hinderer, M., 2017. The local marine reservoir effect at Kalba (UAE) between the Neolithic and Bronze Age: an indicator of sea level and climate changes. Quat. Geochronol. 42, 105–116. http://dx.doi.org/10.1016/j.quageo.2017.09.003.

Liu, M.L., Yund, R.A., 1993. Transformation kinetic of polycristalline aragonite to calcite: new experimental data, modelling and implications. Contrib. Mineral. Petrol. 114, 465–478. http://dx.doi.org/10.1007/BF00321751.

de Lumley, H., 1966. Les fouilles de Terra Amata à Nice. Premiers résultats. Bulletin du Musée d'Anthropologie et Préhistoire de Monaco 13, 29–51.

Maggetti, M., Neururer, C., Ramseyer, D., 2011. Temperature evolution inside a pot during experimental surface (bonfire) firing. Appl. Clay Sci. 53, 500–508. http://dx. doi.org/10.1016/j.clay.2010.09.013.

Mannino, M.A., Thomas, K.D., 2001. Intensive Mesolithic exploitation of coastal resources? Evidence from a shell deposit on the Isle of Portland (Southern England) for the impact of human foraging on populations of intertidal rocky shore molluscs. J. Archaeol. Sci. 1101–1114. http://dx.doi.org/10.1006/jasc.2001.0658.

Mannino, M.A., Thomas, K.D., 2002. Depletion of a resource? The impact of prehistoric human foraging on intertidal mollusc communities and its significance for human settlement, mobility and dispersal. World Archaeol. 33, 452–474. http://dx.doi.org/10.1080/00438240120107477.

Mannino, M.A., Spiro, B.F., Thomas, K.D., 2003. Sampling shells for seasonality: oxygen isotope analysis on shell carbonates of the inter-tidal gastropod Monodonta lineata (da Costa) from populations across its modern range and from a Mesolithic site in southern Britain. J. Archaeol. Sci. 30, 667–679. http://dx.doi.org/10.1016/S0305-4403(02)00238-8.

Mannino, M.A., Thomas, K.D., Leng, M.J., Piperno, M., Tusa, S., Tagliacozzo, A., 2007. Marine resources in the mesolithic and neolithic at the Grotta dell'Uzzo (Sicily): evidence from isotope analyses of marine shells. Archaeometry 49, 117–133. http://dx.doi.org/10.1111/j.1475-4754.2007.00291.x.

Mannino, M.A., Thomas, K.D., Leng, M.J., Sloane, H.J., 2008. Shell growth and oxygen isotopes in the topshell Osilinus turbinatus: resolving past inshore sea surface temperatures. Geo-Mar. Lett. 28, 309–325. http://dx.doi.org/10.1007/s00367-008-0107-5.

Marean, C.W., Bar-Matthews, M., Bernatchez, J.A., Fisher, E.C., Goldberg, P., Herries, A.I.R., Jacobs, Z., Jerardino, A., Karkanas, P., Minichillo, T., Nilssen, P.J., Thompson, E., Watts, I., Williams, H.M., 2007. Early human use of marine resources and pigment in South Africa during the Middle Pleistocene. Nature 449, 906–909. http://dx.doi.org/10.1038/nature06204.

Maritan, L., Mazzoli, C., Freestone, I., 2007. Modelling changes in mollusc shell internal microstructure during firing: implications for temperature estimation in shell-bearing pottery. Archaeometry 49, 529–541. http://dx.doi.org/10.1111/j.1475-4754.2007.00318.x.

McBurney, C.B.M. (Ed.), 1967. The Haua Fteah (Cyrenaica) and the Stone Age of the South-East Mediterranean. Cambridge University Press, Cambridge.

Meehan, B., 1977. Hunters by the seashore. J. Hum. Evol. 6, 363–370.

Meehan, B., 1982. Shell Bed to Shell Midden. Australian Institute of Aboriginal Studies, Canberra.

Menzies, R., Cohen, Y., Lavie, B., Nevo, E., 1992. Niche adaptation in two marine gastropods, Monodonta turbiformis and M. turbinata. Bolletino di Zool. 59, 297–302. http://dx.doi.org/10.1080/11250009209386685.

Milano, S., Prendergast, A.L., Schöne, B.R., 2016. Effects of cooking on mollusc shell structure and chemistry: implications for archeology and palaeoenvironmental reconstruction. J. Archaeol. Sci. Rep. 7, 14–26. http://dx.doi.org/10.1016/j.jasrep.2016.03.045.

Milano, S., Schöne, B.R., Witbaard, R., 2017. Changes of shell microstructural characteristics of Cerastoderma edule (Bivalvia) - a novel proxy for water temperature. Palaeogeogr. Palaeoclimatol. Palaeoecol. 465, 395–406. http://dx.doi.org/10.1016/j.palaeo.2015.09.051.

Miyaji, T., Tanabe, K., Schöne, B.R., 2007. Environmental controls on daily shell growth of Phacosoma japonicum (Bivalvia: Veneridae) from Japan. Mar. Ecol. Prog. Ser. 336, 141–150. http://dx.doi.org/10.3354/meps336141.

Mook, W., 1971. Paleotemperatures and chlorinities [CORRECT?] from stable carbon and oxygen isotopes in shell carbonate. Palaeogeogr. Palaeoclimatol. Palaeoecol. 9, 245–263. http://dx.doi.org/10.1016/0031-0182(71)90002-2.

Moss, M.L., 1993. Shellfish, gender, and status on the northwest coast: reconciling archeological, ethnographic, and ethnohistorical records of the Tlingit. Am. Anthropol. 95, 631–652. http://dx.doi.org/10.1525/aa.1993.95.3.02a00050.

Mougne, C., Dupont, C., Giazzon, D., Quesnel, L., 2014. Shellfish from the Bronze Age Site of Clos des Châtaigniers (Mathieu, Normandy, France). Internet Archaeol. http://dx.doi.org/10.11141/ia.37.5.

Newton, R., Moss, M., 1984. The subsistence lifeway of the Tlingit people: excerpts of oral interviews. In: USDA Forest Service Alaska Region Report No.179. Juneau.

Nishihira, M., Kuniyoshi, M., Shimamura, K., 2002. Size variation in Terebralia palustris (Gastropoda: Potamididae) of Iriomote Isl and, southern Japan, and its effect on some population characteristics. Wetl. Ecol. Manag. 10, 243–247.

Oschmann, W., 2009. Sclerochronology: editorial. Int. J. Earth Sci. 98, 1–2. http://dx.doi.org/10.1007/s00531-008-0403-3.

Percy, G., 1608. Observations Gathered out of a Discourse of the Plantation of the Southern Colony in Virginia by the English, 1606.

Perdikouri, C., Kasioptas, A., Geisler, T., Schmidt, B.C., Putnis, A., 2011. Experimental study of the aragonite to calcite transition in aqueous solution. Geochim. Cosmochim. Acta 75, 6211–6224. http://dx.doi.org/10.1016/j.gca.2011.07.045.

Perić, J., Vučak, M., Krstulović, R., Brečević, L., Kralj, D., 1996. Phase transformation of calcium carbonate polymorphs. Thermochim. Acta 277, 175–186. http://dx.doi.org/10.1016/0040-6031(95)02748-3.

Petchey, F., Ulm, S., David, B., Mcniven, I.J., Asmussen, B., Tomkins, H., Dolby, N., Aplin, K., Richards, T., Rowe, C., Leavesley, M., 2013. High-resolution radiocarbon dating of marine materials in archaeological contexts: radiocarbon marine reservoir variability between Anadara, Gafrarium, Batissa, Polymesoda spp. and Echinoidea at Caution Bay, Southern Coastal Papua New Guinea. Archaeol. Anthropol. Sci. 5, 69–80. http://dx.doi.org/10.1007/s12520-012-0108-1.

Phillips, C.S., Mosseri-Marlio, C.E., 2002. Sustaining change: the emerging picture of the Neolithic to Iron Age subsistence economy at Kalba, Sharjah Emirate, UAE. In: Proceedings of the Fifth International Symposium on the Archaeozoology of Southwestern Asia and Adjacent Areas. ARC-Publicaties, Groningen, The Netherlands.

Plaziat, J.C., 1984. Mollusc distribution in the mangal. In: Por, D., Dor, I. (Eds.), Hydrobiology of the Mangal: The Ecosystem of the Mangrove Forests. Junk, Boston, pp. 111–143.

Prendergast, A.L., Schöne, B.R., 2017. Oxygen isotopes from limpet shells: implications for palaeothermometry and seasonal shellfish foraging studies in the Mediterranean. Palaeogeogr. Palaeoclimatol. Palaeoecol. 484, 33–47. http://dx.doi.org/10.1016/j.palaeo.2017.03.007.

Prendergast, A.L., Azzopardi, M., O'Connell, T.C., Hunt, C., Barker, G., Stevens, R.E., 2013. Oxygen isotopes from Phorcus (Osilinus) turbinatus shells as a proxy for sea surface temperature in the central Mediterranean: a case study from Malta. Chem. Geol. 345, 77–86. http://dx.doi.org/10.1016/j.chemgeo.2013.02.026.

Prendergast, A.L., Stevens, R.E., O'Connell, T.C., Fadlalak, A., Touati, M., Al-Mzeine, A., Schöne, B.R., Hunt, C.O., Barker, G.W., 2016. Changing patterns of eastern Mediterranean shellfish exploitation in the Late Glacial and Early Holocene: oxygen isotope evidence from gastropods in Epipaleolithic to Neolithic human occupation layers at the Haua Fteah cave, Libya. Quat. Int. 407, 80–93. http://dx.doi.org/10.1016/j.quaint.2015.09.035.

Ragir, S., 2000. Diet and food preparation: rethinking early hominid behavior. Evol. Anthropol. 9, 153–155. http://dx.doi.org/10.1002/1520-6505(2000)9:4<153::AIDEVAN4>3.0.CO;2-D.

Reagan, A.B., 1934. Various uses of plants by West Coast Indians. Washingt. Hist. Q. 25, 133–137.

Reimer, P.J., McCormac, F.G., 2002. Marine radiocarbon reservoir corrections for the Mediterranean and Aegean Seas. Radiocarbon 44, 159–166.

Reimer, P.J., Bard, E., Bayliss, A., Beck, J.W., Blackwell, P.G., Bronk, C., Caitlin, R., Hai, E.B., Edwards, R.L., 2013. Intcal13 and marine13 radiocarbon age calibration curves 0–50,000 years cal CP. Radiocarbon 55, 1869–1887. http://dx.doi.org/10.2458/azu_js_rc.55.16947.

Rick, T.C., Lowery, D.L., 2013. Accelerator mass spectrometry 14C dating and the antiquity of shell-tempered ceramics from the Chesapeake Bay and Middle Atlantic. Am. Antiq. 78, 570–579.

Schembri, P.J., Deidun, A., Mallia, A., Mercieca, L., 2005. Rocky shore biotic assemblages of the Maltese Islands (Central Mediterranean): a conservation perspective. J. Coast. Res. 21, 157–166.

Schöne, B.R., 2008. The curse of physiology—challenges and opportunities in the interpretation of geochemical data from mollusc shells. Geo-Mar. Lett. 28, 269–285. http://dx.doi.org/10.1007/s00367-008-0114-6.

Schöne, B.R., Krause, R.A., 2016. Retrospective environmental biomonitoring – Mussel Watch expanded. Glob. Planet. Chang. 144, 228–251. http://dx.doi.org/10.1016/j.gloplacha.2016.08.002.

Schöne, B.R., Freyre Castro, A.D., Fiebig, J., Houk, S.D., Oschmann, W., Kröncke, I., 2004. Sea surface water temperatures over the period 1884-1983 reconstructed from oxygen isotope ratios of a bivalve mollusc shell (Arctica islandica, southern North Sea). Palaeogeogr. Palaeoclimatol. Palaeoecol. 212, 215–232. http://dx.doi.org/10.1016/j.palaeo.2004.05.024.

Schöne, B.R., Fiebig, J., Pfeiffer, M., Gleß, R., Hickson, J., Johnson, A.L.A., Dreyer, W., Oschmann, W., 2005. Climate records from a bivalved Methuselah (Arctica islandica, Mollusca; Iceland). Palaeogeogr. Palaeoclimatol. Palaeoecol. 228, 130–148. http://dx.doi.org/10.1016/j.palaeo.2005.03.049.

Shackleton, N.J., 1973. Oxygen isotope analysis as a means of determining season of occupation of prehistoric midden sites. Archaeometry 15, 133–141. http://dx.doi.org/10.1111/j.1475-4754.1973.tb00082.x.

Shahack-Gross, R., Berna, F., Karkanas, P., Lemorini, C., Gopher, A., Barkai, R., 2014. Evidence for the repeated use of a central hearth at Middle Pleistocene (300 ky ago) Qesem Cave, Israel. J. Archaeol. Sci. 44, 12–21. http://dx.doi.org/10.1016/j.jas.2013.11.015.

Smith, D., 1978. Delia Smith's Complete Cookery Course. BBC Publications, London.

Steinhardt, J., Butler, P.G., Carroll, M.L., Hartley, J., 2016. The application of long-lived bivalve sclerochronology in environmental baseline monitoring. Front. Mar. Sci. 3. http://dx.doi.org/10.3389/fmars.2016.00176.

Taché, K., Craig, O.E., 2015. Cooperative harvesting of aquatic resources and the beginning of pottery production in north-eastern North America. Antiquity 89, 177–190. http://dx.doi.org/10.15184/aqy.2014.36e.

Taylor, V.K., Barton, R.N.E., Bell, M., Bouzouggar, A., Collcutt, S., Black, S., Hogue, J.T., 2011. The Epi-palaeolithic (Iberomaurusian) at Grotte des Pigeons (Taforalt), Morocco: a preliminary study of the land Mollusca. Quat. Int. 244, 5–14. http://dx.doi.org/10.1016/j.quaint.2011.04.041.

Tebano, T., Paulay, G., 2001. Variable recruitment and changing environments create a fluctuating resource: the biology of Anadara uropigimelana (Bivalvia: Arcidae) on Tarawa atoll. Atoll Res. Bull. 488.

Thoms, A.V., 2008. The fire stones carry: ethnographic records and archaeological expectations for hot-rock cookery in western North America. J. Anthropol. Archaeol. 27, 443–460. http://dx.doi.org/10.1016/j.jaa.2008.07.002.

Van Strydonck, M., Boudon, M., Hoefkens, M., G., D.M., 2005. 14C-dating of cremated bones, why does it work? Lunula. Archaeol. Protohistorica 13, 3–10.

Villagran, X.S., Balbo, A.L., Madella, M., Vila, A., Estevez, J., 2011. Experimental micromorphology in Tierra del Fuego (Argentina): building a reference collection for the study of shell middens in cold climates. J. Archaeol. Sci. 38, 588–604. http://dx.doi.org/10.1016/j.jas.2010.10.013.

Wacker, L., Fülöp, R., Hajdas, I., Molnár, M., Rethemeyer, J., 2013. A novel approach to process carbonate samples for radiocarbon measurements with helium carrier gas. Nucl. Inst. Methods Phys. Res. B 294, 214–217. http://dx.doi.org/10.1016/j.nimb.2012.08.030.

Waselkov, G.A., 1987. Shell gathering and shell midden archaeology. Adv. Archeol. Method Theory 10, 93–209.

Wolf, M., Lehndorff, E., Wiesenberg, G.L.B., Stockhausen, M., Schwark, L., Amelung, W., 2013. Towards reconstruction of past fire regimes from geochemical analysis of charcoal. Org. Geochem. 55, 11–21. http://dx.doi.org/10.1016/j.orggeochem.2012.11.002.

Wrangham, R., 2009. Catching Fire: How Cooking Made Us Human. Basic Books, New York.

Wrangham, R., Carmody, R., 2010. Human adaptation to the control of fire. Evol. Anthropol. 19, 187–199. http://dx.doi.org/10.1002/evan.20275.

Wrangham, R., Conklin-Brittain, N., 2003. Cooking as a biological trait. Comp. Biochem. Physiol. - A 136, 35–46. http://dx.doi.org/10.1016/S1095-6433(03)00020-5.

Yoshioka, S., Kitano, Y., 1985. Transformation of aragonite to calcite through heating. Geochem. J. 19, 245–249.

Zolotoyabko, E., Pokroy, B., 2007. Biomineralization of calcium carbonate: structural aspects. CrystEngComm 9, 1156–1161. http://dx.doi.org/10.1039/b710974a.

4.5 Heating Mollusc Shells: A Radiocarbon and Microstructure Perspective from Archaeological Shells recovered from Kalba, Sharjah Emirate, UAE

Susanne Lindauer [a,b], Stefania Milano [c], Axel Steinhof [d], Matthias Hinderer [b]

[a] Curt-Engelhorn-Zentrum Archaeometry gGmbH, Klaus-Tschira-Archaeometry-Centre, C4, 8, 68159 Mannheim, Germany
[b] Institute of Applied Geosciences, Technical University Darmstadt, Schnittspahnstr. 9, 64287 Darmstadt, Germany
[c] Department of Human Evolution, Max Planck Institute for Evolutionary Anthropology, Deutscher Platz 6, 04103 Leipzig, Germany
[d] Max-Planck Institute for Biogeochemistry, Hans-Knöll-Str. 10, 07745 Jena, Germany

Contributions: SL, SM designed the study; SM worked on Raman and SEM; SL, AS produced radiocarbon data; SL, MH collected the samples; SL, SM wrote the paper.
Citation: Lindauer, S., Milano, S., Steinhof, A., Hinderer, M., 2018b. Heating mollusc shells - A radiocarbon and microstructure perspective from archaeological shells recovered from Kalba, Sharjah Emirate, UAE. *Journal of Archaeological Science: Reports* **21***,* 528-537*.*

4.5.1 Abstract

This publication aims to shed light on the influence that prior heating (burning) of mollusc shells during human activity may have on the results of radiocarbon dating. We compare the geochemical and mineralogical composition of heated and unheated shells of *Anadara uropigimelana* and *Terebralia palustris* recovered from Neolithic and Bronze Age archaeological contexts at Kalba, Sharjah Emirate, in the United Arab Emirates (UAE). Our research examined whether the heating of shells impacts on the determination of reservoir effects, or whether in spite of heating, this material remains a viable material for precise ^{14}C measurements. Our results show that both heated and non-heated shells of *A. uropigimelana* and *T. palustris* provide consistent results, although the mineral composition of the shells changes from aragonite to calcite. Our results are important, since some of our selection of shells did not initially appear to have been heated. A heating process will then usually be detected as a greyish, marble like structure when cutting the shells. As a result of this work, we have also developed insights into prehistoric cooking practices of shells collected in Arabia. Our results provide archaeologists and associated researchers with confidence when assessing the results of radiocarbon dating during their studies of shells that might have been heated.

4.5.2 Introduction

Shells provide valuable sources of information within archaeology, whether for establishing chronologies for archaeological sites by means of radiocarbon dating and AAR (Kosnik et al. 2017) or through palaeoclimate and palaeoenvironmental studies (Biagi 1994, Zazzo et al. 2016, Lindauer et al. 2017). This is especially so in arid environments where other organic matter such as peat or humic silt and clay are poorly preserved. Given the abundance of burnt shells in archaeological deposits (Stringer 2008, Barker et al. 2010, Taylor 2011), it is fundamental to understand the effect of heating on the

geochemical composition of the shelly material, which in turn, may have consequences for the determination of reservoir effects during radiocarbon dating.

Depending on the species, shells can provide high-resolution information about palaeoenvironments over decades, centuries or millenia (Wanamaker Jr et al. 2008, Andrus 2011, Scourse et al. 2012, Hallmann et al. 2013, Paul and Mauldin 2013, Lindauer et al. 2017). The information stored in the shell material contains evidence about environmental conditions and food resources throughout their complete lifetime (Culleton et al. 2006, Hallmann et al. 2013, Leng and Lewis 2016, Twaddle et al. 2017). Furthermore, shells can aid our understanding of strategies of food procurement by hunter-gatherer communities (Burchell et al. 2013). In archaeological contexts, large quantities of aquatic shells are found along contemporary or past coastlines, either as discrete shell midden deposits, or associated with settlements (Uerpmann 1990, Biagi 1994, Biagi 1999, Parker and Goudie 2007, Biagi 2013, Fernández-López de Pablo 2016). Sometimes shells are also found in excavations further inland, e.g. as grave goods (Kutterer 2013). In all these contexts, it is critical to know whether or not heated (burnt) shells can still be used to provide chronological control. Furthermore, sometimes it is not obvious at first sight whether shell remains have been heated or not. The most obvious way that shells would be heating is during the cooking process.

In an earlier paper, Milano et al. (2016) focused upon species *Phorcus turbinatus*. The behaviour of shell microstructures and changes associated with the temperature of heating were explored; it was shown that above a temperature of 500 °C a mineralogical transformation from aragonite into calcite and major structural alterations occurred. Milano et al. (2016) also found that exposure to high temperatures resulted in a systematic shift in the oxygen stable isotope content ($\delta^{18}O$), which has significant implications for palaeoclimatic interpretations of sea surface temperatures. The information on altered microstructures is relevant when interpreting the radiocarbon data on heated shells as a change in microstructure might lead to an incorporation of surrounding carbon sources like atmosphere or ash.

When investigating ancient shell midden sites or settlements, shells are often used for radiocarbon dating. However, shells that show evidence of burning are generally excluded from such studies. However, it is important to remember that in some cases it may not be possible to detect burning features at first sight. Thus, cooked shells could unintentionally be selected for dating. It is therefore important to know how heating affects the dates that may potentially result when using shells for radiocarbon dating.

In this paper, we build upon the studies of Milano et al. (2016) and explore the role that heating of mollusc shells may have on radiocarbon analyses based on (shell) material recovered from an archaeological site, Khor Kalba in the United Arab Emirates (UAE).

Shells from archaeological sites in Kalba

Khor Kalba in the Sharjah Emirate, United Arab Emirates, is a city that lies on the Gulf of Oman, between the Hajar Mountains and the present-day coast (Fig. 4.5.1). Since the Neolithic, there has been a lagoon near Kalba where mangroves, mostly *Avicenna marina*, are abundant, providing the local population with food and wood. In Kalba, shell middens dating back to the Neolithic are located in the

vicinity of the mangroves and the surrounding sabkha (salt flats), thus providing potential information about human dietary strategy (Phillips and Mosseri-Marlio 2002, Magee 2014). However, no Neolithic settlements have been found. Nonetheless, north of the shell middens and the city of Kalba, ancient settlement structures, including mudbrick walls, houses and a tower dating from the Bronze Age and the Iron Age have been discovered (Fig. 4.5.1) and investigated archaeologically (Carter 1997, Phillips and Mosseri-Marlio 2002).

In the present study, we focus on two species of marine shell, *Anadara uropigimelana* (Bory de Saint-Vincent, 1827) and *Terebralia palustris* (L), that were identified in large quantities from a shell midden and archaeological settlement near the mangrove at Kalba. These shells show a species-specific radio-carbon reservoir effect, as their lifestyle and diet differ significantly, although both are found in or near mangrove forests. *Anadara uropigimelana* is a filter feeder and lives buried in the sand (Murray-Wallace et al. 2000, Azzoug et al. 2012), whilst in contrast, *Terebralia palustris* feeds on leaf litter (Slim et al. 1997, Fratini et al. 2008) and can be found on the surface of sediments, or attached to mangrove roots. Hence, each of them utilizes different carbon sources. This leads to a different species-specific reservoir effect, as suggested by other studies, for example, in the United States (Culleton et al. 2006). For this study, we sampled a shell midden of late Neolithic date, but with two distinct phases (site code KK1): once in 2013 and again in 2015 (Fig. 4.5.1). We also collected younger specimens of Bronze Age date from a settlement northwest of the modern city of Kalba (site code K4); near a mudbrick wall, we located two shell layers, one on top of the other, and sampled each of them separately. The lower layer, referred to as MBZ1 (Middle Bronze Age 1) turns out to be around 100 years older than the overlying layer MBZ2. The younger layer (MBZ2) consisted mainly of shells, in contrast to the older layer (MBZ1), which comprised a mix of shells, ash and sediment. The age correlations follow those of Carl Philipps (pers. Comm., Phillips and Mosseri-Marlio, 2002, Lindauer et al., 2017).

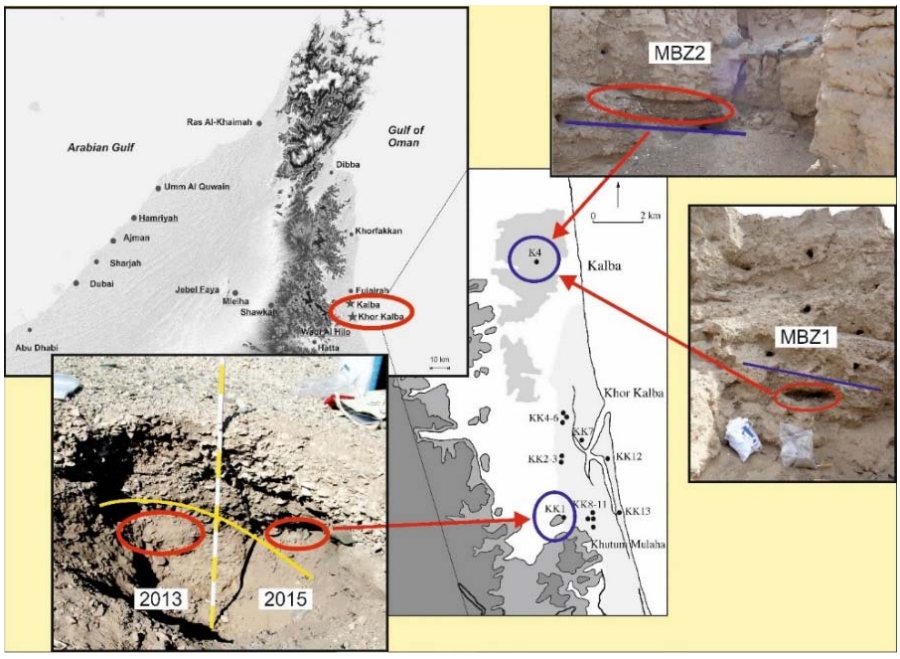

Fig. 4.5.1 Map of Kalba in the United Arab Emirates with sampling sites. KK1 is a Neolithic shell midden covering two different periods (below and above the yellow line) sampled in 2013 and 2015; K4 is a settlement from the Bronze Age where two shell layers on top of each other were sampled (MBZ1 and MBZ2, MBZ meaning Middle Bronze Age).

The environmental conditions of shell growth as well as seasonal patterns are usually investigated using sclerochronology and stable isotopes ($\delta^{13}C$ and $\delta^{18}O$). Kalba is a settlement along a lagoon with occasional inputs of freshwater as a result of heavy rainfall events, which makes $\delta^{13}C$ signals difficult to interpret due to the several overlapping sources of carbon influencing the signal. Shell $\delta^{13}C$ mirrors processes like ecosystem metabolism as well as estuarine mixing, but for marine shells, it is mainly influenced by dissolved inorganic carbon (DIC) in the water (McConnaughey and Gillikin, 2008). In contrast, the $\delta^{18}O$ signature is easier to interpret, since it mainly reflects sea surface temperature and salinity.

For *A. uropigimelana*, its shell grows continuously from autumn until spring but its growth ceases in the summer. The seasonality of shell growth and hence the ability to reflect seasonal environmental changes in *A. uropigimelana* from Kalba had been investigated using growth lines and stable isotopes, $\delta^{13}C$ and $\delta^{18}O$ (Lindauer et al., 2016); it also enables the determination of the season of collection/harvesting of the shell. For *Terebralia palustris*, these factors have not yet been investigated.

Radiocarbon measurements on shells

In coastal archaeological and geochronological studies, shells (marine and terrestrial) are often used for radiocarbon dating, especially in arid areas, where the rate of preservation of organic material is low (Biagi, 1994; Diedrich, 2006). However, dating marine shells is not straightforward. Marine shells usually show ages which appear to be older than contemporary terrestrial materials, due to the old carbon content of the reservoir from which they incorporate carbon (Ascough et al., 2005; Dutta, 2008; Petchey et al., 2013; Petchey, 2011; Southon et al., 2002). Oceans can store carbon for very long timescales, especially when the carbon is transported to great depths, where it can remain for around 1000 years or more (Ascough et al., 2005; Dutta, 2008). During this time, ^{14}C, being radioactive (half-life 5730 ± 40 years), decays and is not replaced by new ^{14}C from the atmosphere. Therefore, deep water becomes depleted in ^{14}C. Due to ocean circulation patterns, this ^{14}C – depleted ("old") water can be brought up to shallower water depths or to the surface, where it can be incorporated by organisms, making their apparent radiocarbon age older than their calendar age. This older age is called reservoir age R (t) (Stuiver and Braziunas, 1993; Stuiver et al., 1986). Hence, for marine material, a specific radiocarbon calibration curve exists. The current marine calibration curve is Marine13 (Reimer et al., 2013), but locally, there can be a difference between the marine calibration curve and the determined reservoir age. This offset is known as local reservoir effect ΔR (Petchey, 2008; Stuiver et al., 1986). For archaeologists working in coastal environments, knowledge of this reservoir effect is fundamental to building chronologies, if shells are to be used to establish chronologies through dating. For palaeoenvironmental research, changes in reservoir effects become important, since they reflect variations in the environmental conditions, such as fluctuations in sea levels.

A previous study (Lindauer et al., 2017) determined a species-specific reservoir effect and its variation between the Neolithic and Bronze Age on shells of *A. uropigimelana* and *T. palustris* from midden KK1 and settlement K4 in Kalba, Sharjah Emirate, UAE (Table 4.5.1). Because *T. palustris* feeds mainly on leaf litter of mangrove leaves, its radiocarbon signal has a terrestrial component, and therefore results in a lower reservoir effect than for *A. uropigimelana*, which feeds exclusively on algae and other marine particulates. Between the Neolithic and Bronze Age, the reservoir effect ΔR decreased significantly,

from 576 ± 90 years to 105 ± 50 for *A. uropigimelana* and 390 ± 66 to -26 ± 46 years for *T. palustris*. As can be seen in Table 4.5.1, the difference between the species is also reduced through time. These time-dependent (species-specific) reservoir effects reflect not only changes in the local environmental conditions (such as sea level, food resources and food quality), but also larger-scale changes in climate, as can be seen when comparing climate estimates with proxy records from other locations (Culleton et al., 2006; Lindauer et al., 2017). The reasons for changes in ΔR over time, and especially the tendency for negative ΔR values for *T. palustris*, are discussed in detail, and compared with other ΔR studies in nearby areas, in Lindauer et al. (2017).

The use of ash as terrestrial counterpart for determining a reservoir effect is always critical. The preferred material for this would be charcoal fragments, preferably from short-lived species or branches. One does not always have the possibility to choose and needs to deal with difficult material. In this case the ash samples were tested using stable isotopes to derive the origin of their main component. As in our case the $\delta^{13}C$ values had been found to be between – 20 to – 23 ‰ these samples can be regarded as being of plant origin. Mangrove leaves and branches have $\delta^{13}C$ values in the range of -20 to -28 ‰. Contamination from attached carbonates etc. is removed during sample preparation. A discussion of this can be found in Lindauer et al. (2017).

Sample	Material	^{14}C age (BP)	ΔR (yrs)
	Shell midden - Neolithic		
KK1-BL	Ash	6117 ± 26	
Anadara sp.	shell marine		*576 ± 90*
Terebralia sp.	shell marine		*389 ± 66*
KK1 ash	Ash	5723 ± 46	
Anadara sp.	shell marine		*200 ± 30*
Terebralia sp.	shell marine		*172 ± 99*
	K4 MBZ1		
K4 BZ Ash	Charcoal	3531 ± 40	
K4 BZ DS	Date stone	3537 ± 35	
Anadara sp.	shell marine		*105 ± 50*
Terebralia sp.	shell marine		*-26 ± 46*
	K4 MBZ2		
K4 SL Ash	*Charcoal*	3425 ± 15	
Anadara sp.	shell marine		*112 ± 44*
Terebralia sp.	shell marine		*-19 ± 36*

Table 4.5.1 Reservoir effects ΔR and corresponding terrestrial ages of *A. uropigimelana* and *T. palustris* from Kalba KK1 and K4. Ash samples had been tested using stable isotope measurements (IRMS), and found δ13C-values of -20 to -23 ‰, corresponding to wood or other C3 plants. See (Lindauer et al., 2017) for details and data.

As found out by Zazzo et al. (2012), an old wood effect from heating the shells with older parts of a tree (for example) should clearly be evident in older radiocarbon ages of the dated material. In our case, when using wood for heating, an old wood effect might cause depleted ^{14}C to be stored in the shell. A similar investigation was conducted on the inclusion of old wood ^{14}C into animal bones when heating them (Snoeck et al., 2016; Zazzo et al., 2012). Zazzo et al. (2012) suggest using $\delta^{13}C$ to determine whether carbon of bone apatite originates from bone or partially from the charcoal used. In order to decide whether this is also necessary in the case of heated shells, we need to know the temperature of combustion, its duration and the type of fuel (old wood) used for the fire. Depending on the heating process and the wood used this might provide a possible explanation if we find older radiocarbon ages for heated shells compared to unprocessed shell material of the same archaeological layer.

Mineralogy

The two common forms of calcium carbonate occurring in shells are aragonite and calcite. Molluscs precipitate their shells, adopting one of these two phases, though in some cases, they precipitate both forms. Shell mineralogical composition can be determined using Confocal Raman Microscopy (CRM) and Scanning Electron Microscopy (SEM). It can also be determined by using Fourier Transform Infrared Spectrometry (FTIR), among other methods. Aragonite is a $CaCO_3$ metastable phase, which tends to convert into the more stable calcite, as a result of diagenetic recrystallization (Loftus et al. 2015). Naturally, diagenesis occurs over significant geological timespans. However, exposure to elevated temperatures can accelerate this process, mimicking the effect of diagenesis on shell structure and composition. During the process of dissolution and recrystallization, all environmental information stored in the carbonate is substantially affected (Loftus et al. 2015). Because aragonite is prone to diagenetic alteration, changes at the geochemical level become severe when carbon depleted in $\delta^{13}C$ and ^{14}C is involved. Since calcite is more stable, there should be no further exchange with the environment, following complete transition. In naturally- and slowly-occurring diagenetic processes, a larger data spread can be expected, since old and new information might be mixed. However, as the heat-induced diagenesis process is significantly faster, a different response can be expected. Geochemical, structural and mineralogical features serve to better understand the transition process itself, and the possible carbon exchange, which can be responsible for potential dating errors.

Methods of heating a shell

Different colour shades on the shell surface, from light grey to dark grey and sometimes white, indicate different heat exposures and potentially, different cooking techniques (Milano et al., 2016). For instance, darker colourations may be related to direct contact with the heat source (i.e. burning in a fire). On the other hand, shells with lighter shades might have been heated through a medium (i.e. boiled in pots) or else burnt only for a short time. Cooking pots have been found in Arabia, dating from the Bronze and Iron Age, but not from Neolithic contexts (Händel, 2014). In this geographical area, details about how the shells were cooked or heated are not well understood. However, an ethnological study of traditional methods of shellfish cooking and burning by aboriginal communities in Australia in the 1970s was published by Meehan (1982). This showed that the shells are placed in a previously cleaned area of sand, hinge side up. Small wooden sticks and dead grass are placed on top of them and ignited. The fire starts at one end of the ‘shell phalanx’ and travels along the shells (Fig. 4.5.2). This fire is designed to be hot and fast, burning for a few minutes only, enough to release the mollusc muscle attachment and to allow the opening of the valves. The mollusc flesh is then extracted and eaten, once the shells have cooled down (Meehan, 1982).

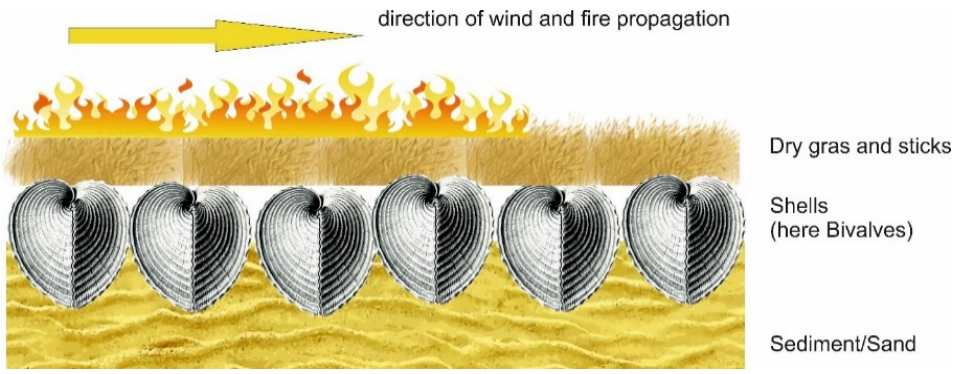

Fig. 4.5.2 Schematic drawing of heating of bivalves as described in Meehan (1982). Grass and small branches on top of the shells are used to make a quick, hot fire, which opens the bivalves.

The traditional processing techniques observed within that study seem to fit, on the whole, with our observations of the colouration of the shells presented in this paper. What makes Meehan's findings even more relevant to our study is that the most common shellfish consumed by these populations were species of *Tapes hiantina*. (in the Arabian Sea, this species is comparable to *Marcia flammea*, *Marcia, marmorata., Protapes sinuosa. and Circenita callipyga*.), and other species which can be found in the Arabian Sea, especially *T. palustris* and *A. uropigimelana*.

Meehan (1982), provides observations on foraging seasons and diet composition and describes several occasions on which shellfish were cooked. These observations indicate that this type of food processing has an important role in the marine resource-based diet of hunter-gatherer communities. The areas used for shellfish processing and cooking were often associated with the dinnertime camps, home bases or processing sites near the beds where the molluscs were collected. The latter case might account for shell middens not always being linked to a specific long-term settlement, as in the case of Kalba. In particular, Meehan (1982) carefully describes a common cooking practice still used by the local populations in the 1970s.

Meehan (1982) also describes the use of steam ovens. This practice is adopted for large quantities of shellfish (ca. 70 kg) prepared for ceremonial gatherings. On these occasions, a large pit measuring around 1 m2 is constructed and firewood placed into it. Numerous empty shells collected from the beach are then placed on top of the charcoal. The shells with living organisms still inside are tipped onto this surface of old shells and charcoal, and then covered with green branches, which prevent steam from escaping. As for the cooking time, the use of this technique takes only a few minutes (around two minutes, Meehan, 1982). The observation that older shells were also used on top of the charcoal to make the fire is important when considering the presence of outliers in radiocarbon data derived from the analysis of shell samples. If older shells are used as a cooking base, and mixed with fresh shells, older ages might be present in the results. Potentially, such results can supply additional information regarding cooking processes, thus providing important archaeological evidence. For this and other reasons (variability between specimens), older dates should not be excluded when reporting datasets and their origins robustly considered.

4.5.3 Material and Methods

Radiocarbon

Here, we present previously published shell data from Kalba, Sharjah Emirate, UAE (Lindauer et al., 2016; Lindauer et al., 2017), but now with respect to the role that heating may have had on the shell material. We also use new material to allow a distinct comparison of the radiocarbon ages of burnt and unburnt shells of different species. The shells we had dated previously were analysed and dated either at: the Curt-Engelhorn-Centre Archaeometry (CEZA) in Mannheim, Germany (Kromer et al., 2013; Lindauer et al., 2016) using a MICADAS system (Synal, 2007); the KCCAMS facility of the University of California, Irvine, USA (Santos and Ormsby, 2013; Santos and Xu, 2016); or at the Max-Planck-Institute for Biogeochemistry (MPI-BGC), Jena, Germany (Steinhof et al., 2004). The new shells measured for comparison were only measured at MPI-BGC. The pretreatment and measurement procedure of all these facilities are described in detail in Lindauer et al. (2017).

The terrestrial ages of these new shell measurements cover the Neolithic as well as the Middle Bronze Age, and are given in Table 4.5.2, accompanied by the radiocarbon ages on contemporaneous ash, charcoal and stone (DS in Table 4.5.2). The ash samples were checked for their wood origin using stable isotope $\delta^{13}C$ measurements, which gave results of -20 to -23 ‰, representing typical wood/plant values of C3 plants. Being adjacent to a mangrove, the wood used for burning, and the charcoal samples derived from it, could be mangrove trees (here *Avicenna marina*). Due to low rainfall in this area, only a few acacia and similar trees are found and these have rather short life-spans.

All calibrations in this publication were carried out using Oxcal 4.2. (Bronk Ramsey and Lee, 2013; Ramsey, 1995) using the Intcal13 and Marine13 dataset (Reimer et al., 2013). The isotope values of $\delta^{13}C$ measured with the AMS system are not given, because they only correct the measurement, but do not allow an interpretation regarding the source of the material. For this purpose a measurement of $\delta^{13}C$ from an Isotope Ratio Mass Spectrometer (IRMS) would be needed.

Table 4.5.2 Calibration of terrestrial radiocarbon ages of contemporaneous material for the shells in our investigation. KK1 is the late Neolithic shell midden, with two distinct phases. K4 is the ancient settlement from the Middle Bronze Age. Calibrated with Oxcal 4.2 using the IntCal13 dataset. Measurements of $\delta^{13}C$ are only given when measured with IRMS (Isotope ratio mass spectrometer), not from AMS measurements.

Labcode	Sample	Material	C14 age	$\delta^{13}C$	cal BC	Mean cal BC
			BP	‰	(2σ)	
MAMS 22875	KK1-BL	Ash	6117 ± 26	-25.2	5207-4957	5038 ± 38
UCIAMS173933	KK1 ash	Ash	5755 ± 20	-20.8	4685-4544	4598 ± 34
UCIAMS173934	KK1 ash	Ash (duplicate)	5690 ± 20	-20.6	4559-4459	4518 ± 15
P 13304	K4 MBZ1 Ash	Charcoal	3531 ± 40		1971-1746	1860 ± 38
P 13305	K4 MBZ1 DS	Date stone	3537 ± 35		1961-1752	1878 ± 32
UCIAMS171125	K4 MBZ2 charcoal	Charcoal	3425 ± 15	-24.0	1770-1683	1718 ± 18
UCIAMS171126	K4 MBZ2 charcoal	Charcoal (dup)	3420 ± 15	-23.0	1758-1665	1717 ± 17

Mineralogy and Microstructures

The shells of *A. uropigimelana* were cut along the growth axis into 3 mm thick sections using a low-speed, precision saw (Buehler Isomet 1000). The sections were then mounted on microscope slides using JB KWIK epoxy resin, and polished using SiC (800 and 1200 grit). After each polish, the samples were rinsed in an ultrasonic bath for 3-4 mins. Subsequently they were polished with Al_2O_3 powder (1 µm).

Changes in the mineralogical composition were investigated with Confocal Raman Microscopy (CRM). Point measurements were taken of each of three shell layers (inner shell layer, middle shell layer, outer shell layer) of both species. A Horiba Jobin Yvon LabRam 800 spectrometer coupled with an Olympus BX41 optical microscope was used (employing a 532.21 nm laser wavelength, a 400 µm confocal hole, a grating with 1800 grooves/mm, an entrance slit width of 100 µm and 50× magnification, long working distance objective lens). The time window for acquisition was 5 s. The mineralogy of sample K4 MBZ1 A1 was analyzed using a WITec alpha 300 R (WITec GmbH, Germany) confocal Raman microscope. Scans of 5100 × 1000 µm and 100 × 100 µm were performed using a 488 nm diode laser. A spectrometer (UHTS 300, WITec, Germany) was used with a 600 mm−1 grating, a 500 nm blaze and an integration time of 0.09 s.

Microstructures were analyzed using a LOT Quantum Design Phenom Pro desktop Scanning Electron Microscope (SEM). To enhance the visibility of the carbonate structures, the sections of shell were first etched in 1 vol% HCl for 5 s and sputter-coated with a 2 nm-thick layer of platinum, using a Leica EM ACE200 Vacuum Coating machine.

4.5.4 Results

Raman measurements

Raman spectroscopy was performed in order to assess the mineralogical conversion of the shell material (Lindauer et al., 2016; Milano et al., 2018). Both *A. uropigimelana* and *T. palustris*, have aragonitic shells that tend to convert into calcite upon heating. The shells are formed in three microstructurally different layers (oSL= outer shell layer; mSL= middle shell layer; iSL= inner shell layer). Fig. 4.5.3 shows an *A. uropigimelana* specimen (K4 MBZ1 A1), appearing unheated on the outside, however when cut, it shows an interesting and unexpected appearance, which is attributable to heating. For this shell, single data points were measured using CRM, both for the internal part of the shell, as well as for the outer shell layer (Fig. 4.5.3). The results indicate that the outer part is composed completely of calcite, as can be seen from the inorganic calcite spectrum, plotted for comparison. In this case, the typical calcite peaks are present at 153 cm-1, 281 cm-1, 713 cm-1 and 1086 cm-1. In contrast, the internal component of the shell shows an extra peak at 206 cm−1, which indicates the presence of aragonite (Fig. 4.5.3).

In order to further understand the extent of incomplete mineralogical transition, large scans were performed using CRM in two areas of interest. One scan was performed near the hinge, an area where the shell had a darker colouration. The second scan was measured toward the ventral margin, in the lighter portion of the shell (Fig. 4.5.4). The maps show that most of the shell is calcite. However, there are some areas, which display the spectrum of the aragonite-calcite transition. These areas are found in the oSL and mSL, whereas no trace of aragonite is found in the iSL. The transition is more visible in the shell portion near the ventral margin, the lighter part of the shell.

Raman results of some of our *T. palustris*. shells can be found in Milano et al (2018) and the results indicated in that paper, too, show that heating of the aragonitic shell results in a transformation to calcite.

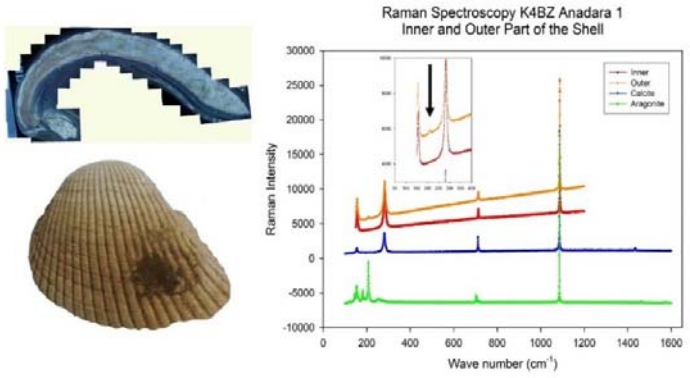

Fig. 4.5.3 *A. uropigimelana* shell K4 MBZ1 A1 from Kalba MBZ1 (Middle Bronze Age), archaeological site K4. Note the shell overall appearance (bottom left) and the slab (top left) cut out along the growth axis, which shows an interesting, marble-like structure. Raman spectra of the single data points measured across the outer and inner part of the shell revealed an incomplete transition from aragonite to calcite (arrow in inset).

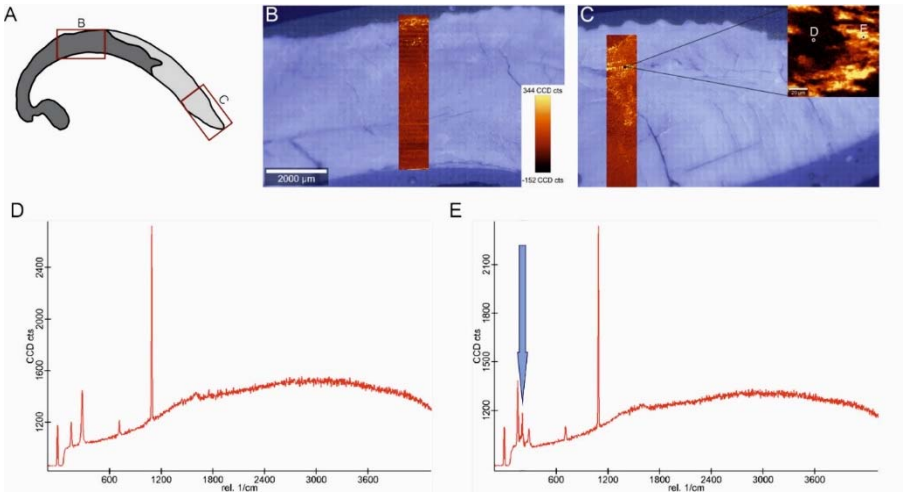

Fig. 4.5.4 Mineralogical composition of *A. uropigimelana* (K4 MBZ1 A1), analysed by using Confocal Raman Microscopy (CRM). (A) Sketch of the shell section, characterized by a variable colouration. Dark grey dominates in the hinge and in the ontogenetically younger shell portion, whereas a lighter shade occurs toward the ventral margin. The rectangles indicate the position of the regions investigated. (B) CRM map of the dark portion. Bright colours in the scan identify the presence of typical aragonite peak (206 cm-1). (C) CRM map of the light grey portion. Colour and scale bars are the same as in (B). As in the darker portion, calcite dominates. However, the ventral margin is characterized by an increased presence of aragonite signal. (D) Raman spectrum of calcite with the characteristic set of peaks at 155, 282, 711 and 1085 cm-1. (E) Raman spectrum of the transitional phase between calcite and aragonite, characterized by the additional band at 206 cm-1 (blue arrow).

Microstructures

Heating of shells is not only reflected in the transition from aragonite to calcite, but also in a morphometric change of the microstructures, as previously suggested by Milano et al. (2018). Here, specimen K4 MBZ1 A1 is compared to a completely heated, and also an unheated, shell of the same species, *A. uropigimelana* (Fig. 4.5.5). SEM images were taken in the darker part, closer to the hinge of the shell, as well as in the lighter part, near the ventral margin. As the shells consist of three distinct layers, all of them were scanned for comparison. The microstructures of K4 MBZ1 A1 oSL show some differences between the light and the dark portion of the shell (Fig. 4.5.5). In both portions, the characteristic oSL branching crossed-lamellar structures (shown in the unheated K4 MBZ2 Ana3) are altered, with their 3-rd order lamellae losing geometric definition and starting to fuse together. However, toward the ventral margin (light portion), the branching of the 1st-order lamellae is still visible, whereas this is not the case for the darker shell portion. This indicates a less severe structural alteration in the oSL of the light portion compared to the dark one (Fig. 4.5.5). As for the mSL and iSL, the differences between the two shell portions are less evident. In both cases, the microstructures are significantly altered in comparison to unheated shells. Generally, all three layers of K4 MBZ1 A1 present microstructure morphometric changes at an intermediate level between the unheated and heated shells (Fig. 4.5.5).

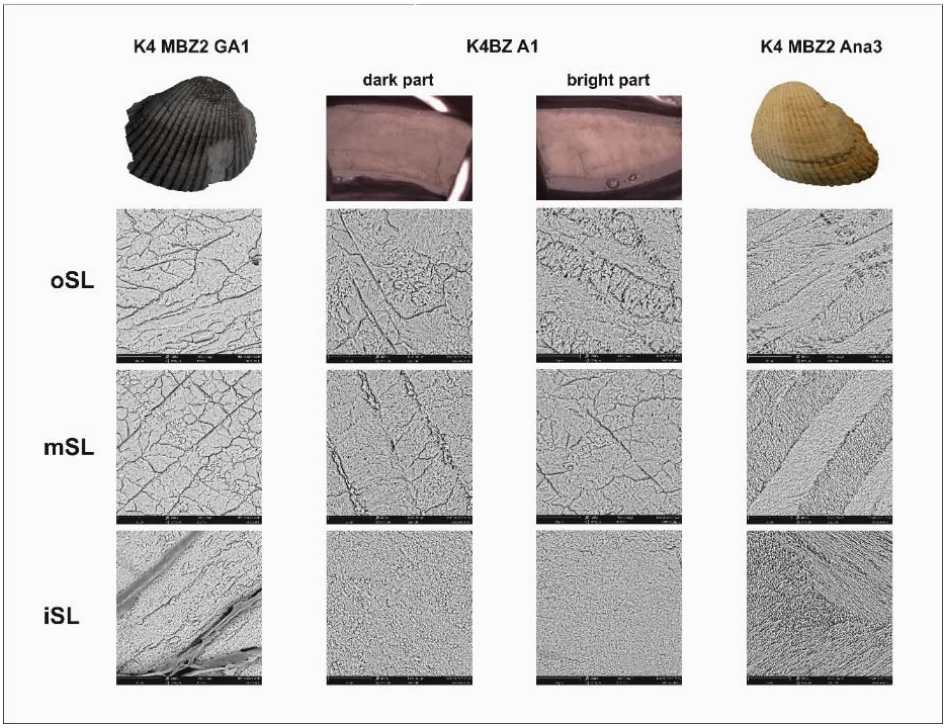

Fig. 4.5.5 Comparison between heated (K4 MBZ2 GA1) and unheated specimens of *A. uropigimelana* (K4 MBZ2 Ana3), with a shell showing signs of transitional phase between aragonite and calcite (K4 MBZ1 A1), hence pointing to incomplete or lower temperature heating. The heated and unheated shell data have been published in Milano et al (2018).

The microstructures of unheated *T. palustris* showed the typical simple and linear-crossed lamellar microstructures. Heated specimens, on the other hand, showed a transformation of lamellar biomineral units into large irregular-shaped assemblages, both in the oSL and the iSL. Examples of microstructures investigated in our heated as well as unheated *Terebralia palustris* shells can be found in Milano et al. (2018).

Radiocarbon

Radiocarbon results are presented in Table 4.5.3 as uncalibrated data in ^{14}C yrs BP, as well as calibrated with Oxcal 4.2. (Bronk Ramsey and Lee, 2013; Ramsey, 1995) with the Intcal13 and Marine13 dataset (Reimer et al., 2013). Prior to analysis, we noted the status of heating of individual shell specimens. Most of the shells from Kalba were presented in Lindauer et al. (2017). The data shows a larger age range, since the results are now all calibrated with the reservoir effects and presented as unmodelled ages. In Lindauer et al. (2017), the results were presented as modelled ages, because they were used to determine a reservoir effect. To adjust the data to the new measurements, we decided to calibrate them all in the same way. In addition, the terrestrial periods are shown in Table 4.5.1. The late Neolithic layers of the shell midden KK1 (Kalba) comprised of two layers, dating to 5038 ± 38 cal BC (7013 ± 69 cal BP) for the lower layer, and 4598 ± 34 cal BC (6557 ± 41 cal BP), immediately on top of the first layer.

The Middle Bronze Age in the settlement K4 at Kalba was found in two phase, which were dated to 1878 ± 32 cal BC (3775 ± 48 cal BP) for the lower layer MBZ1 and to 1718 ± 18 cal BC (3671 ± 28 cal BP) for the layer MBZ2 immediately above it.

Even if the uncalibrated results of heated versus unheated shells differ, there is still the possibility of overlapping results after the calibration process. This overlapping of results would prevent the establishment of a high-resolution chronology for these archaeological sites.

A certain radiocarbon offset between specimens is natural and depending on exact location of habitat, food availability as well as food preference (Claassen, 2009; Culleton et al., 2006). Stress and illness can also lead to changes in carbon uptake and incorporation into the shell material.

The radiocarbon data is consistent for both heated and unheated material.

In addition to the radiocarbon data, we investigated potential differences between heated and unheated shells, focusing on the mean values and their standard deviations (Table 4.5.4). We also looked at the differences in standard deviations of heated and unheated shells and is discussed in more detail in the following section.

Table 4.5.3 Radiocarbon data of heated and unheated shells from Kalba, UAE. All samples except the samples named GA, GT, UA, UT were previously presented in Lindauer et al. (2017).

Period	Labcode	Name	Species	burnt/ unburnt	Mean ^{14}C age (yrs BP)	cal BC 2σ
Neolithic 1 KK1 lower layer	P 14280	KK1 GT2	*T. palustris*	burnt	6944 ± 31	5895-5739
	P 14281	KK1 GT3			6923 ± 30	5877-5734
	P 14282	KK1 UT1		unburnt	6927 ± 30	5880-5736
	P 14283	KK1 UT2			6997 ± 31	5983-5797
	P 14284	KK1 UT3			7003 ± 31	5984-5809
	MAMS 22876	KK1 BL T1			6911 ± 28	5262-4901
	MAMS 22877	KK1 UBL T1			6924 ± 27	5275-4921
Neolithic 2 KK1 upper layer	UCIAMS 171094	KK1 Ana 1	*A. uropigimelana*	burnt	6305 ± 15	4681-4486
	UCIAMS 171095	KK1 Ana 2			6300 ± 20	4681-4476
	UCIAMS 171096	KK1 Ana 3			6295 ± 20	4677-4472
	MAMS 22867	KK1 A2OBL		unburnt	6295 ± 26	4681-4464
	MAMS 22880	KK1 OBL A1			6273 ± 27	4665-4445
	MAMS 22883	KK1 MuGOF			6310 ± 26	4695-4480
	MAMS 22885	KK1 10-15 A1			6272 ± 27	4664-4445
	MAMS 22882	KK1 MuGOF	*T. palustris*	burnt	6257 ± 26	4786-4338
	MAMS 22884	KK1 10-15 T1			6262 ± 26	4791-4341
	P 14279	KK1 GT1			6386 ± 28	4952-4461
Middle Bronze Age 1	P 13306	K4BZ Ana 1	*A. uropigimelana*	burnt	3897 ± 43	2066-1650
	P 13307	K4BZ Ana 2			3859 ± 31	1939-1613
	P 13308	K4BZ Ana 3			3993 ± 38	2100-1730
	P 13309	K4BZ Ana 4			3991 ± 40	2097-1721
	P 13310	K4BZ Ana 5			3951 ± 40	2096-1691
	P 13838	K4BZ GA1			3918 ± 22	1961-1656
	P 13839	K4BZ GA2			3878 ± 22	1908-1614
	P 14287	K4BZ GA3			3887 ± 23	1920-1621
	P 13836	K4BZ UGA1		unburnt	3993 ± 28	2089-1738
	P 13837	K4BZ UGA2			4188 ± 31	2376-1997
	P 14288	K4BZ UA3			3952 ± 24	2011-1691
	P 13311	K4 BZ Ter 1	*T. palustris*	unburnt	3958 ± 42	2224-1866
	P 14286	K4BZ UT3			4275 ± 23	2620-2308
	P 13832	K4BZ UGT1			3763 ± 24	1922-1636
	P 13833	K4BZ UGT2			3803 ± 23	1975-1679
	P 13834	K4BZ GT1		burnt	3740 ± 23	1893-1612
	P 13835	K4BZ GT2			3788 ± 26	1956-1660
	P 13312	K4BZ Ter 2			4188 ± 38	2570-3306
	P 13313	K4BZ Ter 3			3700 ± 35	1946-1616
	P 13314	K4BZ Ter 4			3674 ± 39	1921-1576
	P 13315	K4BZ Ter 5			3767 ± 38	2071-1695
	P 14285	K4BZ GT3			3768 ± 24	1928-1642
Middle Bronze Age 2	P 14289	K4SL GT1	*T. palustris*	burnt	3755 ± 26	1887-1633
	P 14290	K4SL GT2			3767 ± 23	1900-1651
	P 14291	K4SL GT3			3736 ± 23	1869-1621
	P 14292	K4SL UT1		unburnt	3728 ± 24	1865-1612
	P 14293	K4SL UT2			3678 ± 24	1798-1527
	P 14294	K4SL UT3			3723 ± 23	1861-1609
	UCIAMS 171089	K4SL Ter 1			3690 ± 15	1811-1556
	UCIAMS 171090	K4SL Ter 2			3690 ± 15	1811-1556
	UCIAMS 171091	K4SL Ter 3			3715 ± 20	1855-1603
	UCIAMS 171092	K4SL Ter 4			3790 ± 20	1925-1681
	P 14295	K4SL GA1	*A. uropigimelana*	burnt	3850 ± 23	1871-1591
	P 14296	K4SL GA2			3891 ± 22	1902-1630
	P 14297	K4SL GA3			3827 ± 23	1852-1552
	P 14298	K4SL UA1		unburnt	3861 ± 23	1877-1602
	P 14299	K4SL UA2			3805 ± 23	1809-1512
	UCIAMS 171084	K4SL Ana 1			3825 ± 15	1843-1553
	UCIAMS 171085	K4SL Ana 2			3835 ± 15	1857-1576
	UCIAMS 171086	K4SL Ana 3			3830 ± 15	1850-1561
	UCIAMS 171087	K4SL Ana 4			3880 ± 15	1884-1623
	UCIAMS 171088	K4SL Ana 5			3945 ± 15	1967-1692

Table 4.5.4 Mean values and standard deviation of heated and unheated shells from different periods. In addition, the differences of the mean values are listed, as well as the differences of the standard deviations.

Period	Site	Species	Burnt / Unburnt	No. of shells	Mean ^{14}C age		Diff. burnt-unburnt	StDev (b.) - StDev (unb.)
					yrs BP	±	years	years
Neol. 1	KK1	*T. palustris.*	burnt	2	6933	15	-19	-29
			unburnt	5	6952	44		
Neol. 2	KK1	*A. uropigimelana*	burnt	3	6300	5	12	-18
			unburnt	5	6288	18		
MBZ 1	K4BZ	*A. uropigimelana*	burnt	8	3922	51	-123	-75
			unburnt	3	4045	126		
		T. palustris.	burnt	7	3804	174	-146	-58
			unburnt	4	3950	233		
MBZ 2	K4SL	*A. uropigimelana*	burnt	3	3856	32	2	-15
			unburnt	7	3854	47		
		T. palustris.	burnt	3	3752	16	36	-22
			Unburnt	7	3716	38		

4.5.5 Discussion

Our additional analyses have confirmed previous results relating to the thermal effect on shell microstructures and mineralogy. Generally, heating induces the fusion of the basic structural units into much larger, joint aggregates, with a very heterogeneous and disordered spatial arrangement, as previously observed by Milano et al. (2016) and Milano et al., (2018). CRM maps and SEM imaging are helpful tools to identify burnt shells, especially those appearing initially unheated on visual inspection.

In the present study, detailed mineralogical maps allowed the identification of an aragonite - calcite intermediate phase in a heated shell. The persistence of this calcium carbonate phase can be used to infer important information about the heating process. One shell in this study (K4 MBZ1 A1) presented a patchy colouration (dark/light grey) and variable mineralogical composition. The aragonite - calcite transition phase, although limited to some areas of the oSL and mSL, survived in the archaeological record. This indicates its stability through time and allows more precise estimates of heating temperatures than previously thought. According to our previous results (Milano et al., 2018; Milano et al., 2016), mineralogical transitions occur between 300°C and 400°C, suggesting that K4 MBZ1 A1 was heated to this range of temperatures. On the other hand, other specimens (i.e., K4MBZ2 GA1) were exposed to higher temperatures that drove the entire shell to transform into calcite.

The overall colour variability of specimen K4 MBZ1 A1 conforms well to the cooking practice described in the section about heating of shells and illustrated in Fig. 4.5.2. The dark grey colour near the hinge, shading into a creamy colour towards the ventral margin, is most likely associated with a heating process in which the shells are placed, hinge up, into the sand and a fire is then ignited overtop of them.

Our results, together with the ethnographic observations of Meehan (1982), suggest that a similar heating technique was known in Arabia during the Middle Bronze Age. Of course the modern study of

Meehan was an observation from Australian aboriginal groups and is not from Arabia and so cannot be compared directly to Neolithic and Bronze Age. However, the shells being *T. palustris* and *A. uropigimelana*, too, and the microstructure pattern together with the lack of charcoal fragments throughout the late Neolithic shell midden are supporting evidence for a similar method of shell processing. The hinge was found to be totally calcitic because it had experienced the highest temperature, whereas the ventral margin was subjected to lower temperatures, and therefore it still contained traces of the mineralogical interface. It is proposed that the duration of heating was rather short, thus preventing the whole shell from transforming completely mineralogically. However, the mineralogical variability of the shell might well assist in understanding the mechanism of heat transfer. It is rather unexpected that the outer shell layer (oSL) shows signs of being exposed to lower temperatures than the inner shell layer (iSL). This would seem to imply a stronger heat transfer through the hinge than along the outer part. Possibly, the air between the shells may function as a cooling mechanism, whereas the closed inner part with the animal inside may transfer the heat more readily. In general, it can be said that the different types of microstructure may respond differently to the thermal exposure. The oSL might be more resistant to mineralogical transformation than the other layers, as previously suggested by Milano et al. (2016).

From a methodological perspective CRM maps are more efficient than point measurements because they take into account the complexity of biogenic carbonates and their potential variable thermal responses.

The results of the radiocarbon measurements do not indicate a significant difference in age between heated and unheated shells. This becomes obvious when we consider data mean values and their standard deviations, as presented in Table 4.5.3. The difference of the mean values for heated and unheated shells is less than their individual standard deviations, and are thus not statistically significant. Furthermore, the heated material is sometimes older and sometimes younger than the unheated material, which indicates that there is no systematic difference. The data, nevertheless, present a larger scatter in the unheated shells, compared to the heated ones. Furthermore, the average data of the unheated material has a narrower standard deviation than the heated one. Therefore, we examined the difference of the standard deviations of the mean values. Although still rather small, here we can see a trend that this difference is negative in all cases, thus pointing to a systematically smaller standard deviation in the heated material. Further studies with more specimens will be needed to build more robust statistical evidence base to allow further discussion. Therefore, Table 4.5.4 is to be regarded as a first approximation, until a statistically relevant population has been investigated for each layer. The aim of the present work is to provide the basic knowledge on which future research can be built. Our results indicate that the narrower variability of the radiocarbon data from heated shells reflects the general assumption that calcite is more stable than aragonite, and that therefore it does not exchange carbon with the environment to the same extent. The system seems to be isolated against influences from the surroundings, which therefore prevents exchanges with surrounding radiocarbon sources, such as, for instance, limestone detritus in the sediment matrix. This would explain the obviously reduced data scatter.

Our results suggest that the heating processes do not alter radiocarbon ages of *A. uropigimelana* and *T. palustris*. Therefore, heated shells continue to be useful material which can be used with confidence for dating archaeological contexts and sites, and in palaeoclimate studies.

4.5.6 Conclusions

An important result of our study has been to explore the link between modern ethnological studies of shell foraging and processing (heating) in Australia (Meehan, 1982) and ancient food processing methods in Arabia. Previously, the details of shellfish consumption in this latter region in later prehistory were largely unknown. Our data suggest that the shells were mainly used as food and they were likely being processed below short-lived, but hot fires. This conclusion sheds light on the dietary and cooking habits of the local populations, thus contributing to a better understanding of their lifestyle during the late Neolithic.

Shell structure and mineralogical composition are shown to be strongly influenced by heating. One of our shells clearly showed transitional phases from aragonite to calcite, which allowed us to come to a conclusion about the heating procedure.

From the microstructural perspective, high temperatures lead to a loss in microstructure, with a typical design resulting in a decrease in material resistance to mechanical stress, and thus resulting in more frequent breakage. In addition, temperatures above 300-400 °C cause a mineralogical change from aragonite to calcite. Given the intermediate microstructural and mineralogical properties of one of our shells, our results suggest an interpretation of the heating processes used during the Middle Bronze Age. As described by Meehan (1982), shells would likely be prepared using a fire on top of the shells, which are first aligned on a sandy substrate, with their hinges pointing down.

For the radiocarbon ages, heating has no influence on the measured age itself. Moreover, the rapid exposure to elevated temperatures appears to induce closure of the shell structures, thus preventing external carbon sources from entering the shell structure itself. This is reflected in the larger spread in ages of unheated shells versus the narrower age range of heated shells from the same stratigraphic layers of the shell midden and settlement site.

Being aware that there is no significant influence of the heating treatment on the shell radiocarbon geochemistry, heated shells are assessed as providing valuable material for radiocarbon dating, without applying any further corrections.

Acknowledgements

The authors would like to thank Dr. Sabah Jasim and Eisa Yousif from the Directorate of Antiquities, Department of Culture & Information, Sharjah, UAE, as well as Prof. Dr. Hans-Peter Uerpmann and Dr. Margarethe Uerpmann for their continuous support and help with the field work. Dr Carl. S. Phillips kindly shared his knowledge and his experience about the excavations in Kalba with us, which provided invaluable insights for our work. We gratefully acknowledge the support of Dr. Gernot Nehkre and Dr.

Tobias Häger from AWI, Bremerhaven, Germany, for helping with the Raman measurements, and Prof. Bernd Schöne, University Mainz, Germany, for providing the SEM facilities. We would like to thank Dr. Meghan Burchell, Department of Anthropology, Memorial University, Newfoundland and Labrador, Canada, and Michael Simon Krochmal, Autoscan Systems Pty. Ltd., Melbourne, Australia, for fruitful discussions. Dr. Andy Howard, Landscape Research & Management, UK, was a great help in optimizing the final draft. Two anonymous reviewers provided helpful advice which significantly helped to improve the manuscript.

4.5.7 References:

Andrus, C.F.T., 2011. Shell midden sclerochronology. Quaternary Science Reviews 30, 2892-2905.

Ascough, P., Cook, G., Dugmore, A., 2005. Methodological approaches to determining the marine radiocarbon reservoir effect. Progress in Physical Geography 29, 532-547.

Azzoug, M., Carré, M., Schauer, A.J., 2012. Reconstructing the duration of the West African Monsoon season from growth patterns and isotopic signals of shells of *Anadara senilis* (Saloum Delta, Senegal). Palaeogeography, Palaeoclimatology, Palaeoecology 346-347, 145-152.

Barker, G., Antoniadou, A., Armitage, S., Brooks, I., Candy, I., Connell, K., Douka, K., Drake, N., Farr, L., Hill, E., Hunt, C., Inglis, R., Jones, S., Lane, C., Lucarini, G., Meneeley, J., Morales, J., Mutri, G., Prendergast, A., Rabett, R., Reade, H., Reynolds, T., Russell, N., Simpson, D., Smith, B., Stimpson, C., Twati, M., White, K., 2010. The Cyrenaican Prehistory Project 2010: the fourth season of investigations of the Haua Fteah cave and its landscape, and further results fromthe 2007–2009 fieldwork. Libyan Stud 41, 63-88.

Biagi, P., 1994. A radiocarbon chronology for the aceramic shell-middens of coastal Oman. Arabian Archaeology and Epigraphy 5, 17-31.

Biagi, P., 2013. The shell middens of Las Bela coast and the Indus delta (Arabian Sea, Pakistan). Arabian Archaeology and Epigraphy 24, 9-14.

Biagi, P.N., Renato, 1999. The shell-midden sites of RH5 and RH6 (Muscat, Sultanate of Oman) in their environmental setting. Archaeologia Polonia 37, 31-47.

Bronk Ramsey, C., Lee, S., 2013. Recent and Planned Developments of the Program OxCal.

Burchell, M., Cannon, A., Hallmann, N., Schwarcz, H.P., Schöne, B.R., 2013. Inter-site variability in the season of shellfish collection on the central coast of British Columbia. Journal of Archaeological Science 40, 626-636.

Carter, R., 1997. The Wadi Suq period in south-east Arabia: a reappraisal in the light of excavations at Kalba, UAE. Proceedings of the Seminar for Arabian Studies 27, 87-98.

Claassen, C., 2009. Shells Cambridge University Press.

Culleton, B.J., Kennett, D.J., Ingram, B.L., Erlandson, J.M., Southon, J.R., 2006. Intrashell Radiocarbon Variability in Marine Molluscs. Radiocarbon 48, 387-400.

Diedrich, C.G., 2006. Discoveries of Neolithic prehistoric sites at Pleistocene carbonate rock shelters on the east coast of the UAE. Arabian Archaeology & Epigraphy 17, 131-138.

Dutta, K., 2008. Marine 14C Reservoir Age and Suess Effect in the Indian Ocean. Journal of Earth Science India I, 175-188.

Fernández-López de Pablo, J., 2016. The timing of postglacial coastal adaptations in Eastern Iberia: A Bayesian chronological model for the El Collado shell midden (Oliva, Valencia, Spain). Quaternary International 407, Part B, 94-105.

Fratini, S., Vannini, M., Cannicci, S., 2008. Feeding preferences and food searching strategies mediated by air- and water-borne cues in the mud whelk Terebralia palustris (Potamididae: Gastropoda). Journal of Experimental Marine Biology and Ecology 362, 26-31.

Hallmann, N., Burchell, M., Brewster, N., Martindale, A., Schöne, B.R., 2013. Holocene climate and seasonality of shell collection at the Dundas Islands Group, northern British Columbia, Canada—A bivalve sclerochronological approach. Palaeogeography, Palaeoclimatology, Palaeoecology 373, 163-172.

Händel, M., 2014. Al-Hamriya - Dynamik einer Muschelhaufenlandschaft in den Vereinigten Arabischen Emiraten. Archaeologia Austriaca 97-98, 77-96.

Kosnik, M.A., Hua, Q., Kaufman, D.S., Kowalewski, M., Whitacre, K., 2017. Radiocarbon-calibrated amino acid racemization ages from Holocene sand dollars (Peronella peronii). Quaternary Geochronology 39, 174-188.

Kromer, B., Lindauer, S., Synal, H.-A., Wacker, L., 2013. MAMS - A new AMS facility at the Curt-Engelhorn-Centre for Achaeometry, Mannheim, Germany. Nuclear Instruments and Methods in Physics Research Section B: Beam Interactions with Materials and Atoms 294, 11-13.

Kutterer, J., 2013. The Archaeological Site HLO1 A Bronze Age Copper Mining and Smelting Site in the Emirate of Sharjah (U.A.E.), Mathematisch-Naturwissenschaftlichen Fakultät. Eberhard-Karls-Universität Tübingen, p. 232.

Leng, M.J., Lewis, J.P., 2016. Oxygen isotopes in Molluscan shell: Applications in environmental archaeology. Environmental Archaeology 21, 295-306.

Lindauer, S., Marali, S., Schöne, B.R., Uerpmann, H.-P., Kromer, B., Hinderer, M., 2016. Investigating the Local Reservoir Age and Stable Isotopes of Shells from Southeast Arabia. Radiocarbon 59, 355-372.

Lindauer, S., Santos, G.M., Steinhof, A., Yousif, E., Phillips, C., Jasim, S.A., Uerpmann, H.-P., Hinderer, M., 2017. The local marine reservoir effect at Kalba (UAE) between the Neolithic and Bronze Age: An indicator of sea level and climate changes. Quaternary Geochronology 42, 105-116.

Loftus, E., Rogers, K., Lee-Thorp, J., 2015. A simple method to establish calcite:aragonite ratios in archaeological mollusc shells. Journal of Quaternary Science 30, 731-735.

Magee, P., 2014. The Archaeology of Prehistoric Arabia: Adaptation and Social Formation from the Neolithic to the Iron Age. Cambridge University Press, Cambridge.

McConnaughey, T.A., Gillikin, D.P., 2008. Carbon isotopes in mollusc shell carbonates. Geo-Marine Letters 28, 287-299.

Meehan, B., 1982. Shell Bed to Shell Midden. Australian Institute of Aboriginal Studies, Canberra.

Milano, S., Lindauer, S., Prendergast, A.L., Hill, E.A., Hunt, C.O., Barker, G., Schöne, B.R., 2018. Mollusc carbonate thermal behaviour and its implications in understanding prehistoric fire events in shell middens. Journal of Archaeological Science: Reports 20, 443-457.

Milano, S., Prendergast, A.L., Schöne, B.R., 2016. Effects of cooking on mollusc shell structure and chemistry: Implications for archeology and paleoenvironmental reconstruction. Journal of Archaeological Science: Reports 7, 14-26.

Murray-Wallace, C.V., Beu, A.G., Kendrick, G.W., Brown, L.J., Belperio, A.P., Sherwood, J.E., 2000. Palaeoclimatic implications of the occurrence of the arcoid bivalve Anadara trapezia (Deshayes) in the Quaternary of Australasia. Quaternary Science Reviews 19, 559-590.

Parker, A.G., Goudie, A.S., 2007. Development of the Bronze Age landscape in the southeastern Arabian Gulf: new evidence from a buried shell midden in the eastern extremity of the Rub´ al-Khali desert, Emirate of Ras al-Khaimah, U.A.E. Arabian Archaeology & Epigraphy 18, 132-138.

Paul, D., Mauldin, R., 2013. Implications for Late Holocene climate from stable carbon and oxygen isotopic variability in soil and land snail shells from archaeological site 41KM69 in Texas, USA. Quaternary International 308-309, 242-252.

Petchey, F., Ulm, S., David, B., McNiven, I., Asmussen, B., Tomkins, H., Dolby, N., Aplin, K., Richards, T., Rowe, C., Leavesley, M., Mandui, H., 2013. High-resolution radiocarbon dating of marine materials in archaeological contexts: radiocarbon marine reservoir variability between Anadara, Gafrarium, Batissa, Polymesoda spp. and Echinoidea at Caution Bay, Southern Coastal Papua New Guinea. Archaeological and Anthropological Sciences 5, 69-80.

Petchey, F.A., A; Zondervan, A; Ulm, S; Hogg, A., 2008. New Marine DR Values For The South Pacific Subtropical Gyre Region. Radiocarbon 50, 373-397.

Petchey, F.C., Geoffrey, 2011. Tongatapu hardwater: Investigation into the 14C marine reservoir offset in lagoon, reef and open ocean environments of a limestone island. Quaternary Geochronology 6, 539-549.

Phillips, C.S., Mosseri-Marlio, C.E., 2002. Sustaining Change: The Emerging Picture of the Neolithic to Iron Age Subsistence Economy at Kalba, Sharjah Emirate, UAE, In: Buitenhuis, H., Choyke, A.M., Mashkour, M., Al-Shiyab, A.H. (Eds.), Fifth International Symposium on the Archaeozoology of southwestern Asia and adjacent areas. ARC-Publicaties Groningen, Amman, Jordan, pp. 195-210.

Ramsey, C.B., 1995. Radiocarbon calibration and analysis of stratigraphy; the OxCal program. Radiocarbon 37, 425-430.

Reimer, P.J., Bard, E., Bayliss, A., Beck, J.W., Blackwell, P.G., Bronk Ramsey, C., Buck, C.E., Cheng, H., Edwards, R.L., Friedrich, M., Grootes, P.M., Guilderson, T.P., Haflidason, H., Hajdas, I., Hatté, C., Heaton, T.J., Hoffmann, D.L., Hogg, A.G., Hughen, K.A., Kaiser, K.F., Kromer, B., Manning, S.W., Niu, M., Reimer, R.W., Richards, D.A., Scott, E.M., Southon, J.R., Staff, R.A., Turney, C.S.M., van der Plicht, J., 2013. IntCal13 and Marine13 Radiocarbon Age Calibration Curves 0–50,000 Years cal BP. Radiocarbon 55, 1869-1887.

Santos, G.M., Ormsby, K., 2013. Behavioral Variability in ABA Chemical Pretreatment Close to the 14C Age Limit. Radiocarbon 55, 534-544.

Santos, G.M., Xu, X., 2016. Bag of Tricks: A Set of Techniques and other Resources to Help 14C Laboratory Setup, Sample Processing, and Beyond. Radiocarbon 59, 785-801.

Scourse, J.D., Wanamaker Jr, A.D., Weidman, C., Heinemeier, J., Reimer, P.J., Butler, P.G., Witbaard, R., Richardson, C.A., 2012. The Marine Radiocarbon Bomb Pulse across the Temperate North Atlantic: A Compilation of Δ 14 C Time Histories from Arctica islandica Growth Increments. Radiocarbon 54, 165-186.

Slim, F.J., Hemminga, M.A., Ochieng, C., Jannink, N.T., Cocheret de la Morinière, E., van der Velde, G., 1997. Leaf litter removal by the snail Terebralia palustris (Linnaeus) and sesarmid crabs in an East African mangrove forest (Gazi Bay, Kenya). Journal of Experimental Marine Biology and Ecology 215, 35-48.

Snoeck, C., Schulting, R.J., Lee-Thorp, J.A., Lebon, M., Zazzo, A., 2016. Impact of heating conditions on the carbon and oxygen isotope composition of calcined bone. Journal of Archaeological Science 65, 32-43.

Southon, J., Kashgarian, M., Fontugne, M., Metivier, B., Yim, W.W.-S., 2002. Marine Reservoir Corrections for the Indian Ocean and Southeast Asia. Radiocarbon 44, 167-180.

Steinhof, A., Adamiec, G., Gleixner, G., van Klinken, G.J., Wagner, T., 2004. The New 14C Analysis Laboratory in Jena, Germany. Radiocarbon 46, 51-58.

Stringer, C.B., Finlayson, J.C., Barton, R.N.E., Fernández-Jalvo, Y., Cáceres, I., Sabin, R.C., Rhodes, E.J., Currant, A.P., Rodríguez-Vidal, J., Giles-Pacheco, F., Riquelme-Cantal, J.A., 2008. Neanderthal exploitation of marine mammals in Gibraltar. Neanderthal exploitation of marine mammals in Gibraltar 105, 14319–14324.

Stuiver, M., Braziunas, T.F., 1993. Modeling atmospheric (super 14) C influences and (super 14) C ages of marine samples to 10,000 BC. Radiocarbon 35, 137-189.

Stuiver, M., Pearson, G.W., Braziunas, T.F., 1986. Radiocarbon age calibration of marine samples back to 9000 cal yr BP. Radiocarbon 28, 980-1021.

Synal, H.-A.S., Martin; Suter, Martin, 2007. MICADAS: A new compact radiocarbon AMS system. Nuclear Instruments and Methods in Physics Research Section B: Beam Interactions with Materials and Atoms 259, 7-13.

Taylor, V.K., Barton, R.N.E., Bell, M., Bouzouggar, A., Collcutt, S., Black, S., Hogue, J.T., 2011. The Epipalaeolithic (Iberomaurusian) at Grotte des Pigeons (Taforalt), Morocco: A preliminary study of the land Mollusca. Quaternary International 244, 5-14.

Twaddle, R.W., Wurster, C.M., Bird, M.I., Ulm, S., 2017. Complexities in the palaeoenvironmental and archaeological interpretation of isotopic analyses of the Mud Shell Geloina erosa (Lightfoot, 1786). Journal of Archaeological Science: Reports 12, 613-624.

Uerpmann, H.-P., 1990. Radiocarbon Dating of shell middens in the Sultanate of Oman. PACT 29, 335-347.

Wanamaker Jr, A.D., Heinemeier, J., Scourse, J.D., Richardson, C.A., Butler, P.G., Eiríksson, J., Knudsen, K.L., 2008. Very Long-Lived Molluscs Confirm 17th Century AD Tephra-Based Radiocarbon Reservoir Ages for North Icelandic Shelf Waters. Radiocarbon 50, 399-412.

Zazzo, A., Munoz, O., Badel, E., Béguier, I., Genchi, F., Marcucci, L.G., 2016. A Revised Radiocarbon Chronology of the Aceramic Shell Midden of Ra's Al-Hamra 6 (Muscat, Sultanate of Oman): Implication For Occupational Sequence, Marine Reservoir Age, and Human Mobility. Radiocarbon 58, 383-395.

Zazzo, A., Saliége, J.-F., Lebon, M., Lepetz, S., Moreau, C., 2012. Radiocarbon Dating of Calcined Bones: Insights from Combustion Experiments under Natural Conditions. Radiocarbon 54, 855-866.

4.6 Radiocarbon measurements of *Zootecus insularis* and *Melanoides tuberculata* in the light of different geological settings in the United Arab Emirates

Susanne Lindauer[1,2], Axel Steinhof[3], Matthias Hinderer[2]

[1] Curt-Engelhorn-Zentrum Archaeometry, Klaus-Tschira-Archaeometry-Centre, C4, 8, 68159 Mannheim, Germany;

[2] Institute of Applied Geosciences, Technical University Darmstadt, Schnittspahnstr. 9, 64287 Darmstadt, Germany;

[3] Max-Plack Institute for Biogeochemistry, Hans-Knöll-Str. 10, 07745 Jena, Germany

Contributions: SL, MH designed the study; SL, AS produced the radiocarbon data; SL, MH wrote the paper.

No citation, Under review, Journal of Arid Environments

4.6.1 Abstract:

Landsnails of species *Zootecus insularis* are often found during excavations in SE Arabia and other arid zones. We present a pilot study while sampling shells from different archaeological and geological settings throughout the United Arab Emirates (UAE) to determine their apparent radiocarbon age and possible hardwater effect. The results confirm expected trends for *Zootecus insularis* shells with a higher hardwater effect in limestone and mixed bedrock terrains (up to 3500 years), and a much younger age in ophiolitic terrains. However, most sites show a large variability of radiocarbon ages. The reason can be answered only speculatively at the moment, because no living specimen was found. *Melanoides tuberculata* shells were found only in ophiolitic terrains in the southeast. It shows no or a much lower hardwater effect. At Kalba, shells of both gastropod genera could be sampled in a mud-brick wall (3500 cal BP). Here, *Zootecus insularis* had a strong hardwater effect (over 3000 years). In contrast, *Melanoides tuberculata* is close age of the wall. In summary, our results are encouraging and show that future application of gastropod dating for archaeological chronologies in Arabia is possible, but needs a thorough calibration for local geological, morphological, hydrological and environmental conditions.

Keywords: Radiocarbon, Hardwater effect, United Arab Emirates, Geology, *Zootecus insularis*, *Melanoides tuberculata*

4.6.2 Introduction

Building radiocarbon chronologies for different archaeological contexts is quite challenging in South East Arabia due to the lack of well-preserved organic material suitable for radiocarbon dating (Uerpmann 1990, Zazzo et al. 2012). Hence the idea came up whether *Zootecus insularis* shells would be a suitable material for radiocarbon dating as this species occurs quite frequently and usually is well preserved over centuries and millennia. *Zootecus insularis* is a landsnail that is often found on the Arabian peninsula, Africa and the Indian subcontinent (Neubert 2003, Girod and Balzarini 2017). Because of their limited size and short life time it is hard to find live specimen. At some locations we also found *Melanoides tuberculata* shells, a freshwater snail that would help us to interpret whether the riverine systems flowing through wadis after strong rainfalls can dissolve limestone, if present, in significant amounts. However, with a knowledge about carbon sources, landsnails and also freshwater molluscs can help to understand to what extend carbonaceous material is available for transport.

Radiocarbon on shells and hardwater effect

Molluscs incorporate carbon through food and water uptake. If incorporated carbon originates from limestone or other geological sources it is depleted in radiocarbon (Goodfriend and Hood 1983, Goodfriend and Stipp 1983, Goodfriend 1987). This effect is called hardwater effect for freshwater sources. The hardwater effect describes the apparently older age of a material used for radiocarbon dating with respect to the calender age as obtained by other contemporaneous terrestrial material (e.g. plants) and is strongly dependent on carbon intake and its incorporation into the shell. Not all landsnails are subject to a hardwater effect. For example species like *Scutalus spp*. in Peru live in semi-

dry environment but do not show a reservoir effect (Mächtle et al. 2010, Lindauer and Kromer 2013). Detailed knowledge about a hardwater effect is indispensable when using a snail for chronological purposes.

The ideal way to derive a possible hardwater effect would be to sample several live specimen of the molluscan species of interest or to have a well-defined contemporary pair of shell and terrestrial component like plants. As these shells seem to bury and are rather small, finding live specimen is a challenge in which we did not succeed. As a hint regarding limestone solution in freshwater we use *Melanoides tuberculata* shells found at some of our sampling sites. *Melanoides tuberculata* is a freshwater snail that occurs nearly as often as *Zootecus insularis*. Here, too, we only found empty shells and no live specimen and we did not find *M. tuberculata* at all sites.

In an earlier publication we had found that the marine reservoir effect is species-specific and changes over time (Lindauer et al. 2017). Therefore the two species, *Z. insularis* and *M. tuberculata*, will be treated separately.

Landsnails *Zootecus insularis*

The tiny landsnail *Zootecus insularis* (Fig. 4.6.1, left) is often found on the Arabian Peninsula. Its size of up to 15 mm makes it a rather unobtrusive companion in archaeological excavations. However, it is quite common, but not thoroughly investigated with respect to its food resources, preferred habitat or possible life span. Maybe depending on locality, some authors mentioned that they occur only in humid and semi-arid areas (Pietsch et al. 2010). Other authors emphasize that the snail occurs in arid to semi-arid areas (Neubert 1998, Girod and Balzarini 2017). Regarding habitat, Girod and Balzani (2017) sampled at different sites in Pakistan. They found *Zootecus insularis* to be a petricalous genus which prefers to stay on stony ground, under boulders and on hills and mountain slopes (Feulner and Green 2003, Girod and Balzarini 2017). *Zootecus insularis* collected from houses, parks and agricultural fields in Qatar are described by Al-Khayat and Jones (1999). They found this species to prefer moist soil and shade, but also found them attached to leaves (Al-Khayat and Jones 1999). In the Egyptian Red Sea area they were found as burying themselves into sandy substrate and are found in substrates with more calcareous, sandy nature (Vermeersch and Kweakason 2008)

This leaves us with the impression that *Zootecus insularis* can adjust to a variety of habitats offered, ranging from semi-arid to arid environments but with occasional water resources, maybe damp or water droplets on plants. This might be the reason why it is widespread and occurs since ancient times. With only few basic information about this species, especially food resources and differing information about habitat, it was difficult to judge about the suitability without testing several specimen for a possible hardwater effect.

Freshwater snail *Melanoides tuberculata*

The freshwater snail *Melanoides tuberculata* (Fig. 4.6.1, right) is a wide-spread species that occupies fresh as well as brackish water bodies (Brown and Gallagher 1985). It can tolerate salinities of 7-8% and can also be found in or near ravines (Elkarmi and Ismail 2007). In Oman, it covers areas near the sea level until up to 600 m altitude. Usually it can be found on algal mats or algae-covered stones in

shallow waters as it feeds algivorous as well as detrivorous depending on possibilities. *Melanoides tuberculata* can become up to 5 years old depending on environmental conditions like temperature (Elkarmi and Ismail 2007). Elkarmi and Ismail (2007) found out that *M. tuberculata* living in hot springs can reach an age of 5 years whereas the same species in a pool nearby but at 7°C lower temperature only lived up to 4 years. The species living in the hot springs also was found to be larger which means that these shells can adapt to varying environments.

Fig. 4.6.1 Left *Zootecus insularis*; right: *Melanoides tuberculata (old specimen below, recent one above)*.

Geology of the area and expected hardwater effect

In the eastern United Arab Emirates contrasting lithologies exist with respect to carbonate content. They belong to distinctly different tectonic realms: the autochthonous UAE foreland basin with a succession of Late Permian to Late Cretaceous shelf sediments in the northeast, mostly carbonates, and a set of allochthonous thrust sheets in the southeast of which the uppermost Semail Ophiolite has the largest extension. The boundary between both tectonic realms is marked by the Dibba Zone, which shows mixed lithology (Fig. 4.6.2). Whereas the Arabian Plate subsides north of the Dibba Zone due to subduction under the Eurasian Plate along the Zagros Belt and Makaran Subduction Zone, the region south of it is still uplifting (Glennie 2005).

The autochthonous shelf sediments in northern UAE making up the Musadam Peninsula are summarized as Hajar Supergroup (Phillips et al. 2006). This supergroup represents a carbonate platform with dolomites, dolomitic limestones, different types of limestones and intercalated mudstones. Sandstones and sandy limestones are rare. Some limestones bear chert nodules (Phillips et al. 2006). The Dibba Zone shows a mixture of sedimentary, metamorphic and igneous rocks (Cooper et al. 2016). Here, the Hawasina Complex, the Haybi Complex, and the Semail ophiolite are thrusted over each other (Ali and Watts 2009). The Hawasina and Haybi complexes represent time-equivalent distal oceanic sediments and consists of cherts, siliceous mudstones, turbiditic clastic limestones (calcarenites), calcareous conglomerates (calcirudites), thinnly bedded limestones, and mudstones (Phillips et al., 2006; Searle & Ali 2009). In addition, the metamorphic basement of the foreland is exposed as a thrust-bound unit (Ghub outlier) and as a tectonic window (Masafi-Ismah Metamorphic Window). They bear

greenschists to metasedimentary and meta-igneous rocks. The meta-sediments are mainly quartz-chlorite-schists and chlorite schists, which contain occasional lenses or layers of metamafite, calc-silicate rock, metalimestone and metachert (Phillips et al. 2006).

South of the Dibba Zone, the Semail Ophiolite complex forms the Hajar Mountains. The Semail Ophiolite represents an 8 to 15 km thick Cenomanian oceanic crust and upper mantle with layered gabbros and peridodites (harzburgites, dunites), respectively. It was obducted in the late Cretaceous from the southeast. The layered gabbros become dominant towards the south, whereas the north is dominated by mantle rocks. Primarily, all these rocks are free of calcite. However, carbonate can be produced by weathering. Hereby, calcium is mobilized from mafic minerals such as pyroxene, amphibole, and olivine as well as from the felsic mineral feldspar (anorthitic plagioclase) by hydrolysis. Bicarbonate is provided by dissociation of CO_2 from the atmosphere or the soil air, hence, the carbon in ophiolitic rocks is newly formed by chemical weathering and contains ^{14}C at the time of precipitation. In contrast, carbonate rocks composed of calcite ($CaCO_3$) and/or dolomite ($(CaMg)_2CO_3$) dissolve directly during weathering, i.e. half of the dissolved bicarbonate contains old carbon devoid of ^{14}C. This leads to the observed hardwater effect, when organisms take water or food from carbonaceous terrains. At the western margin of the Hajar Mountains along the Semail thrust carbonate-bearing rocks of the Haybi and Hawasina complexes are again exposed below and in front of the Semail ophiolite (not represented in Fig. 4.6.2). In addition, some anticlines with post-orogenic Maastrichtian to Cenozoic sediments of the foreland basin emerge in front of the Hajar Mountains. This sediment succession starts with deep-marine mudstones and grade into carbonate-dominated, shallow marine limestones.

The entire western part of the United Arab Emirates (UAE) is covered by Quaternary sediments ("superficial deposits" in Fig. 4.6.2). From the Hajar Mountains, large alluvial fans were shed which consist of gravels and sands, frequently being carbonate-cemented. In addition, active sand dunes occur on their surface and at their margins. Quaternary deposits are omnipresent as pediments and terraces along the wadis also within the Hajar Mountains. Partly, they bear pedogenic carbonate. These alluvial deposits were deposited during more humid periods in the late Pleistocene around 30 kyr BP and 10 ky BP (Parton et al. 2013). The source of carbonate in the Quaternary sediments is either in-situ chemical weathering or deposition of carbonate-bearing aeolian dust, most probably from coastal sites.

Our sampling locations cover all three bedrock lithologies, i.e. carbonate, mixed and ophiolitic terrains. In theory, shells from gastropodes living on ophiolithic substrate should show no hardwater effect, whereas those on carbonaceous substrate should show a strong effect. Mixed terrains are expected to lie between these extremes. Pedogenic carbonates in Quaternary deposits may contribute old carbon also in ophiolithic terrains.

4.6.3 Material and Methods:

Sampling strategy

As it was unclear where to best find living gastropods, we first looked for modern shells in and around active wadis where episodic water may provide temporally favorable conditions for snails. We found

empty shells of species *Z. insularis* mostly in stony wadis where trees or plant fragments are present. This of course leaves an open question as to whether the shells chose this place for living or whether the empty shells had been transported there by wind or water. Therefore, we tried to sample several specimen because the probability of having many shells of the same age transported to the same place should be rather low. Hence, several shells showing the same age might be an indicator for in situ or nearly in situ placement. We did not find information in the literature whether these snails live in groups. During sampling in December 2015, we did not find any live specimen of *Zootecus insularis,* but localities with apparently recent enrichment of shells.

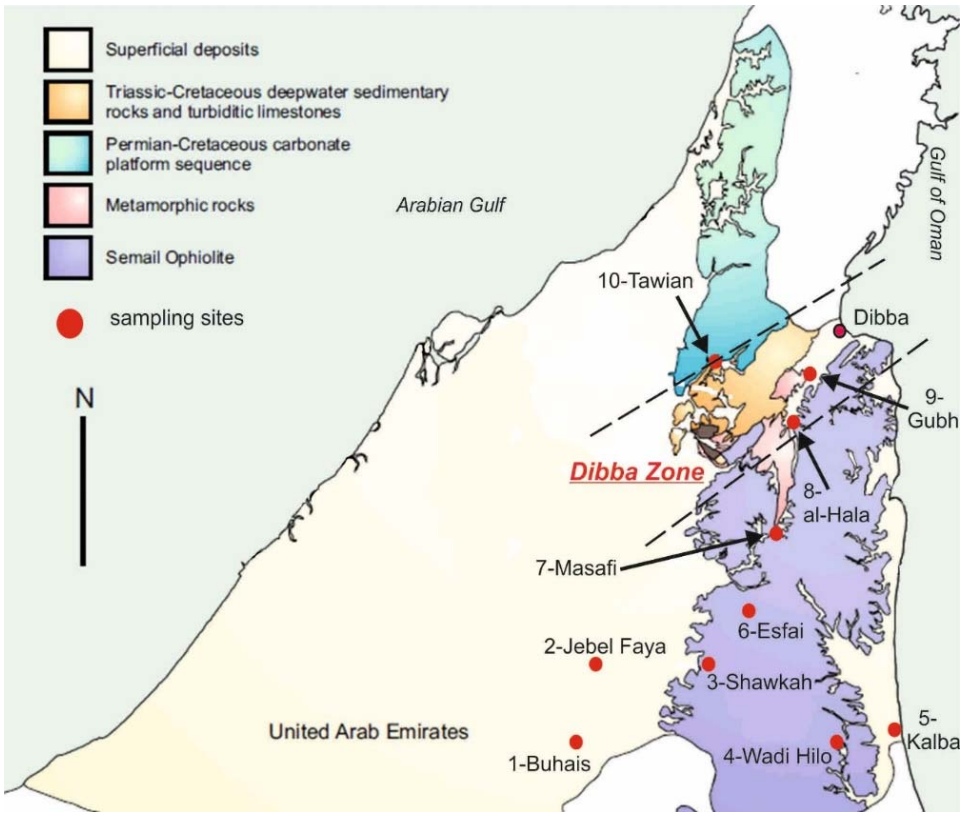

Fig. 4.6.2 Simplified geological map of the United Arab Emirates with sampling sites marked in red. Note that the Dibba fracture Zone is marked with approximate boundaries. The map is modified from (Styles et al. 2005), British Geological Survey.

Primarily, we wanted to test the hardwater effect for different bedrock lithologies and sampled along wadis in different lithological terrains. Secondly, we sampled at or around archaeological sites such as Wadi al-Hilo and Kalba. Most of the *Z. insularis* shells were well preserved lying in the lee of pebbles or obstacles in the dry river bed or on terraces, sometimes caught by grass and roots. If possible several specimen were collected. Surprisingly, no snail shells could be found in the northernmost part of the Hajar Mountains close to the Oman border (Musandam), like Wadi Galilah, although the morphological and hydrodynamic situation was comparable to the south and we carefully searched the wide wadi beds there. Therefore, the dam near Tawian was our northernmost sampling point (Fig. 4.6.2). If possible, several snails were collected per site.

Sampling locations

Geological sites without archaeological background were chosen in the Hajar Mountains following different geological terrains, i.e. carbonaceous, mixed, and ophiolitic terains. In addition, we sampled alluvial and dune areas west and east of the Hajar Mountains. In a Wadi leading to Esfai, hence called "Wadi to Esfai" (WE, No 6), we sampled in the streambed (WEB) and on a Terrace about 1 m above the streambed (WET). Next to the road from Masafi to Dibba was a small Wadi where we found two snails and called the location Terrace near Masafi (TMas, No 7). Further along this road in a Wadi opposite to the village al-Hala was our next location, to which we refer to as Wadi near al-Hala (WaH, No 8). The great dam near Gubh (GD, No 9) was our final point along this road and in this area. The northernmost location was Tawian Dam (TD, No 10) northwest of Gubh. In particular, interdune areas beneath Jebel Buhais delivered hundreds of *Zootecus insularis*. Obviously, they had been flushed to the surface or washed together during rainfall just shortly before our arrival. As these hundreds or thousands of snails made the dunes look like snow, we called them "Buhais snow snails" (BSS, No 1).

Important archaeological sites in the UAE are Jebel Faya (excavation finished) and Wadi al-Hilo (at that time ongoing), both led by Hans-Peter Uerpmann (Kutterer et al. 2012, Uerpmann et al. 2018) and coastal sites around the city of Kalba, excavated by Carl Phillips (Phillips and Mosseri-Marlio 2002). Only few snails were found around Jebel Faya (JF, No 2) near the sites where the excavations had taken place (Uerpmann et al. 2013). Shawkah (No 3) with dam (SD), and palm garden (SP) provided *Zootecus insularis* as well as the freshwater snail *Melanoides tuberculata* and living palms as modern analogues. Wadi al-Hilo (No 4, WH) was sampled in the streambed below the excavation site on the terrace (Uerpmann et al. 2018) as well as upstream in a wadi north of the excavation site few meters from the junction with the main wadi to be sure not to have relocated *Zootecus insularis* specimen from the excavation. Close to Wadi al-Hilo directly at the Gulf of Oman lies the city of Kalba (No 5) where we also sampled few specimen of *Z. insularis* on a hill adjacent to a Neolithic shell midden "KK1" and few specimen, including a single *Melanoides tuberculata* shell, were found in the mud brick wall of the old settlement "K4" dating to the Bronze Age. Both sites are described in (Phillips and Mosseri-Marlio 2002, Lindauer et al. 2017).

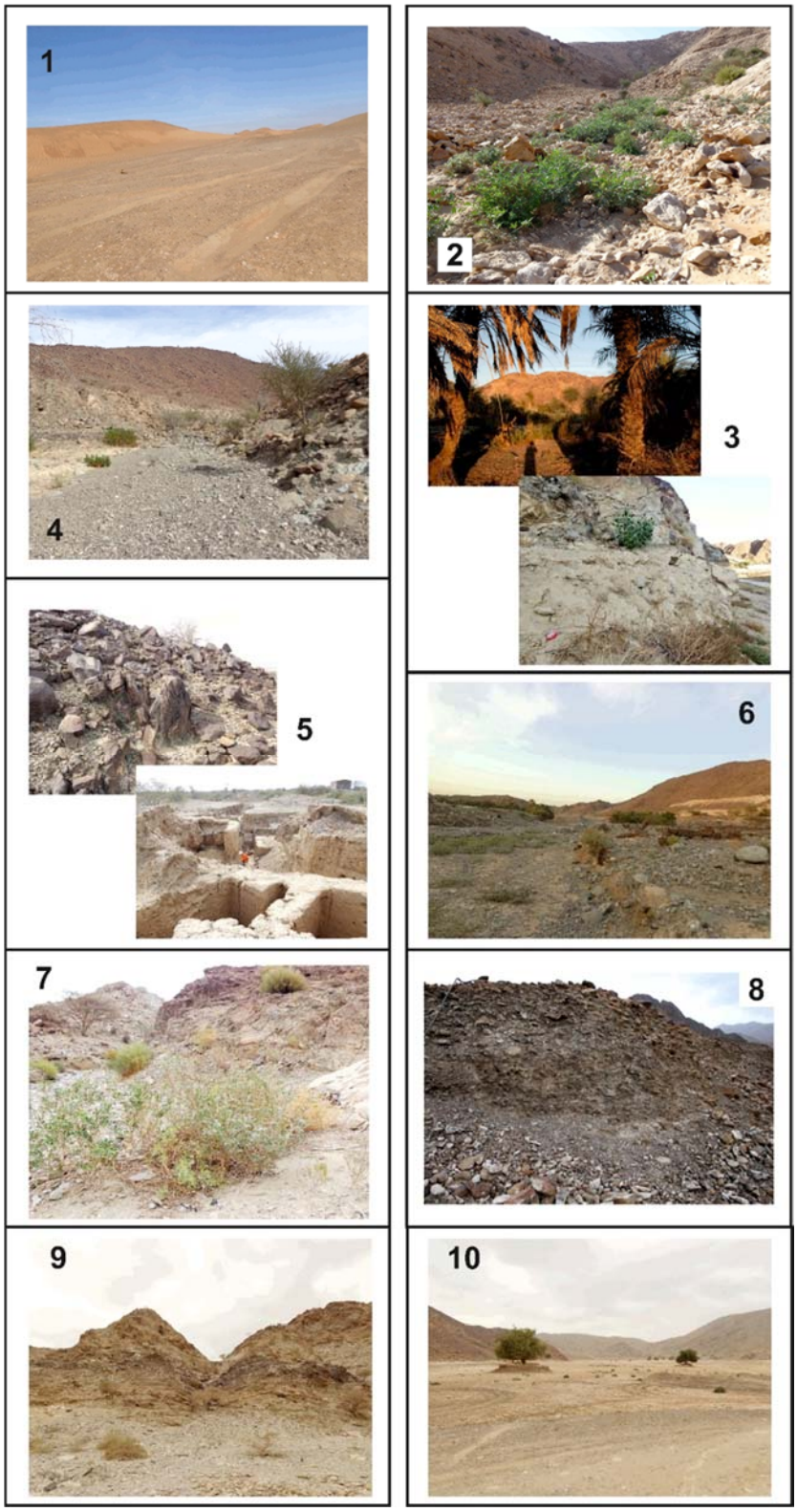

Fig. 4.6.3 Photos of the sampling sites of *Zootecus insularis* and Melanoides tuberculata in different geological settings. Numbers refer to site numbers of Table 1. 1 = Buhais, 2 = Jebel Faya, 3 = Shawkah (top: Palm garden, bottom behind dam), 4 = Wadi al-Hilo (here Wadi North of Main Wadi, at junction), 5 = Kalba (top: hill behind shell midden KK1, bottom: archaeological site K4), 6 = Wadi to Esfai (to the right terrace with old palm garden, left streambed), 7 = Terrace near Masafi, 8 = Wadi opposite al-Hala, 9 = Great Dam near Gubh, 10 = close to Tawian Dam.

Table 4.6.1 Sampling locations and descriptions of *Zootecus insularis and Melanoides tuberculata.*

Sample code	Loc. No	Area	Lith.	Period	Lat. (°N)	Long. (°E)	Height (m)	Description
BSS A	1a	Buhais	I	a	24.983	55.7582	137	"Snow Snails" in dunes
BSS B	1b				24.983	55.7582	137	
JF 2013	2a	Jebel Faya	I	a	25.124	55.8394	169	sampled in 2013
JF 2015	2b				25.119	55.8481	144	sampled in 2015
ShPG	3a	Shawkah	II	a	25.103	56.0393	287	old Palm Garden
ShD	3b				25.107	56.0444	306	behind Dam
WHN	4a	Wadi al-Hilo	II	c	24.993	56.2186	349	Wadi North of Main Terrasse, connecting to main Wadi
WH	4b				24.99	56.218	342	Wadi al-Hilo below Terrasse, main Wadi
K4 MBZ1								Middle Bronze Age 1
K4 MBW	5a	Kalba K4	IV	b	25.086	56.345	25	Mud Brick Wall
K4 MBZ2								Middle Bronze Age 2
KK1 HB	5b	Kalba KK1		a	24.99	56.35	30	Hill adjacent to neolithic shell midden ("Hill behind")
WEB	6a	Wadi to Esfai	II	a	25.144	56.1087	309	Streambed
WET	6b							Terrasse, former Palm Garden
Tmas	7	Masafi	IV	a	25.353	56.1632	490	Terrasse near Masafi along road to Dibba
WaH	8	Wadi al Hala	III	a	25.474	56.1887	160	Wadi near al Hala along road to Dibba
GDG	9	Great Dam Gubh	III	c	25.531	56.2022	90	Great dam near Gubh at road to Dibba
TD	10	Tawian Dam	III	c	25.562	56.0539	114	Wadi leading to the dam at Tawian

Lithology (Lith.): I - Alluvial (Quaternary), II - Ophiolite, III - Carbonaceous, IV - Mixed

Period: a - supposed to be modern, b - archaeological (Bronze Age), c - unclear

Radiocarbon Dating:

The snail shells were cleaned of sand and pretreated in diluted acid (1% hydrochloric acid, HCl) to remove adherent contamination. Some of the shells were measured at the radiocarbon laboratory at CEZ Archaeometry in Mannheim, Germany, labcode MAMS. The others were measured at the radiocarbon laboratory of the Max-Planck Institute for Biogeochemistry in Jena, labcode P.

In Mannheim, phosphoric acid (85%) is used with an autosampler system (IONPLUS) to extract the aragonitic CO_2 which is reduced to elemental carbon (graphite) using hydrogen with iron as catalyst in an AGE III graphitization system (IONPLUS) as described in (Lindauer et al. 2016, Lindauer et al. 2017). The graphite was then measured in a 200kV MICADAS AMS system (Kromer et al. 2013, Lindauer and Kromer 2013).

In Jena samples were extracted using a headspace extraction at a special inlet to the graphitization system and measured using the 3 MV Tandetron accelerator (HVEE, Amersfoort, Netherlands) at the Max-Planck-Institute for Biogeochemistry in Jena (Steinhof et al. 2004, Lindauer et al. 2017).

As we have no contemporaneous terrestrial material for comparison apart from plant fragments of modern palm trees in Shawkah, we do not calibrate the data received, but instead give the fraction modern (pmC) and ^{14}C ages BP with respect to usual convention. The data is corrected for isotope

fractionation. The plant material was pretreated with a standard ABA (acid-base-acid) protocol (Lindauer et al. 2016), then graphitized and measured as described in (Lindauer and Kromer 2013).

4.6.4 Results and Discussion:

The results of the radiocarbon measurements of shell and palm fragments are presented in Table 4.6.2. Modern or post-bomb results are presented as fraction modern and not listed as uncalibrated years BP.

Shells of *Zootecus insularis* from modern environments

First, most sites show a large variety in radiocarbon data like Wadi al-Hilo, Shawkah, Wadi to Esfai, Great Dam Gubh and Tawian Dam. However, there is a striking correspondence in *Z. insularis* ages along the wadi that streches from Masafi to Dibba (compare Fig. 4.6.4) following the narrow Dibba Fracture Zone. Masafi as well as al-Hala consistently show ages over 3000 years BP whereas Gubh at the end of this wadi shows a larger variation and also younger ages. This might be due to the fact that the carbonate-bearing rocks or alluvial deposits of the upstream setting deliver a more homogenous signal, whereas in the downstream setting shells are mixed by episodic water transport from different lithologies with and without carbonate. The data from al-Hala are all elevated, although the catchment is composed of harzburgites. Here we could observe intensively lime-encrusted old terrace deposits, possibly of Pleistocene age. Instead, the reduced hardwater effect of some snails at Gubh can be explained from episodic storage of surface water in the reservoir. Most probably, this is due to a mixture of snail shells from terrestrial upstream habitats with those living at the reservoir, which is episodically flooded by surface waters with reduced reservoir effect. This interpretation is supported by the Tawian reservoir in the north, where a similar scatter between 1164 +/- 26 and 3372 +/- 31 yrs BP is observed.

The oldest age spectrum of shells was found in interdune areas near Buhais. There are two possible explanations. The habitat and food resources provided the snails with old carbon depleted in ^{14}C. If *Zootecus insularis* would be a burrowing species as suggested by some authors this would imply that the shells in Buhais are in situ and might have passed away not too long ago. Hence, the age would represent a hardwater effect of over 2500 years. The second option is that at least some of the collected specimens originate from older interdune sediments which are eroded presently. The ages from the nearby Jebel Faya are also relatively high ranging from 1840 +/- 20 to 3322 +/- 22 ^{14}C yrs BP from unburied specimen. Here previous burial is very unlikly and the high ages can be explained by uptake of old carbon from the surrounding limestones and the lower ones by taking up episodic surface water.

The sampling sites in the ophiolitic terrains of the southeastern UAE, i.e. Wadi to Esfa, Shawka, and Wadi al-Hilo, all show ages for *Z. insularis* below 3000 ^{14}C yrs BP. Ages below 2000 ^{14}C yrs BP and even below 1000 ^{14}C yrs BP are common. The lowest ages are observed in the most central mountainous setting at Wadi al-Hilo surrounded by gabbros. Wadi al-Hilo was the only location where a specimen of *Z. insularis* was found that yielded a modern age pointing to no hardwater effect in the ophiolite dominated area as far as other old carbon sources are absent. Two explanations are possible for the older ages at these settings.

Table 4.6.2 Radiocarbon data on the shells of *Zootecus insularis, Melanoides tuberculata* and palm tree plant fragments.

Labcode	Sample	Species	C14 age		$F^{14}C$		Location
			yrs BP	±		±	
P 13282	BSS A Z1	*Z. insularis*	2755	23	0.7096	0.0020	1a/b Buhais "snow snails" locations 1 and 2
P 13283	BSS A Z2	*Z. insularis*	3316	32	0.6618	0.0026	
P 14272	BSS A Z3	*Z. insularis*	3570	25	0.6412	0.0020	
P 13828	BSS B Z1	*Z. insularis*	3147	21	0.6759	0.0018	
P 13829	BSS B Z2	*Z. insularis*	4537	25	0.5685	0.0018	
P 17766	BSS B Z3	*Z. insularis*	4022	20	0.6061	0.0015	
MAMS 23894	JF 2013 Z1	*Z. insularis*	1840	20	0.7953	0.002	2a/b Jebel Faya
MAMS 23895	JF 2013 Z2	*Z. insularis*	3322	22	0.6613	0.0018	
P 17768	JF 2013 Z4	*Z. insularis*	3013	19	0.6872	0.0016	
P 13289	JF 2015 Z3	*Z. insularis*	3883	22	0.6167	0.0017	
MAMS 21278	*ShPG palm*	Palmtree	*modern*		*1.137*	*0.0024*	3a Shawkah palm garden
MAMS 21276	ShPG Z1	*Z. insularis*	2230	19	0.7576	0.0018	
P 13820	ShPG Z2	*Z. insularis*	2405	26	0.7413	0.0024	
P 14275	ShPG Z3	*Z. insularis*	1724	20	0.8069	0.0020	
P 13821	ShPG Mel1	*M. tuberculata*	499	20	0.9398	0.0023	
P 17763	ShPG Mel2	*M. tuberculata*	modern		1.0034	0.0021	
MAMS 21279	*ShD palme*	Palmtree	*modern*		*1.1295*	*0.0024*	3b Shawkah dam
MAMS 21277	ShD Z1	*Z. insularis*	2205	17	0.7599	0.0017	
P 13818	ShD Z2	*Z. insularis*	1448	24	0.8351	0.0025	
P 14276	ShS Z3	*Z. insularis*	1781	21	0.8011	0.0021	
P 13819	ShD Mel1	*M. tuberculata*	49	20	0.9939	0.0025	
P 17761	ShD Mel 2	*M. tuberculata*	14	15	0.9982	0.0019	
P 17762	ShD Mel 3	*M. tuberculata*	modern		1.0044	0.002	
P 13272	WHN 1	*Z. insularis*	1438	39	0.8361	0.0040	4a Wadi al-Hilo North
P 13273	WHN 2	*Z. insularis*	753	35	0.9105	0.0039	
P 14277	WHN 3	*Z. insularis*	2577	21	0.7256	0.0019	
MAMS 22874	WH Z1	*Z. insularis*	modern		1.1746	0.0030	4b Wadi al-Hilo main Wadi
MAMS 23893	WH Z2	*Z. insularis*	1443	24	0.8355	0.0025	
P 17767	WH Mel1	*M. tuberculata*	821	17	0.9029	0.0019	
P 13286	K4 MBZ1 Mel	*M. tuberculata*	3704	30	0.6306	0.0023	5a Kalba K4
MAMS 36342	K4 MBW Z1	*Z. insularis*	5648	28	0.4950	0.0017	
P 13823	K4 MBW Z2	*Z. insularis*	6427	27	0.4493	0.0015	
P 13287	K4 MBZ2 Z1	*Z. insularis*	5909	37	0.4792	0.0022	
P 13288	K4 MBZ2 Z2	*Z. insularis*	7591	29	0.3887	0.0014	
P 13826	KK1 HB1	*Z. insularis*	2174	21	0.7629	0.002	5b Kalba KK1
P 13827	KK1 HB2	*Z. insularis*	942	33	0.8893	0.0036	
P 14274	KK1 HB3	*Z. insularis*	969	20	0.8864	0.0022	
P 17765	KK1 HB4	*Z. insularis*	562	16	0.9324	0.0019	
P 13284	WEB 1	*Z. insularis*	2879	28	0.6988	0.0024	6a Wadi to Esfai Bachbett (B)
P 13285	WEB 2	*Z. insularis*	946	25	0.8889	0.0028	
P 17760	WEB 3	*Z. insularis*	3180	13	0.6731	0.0011	
P 17758	WEB Mel1	*M. tuberculata*	592	16	0.9289	0.0019	
P 17759	WEB Mel2	*M. tuberculata*	2233	18	0.7573	0.0017	
P 13830	WET 1	*Z. insularis*	2553	21	0.7277	0.0019	6b Wadi to Esfai Terrasse (T)
P 13831	WET 2	*Z. insularis*	1158	20	0.8657	0.0022	
P 14273	WET 3	*Z. insularis*	1448	20	0.8351	0.0021	
P 13274	TMas 1	*Z. insularis*	3040	32	0.6850	0.0027	7 Terrace near Masafi
P 13275	TMas 2	*Z. insularis*	3116	33	0.6785	0.0028	
P 13276	WaH 1	*Z. insularis*	3129	23	0.6774	0.0019	8 Wadi al Hala
P 13277	WaH 2	*Z. insularis*	3510	24	0.6460	0.0019	
P 14278	WaH 3	*Z. insularis*	3357	22	0.6584	0.0018	
P 17764	WaH 4	*Z. insularis*	3501	22	0.6467	0.0018	
P 13280	GDG 1	*Z. insularis*	3372	31	0.6572	0.0025	9 Great Dam Gubh
P 13281	GDG 2	*Z. insularis*	2145	21	0.7657	0.0020	
P 13825	GDG 3	*Z. insularis*	1288	20	0.8519	0.0021	
P 14271	GDG 4	*Z. insularis*	1616	23	0.8178	0.0023	
P 13278	TD 1	*Z. insularis*	3203	30	0.6712	0.0025	10 Tawian Dam
P 13279	TD 2	*Z. insularis*	1164	26	0.8651	0.0028	
P 13824	TD 3	*Z. insularis*	1486	20	0.8311	0.0021	
P 14270	TD 4	*Z. insularis*	2028	27	0.7769	0.0026	

First, shells with higher ages show their original age and were buried in terrace sediments. From there they have been transported due to natural riverbank erosion or from dump sites of the ongoing archeological excavations. Even if we sampled upstream to dumping sites, we cannot rule out that some shells have been outwashed or transported by wind. A second option is that the ages represent a hardwater effect. Taking this scenario, some of the snails retrieved old carbon from weathering crusts and/or carbonate-bearing terrace sediment. Similar scenarios can be applied to Shawka and Wadi to Esfai.

At Kalba, gastropod shells have been collected uphill of the Neolithic shell midden KK1 which is composed of gabbros. The ages are comparably low as Wadi al-Hilo and spread from 562 +/- 16 up to 2174 +/- 21 ^{14}C yrs BP. Here no terrace sediments are present and a scenario of temporal burial can be excluded. The same applies to far-distance transport and mixture of shells from different localities. This means that the higher ages must be due to uptake of old carbon from the local environment. The hill fits well to the description of a stony habitat by Girod and Balzarini (2017) consisting of big blocks between them weathering products as well as eolian dust are trapped from the nearby sabkha. Both contain carbonate. The dust from the sabkha is expected to bear marine carbonate from mangrove sediments having already a reservoir effect (Lindauer et al. 2016). Hence we interpret the two younger dates as being rather contemporary which would result in a hardwater effect of around 500 years for *Zootecus insularis*.

Shells of Melanoides tuberculata from modern environments

Fig. 4.6.5 shows radiocarbon ages for *Melanoides tuberculata*. The findings of this species area restricted to the ophiolithic settings in the southeastern UAE. Except one shell, all ages are below 1000 ^{14}C yrs BP, and two shells have modern ages, i.e. they show no hardwater effect. Wadi al-Hilo and Wadi to Esfai delivered ages of 821 +/- 17, 592 +/- 16, and 2233 +/- 18 ^{14}C yrs BP. At Shawkah two sites were sampled, beneath a reservoir and in an old palm garden closer to the settlement (Fig. 4.6.4 and Fig. 4.6.5). At both sites also plant material was sampled for excluding, that soil water uptake by plants already lead to a hardwater effect due to the diet of snails. However, plant fragments of the palm trees all were modern. At both sites, modern ages of *Melanoides tuberculata* influenced by bomb radiocarbon, as well as older specimen (50 to 500 years BP) were found. The palm garden lies downstream of the reservoir, i.e. through-passing water has the same origin except some direct rainwater input. Interestingly, the youngest ages of *Z. insularis* at both sites are much higher and yielded ages of around 1400 and 2000 ^{14}C yrs BP. This point to a different life habitat of both snail genus. The hardwater effect of *Melanoides tuberculata* appears to represent the hardwater effect of the surface water in the wadi, whereas *Zootecus insularis* must have an additional carbon source from its more terrestrial life habitat. Here, it seems to take up old carbon from weathering crust and/or carbonaceous dust.

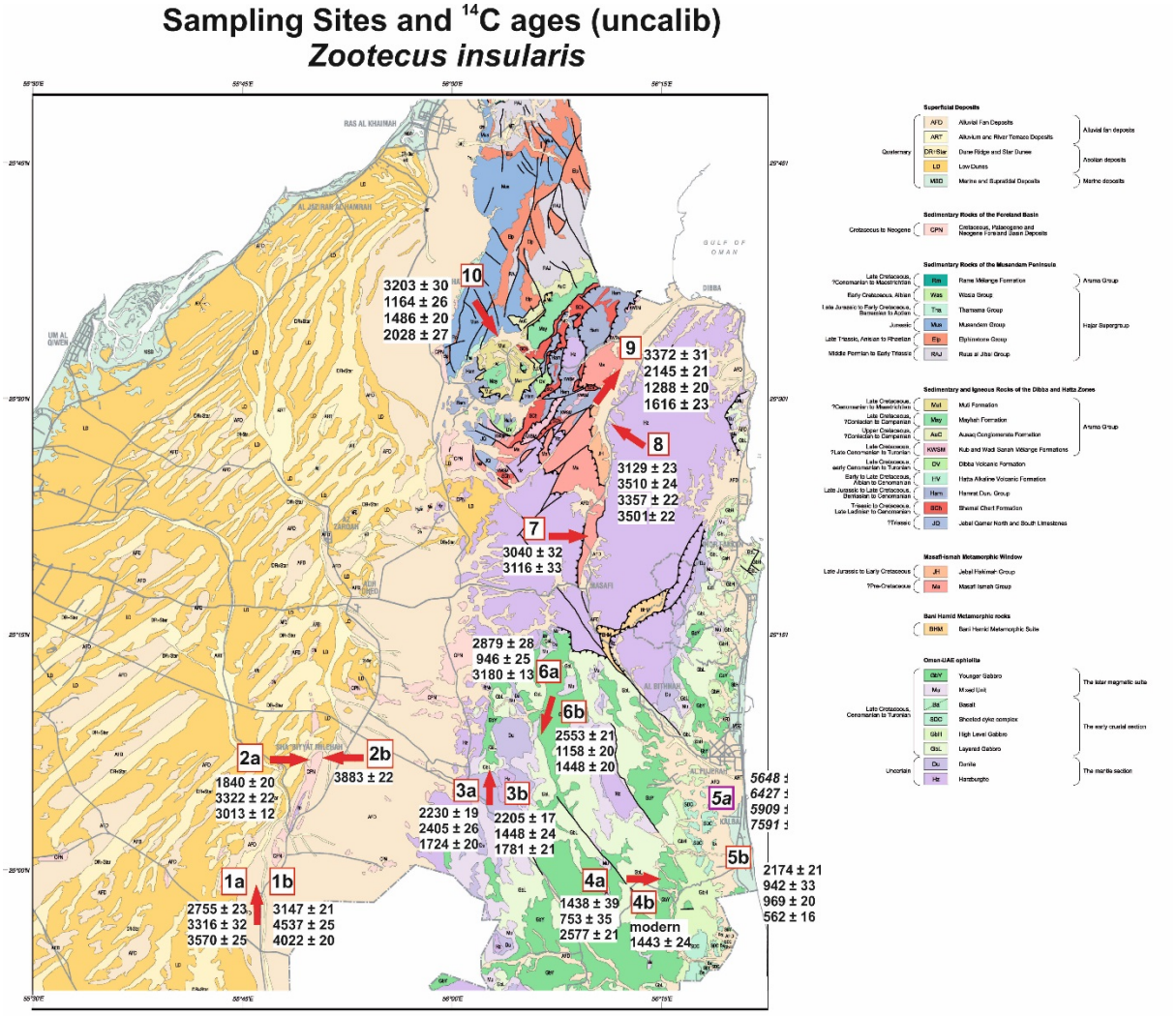

Fig. 4.6.4 Shell data of *Zootecus insularis* for the different geological sites. Map modified from UAQ map of the British Geological Survey. Archaeological Sites in italic and number framed in purple, numbers of geological sites framed in red.

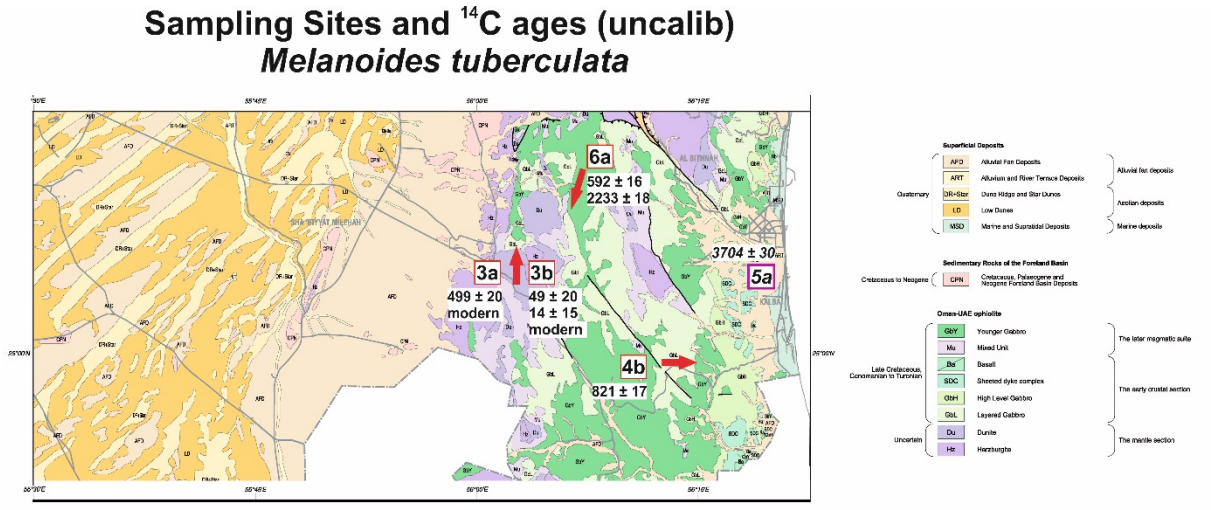

Fig. 4.6.5 Extract of the geologial map of the UAE with radiocarbon ages from sites where freshwater snail *Melanoides tuberculata* was found. Map modified from UAQ map of the British Geological Survey. Archaeological Sites in italic and number framed in purple, numbers of geological sites framed in red.

Shells of *Zootecus insularis* and *Melanoides tuberculata* from archeological sites

At Kalba, both snail species could be found in archaeological excavations beneath marine shells and charcoal. The excavations are documented in Phillips and Mosseri-Marlio (2002).In the two layers MBZ1 and MBZ2, we have calibrated ages for marine shells and charcoal (Lindauer et al. 2017). These layers are dated to around 3500 BP (MBZ1, charcoal measurements ca.3870 – 3640 cal BP, 2σ) for the lower layer and to 3400 BP (MBZ2, charcoal measurements ca. 3720 - 3610 cal BP, 2σ) for the overlying layer. For both layers radiocarbon ages of *Z. insularis* are much too old and show a large spread from 5600 to 7600 ^{14}C yrs BP. This means that if *Zootecus insularis* really belongs to this period, it shows a hardwater effect of around 3000 to 4000 years before being buried. This is comparable to a maximum hardwater effect in modern environments with carbonate-bearing mixed lithologies, e.g. Wadi Al Hawa and Masafi.

In contrast, the freshwater shell of *M. tuberculata* is close to the age of MBZ1, i.e. it had no or only little hardwater effect when being buried. This confirms the finding in modern environments made before that *Melanoides tuberculata* is much less affected by a hardwater effect than *Zootecus insularis* due to its more aquatic habitat. In contrast, *Zootecus insularis* is adapted to more terrestrial habitats, which leads to uptake of old carbon from underlying limestones, weathering crusts, terrace deposits, and eolian dust, except during episodic and/or seasonal humid conditions with flowing and ponded surface water. Eolian processes appear an efficient distributor for carbonate in the east at Kalba due to landward-directed winds, which can easily deflate sand and dust from the broad coastal sabkha of Kalba. The carbon in the sabkha is mostly of marine origin and has a strong reservoir effect as can be shown from marine shells (Lindauer et al. 2016, Lindauer et al. 2017). Storage of the dust in the terrestrial environment leads to an additional time lag and increase the radiocarbon age of soils upon which *Zootecus insularis* live. (see Fig. 4.6.4).

4.6.5 Conclusions

This paper can be regarded as pilot study to test the usefulness of gastropod shells in assisting archaeological dating in the UAE. To create a first data base, we sampled two common gastropod species over different geological settings in the UAE. Basic hypotheses are supported by this study: (i) shells from carbonate-bearing terrains show a stronger hardwater effect than others, (ii) *Zootecus insularis* shows a stronger hardwater effect than *Melanoides tuberculata* due to its more terrestrial life style. Whereas the maximum hardwater effect of *Zootecus insularis* is around 3500 years and rarely below 1000 years, the hardwater effect of *Melanoides tuberculata* mostly is less than 1000 years and no or little hardwater effect is common. In addition it shows that freshwater, usually only occurring after stronger rainfall, does not stay long enough to dissolve sufficient amounts of limestone. This is confirmed by partly reduced ages of *Zootecus insularis* at reservoirs with episodic flooding.

Our results also show some pitfalls. In contrast to our expectations, variability of radiocarbon ages from different individuals at one site are significant. Possible reasons of this wide scatter can be given, however, we could not further test this. Reasons for wide age spectra are: (i) carbonate is present in weathering crusts also in primarily carbonate-free lithologies (here: ophiolites). This argument seems

mostly valid for mountainous regions in the UAE with higher humidity, (ii) carbonate is deposited in carbonate-free lithologies via eolian dust transport. This seems to be most applicable to coastal regions in the UAE, (iii) shells originate from different geological terrains and are mixed via transport, and (iv) shells had been temporarily buried in river terraces and the river bed. Such intermittent storage may reach from few years to thousands of years. Only reasons (i) and (ii) yield a hardwater effect. Reasons (iii) and (iv) are artefacts due to translocation of the shell from its original life habitat and time lag, respectively.

For future application of gastropod radiocarbon dating, these processes must be studied further. One strategy is to systematically compare the terrestrial genus *Zootecus insultaris* with the aquatic genus *Melanoides tuberculata*. The latter shows a much weaker reservoir effect and most probably records the age of the water they live in. In wadis rain water reflecting atmospheric (modern) carbon composion may mix with fossil groundwater of high age. Here, groundwater age and proportional mixing of surface water must be known before assessing the hardwater effect. A positive message of our pilot study is that the difference in the hardwater effect among the two genus in modern settings appear to be similar in archeological settings. This could be shown in excavation of the Bronze Age at Kalba. In summary, our results are encouraging and show that future application for archeological dating is possible, but needs a thorough calibration for local geologial, morphological, hydrological and environmental conditions.

Acknowledgements:
The authors would like to thank Hans-Peter Uerpmann, University of Tübingen, Germany, for encouraging us to start this pilot study. This research did not receive any specific grant from funding agencies in the public, commercial, or not-for-profit sectors.

4.6.6 References

Al-Khayat, J. A. and D. A. Jones (1999). A Comparison of the Macrofauna of Natural and Replanted Mangroves in Qatar. *Estuarine, Coastal and Shelf Science* 49, Supplement 1(0): 55-63.

Brown, D. S. and M. D. Gallagher (1985). Freshwater snails of Oman, South Eastern Arabia. *Hydrobiologia* 127(2): 125-149.

Cooper, D. J. W., et al. (2016). Evolution of the Arabian continental margin of the northern Dibba Zone, eastern United Arab Emirates and Oman. *Journal of Asian Earth Sciences* 129: 254-275.

Elkarmi, A. Z. and N. S. Ismail (2007). Growth models and shell morphometrics of two populations of Melanoides tuberculata (Thiaridae) living in hot springs and freshwater pools. *2007* 66(2): 7.

Feulner, G. R. and S. A. Green (2003). Terrestrial Molluscs of the United Arab Emirates. *Mitteilungen der deutschen malakozoologischen Gesellschaft* 69/70: 23-34.

Girod, A. and A. Balzarini (2017). The local forms of Zootecus (Gastropoda: Pulmonata: Subulinidae) of Pakistan: an archaeomalacological case study. *Natural History Sciences. Atti Soc. it. Sci. nat. Museo civ. Stor. nat. Milano* 4(1): 31-42.

Glennie, K. W. (2005). The geology of the Oman Mountains: an outline of their origin, Scientific Press.

Goodfriend, G. A. (1987). Radiocarbon age anomalies in shell carbonate of land snails from semi-arid areas. *Radiocarbon* 29(2): 159-167.

Goodfriend, G. A. and D. G. Hood (1983). Carbon isotope analysis of land snail shells; implications for carbon sources and radiocarbon dating. *Radiocarbon* 25(3): 810-830.

Goodfriend, G. A. and J. J. Stipp (1983). Limestone and the problem of radiocarbon dating of land-snail shell carbonate. *Geology* 11: 575-577.

Kromer, B., et al. (2013). MAMS - A new AMS facility at the Curt-Engelhorn-Centre for Achaeometry, Mannheim, Germany. *Nuclear Instruments and Methods in Physics Research Section B: Beam Interactions with Materials and Atoms* 294(0): 11-13.

Kutterer, A. U., et al. (2012). Neolithic cremation in south-east Arabia: archaeological and anthropological observations at FAY- NE10 in the Emirate of Sharjah (UAE). Arabian Archaeology & Epigraphy, Wiley-Blackwell. **23:** 125-144.

Lindauer, S. and B. Kromer (2013). Carbonate Sample Preparation for ^{14}C Dating Using an Elemental Analyzer. *Radiocarbon* 55(2-3): 364-372.

Lindauer, S., et al. (2016). Investigating the Local Reservoir Age and Stable Isotopes of Shells from Southeast Arabia. *Radiocarbon*: 1-18.

Lindauer, S., et al. (2016). Investigating the Local Reservoir Age and Stable Isotopes of Shells from Southeast Arabia. *Radiocarbon* 59(2): 355-372.

Lindauer, S., et al. (2017). The local marine reservoir effect at Kalba (UAE) between the Neolithic and Bronze Age: An indicator of sea level and climate changes. *Quaternary Geochronology* 42(Supplement C): 105-116.

Mächtle, B., et al. (2010). Molluscs as evidence for a late Pleistocene and early Holocene humid period in the southern coastal desert of Peru (14.5°S). *Quaternary Research* 73(1): 39-47.

Neubert, E. (1998). Annotated checklist of the terrestrial and freshwater molluscs of the Arabian Peninsula with description of new species. *Fauna of Arabia* 17: 333-461.

Neubert, E. (2003). The continental malacofauna of Arabia and adjacent areas, II The genus *Zootecus* Westerlund 1887. *Arch. Molluskenkunde* 132(1/2): 153-160.

Parton, A., et al. (2013). An early MIS 3 pluvial phase in Southeast Arabia: Climatic and archaeological implications. *Quaternary International* 300(0): 62-74.

Phillips, C. S. and C. E. Mosseri-Marlio (2002). Sustaining Change: The Emerging Picture of the Neolithic to Iron Age Subsistence Economy at Kalba, Sharjah Emirate, UAE. Fifth International Symposium on the Archaeozoology of southwestern Asia and adjacent areas, Amman, Jordan, ARC-Publicaties Groningen.

Pietsch, D., et al. (2010). Holocene soils and sediments around Ma'rib Oasis, Yemen: Further Sabaean treasures? *The Holocene* 20(5): 785-799.

Steinhof, A., et al. (2004). The New 14C Analysis Laboratory in Jena, Germany. *Radiocarbon* 46(1): 51-58.

Styles, M., et al. (2005). Mapping ancient oceans. *Earthwise* 22: 14-15.

Uerpmann, H.-P. (1990). Radiocarbon Dating of shell middens in the Sultanate of Oman. *PACT* 29(IV.5): 335-347.

Uerpmann, H.-P., et al. (2013). The Neolithic period in the Central Region of the Emirate of Sharjah (UAE). *Arabian Archaeology and Epigraphy* 24(1): 102-108.

Uerpmann, M., et al. (2018). HLO1-south: An Early Neolithic site in Wadi al-Hilo (Sharjah, UAE). *Arabian Archaeology and Epigraphy* 29(0): 1-9.

Vermeersch, P. M. and A. P. Kweakason (2008). A Holocene Prehistoric Sequence in the Egyptian Red Sea Area: The Tree Shelter, Cornell University Press.

Zazzo, A., et al. (2012). Variability in the marine radiocarbon reservoir effect in Muscat (Sultanate of Oman) during the 4th millennium BC: reflection of taphonomy or environment? *Journal of Archaeological Science* 39(7): 2559-2567.

5 Discussion

This thesis aims for a systematic approach to determine the marine reservoir effect of two abundant shell species associated with archaeological sites in SE Arabia. The difference of this study compared to other published data lies in the detailed analysis of the shells and their suitability for radiocarbon dating and environmental reconstruction. So far, reservoir effects are rarely determined as species-specific but rather measured from combined datasets using different shell data (Saliege 2005, Zazzo et al. 2012). If the reservoir effect cannot be determined, literature data on live-collected pre-bomb shells from museum collections are used where the data is taken again as a mean value of several species (Southon et al. 2002, Dutta 2008). This leads to diverging age results between terrestrial and marine material and difficulties to connect different sites due to differing opinions about which reservoir effect to use (Uerpmann 1990, Charpentier et al. 2000, Saliege 2005, Zazzo et al. 2012). Furthermore, temporal variations of the reservoir effect have never been taken into account in this area.

In the first part, the information stored in the shell carbonate of *Anadara uropigimelana* was accessed through stable isotope analysis ($\delta^{13}C$, $\delta^{18}O$) and combined with sclerochronology. The results are significant because they give insight into the seasonality of the shell growth of this species which ceases to grow during summer (Lindauer et al. 2016). Consequentially, information stored in the shell material during summer should be regarded incomplete. However, freshwater input is recorded during the winter months when rainfall is more typical. The response time to changes in the environment and consequent implementation into the shell material is relatively immediate (Lindauer et al. 2016). This is reflected in the daily growth lines visible in parts of the several thousand years old *A. uropigimelana* shells investigated in this thesis. In addition, the $\delta^{18}O$ data yields information about the seasonal temperature variation of around 8 – 10 °C in the lagoon of Kalba, which fits nicely to the literature data of seasonally fluctuating sea surface temperature (SST) of the Gulf of Oman between 22 and 32 °C even though the summer data shows a lower resolution than the winter data within the shell (Michael Reynolds 1993, Watanabe et al. 2017).

Confident about the suitability for environmental monitoring of the shell species of interest, *Anadara uropigimelana* and *Terebralia palustris*, in a next step the reservoir ages for each species were determined by comparison of the shell radiocarbon measurements to ^{14}C ages of terrestrial counterparts, here ash and charcoal, as well as charred date stones. Because shells from four layers had been sampled, two at a Neolithic shell midden KK1 and two layers at the settlement Kalba K4 that dates to the Middle Bronze Age, a reservoir effect for each species from each layer could be determined separately (Lindauer et al. 2017). The differing results lead to the conclusion that one has to deal with a species-specific reservoir effect ΔR that changes considerably over time. This discrepancy for different molluskan species is not unexpected. The dietary habits of *A. uropigimelana* and *T. palustris* differ significantly. With a terrestrially influenced diet from mangrove leaf litter, *T. palustris* shows a lower reservoir effect than *A. uropigimelana* that reflects purely marine food resources. Within a rather short period, the reservoir effect for *A. uropigimelana* decreases from 576 ± 90 years (7013 ± 69 cal BP, 5064 ± 69 cal BC) to 200 ± 30 years (6557 ± 411 cal BP, 4608 ± 41 cal BC). At the same time, ΔR for *T. palustris* drops from 389 ± 66 to 172 ± 99 years. A comparison with other published data from the Neolithic on

Anadara antiquata shells collected from Ras al-Hamra, an archaeological site near Muscat (Oman), revealed a significant difference between the two sites. Here, the reservoir effect corresponding to the lowermost layer at Kalba is determined as 202 ± 96 years (7077 ± 49 cal BP) and also decreases quickly to 144 ± 25 years (6675 ± 31 cal BP) (Zazzo et al. 2016). In Kalba, ΔR of *A. uropigimelana* continues to drop to 112 ± 44 years during the Bronze Age (3671 ± 28 cal BP, 1722 ± 28 cal BC) and of *T. palustris* to -19 ± 36 years. Unfortunately, no reservoir effect data from Ras al-Hamra during the Bronze Age or for *Terebralia palustris* of either period is available. In consequence, this drastic decrease in species-specific ΔR between Neolithic and Bronze Age is also different at differing locations and needs to be explained. The marine reservoir effect reflects the amount of old carbon (radiocarbon depleted waters) transported from the deep sea to the surface waters by upwelling.

Foraminifera in marine sediments of the Arabian Sea show a large variation in frequency per species in the period between 10 – 8.4 ka BP (Fig. 5.1). This can be explained by a century scale variability accompanied by a strong southwest monsoon causing a strong upwelling along the coast of Oman, Pakistan, and Iran (Staubwasser et al. 2002, Thamban et al. 2007). Since the mid-Holocene (from ca.7000 BP), the upwelling is reduced in strength (Fig. 5.1) (Staubwasser et al. 2002). Therefore, less old carbon is transported to the surface. These changes of reduced upwelling and climate are reflected in the radiocarbon data of the materials investigated. Reduced upwelling is a consequence of reduced monsoon which causes a reduced precipitation on land. This reduced upwelling causes a lower reservoir effect for the marine organisms involved. Marine radiocarbon chronologies suffer from unknown and certainly variable reservoir effects, bioturbation and varying depositional events. This hinders precise chronologies (Staubwasser et al. 2002). For example, relatively high reservoir ages of between 640 and 1120 years are reported from foraminifera between the onset of the Younger Dryas to the mid Holocene, therefore clearly showing temporal variations with a decreasing trend towards younger ages (Staubwasser et al. 2002). By way of comparison, values of over 1000 yrs today are only reached at ocean depths of just above 1000 m, a region below being affected by upwelling and surface convection as well as bomb radiocarbon penetration (Staubwasser et al. 2002). In the Arabian Sea (AS), the reconstructed $\Delta^{14}C$ content of the sea surface during the early Holocene is reconstructed to be in the range of 70 – 80 ‰, which converts to an age of 580 to 670 years (Staubwasser et al. 2002). In addition, the $\Delta^{14}C$ of the AS shows a distinct S-N decreasing gradient. Reservoir ages of the Arabian Sea are controlled by: a) summer monsoon upwelling; b) winter monsoon surface convection; c) reservoir ages of the AS thermocline water as inherited from its region of formation in the Southern Ocean (Staubwasser et al. 2002). Higher reservoir ages in the early Holocene hence can point to several effects: a lower or more depleted ^{14}C concentration of the Southern Ocean than today, a southward shift of the formation of thermocline water, hence also different ocean conditions of the Southern Ocean during the early Holocene (Staubwasser et al. 2002).

By trend, early Holocene reservoir ages of foraminifera exceeded 1000 yrs and decreased since then. In Fig. 5.1 this is represented by the amount of *G. bulloides* decreasing by about 5% between Neolithic and Bronze Age (mean value for the periods of the ΔR values). *G. bulloides* is a marker for upwelling and mixing of the water column.

The change in Southern Ocean conditions and therefore in upwelling of ^{14}C depleted waters is responsible for the continuous decrease of the reservoir effect over time since the early Holocene. Nevertheless, it would still induce a local reservoir effect that should be higher at Ras al-Hamra compared to Kalba because Ras al-Hamra lies further south and therefore closer to the coast where the upwelling takes place. Upwelling is restricted to the coast of Yemen and Oman until Ras al-Hadd, southeast of Muscat. In Kalba, no direct upwelling current is found. Therefore, an additional resource of radiocarbon depleted water must be responsible for the higher local reservoir effect at Kalba. The higher values at Kalba can be explained by the outflow of the dense, saline waters of the Arabian Gulf which are depleted in radiocarbon because they are rich in old carbon from sediments. Modern data on water samples from the mangroves at Kalba and Umm al-Qwain showed slightly depleted radiocarbon content for UAQ even today (see Chapter 3, Table 3.1.1). Today, oceans show hardly any or no reservoir effect in the sea surface region because of the bomb radiocarbon inventory (see Chapter 3). Therefore, measuring a difference between Kalba at the Gulf of Oman and Umm al-Qwain at the coast of the Arabian Gulf (AG) even today allows to interpret that the difference must have been even more pronounced in the past. It is even more significant when taking into account how flat the AG is which allows a constant exchange of the complete water column with atmospheric CO_2.

During the mid-Holocene, the sea level of the Arabian Gulf is still rising (Bernier et al. 1995, Lambeck 1996, Parker et al. 2018), as can be seen in Fig. 5.1. At the time when Kalba shows its highest reservoir effect (7013 ± 69 cal BP, 5064 ± 69 cal BC), the AG sea level was still below today´s level, but rises to more than 1 m above modern level until the second, much lower reservoir effect determination (6557 ± 41 cal BP, 4608 ± 41 cal BC) as can be seen in Fig. 5.1. Monitoring the seasonal inflow of rainfall into the AG was beyond the scope of this thesis and would require sclerochronology and stable isotopes on shells at several locations along the Arabian Gulf. However, at Kalba we can observe seasonality within the shells growth pattern and stable isotopes, but also in the high resolution ^{14}C measurements, but we cannot assign distinct freshwater input to the data due to the large error of the high resolution radiocarbon measurements made on two shells. Because *Anadara uropigimelana* ceases to grow during summer, it is not possible to achieve the same resolution in environmental monitoring as during winter. Due to the high background level during highly resolved measurements and large measurements errors because of extremely small amounts of carbon (down to 4 µg C instead of 30 µg needed with this configuration, see below), it is also not possible to use the data to trace the seasonal changes in reservoir effect.

One possible explanation is, that a higher sea level in AG and GO allows for a better mixing and hence dilution of the AG waters with respect to salinity and carbonate content. The ocean circulation within the AG and across the Straits of Hormuz might also allow for a better transport of atmospheric CO_2 into the water column. The stronger mixing and therefore homogenization of the waters should result in a reduced – or even negative – reservoir effect ΔR at Kalba and a reduced difference between the sites along the coast which is noticeable during the Bronze Age. Of course this interpretation suffers from the lack of reservoir effect data between ca. 6500 cal BP and ca. 3500 cal BP. The effect of sea level change of the Arabian Gulf and the amount of outflow on the reservoir effect in Kalba still needs to be investigated using sites along the Arabian Gulf of the same periods as Kalba. From the reconstructed sea level curve of the Arabian Gulf at Dosariayah (Parker et al. 2018) modified and included

in Fig. 5.1, the highest reservoir effect at Kalba can be linked to a period where the transgression just started to rise to a point allowing for some mixing of Arabian Gulf waters with water from the Gulf of Oman. The second reservoir effect around 400 years later marks a period of still rising sea level in the Arabian Gulf and therefore better mixing with waters from the Gulf of Oman that contain less dissolved inorganic carbon and therefore less radiocarbon depleted carbon. It should be noted that while several sea level curves are published for the Arabian Gulf, only few of them rely on calibrated radiocarbon ages taking into account reservoir effects. The study by Parker et al. (2018) did not only provide reliable data that is calibrated taking into account at least a certain reservoir effect, but also included sea level index points to reconstruct shores and sea level. Data gained by optically stimulated luminescence provides additional information on the ages of sedimentation.

The reduced ΔR at higher sea levels supports the idea that better mixing and reduced outflow of carbonate saturated waters over time is responsible for a significantly different ΔR at Kalba as compared to Muscat. During the Bronze Age, the reservoir effects calculated for Kalba are further reduced and seem to lie within a range of sea level where still increased sea levels in the AG are possible, resulting in an even more reduced carbonate saturation of the water (Fig. 5.1). Another factor contributing to the seasonal or temporal changes in ^{14}C depletion might be freshwater input as a consequence of increased rainfall. When the rainwater passes through limestone-rich environment and has enough time to dissolve significant amounts of radiocarbon depleted inorganic carbon, it will lead to an increase in reservoir effect in the lagoon where it enters the sea. If it does not pass through limestone-rich areas or does not have enough time to dissolve enough limestone, it will show a radiocarbon age close to the atmospheric value and therefore decrease the reservoir effect at the lagoon for a while. This seems to be the case for Kalba where the wadis feeding the mangrove forest after strong rainfalls pass through ophiolite, here especially Harzburgite, which does not contain significant amounts of limestone before it reaches the shoreline. Another indicator for rainfall and freshwater availability are the aquifers that store freshwater. Not many investigations were done on freshwater aquifers in the UAE, but results show that significant recharge of the aquifer at Liwa near Abu Dhabi stopped after 5500 cal BP (Wood and Imes 2003). This is interpreted as a reduction in rainfall from ca. 500 mm/yr to around 50 mm/yr as a results of a southward shift of the monsoon and the Intertropical Convergence Zone (Wood and Imes 2003).

In short, the ocean circulation that shows a seasonal pattern (correlated to monsoon and Westerlies) with respect to outflow of saline and carbonate rich Arabian Gulf waters passing along Kalba but not along Ras al-Hamra helped to understand the local differences. The carbonate–rich, radiocarbon-depleted outflow from the Arabian Gulf passes near Kalba, causing a higher reservoir effect at Kalba compared to settlements further south like Muscat, Ras al-Hamra or Ras al-Hadd. Nevertheless, it could be a consequence of two effects: sea-level rise with the consequence of diluted outflow from the AG and the decrease in upwelling because of reduced monsoon strength. In favour of a combination of the effects speaks the fact that also in Ras al-Hamra, which is influenced by upwelling but not by AG outflow, a reduction in reservoir effect can be seen during the period 7000 – 6500 cal BP, although less pronounced. The stronger effect at Kalba, however, can then be attributed to a reduced outflow (or increased mixing) and therefore a reduced availability of radiocarbon – depleted AG waters. The con-

tinuing decrease in ΔR of the purely marine and mixed (marine and terrestrially influenced) shell species between Neolithic and Bronze Age (Fig. 5.1) obviously reflects a continuous development in marine and terrestrial conditions. To monitor details between 6000 cal BP and 3000 cal BP, a continuous series of shell – charcoal pairs or at least some more data points over this period of around 3000 years would have been ideal. The drop in ΔR during the Bronze Age is less significant compared to the decrease during the Neolithic, but mirrors the continuing reduction in upwelling conditions along the coast of Oman and consequently at Kalba. The ΔR data during the Bronze Age period still lies on the elevated part of the sea level curve for the Arabian Gulf representing a better mixing with waters from the Gulf of Oman. This leads to a reduced saturation with carbonates and therefore a reduction in radiocarbon depleted water and consequently a decrease in ΔR (Fig. 5.1).

Apart from the general trend in environmental conditions, marine as well as terrestrial, another aspect to be taken into account is the periodic occurrence of molluskan species. Because only a few specimens of *Anadara uropigimelana* could be recovered in the oldest layer at the Neolithic shell midden in Kalba, this phase of the shell midden might coincide with the timing of the first *A. uropigimelana* mollusks to settle in this lagoon during the mid-Holocene, hence its first occurrence here. This, too, could be a parameter to contribute to an increased reservoir effect for a species that still needs to find its niche in this environment with respect to habitat and dietary preferences. For example, when the first specimens settled further outside the lagoon and fed from other, more radiocarbon depleted foraminifera and algae they might show older ages than inside the lagoonal environment. This would result in older radiocarbon ages and therefore an increased reservoir effect compared to later specimens that settled in the well protected lagoon with maybe different food resources. So far, this effect has never been taken into account or investigated. The occurrence of a new species usually marks changes in the environmental conditions that permit a new species to settle. In contrast, environmental changes like increased salinity can lead to the loss of a species. *Terebralia palustris*, for example, died out in the Arabian Gulf during an unknown period, probably because the increasing salinity started to dissolve the shell material. Higher salinity has a direct influence on the species diversity in the past as well as today (Coles and McCain 1990, Apel and Türkay 1999) This must have happened after the Iron Age period because *T. palustris* shells are still found at Tell Abraq (Arabian Gulf) during this period (Magee et al. 2017). Some authors found dead *Terebralia palustri*s shells dating to the Islamic era near Abu Dhabi, but it is commonly acknowledged that this species appeared in significant amounts along the Arabian Gulf predominantly during the Neolithic and their amount decreased since the Bronze Age (Hellyer and Aspinall 2006, Händel 2014)

The mangrove forest at Kalba shows its largest extend during the Neolithic denoted by the extension of the sabkha as seen today (Phillips and Mosseri-Marlio 2002). This, too, points to a higher sea level in the Gulf of Oman for the mid-Holocene (some unpublished shells by the author of this thesis from the sabkha were measured as 6000 ^{14}C yrs BP, and similar measurements mentioned in Phillips and Mosseri-Marlio, 2002).

The stronger drop in ΔR for *A. uropigimelana* from 576 ± 90 to 112 ± 44 years compared to the slightly lower drop in ΔR for *Terebralia palustris* from 389 ± 66 to 19 ± 36 years in the Neolithic should be due to the completely marine habitat and diet of the former, but might also be a consequence of change

in diet. With an exclusively marine diet, *Anadara uropigimelana* shows a completely marine radiocarbon signal and therefore a marine reservoir effect. *Terebralia palustris*, however, feeds mostly on leaf litter from the mangrove forest which is reflected in a mixed marine and terrestrial radiocarbon signal and therefore lower reservoir effect as *A. uropigimelana*. To account for the different contributions of upwelling and AG outflow towards the reservoir effect, investigations of several settlements along the coast would have been helpful. Both strategies could not be realized in the frame of this thesis.

Until the Bronze Age, the reservoir effect continues to decrease to a value of 105 ± 50 years for *A. uropigimelana* and -26 ± 46 years for *T. palustris* around 3811 ± 58 cal BP (1862 ± 58 cal BC). Overlapping results are found for the period a hundred years later with 112 ± 44 years at 3671 ± 28 cal BP (1722 ± 28 cal BC) and -19 ± 36 years for the respective species. This points to a rather stable environment for this period or changes that are rather long-term. In contrast to the mid-Holocene data, when taking a closer look at the archives it seems clear that this decrease follows after the drastic processes visible during the mid-Holocene and discussed above. The altered environmental conditions of decreased upwelling and reduced precipitation continued until the period monitored by the measured reservoir effects (Fig. 5.1).

The ΔR results and interpretations of marine shells can also be cross-checked with other paleoclimate archives such as stalagmites (Fig. 5.1). Stalagmites provides high resolution information about environmental conditions such as precipitation and in consequence about flora and sediment above the cave. The drop in species-specific reservoir effect detected at Kalba matched particularly well with the stalagmite records from Hoti cave (Fig. 5.1), near Muscat, Oman (Fleitmann et al. 2007, Fleitmann and Matter 2009). This cave is the nearest one where high resolution stalagmite data was measured. $\delta^{18}O$ in stalagmite records monitors precipitation where a shift towards positive values indicates a reduction in water availability. The isotopic ratio $\delta^{13}C$ used to interpret vegetation changes above the cave (Bar-Matthews and Ayalon 2004). The stalagmites in Hoti show rising $\delta^{18}O$ isotope values around 4200 BC and ceased to grow when the shell data shows the drop in ΔR which is interpreted as increasing aridity due to a lack of precipitation from the monsoon (Fig. 5.1). It, too, allows the interpretation that the ITCZ had moved further south during this period (Fleitmann et al. 2007) and caused enough rain for southern parts of Oman but excluded the northern parts from the cyclone system. This interpretation is corroborated by the continuous stalagmite data from Qunf cave, South Oman (Fig. 5.1) (Fleitmann et al. 2007, Fleitmann and Matter 2009, Van Rampelbergh et al. 2013) where the continuous rainfall is recorded but also shows a trend to reduced rainfall compared to the mid-Holocene. Around 4500 cal BC (ca.6500 cal BP) the Qunf cave signal start to shift towards more positive $\delta^{18}O$ values, but still oscillates until it stays at an elevated mean value after around 3500 cal BC (ca.5500 cal BP) just when Hoti cave fails to record. This marks the time when the monsoon shifts south and the rainfall in the North becomes too weak for the stalagmites in Hoti cave to grow. The monsoon gets weaker and in consequence fails to transport the same amount of nutrient rich water as upwelling to the Arabian Sea as it did before. Apart from the exchange with the waters of the Arabian Sea, the waters of the Arabian Gulf are now fed by freshwater caused only by rain transported with the Westerlies. A shift of the monsoonal system southward and therefore a shift to the Westerlies as the main resource of rainfall for the UAE leads to a reduced upwelling along the coast of Oman and therefore a reduced reservoir effect for marine species along the coast of Oman in the Arabian Sea and the Gulf of Oman,

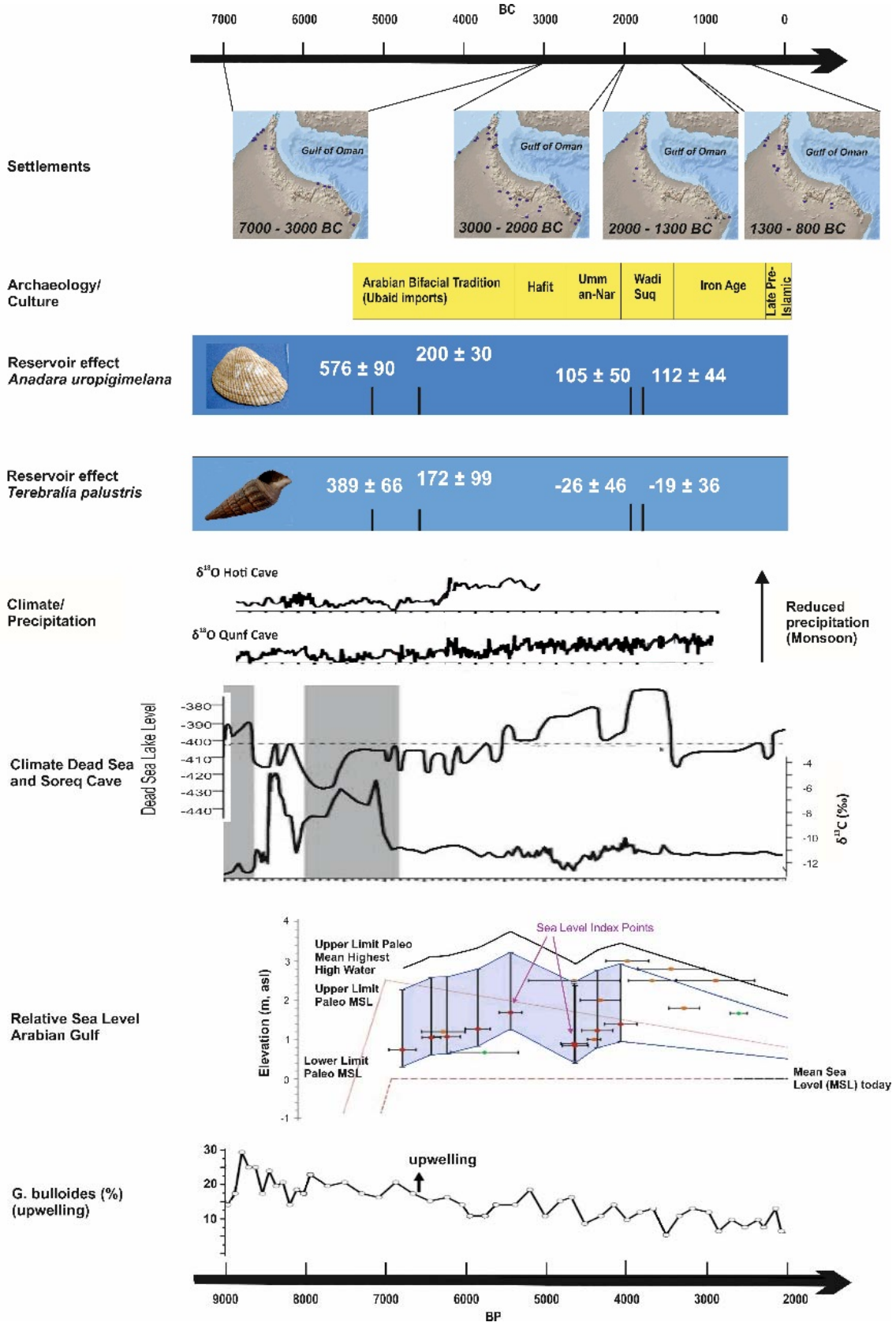

Fig. 5.1 Marine shell reservoir effects data from Kalba in the context of archaeology, climate (stalagmite data from Hoti cave and Qunf cave, modified from Parker et al., 2016), Relative Sea Level of the Arabian Gulf modified from (Parker et al. 2018) and upwelling as recorded by *G. bulloides* (modified from Balakrishnan Nair, 2006). The data from Soreq cave was modified from (Weninger et al. 2009).

With respect to terrestrial records, several paleolake investigations are published (Parker et al. 2006, Preston et al. 2015) where an increase in sedimentation by intake of aeolian sediments and a lack of precipitation or water resources is assigned to the periods of interest between early Holocene and Iron Age as well (Parker et al. 2006). The pollen and phytolith records of Awafi lake point to a C3 vegetation during the early to mid-Holocene (8500 – 5900 ka) representing a relatively moist phase. Pollen records of Awafi and Wahala lakes indicate a change to C4 plants that occur in zones with more arid climate. Geochemical analysis (Ti, Al, Fe, K, for information see chapter 2.3) of the lake sediments reveals a rapid dune activation together with increased influx of allogenic material into the lake system. This is interpreted as the onset of major desertification, drop in sea level and strengthening of the Shamal winds accompanied by a loss in vegetation (Parker et al. 2006). This increase in aeolian deposition starts around 5400 cal BP and peaks approximately at 5200 cal BP. A shallow lake remains between 5200 and 4200 cal BP due to dominant winter rainfall derived from Westerlies before the lakes (Awafi and Wahalah) fall dry around 3900 years ago. The reservoir effect data from Kalba connects to the results from Parker et al. (2006) indicating higher values before the onset of increased aridity and shortly before the lakes fell dry with low or, in the case of *Terebralia palustris*, even negative ΔR. In general it can be concluded that the local paleoenviromental records point to a significant desertification between 5500 and 4000 BP. This constant decline in humid conditions shows the same trend as the decrease in reservoir effect.

Climate on the Arabian Peninsula is also influenced by the Westerlies mentioned earlier, a wind transporting Mediterranean climate, in particular in the Levant region. Therefore, Soreq cave near Jerusalem and Dead Sea lake level provide palaeorecords of the intensities of the Westerlies (Bar-Matthews and Ayalon 2004, Migowski et al. 2006). The stable isotope data from Soreq cave shows several distinct features in its signal roughly contemporary to the features at the caves in Oman. Anomalously high pulses in $\delta^{13}C$ around 8500 cal BP and 7000 cal BP (Fig. 5.1) in combination with rather low $\delta^{18}O$ values were in this case interpreted as humid conditions. Another sharp but short event (ca.200 years) of increased $\delta^{18}O$ signal pointing to reduced rainfall occurs around 5200 cal BP, coinciding with the lake records from Awafi. A longer period of approximately 400 years duration with increased $\delta^{18}O$ and $\delta^{13}C$ data occurs between 4600 to 4000 cal BP. The latter event of parallel rise of both stable isotopes is interpreted as an increase of the relative proportion of C4 plants, coinciding with archaeological disaster events such as the collapse of the Akkadian Empire and the Egyptian Kingdom probably due to a significant drop in Nile water (Bar-Matthews and Ayalon 2004). At Soreq cave, $\delta^{13}C$ reflects interactions between rain water, soil CO_2 from, mostly, C3 vegetation and host dolomite rocks in a closed or open-closed system. Therefore, a sharp increase of $\delta^{13}C$ can also correspond to a removal of soil and stronger proportion of rock and atmospheric CO_2 signal (Bar-Matthews and Ayalon 2004).

Not too far from Soreq cave, the Dead Sea lake level is also an indicator for environmental changes. Like Soreq cave, the Dead Sea level mirror the influence of the Westerlies from the Mediterranean. Their influence is visible in southeast Arabia as well, but to a lesser amount as in Jordan. During the Holocene, the data points to significant changes in environmental conditions, here influence of Westerly winds, also in this area (Fig. 5.1). The higher seal level of the Dead Sea before 7700. cal BP coincides with the general trend of a more humid phase during the early Holocene. Apart from certain wiggles in the data, the Dead Sea lake level shows a trend to rising sea level between ca.7500 to ca.3500 cal

BP after a downward trend until 7700 cal BP. The relatively low level conditions lasted until ca. 5600 cal BP marked by the appearance of aragonite, gypsum and sand layers in the sediment cores (Migowski et al. 2006). An amelioration of climatic conditions began in 5400 cal BP and lasted until 3500 cal BP with an interruption of a drier period around 4200 cal BP corroborating the interpretation from the Soreq cave data (Fig. 5.1). Because the Westerlies become a major carrier of rainfall to Arabia after retreating monsoon, it is concluded that the changes in reservoir effect at Kalba seem to reflect not only environmental conditions on a local scale, but also on a global scale and follows the trends detected in other archives in Oman as well as in Israel.

Several studies on corals around the Great Barrier Reef in Australia, however, also support the interpretation of the shell data from Kalba results in the context of environmental change and weakening monsoon systems and upwelling waters (Yu et al. 2007, Hua et al. 2015).The Great Barrier Reef is also affected by upwelling waters from the Southern Ocean that divides south of the Arabian Sea. Part of the deep current then takes the route along east Africa to the Arabian Sea, the second part travels eastward along the equator to Oceania and South America. The ocean circulation is far more complex here with many islands and the south equatorial current (SEC) flowing westward and transporting upwelling waters from Peru across the Pacific as a second resource for upwelled and therefore radiocarbon depleted waters apart from the Subantarctic Mode Water (SAMW) that deviates from the Antarctic Circumpolar Current. The reservoir effect data in this case was determined on corals from the Great Barrier Reef and compared to other data (Druffel et al. 2007, Hua et al. 2015). Even though the environmental conditions are not the same, they might allow for a comparison of both locations with respect to global or, here, Southern Hemisphere events. Hua et al. (2015) link the changes in reservoir effect to the variations in ocean circulation associated with changing climate conditions (especially El Niño/La Niña, easterly trade winds, positions of the Intertropical Convergence Zone as well as the South Pacific Convergence Zone) (Hua et al. 2015). Even though the changes in ΔR for the corals are less distinctive (Yu et al. 2007, Hua et al. 2015), these studies reported a large scatter in the data but an overall tendency towards a decrease in ΔR over the years. For one site, Moreton Bay, the ΔR dropped from 300 to 50 years between 6000 to 2500 cal BP. In Kalba, the more pronounced change in species-specific reservoir effects compared to the change at the Great Barrier Reef allows the interpretation that the changes in environmental conditions were stronger in Kalba and more straightforward maybe due to a less complicated ocean circulation.

The observations made in marine and terrestrial archives such as increasing aridity, reduced rainfall, etc., directly influence cultural developments as identified by archaeologists. As the shells used for radiocarbon dating are usually recovered from archaeological excavations, this aspect also needs some attention and helps to link the data to environmental conditions experienced by the people collecting the shells. Neolithic and Bronze Age cultural developments are linked to patterns of increasing contact and exchange (e.g. with Mesopotamia and Iran), as monitored in the amount of archaeological sites and their finds as well as complex technologies like copper production (Fig. 5.1). During the Neolithic period (Arabian bifacial tradition), archaeological data already shows a variety of settlements, mainly along the coast (Fig. 5.1), including significant changes in mortuary practice over time from the Hafit to Umm an-Nar to Wadi Suq periods (Fig. 5.1). Intensive agriculture develops between the Bronze and

Iron Age, including the emergence of *falaj* irrigation technologies. The Bronze Age also marks the development of long-distance trade, with evidence for contacts with regions as far as the Indus and Mesopotamia. Environmental changes toward a more arid climate with reduced upwelling and therefore less rich waters is likely linked to the necessity to invent/adopt novel technologies and to develop social networks with neighboring regions. Therefore, the increasing aridity seems to push sustainable progress and cultural developments as survival strategy with increasing necessity.

To test whether it is also possible to monitor seasonal changes of the environment via ^{14}C of the shell, high resolution ^{14}C measurements were measured from two specimens of *Anadara uropigimelana*, one from the Neolithic shell midden Kalba KK1, the second from the Bronze Age settlement Kalba K4 (Lindauer et al. 2018). Inspired by the high resolution and amount of data points per shell specimen achieved from the stable isotope measurements, small shell subsamples were tested for radiocarbon (^{14}C) parallel to the sample holes of the stable isotope samples to recover the same growth period. The measurements produced quite large errors because of the small sample size (4 – 25 µg C). Small amounts of elemental carbon (C) only allow a short measurement period in the AMS, resulting in few data points in larger scatter and therefore a larger error. In addition, a gas-ion source needs to be used which means that the carbon is fed as gaseous CO_2 into the accelerator instead of a solid target. The gaseous CO_2 is more difficult to ionize than the solid carbon because it is not stationary. Therefore, more cesium at elevated temperatures (160 °C compared to 135 °C during a measurement with solid C) is needed to ionize the carbon, which also provides higher energies for the gas to move in the ionization chamber. Ideally, for radiocarbon measurements a sample size of 1 mg elementary carbon (C) is needed. The error depends on the size of the sample and is bigger for smaller samples. In addition the blank assessment revealed cross-contamination effects of up to 6% between successive samples which is not a problem for samples of the same age, but can spoil the measurement when samples with significantly different ^{14}C content are measured. In this case, oxalic acid Ox II (134.08 pmC), the international standard for radiocarbon dating, was measured before a blank sample (marble, IAEA C2) and caused significantly elevated ^{14}C measurements. However, with respect to dating possibility the combination of shells dissolved in a carbonate handling system and fed through the gas ion source into the accelerator can provide reliable data when several blanks (marble) are measured between oxalic acid and shell sample to clean the system. A proper blank assessment as suggested enables better data handling due to reduced error of the blank data itself and in consequence a reduced error of the sample data. In the case presented in chapter 4.3, the ideal sample size would have been at least 30 µg C to allow for an interpretation with respect to environmental conditions. With the smaller amounts of C and elevated backgrounds in combination with cross-contamination effects, only trends could be read from the data. The trend in ^{14}C of the Neolithic shell sample providing 62 subsamples followed the general trend of the $\delta^{13}C$ measurements with some exceptions where significant changes in $\delta^{18}O$ are recorded. For a detailed interpretation of these patterns, improved measurements would be necessary. With respect to the instrument, improvements would be necessary to prevent cross-contamination and memory effects of the zeolith involved that serves as a trap to collect the CO_2. Meanwhile, measurement problems are solved, as could be seen from the blank measurements with the gaseous CO_2 blank and with proper blank-cleaning of the system after oxalic acid measurements (Lindauer et

al. 2018). Therefore, future measurements of high resolution ^{14}C parallel to sampling positions of stable isotope samples will prove to be suitable for detailed interpretations of the seasonal variation when it comes to interpreting the $\delta^{13}C$ data. So far, this pilot study revealed the drawbacks of the system used, allowed for improvements of the method and provided data that provided information on trends in the seasonality, but not details of the origin of the carbon with respect to freshwater input.

To gain all these measurements for ΔR, stable isotopes and high resolution ^{14}C, many shells had to be processed. For some shells, influences of heat on the shell material were obvious and immediately visible as greyish colour which could not be removed by washing the shell. At archaeological sites, often shells are found that had been heated to remove the flesh from the shell material or to open the valves in case of a bivalve (Händel 2014). It is commonly thought though not tested that heated shells cannot be used for radiocarbon dating. As it was never tested, this was another important aspect of the thesis, because it is not always possible to exclude heated shells from dating. Occasionally, a heat influence is not immediately visible. It can then only be detected when cutting the shell material, e.g. for stable isotope analysis or sclerochronological purposes (Lindauer et al. 2018, Milano et al. 2018). Both species used in this thesis, *A. uropigimelana* and *T. palustris*, consist of aragonite. But when heated above a certain temperature (ca. 500 °C), the mineralogy turns into the more stable calcite (Lindauer et al. 2018, Milano et al. 2018). In addition, the microstructure changes from layered structures with lamellae to a rather coarsely granular pattern (Milano et al. 2018). With respect to stable isotopes, the heating process causes a shift especially in $\delta^{18}O$ and therefore heated shells are not reliable for this purpose. The radiocarbon measurements of heated and unheated shells of *Anadara uropigimelana* and *Terebralia palustris* from the same layers yield the same results and do not differ at all (Lindauer et al. 2018). This also means the heating process must be very fast, so that the change in mineralogy does not allow to incorporate carbon from other sources in the surrounding (charcoal, air, etc.). Hence, it follows that heated shells work well for radiocarbon dating and consequently for chronologies, but not for stable isotopes and environmental research.

One of the radiocarbon dated shells of species *A. uropigimelana*, however, showed signs of heating when cut for stable isotope analysis, but not throughout the shell. This specimen consisting of calcite with some minor relicts of aragonite towards the central margin enabled to find out about the heating mechanism. From literature research, a description in a modern (1980s) ethnological study from the prehistoric Australia on similar shell species was found (Meehan 1982). The process involved arranging the shells to be heated in a kind of phalanx with the umbo upwards. They were covered with dry leaves, dry grass and small sticks. This resulted in a very fast and hot fire propagating along the shell phalanx. The heating only takes up to two minutes. This was the first time ever that a shell could be assigned the method of heating which provided another method of shell processing on the Arabian Peninsula.

The terrestrial version of the marine ΔR is referred to as hardwater effect and can deviate even more from the calendar age when the underlying substrate or dissolved carbon in the case of freshwater is of geological origin (limestone for example) and therefore does not contain any ^{14}C. Limestone in the sediment or dissolved in the water can shift the radiocarbon ages even further towards older ages than the upwelled marine waters and result in possible hardwater effects of as much as several thousand years. Hence, as the marine reservoir effect is not assignable to terrestrial or freshwater molluscs, the

attention was drawn to the landsnails of species *Zootecus insularis* and the freshwater gastropod *Melanoides tuberculata*. Like the marine shells investigated so far, these two species are abundant and often found in sediment layers and archaeological sites. The idea behind this was to detect changes in hardwater effect as a result of different geological settings, such as ophilitic bedrocks, carbonate rich environments as well as mixed bedrocks, but also with respect to dissolved carbon in the freshwater. Unfortunately, no live specimens were found to directly derive a hardwater effect for these species which would have provided a well-defined starting point. Nevertheless, samples recovered from archaeological sites for this pilot study, shed light on possible hardwater effects of these species. These vary from no hardwater effect to around 500 years for the freshwater snail *M. tuberculata* and peaked in hardwater effects of several hundred years for *Z. insularis* in Kalba to nearly 4000 years for specimen found in dunes near Buhais. As expected, terrestrial snails show a significantly higher hardwater effect with increasing content of limestone or other carbonate rich bedrocks. This is the case for sites like in the Dibba fracture zone between Masafi and Dibba where the hardwater effect is found to be around 2500 years. Towards the greater plains on the west of the Hajar Mountains, the dunes carry enough carbonaceous sediment to also contribute to a high hardwater effect of the terrestrial snail in the range of nearly 4000 years. In areas with bedrock of no or only minor carbon content like Wadi Hilo where Gabbro and Harzburgite dominate the landscape, hardwater effects of zero are possible, some elevated values can be explained by pedogenic carbonates in Quaternary river terraces. The archaeological site of Kalba yielded hardwater effects of several hundred years. Although the underlying bedrock is dominated by ophiolite and Gabbro, the carbonate-rich sediment of the coast provides enough radiocarbon depleted material to produce a significant shift. The hardwater effects of these terrestrial shells on the other hand can only be regarded as preliminary as far as no live specimens can be found. The study showed, that trends with respect to rock types can be observed, however, an accurate calibration for each archaeological site is necessary. Moreoever, nothing is known about the diet of terrestrial and freshwater gastropods and its imprint on the hardwater effect.

Many aspects of shells from archaeological contexts have been described in this thesis. Figure. 5.2 tries to take the most important aspects mentioned so far into account to provide some suggestions as to the best way to plan dating or investigating marine shells. For terrestrial shells, the possibilities are rather limited and hardly go beyond radiocarbon dating and stable isotopes (or other elements than carbon and oxygen). The recommendations given in the graphic are of course not complete and only based on the findings of this thesis. Regarding possibilities apart from radiocarbon dating, suggestions are made towards sclerochronology and stable isotopes $\delta^{13}C$ and $\delta^{18}O$.

In figure. 5.2, the blue arrows denote the line of action or the questions coming up when using a shell. If a shell is fragmented or only a fragment recovered, it can only be used for radiocarbon dating. Even stable isotopes might not be very conclusive as the position the fragment had in the shell might not be unambiguous therefore it will not help to understand or reconstruct environmental conditions. If the shell or a complete valve in case of a bivalve is conserved, it can be used for a variety of methods apart from radiocarbon. Several specimens of the same species will provide a more representative dataset and if even several species with several specimens can be used, a reliable reconstruction of the environment during a certain time interval can be achieved. Sclerochronology will provide information on

the lifespan of this specimen and stable isotopes contribute information about growth periods and seasonality in combination with data on salinity and water temperature (Fig. 5.2). Ideally, contemporaneous terrestrial material is found and allows for a calculation or modelling of a species-specific reservoir effect. Using information on habitat, lifespan (in general), juvenile phase (duration, habitat if different) from the literature in combination with archaeological findings and comparison with other (paleo-) climate records yields a good dataset to contribute to environmental monitoring. It must be kept in mind though that stable isotopes cannot be applied on heated shell material. In case of a heated shell sclerochronology, too, does not provide information as the heating process destroys the crystal structures as mentioned above. Therefore, growth lines cannot be detected and measured successfully. It should be kept in mind, however, that in the context of radiocarbon dating sclerochronology and stable isotopes do not directly contribute to the determination of the reservoir effect. However, they are an important tool to judge whether the shells can be used for environmental monitoring in addition to radiocarbon dating. Stable isotope measurements can also provide information on whether the shell remained stationary throughout its lifespan or whether it, as in the case of *Terebralia palustris*, grew up offshore and moved closer to the coast after a certain period. This knowledge helps to avoid sampling positions for radiocarbon dating that would lead to erroneous ages.

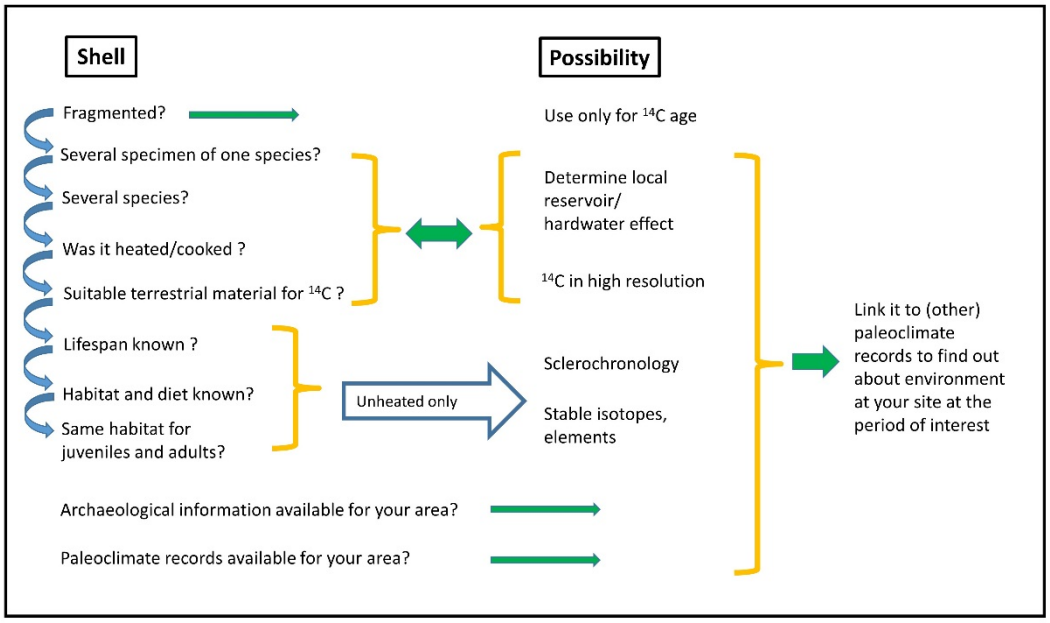

Fig. 5.2 Suggestions for best practice and possibilities when dealing with shells.

This thesis provides an interpretation for the differing results published on shells in SE Arabia so far and gives advices on how to determine a proper species-specific reservoir effect, taking into account temporal variability and shell characteristics for the first time. Hereupon shells can be used for precise chronologies as environmental archives. In effect, shell characteristics such as reactivity to environmental changes, habitat or even diet are used in this work for a better understanding of the shell species. The combination of stable isotopes with knowledge about diet and habitat prior to radiocarbon dating was never used before to understand reservoir effect data and allows to interpret differences in the reservoir effect between species.

6 Conclusions

This study is the first systematic approach to use shells of different species, including the environmental information stored in them, over different periods in time for paleoenvironmental and archaeological chronologies.

Most aims specified earlier could be achieved:

a) A species-specific reservoir effect ΔR was modeled for the marine bivalve *Anadara uropigimelana* and the marine gastropod *Terebralia palustris*;

b) Determining a reservoir effect for each archaeological layer between Neolithic and Bronze Age, it was found that the species - specific ΔR changes significantly between these periods - *A. uropigimelana* drops from 576 ± 90 to 112 ± 44 years, for *T. palustris* the value decreases from 389 ± 66 to -19 ± 36 years;

c) Using stable isotopes it turned out that *A. uropigimelana* reacts fast to changes in the environment. The information stored is more detailed during winter than during summer as this species shows reduced growth during summer and therefore stores less details during this season. The SST range in the lagoon was derived from $\delta^{18}O$. The origin of $\delta^{13}C$ (water DIC and diet) does not allow a unique interpretation, but first tests on high resolution ^{14}C measurements parallel to the stable isotopes helps to at least derive trends like freshwater input;

d) A significant number of shells turned out to be heated after foraging. The mineralogy for both shell species changes from aragonite to calcite and microstructures are completely lost. One shell that shows signs of incomplete heating allowed for detecting transition zones and for the first time to identify the exact heating procedure by comparison with ethnological studies on similar species;

e) The pilot study on terrestrial snails of species *Zootecus insularis* and freshwater gastropod *Melanoides tuberculata* led to some preliminary results for hardwater effects. The geology of the sites plays a crucial role that can only be transferred into a hardwater effect when live specimen can be recovered or other well-defined settings like archaeological context are available. Terrestrial snails, however, remain difficult to interpret at this early stage of the study;

f) The reservoir effect data and the calibrated ages of the shell - charcoal pairs could be linked to other environmental proxies like stalagmites, paleolakes, sea level change, changes in upwelling, etc. This led to the conclusion that the drop in ΔR was caused by changes in upwelling intensity in the Arabian Sea, reduced outflow of old carbon from Arabian Gulf waters.

g) From the manifold investigations undertaken at the shells, some advice in the form of a chart could be gathered (Fig. 5.2) will be helpful when shells had been recovered and so far using them was not planned. It will also provide help when planning studies where shells shall be involved.

This work shows a state of the art approach to reservoir effect determination. With the data on reservoir effect of the two periods determined here, this work contributes to a better understanding of local and global climate aspects. Systematically monitoring reservoir effects of purely marine shells as well

as shells of mixed influence - as provided here – at other locations, too, would result in a better understanding of global effects of wind patterns and corresponding ocean circulation in combination with estimates on purely local contributions. When sampled with higher temporal resolution, it will be possible to differ between local and global contributions. This result reaches a lot further than just the contribution to more detailed chronologies for archaeology and geosciences.

References

Al-Abri, A., et al. (2012). Pleistocene-Holocene boundary in Southern Arabia from the perspective of human mtDNA variation. *American Journal of Physical Anthropology* 149(2): 291-298.

Al-Farraj, A. (2005). An evolutionary model for sabkha development on the north coast of the UAE. *Journal of Arid Environments* 63: 740-755.

Al-Khayat, J. A. and D. A. Jones (1999). A Comparison of the Macrofauna of Natural and Replanted Mangroves in Qatar. *Estuarine, Coastal and Shelf Science* 49, Supplement 1(0): 55-63.

Al-lazki, A., et al. (2002). A crustal transect across the Oman Mountains on the eastern margin of Arabia. *GeoArabia* 7(1): 47-78.

Ali, M. Y. and K. F. Watts (2009). Subsidence history, gravity anomalies and flexure of the United Arab Emirates (UAE) foreland basin. *GeoArabia* 14(2): 17-44.

AlSarmi, S. and R. Washington (2011). Recent observed climate change over the Arabian Peninsula. *Journal of Geophysical Research: Atmospheres* 116(D11).

Alves, E., et al. (2015). Marine Reservoir Corrections on the Southeastern Coast of Brazil: Paired Samples from the Saquarema Shellmound. *2015* 57(4): 517-525.

Alves, E., et al. (2015). Radiocarbon reservoir corrections on the Brazilian coast from pre-bomb marine shells. *Quaternary Geochronology* 29: 30-35.

Alves, E., et al. (2016). Corrigendum to 'Radiocarbon reservoir corrections on the Brazilian coast from prebomb marine shells' [Quat. Geochronol. 29 (2015) 30–35]. *Quaternary Geochronology* 31: 1-2.

Andrus, C. F. T. (2011). Shell midden sclerochronology. *Quaternary Science Reviews* 30(21-22): 2892-2905.

Apel, M. and M. Türkay (1999). Taxonomic Composition, Distribution and Zooeoahic Relationships of the Grapsid and Ocypodid Crab Fauna of Intertidal Soft Bottoms in the Arabian Gulf. *Estuarine, Coastal and Shelf Science* 49, Supplement 1(0): 131-142.

Armitage, S. J., et al. (2011). The Southern Route 'Out of Africa': Evidence for an Early Expansion of Modern Humans into Arabia. *Science* 331(6016): 453-456.

Arz, H. W., et al. (2006). A pronounced dry event recorded around 4.2 ka in brine sediments from the northern Red Sea. *Quaternary Research* 66(3): 432-441.

Ascough, P., et al. (2005). Methodological approaches to determining the marine radiocarbon reservoir effect. *Progress in Physical Geography* 29(4): 532-547.

Ascough, P. L., et al. (2005). Influence of Mollusk Species on Marine ΔR Determinations. *Radiocarbon* 47(3): 433-440.

Ascough, P. L. C., G.T.; Dugmore, A.J. (2009). North Atlantic marine ^{14}C reservoir effects: implications for late-Holocene chronological studies. *Quaternary Geochronology* 4: 171-180.

Azzoug, M., et al. (2012). Reconstructing the duration of the West African Monsoon season from growth patterns and isotopic signals of shells of Anadara senilis (Saloum Delta, Senegal). *Palaeogeography, Palaeoclimatology, Palaeoecology* 346-347(0): 145-152.

Balakrishnan Nair, T. M. (2006). Monsoon control on trace metal fluxes in the deep Arabian Sea. *Journal of Earth System Science* 115(4): 461-472.

Bar-Matthews, M. and A. Ayalon (2004). Speleothems as palaeoclimate indicators, a case study from Soreq Cave located in the Eastern Mediterranean Region, Israel. Past climate variability through Europe and Africa, Springer**:** 363-391.

Barker, G., et al. (2010). The Cyrenaican Prehistory Project 2010: the fourth season of investigations of the Haua Fteah cave and its landscape, and further results fromthe 2007–2009 fieldwork. *Libyan Stud* 41: 63-88.

Beech, M., et al. (2005). New evidence for the Neolithic settlement of Marawah Island, Abu Dhabi, United Arab Emirates. *Proceedings of the Seminar for Arabian Studies* 35: 37-56.

Berger, J.-F., et al. (2005). Évolution paléogéographique du Ja'alan (Oman) à l'Holocène moyen : impact sur l'évolution des paléomilieux littoraux et les stratégies d'adaptation des communautés humaines. *Paléorient*: 46-63.

Berger, J. F., et al. (2013). The dynamics of mangrove ecosystems, changes in sea level and the strategies of Neolithic settlements along the coast of Oman (6000-3000 cal. BC). *Journal of Archaeological Science* 40: 3087-3104.

Bernier, P., et al. (1995). Holocene shoreline variations in the Persian Gulf: Example of the Umm al-Qowayn lagoon (UAE). *Quaternary International* 29–30: 95-103.

Beverly, R. K., et al. (2010). The Keck Carbon Cycle AMS Laboratory, University of California, Irvine: status report. *Radiocarbon* 52(2): 301-309.

Biagi, P. (1994). A radiocarbon chronology for the aceramic shell-middens of coastal Oman. *Arabian Archaeology and Epigraphy* 5(1): 17-31.

Biagi, P. (2013). The shell middens of Las Bela coast and the Indus delta (Arabian Sea, Pakistan). *Arabian Archaeology and Epigraphy* 24(1): 9-14.

Biagi, P. N., Renato (1999). The shell-midden sites of RH5 and RH6 (Muscat, Sultanate of Oman) in their environmental setting. *Archaeologia Polonia* 37: 31-47.

Bieler, R., et al. (2004). Periglypta listeri (J. E. Gray, 1838) (Bivalvia:Veneridae) in the western Atlantic: Taxonomy,, Anatomy, Life Habits and Distribution. *Malacologia* 46(2): 427-458.

Blau, S. and M. Beech (1999). One woman and her dog: an Umm an-Nar example from the United Arab Emirates. *Arabian Archaeology and Epigraphy* 10(1): 34-42.

Böhm, E., et al. (1999). The Ras al Hadd Jet: Remotely sensed and acoustic Doppler current profiler observations in 1994–1995. *Deep Sea Research Part II: Topical Studies in Oceanography* 46(8): 1531-1549.

Boivin, N. and D. Fuller (2009). Shell Middens, Ships and Seeds: Exploring Coastal Subsistence, Maritime Trade and the Dispersal of Domesticates in and Around the Ancient Arabian Peninsula. *Journal of World Prehistory* 22(2): 113-180.

Braadbaart, F., et al. (2012). Fuel, Fire and Heat: an experimental approach to highlight the potential of studying ash and char remains from archaeological contexts. *Journal of Archaeological Science* 39(4): 836-847.

Bretzke, K., et al. (2013). The environmental context of Paleolithic settlement at Jebel Faya, Emirate Sharjah, UAE. *Quaternary International* 300(0): 83-93.

Broecker, W. S., et al. (1960). Natural radiocarbon in the Atlantic Ocean. *Journal of Geophysical Research* 65: 2903-2931.

Bronk Ramsey, C. (2008). Radiocarbon Dating: Revolutions in Understanding. *Archaeometry* 50(2): 249-275.

Bronk Ramsey, C. and S. Lee (2013). Recent and Planned Developments of the Program OxCal.

Brown, D. S. and M. D. Gallagher (1985). Freshwater snails of Oman, South Eastern Arabia. *Hydrobiologia* 127(2): 125-149.

Burchell, M., et al. (2013). Inter-site variability in the season of shellfish collection on the central coast of British Columbia. *Journal of Archaeological Science* 40(1): 626-636.

Burns, S. J., et al. (2001). Speleothem evidence from Oman for continental pluvial events during interglacial periods. *Geology* 29(7): 623-626.

Butler, P. G., et al. (2009). Continuous marine radiocarbon reservoir calibration and the 13C Suess effect in the Irish Sea: Results from the first multi-centennial shell-based marine master chronology. *Earth and Planetary Science Letters* 279(3–4): 230-241.

Butler, P. G., et al. (2011). Long-term stability of d13C with respect to biological age in the aragonite shell of mature specimens of the bivalve mollusk Arctica islandica. *Palaeogeography, Palaeoclimatology, Palaeoecology* 302(1-2): 21-30.

Carter, R. (1997). The Wadi Suq period in south-east Arabia: a reappraisal in the light of excavations at Kalba, UAE. *Proceedings of the Seminar for Arabian Studies* 27: 87-98.

Charpentier, V., et al. (2000). Autour de la mangrove morte de Suwayh, l'habitat VI ^e –V ^e millénaires de Suwayh SWY-11, Sultanat d'Oman. *Proceedings of the Seminar for Arabian Studies* 30: 69-85.

Coles, S. L. and J. C. McCain (1990). Environmental factors affecting benthic infaunal communities of the Western Arabian gulf. *Marine Environmental Research* 29(4): 289-315.

Colonese, A. C., et al. (2017). Shell sclerochronology and stable isotopes of the bivalve Anomalocardia flexuosa (Linnaeus, 1767) from southern Brazil: Implications for environmental and archaeological studies. *Palaeogeography, Palaeoclimatology, Palaeoecology* 484: 7-21.

Cooper, D. J. W., et al. (2014). Structure of the northern Oman Mountains from the Semail Ophiolite to the Foreland Basin.

Cooper, D. J. W., et al. (2016). Evolution of the Arabian continental margin of the northern Dibba Zone, eastern United Arab Emirates and Oman. *Journal of Asian Earth Sciences* 129: 254-275.

Culleton, B. J., et al. (2006). Intrashell Radiocarbon Variability in Marine Mollusks. *Radiocarbon* 48(3): 387-400.

Dalongeville, R. and P. Sanlaville (2005). L'évolution des espaces littoraux du golfe Persique et du golfe d'Oman depuis la phase finale de la transgression post-glaciaire. *Paléorient* 31(1): 9-26.

Das, M., et al. (2017). Holocene strengthening of the Oxygen Minimum Zone in the northwestern Arabian Sea linked to changes in intermediate water circulation or Indian monsoon intensity? *Palaeogeography, Palaeoclimatology, Palaeoecology* 483: 125-135.

de Villiers, M. P. (2010). Predicting the development of weather phenomena that influence aviation at Abu Dhabi International Airport. PhD, University of Pretoria.

Debenay, J. P., et al. (1994). Environmental Conditions, Growth and Production of Anadara Senilis (Linnaeus, 1758) in a Senegal Lagoon. *Journal of Molluscan Studies* 60(2): 113-121.

Dettman, D. L., et al. (2015). 14C and Marine Reservoir Effect in Archaeological Samples from the Northeast Gulf of California. *Radiocarbon* 57(5): 785-793.

Diaz, M., et al. (2016). Radiocarbon Marine Reservoir Effect on the Northwestern Coast of Cuba. *Radiocarbon* 59(2): 333-341.

Druffel, E. R. M., et al. (2007). Oceanic climate and circulation changes during the past four centuries from radiocarbon in corals. *Geophysical Research Letters* 34(9).

Dutta, K. (2008). Marine ^{14}C Reservoir Age and Suess Effect in the Indian Ocean. *Journal of Earth Science India* I(III): 175-188.

Eddisford, D. and C. S. Phillips (2009). Kalba in the third millenium (Emirate of Sharjah, UAE). *Proceedings of the Seminar for Arabian Studies* 39: 111-124.

Eddy, J. A. (1976). The Maunder Minimum. *Science* 192(4245): 1189-1202.

Elkarmi, A. Z. and N. S. Ismail (2007). Growth models and shell morphometrics of two populations of Melanoides tuberculata (Thiaridae) living in hot springs and freshwater pools. *2007* 66(2): 7.

Engelhardt, I., et al. (2013). Impact of Preboreal to Subatlantic shifts in climate on groundwater resources on the Arabian Peninsula.

Engelhardt, I., et al. (2013). Impact of Preboreal to Subatlantic shifts in climate on groundwater resources on the Arabian Peninsula. *Environmental Earth Sciences* 69(2): 557-570.

Enzel, Y., et al. (2015). The middle Holocene climatic records from Arabia: Reassessing lacustrine environments, shift of ITCZ in Arabian Sea, and impacts of the southwest Indian and African monsoons. *Global and Planetary Change* 129: 69-91.

Favier Dubois, C. M. and A. J. T. Jull (2017). Marine Reservoir Effect Values from Shell-Middens of San Matías Gulf, Northern Patagonia (Argentina): A 5000-yr Record. *Radiocarbon* 60(2): 419-424.

Fernández-López de Pablo, J. (2016). The timing of postglacial coastal adaptations in Eastern Iberia: A Bayesian chronological model for the El Collado shell midden (Oliva, Valencia, Spain). *Quaternary International* 407, Part B: 94-105.

Feulner, G. R. (2000). The Large Mangrove Mud Creeper Terebralia palustris (Linneaus, 1767) in Non-Mangrove Environments in Southeast Arabia. *Tribulus* 10(2): 15-26.

Feulner, G. R. and S. A. Green (2003). Terrestrial Molluscs of the United Arab Emirates. *Mitteilungen der deutschen malakozoologischen Gesellschaft* 69/70: 23-34.

Fleitmann, D., et al. (2007). Holocene ITCZ and Indian monsoon dynamics recorded in stalagmites from Oman and Yemen (Socotra). *Quaternary Science Reviews* 26(1â€“2): 170-188.

Fleitmann, D., et al. (2011). Holocene and Pleistocene pluvial periods in Yemen, southern Arabia. *Quaternary Science Reviews* 30(7-8): 783-787.

Fleitmann, D. and A. Matter (2009). The speleothem record of climate variability in Southern Arabia. *Comptes Rendus Geoscience* 341(8-9): 633-642.

Fratini, S., et al. (2008). Feeding preferences and food searching strategies mediated by air- and water-borne cues in the mud whelk Terebralia palustris (Potamididae: Gastropoda). *Journal of Experimental Marine Biology and Ecology* 362(1): 26-31.

Frifelt, K. (1971). Jamdat Nasr fund fra Oman (Jamdat Nasr graves in the Oman). *Kuml*: 355-383.

Füllenbach, C. S., et al. (2015). Strontium/lithium ratio in aragonitic shells of Cerastoderma edule (Bivalvia) — A new potential temperature proxy for brackish environments. *Chemical Geology* 417: 341-355.

Girod, A. and A. Balzarini (2017). The local forms of Zootecus (Gastropoda: Pulmonata: Subulinidae) of Pakistan: an archaeomalacological case study. *Natural History Sciences. Atti Soc. it. Sci. nat. Museo civ. Stor. nat. Milano* 4(1): 31-42.

Glennie, K. W. (1992). Plate Tectonics and the Oman Mountains. *Tribulus* 2(2): 11-21.

Glennie, K. W. (2005). The geology of the Oman Mountains: an outline of their origin, Scientific Press.

Godwin, H. (1962). Half-life of Radiocarbon. *Nature* 195: 984.

Goodfriend, G. A. (1987). Radiocarbon age anomalies in shell carbonate of land snails from semi-arid areas. *Radiocarbon* 29(2): 159-167.

Goodfriend, G. A. (1990). Rainfall in the Negev Desert during the middle Holocene, based on 13C of organic matter in land snail shells. *Quaternary Research* 34(2): 186-197.

Goodfriend, G. A. (1992). The use of land snail shells in paleoenvironmental reconstruction. *Quaternary Science Reviews* 11(6): 665-685.

Goodfriend, G. A., et al. (1999). Radiocarbon age anomalies in land snail shells from Texas; ontogenetic, individual, and geographic patterns of variation. *Radiocarbon* 41(2): 149-156.

Goodfriend, G. A. and D. G. Hood (1983). Carbon isotope analysis of land snail shells; implications for carbon sources and radiocarbon dating. *Radiocarbon* 25(3): 810-830.

Goodfriend, G. A. and J. J. Stipp (1983). Limestone and the problem of radiocarbon dating of land-snail shell carbonate. *Geology* 11: 575-577.

Gupta, A. K., et al. (2003). Abrupt changes in the Asian southwest monsoon during the Holocene and their links to the North Atlantic Ocean. *Nature* 421: 354.

Hadden, C. S. and A. Cherkinsky (2017). Carbon Reservoir Effects in Eastern Oyster from Apalachicola Bay, USA. *Radiocarbon* 59(5): 1497-1506.

Hadden, C. S., et al. (2018). Carbon Isotopes (δ13C and Δ14C) in Shell Carbonate, Conchiolin, and Soft Tissues in Eastern Oyster (Crassostrea Virginica). *Radiocarbon* 60(4): 1125-1137.

Hallmann, N., et al. (2013). Holocene climate and seasonality of shell collection at the Dundas Islands Group, northern British Columbia, Canada—A bivalve sclerochronological approach. *Palaeogeography, Palaeoclimatology, Palaeoecology* 373(0): 163-172.

Händel, M. (2014). Al-Hamriya - Dynamik einer Muschelhaufenlandschaft in den Vereinigten Arabischen Emiraten. *Archaeologia Austriaca* 97-98: 77-96.

Hellyer, P. and S. Aspinall (2006). An archaeological and ecological curiosity - Terebralia palustris (Linnaeus, 1767) in the north-east of the Emirate of Abu Dhabi. *Tribulus* 16.1.

Hoffmann, G., et al. (2015). Geo-archaeological evidence for a Holocene extreme flooding event within the Arabian Sea (Ras al Hadd, Oman). *Quaternary Science Reviews* 113: 123-133.

Hoffmann, G., et al. (2016). Field Guide to the Geology of Northeastern Oman, Borntraeger Science Publishers.

Hoffmann, G., et al. (2013). Review of the long-term coastal evolution of North Oman- subsidence versus uplift (Review der langfristigen Küstenentwicklung Nordomans- Senkung und Hebung). *Zeitschrift der Deutschen Gesellschaft für Geowissenschaften* 164(2): 237-252.

Hosseinibalam, F., et al. (2011). Three-dimensional numerical modeling of thermohaline and wind-driven circulations in the Persian Gulf. *Applied Mathematical Modelling* 35(12): 5884-5902.

Hua, Q. and M. Barbetti (2004). Review of Tropospheric Bomb ^{14}C Data for Carbon Cycle Modeling and Age Calibration Purposes. *Radiocarbon* 46(3): 1273-1298.

Hua, Q., et al. (2015). Large variations in the Holocene marine radiocarbon reservoir effect reflect ocean circulation and climatic changes. *Earth and Planetary Science Letters* 422: 33-44.

Jacobsson, P., et al. (2017). Refining the Hallstatt Plateau: Short-Term 14C Variability and Small Scale Offsets in 50 Consecutive Single Tree-Rings from Southwest Scotland Dendro-Dated to 510–460 BC. *Radiocarbon* 60(1): 219-237.

Jenkins, W. J. e. a. (2010). The Passage of the Bomb Radiocarbon Pulse into the Pacific Ocean. *Radiocarbon* 52(2-3): 1182-1190.

Jennings, R. P., et al. (2015). The greening of Arabia: Multiple opportunities for human occupation of the Arabian Peninsula during the Late Pleistocene inferred from an ensemble of climate model simulations. *Quaternary International* 382: 181-199.

Johns, W. E., et al. (2000). Arabian marginal seas and gulfs. Technical Report 2000-01, University of Miami RSMAS**:** 60.

Johns, W. E., et al. (2003). Observations of seasonal exchange through the Straits of Hormuz and the inferred heat and freshwater budgets of the Persian Gulf. *Journal of Geophysical Research: Oceans* 108(C12).

Jones, D. S., et al. (1989). Sclerochronological records of temperature and growth from shells of Mercenaria mercenaria from Narragansett Bay, Rhode Island. *Marine Biology* 102: 225-234.

Jull, A. J. T., et al. (2018). Radiocarbon Dating and Intercomparison of Some Early Historical Radiocarbon Samples. *Radiocarbon* 60(2): 535-548.

Kämpf, J. and M. Sadrinasab (2005). The circulation of the Persian Gulf: a numerical study. *Ocean Science Discussions* 2(3): 129-164.

Khan, A. A. (1997). Quarts and Dolomite content variations and climate changes in late Pleistocene Sediments of the Nort Arabian Sea.

Khim, B.-K., et al. (2003). Seasonal discharge of estuarine freshwater to the western Chukchi Sea shelf identified in stable isotope profiles of mollusk shells. *Journal of Geophysical Research: Oceans* 108(C9): 3300.

Kömüşcü, A. Ü. (2017). Long-term mean monthly temperatures trends of the United Arab Emirates.

Kosnik, M. A., et al. (2017). Radiocarbon-calibrated amino acid racemization ages from Holocene sand dollars (Peronella peronii). *Quaternary Geochronology* 39: 174-188.

Kromer, B., et al. (2013). MAMS - A new AMS facility at the Curt-Engelhorn-Centre for Achaeometry, Mannheim, Germany. *Nuclear Instruments and Methods in Physics Research Section B: Beam Interactions with Materials and Atoms* 294(0): 11-13.

Kusky, T., et al. (2005). Tertiary-Quaternary faulting and uplift in the northern Oman Hajar Mountains.

Kutterer, A. U., et al. (2012). Neolithic cremation in south-east Arabia: archaeological and anthropological observations at FAY- NE10 in the Emirate of Sharjah (UAE). Arabian Archaeology & Epigraphy, Wiley-Blackwell. **23:** 125-144.

Kutterer, J. (2013). The Archaeological Site HLO1 A Bronze Age Copper Mining and Smelting Site in the Emirate of Sharjah (U.A.E.). PhD thesis, Eberhard-Karls-Universität Tübingen.

Lambeck, K. (1996). Shoreline reconstructions for the Persian Gulf since the last glacial maximum. *Earth and Planetary Science Letters* 142(1-2): 43-57.

Lambeck, K., et al. (2011). Sea level and shoreline reconstructions for the Red Sea: isostatic and tectonic considerations and implications for hominin migration out of Africa. *Quaternary Science Reviews* 30(25–26): 3542-3574.

Lendt, R. (2000). Reaktionen des oberflächennahen marinen Karbonatsystems im nordwestlichen Arabischen Meer auf den Südwest-Monsun. PhD, University of Hamburg.

Leng, M. J. (2006). Isotopes in Palaeoenvironmental Research, Springer Netherlands.

Leng, M. J., et al. (1999). Palaeoclimatic implications of isotopic data from modern and early Holocene shells of the freshwater snail *Melanoides tuberculata*, from lakes in the Ethiopian Rift Valley. *Journal of Paleolimnology* 21: 97-106.

Leng, M. J. and J. P. Lewis (2016). Oxygen isotopes in Molluscan shell: Applications in environmental archaeology. *Environmental Archaeology* 21(3): 295-306.

Leuschner, D. C. and F. Sirocko (2003). Orbital insolation forcing of the Indian Monsoon - a motor for global climate changes? *Palaeogeography, Palaeoclimatology, Palaeoecology* 197(1-2): 83-95.

Lindauer, S., et al. (2018). Highly-resolved radiocarbon measurements on shells from Kalba, UAE, using carbonate handling system and gas ion source with MICADAS. *Nuclear Instruments and Methods in Physics Research Section B: Beam Interactions with Materials and Atoms* in press.

Lindauer, S. and B. Kromer (2013). Carbonate Sample Preparation for ^{14}C Dating Using an Elemental Analyzer. *Radiocarbon* 55(2-3): 364-372.

Lindauer, S., et al. (2016). Investigating the Local Reservoir Age and Stable Isotopes of Shells from Southeast Arabia. *Radiocarbon* 59(2): 355-372.

Lindauer, S., et al. (2016). Investigating the Local Reservoir Age and Stable Isotopes of Shells from Southeast Arabia. *Radiocarbon*: 1-18.

Lindauer, S., et al. (2018). Heating mollusc shells - A radiocarbon and microstructure perspective from archaeological shells recovered from Kalba, Sharjah Emirate, UAE. *Journal of Archaeological Science: Reports* 21: 528-537.

Lindauer, S., et al. (2018). Heating mollusc shells – A radiocarbon and microstructure from archaeological shells recovered from Kalba, Sharjah Emirate, UAE. *Journal of Archaeological Science: Reports* 21: 528-537.

Lindauer, S., et al. (2017). The local marine reservoir effect at Kalba (UAE) between the Neolithic and Bronze Age: An indicator of sea level and climate changes. *Quaternary Geochronology* 42(Supplement C): 105-116.

Loftus, E., et al. (2015). A simple method to establish calcite:aragonite ratios in archaeological mollusc shells. *Journal of Quaternary Science* 30(8): 731-735.

Lokier, S. W., et al. (2017). Late Quaternary sea-level changes of the Persian Gulf. *Quaternary Research* 84(1): 69-81.

Mächtle, B., et al. (2010). Molluscs as evidence for a late Pleistocene and early Holocene humid period in the southern coastal desert of Peru (14.5°S). *Quaternary Research* 73(1): 39-47.

Magee, P. (2007). Beyond the Desert and the Sown: settlement Intensification in Late Prehistoric Southeastern Arabia. *Bulletin of the American Schools of Oriental Research* 347: 83-105.

Magee, P. (2014). The Archaeology of Prehistoric Arabia: Adaptation and Social Formation from the Neolithic to the Iron Age. Cambridge, Cambridge University Press.

Magee, P., et al. (2017). Tell Abraq during the second and first millenia BC: site layout, spatial organisation and economy. *Arabian Archaeology & Epigraphy* 28: 209-237.

Marali, S. and B. R. Schöne (2015). Oceanographic control on shell growth of Arctica islandica (Bivalvia) in surface waters of Northeast Iceland — Implications for paleoclimate reconstructions. *Palaeogeography, Palaeoclimatology, Palaeoecology* 420(0): 138-149.

Marali, S., et al. (2017). Reproducibility of trace element time-series (Na/Ca, Mg/Ca, Mn/Ca, Sr/Ca, and Ba/Ca) within and between specimens of the bivalve Arctica islandica – A LA-ICP-MS line scan study. *Palaeogeography, Palaeoclimatology, Palaeoecology* 484: 109-128.

Martins, J. M. M. and A. M. M. Soares (2013). Marine Radiocarbon Reservoir Effect in Southern Atlantic Iberian Coast. *Radiocarbon* 55(2-3): 1123-1134.

Matter, A., et al. (2015). Palaeo-environmental implications derived from lake and sabkha deposits of the southern Rub' al-Khali, Saudi Arabia and Oman. *Quaternary International* 382: 120-131.

Mattern, F. and A. Scharf (2017). Postobductional extension along and within the Frontal Range of the Eastern Oman Mountains.

Mayewski, P. A., et al. (2004). Holocene climate variability. *Quaternary Research* 62(3): 243-255.

McConnaughey, T. A. and D. P. Gillikin (2008). Carbon isotopes in mollusk shell carbonates. *Geo-Marine Letters* 28(5): 287-299.

Meehan, B. (1982). Shell Bed to Shell Midden. Canberra, Australian Institute of Aboriginal Studies.

Michael Reynolds, R. (1993). Physical oceanography of the Gulf, Strait of Hormuz, and the Gulf of Oman—Results from the Mt Mitchell expedition. *Marine Pollution Bulletin* 27: 35-59.

Michelsen, N., et al. (2015). Isotopic and chemical composition of precipitation in Riyadh, Saudi Arabia. *Chemical Geology* 413: 51-62.

Migowski, C., et al. (2006). Holocene Climate Variability and Cultural Evolution in the Near East from the Dead Sea Sedimentary Record. *Quaternary Research* 66(3): 421-431.

Milano, S., et al. (2018). Mollusk carbonate thermal behaviour and its implications in understanding prehistoric fire events in shell middens. *Journal of Archaeological Science: Reports* 20: 443-457.

Milano, S., et al. (2015). Changes of shell microstructural characteristics of Cerastoderma edule (Bivalvia) — A novel proxy for water temperature. *Palaeogeography, Palaeoclimatology, Palaeoecology*.

Murray-Wallace, C. V., et al. (2000). Palaeoclimatic implications of the occurrence of the arcoid bivalve Anadara trapezia (Deshayes) in the Quaternary of Australasia. *Quaternary Science Reviews* 19(6): 559-590.

Neubert, E. (1998). Annotated checklist of the terrestrial and freshwater molluscs of the Arabian Peninsula with description of new species. *Fauna of Arabia* 17: 333-461.

Neubert, E. (2003). The continental malacofauna of Arabia and adjacent areas, II The genus *Zootecus* Westerlund 1887. *Arch. Molluskenkunde* 132(1/2): 153-160.

Olsson, I. U. (2009). Radiocarbon Dating History: Early Days, Questions, and Problems met. *Radiocarbon* 51(1): 1-43.

Olsson, I. U. (2009). Radiocarbon Dating History: Early Days, Questions, and Problems Met.

Omer, W. M. M. (2010). Ocean Acidification in the Arabian Sea and the Red Sea. MSc, University of Bergen.

Pape, E., et al. (2008). Size-dependent distribution and feeding habits of Terebralia palustris in mangrove habitats of Gazi Bay, Kenia. *Estuarine, Coastal and Shelf Science* 76: 797-808.

Parker, A., et al. (2018). Geomorphology, Geoarcheology and Paleoenvironments. Dosariyah Reinvestigating a Neolithic coastal community in eastern Arabia, Archaeopress Publishing Ltd**:** 21-55.

Parker, A., et al. (2006). The early to mid-Holocene moist period in Arabia: some recent evidence from lacustrine sequences in eastern and south-western Arabia. *Proceedings of the Seminar for Arabian Studies* 36: 243-255.

Parker, A. G., et al. (2004). Holocene vegetation dynamics in the northeastern Rub' al-Khali desert, Arabian Peninsula: a phytolith, pollen and carbon isotope study. *Journal of Quaternary Science* 19(7): 665-676.

Parker, A. G. and A. S. Goudie (2007). Development of the Bronze Age landscape in the southeastern Arabian Gulf: new evidence from a buried shell midden in the eastern extremity of the Rub´ al-Khali desert, Emirate of Ras al-Khaimah, U.A.E. *Arabian Archaeology & Epigraphy* 18: 132-138.

Parker, A. G., et al. (2006). A record of Holocene climate change from lake geochemical analyses in southeastern Arabia. *Quaternary Research* 66: 465-476.

Parker, A. G., et al. (2016). Low-latitude Holocene hydroclimate derived from lake sediment flux and geochemistry. *Journal of Quaternary Science* 31(4): 286-299.

Parton, A., et al. (2013). An early MIS 3 pluvial phase in Southeast Arabia: Climatic and archaeological implications. *Quaternary International* 300(0): 62-74.

Patel, B., et al. (1978). Flux of certain radionuclides in the blood-clam Anadara granosa Linneaus under environmental conditions. *Journal of Experimental Marine Biology and Ecology* 35(2): 177-195.

Paterne, M., et al. (2018). Reservoir Ages in the Western Tropical North Atlantic from One Coral off Martinique Island (Lesser Antilles). *Radiocarbon* 60(2): 639-652.

Paul, D. and R. Mauldin (2013). Implications for Late Holocene climate from stable carbon and oxygen isotopic variability in soil and land snail shells from archaeological site 41KM69 in Texas, USA. *Quaternary International* 308-309(0): 242-252.

Penha-Lopes, G., et al. (2009). Population structure, density and food sources of Terebralia palustris (Potamididae: Gastropoda) in a low intertidal Avicennia marina mangrove stand (Inhaca Island, Mozambique). *Estuarine, Coastal and Shelf Science* 84(3): 318-325.

Petchey, F. and G. Clark (2011). Tongatapu hardwater: Investigation into the ^{14}C marine reservoir offset in lagoon, reef and open ocean environments of a limestone island. *Quaternary Geochronology* 6: 539-549.

Petchey, F., et al. (2013). High-resolution radiocarbon dating of marine materials in archaeological contexts: radiocarbon marine reservoir variability between Anadara, Gafrarium, Batissa, Polymesoda spp. and Echinoidea at Caution Bay, Southern Coastal Papua New Guinea. *Archaeological and Anthropological Sciences* 5(1): 69-80.

Petchey, F. A., A; Zondervan, A; Ulm, S; Hogg, A. (2008). New Marine DR Values For The South Pacific Subtropical Gyre Region. *Radiocarbon* 50(3): 373-397.

Phillips, C. S. and C. E. Mosseri-Marlio (2002). Sustaining Change: The Emerging Picture of the Neolithic to Iron Age Subsistence Economy at Kalba, Sharjah Emirate, UAE. Fifth International Symposium on the Archaeozoology of southwestern Asia and adjacent areas, Amman, Jordan, ARC-Publicaties Groningen.

Pietsch, D., et al. (2010). Holocene soils and sediments around Ma'rib Oasis, Yemen: Further Sabaean treasures? *The Holocene* 20(5): 785-799.

Pigati, J. S., et al. (2010). Radiocarbon dating of small terrestrial gastropod shells in North America. *Quaternary Geochronology* 5(5): 519-532.

Pillevuit, A., et al. (1997). The Oman Exotics: a key to the understanding of the Neotethyan geodynamic evolution. *Geodinamica Acta* 10(5): 209-238.

Piontkovski, S. A., et al. (2012). Interannual Changes in the Sea of Oman Ecosystem. *The Open Marine Biology Journal* 6(1): 38-52.

Plaziat, J.-C. and W. R. Younis (2005). The modern environments of Molluscs in southern Mesopotamia, Iraq: A guide to paleogeographical reconstructions of Quaternary fluvial, palustrine and marine deposits. *Notebooks on Geology* 2005/1.

Pous, S. P., et al. (2004). Hydrology and circulation in the Strait of Hormuz and the Gulf of Oman—Results from the GOGP99 Experiment: 2. Gulf of Oman. *Journal of Geophysical Research: Oceans (1978–2012)* 109(C12).

Prendergast, A. L., et al. (2017). New research on the development of high-resolution palaeoenvironmental proxies from geochemical properties of biogenic carbonates. *Palaeogeography, Palaeoclimatology, Palaeoecology* 484: 1-6.

Preston, G. W., et al. (2015). A multi-proxy analysis of the Holocene humid phase from the United Arab Emirates and its implications for southeast Arabia's Neolithic populations. *Quaternary International* 382: 277-292.

Purser, B. H. (1973). The Persian Gulf : Holocene carbonate sedimentation and diagenesis in a shallow epicontinental sea / edited by B.H. Purser. Berlin, Springer-Verlag.

Rech, J. A., et al. (2016). Assessing Open-System Behavior of 14C in Terrestrial Gastropod Shells. *Radiocarbon* 53(2): 325-335.

Reid, D. G., et al. (2008). Mudwhelks and mangroves: The evolutionary history of an ecological association (Gastropoda: Potamididae). *Molecular Phylogenetics and Evolution* 47(2): 680-699.

Reimer, P. J., et al. (2013). IntCal13 and Marine13 Radiocarbon Age Calibration Curves 0–50,000 Years cal BP. *Radiocarbon* 55(4): 1869-1887.

Reimer, P. J. B., T A; Reimer, R W. (2004). Discussion: Reporting and Calibraion of Post-Bomb ^{14}C Data. *Radiocarbon* 46(3): 1299-1304.

Richardson, C. A. (1987). Microgrowth patterns in the shell of the Malaysian cockle Anadara granosa (L.) and their use in age determination. *Journal of Experimental Marine Biology and Ecology* 111(1): 77-98.

Rodelli, M. R., et al. (1984). Stable isotope ratio as a tracer of mangrove carbon in Malaysian ecosystems. *Oecologia* 61(3): 326-333.

Rollins, H. B., et al. (1987). Growth increment and stable isotope analysis of marine bivalves: Implications for the geoarchaeological record of El Niño. *Geoarchaeology* 2(3): 181-197.

Rollins, H. B., et al. (1990). Mollusks and coastal archaeology; A review. Decade of North American Geology, Centennial Special Volume 4 "Archaeological Geology of North America". J. D. D. N.P. Lasca, Geological Society of America**:** 467-478.

Saliege, J.-F. L., A.-M.;Cleuziou, S. (2005). Estimation de l'effet reservoir 14C marin en mer d'Arabie. *Paleorient*: 64-69.

Santos, G. M. and K. Ormsby (2013). Behavioral Variability in ABA Chemical Pretreatment Close to the 14C Age Limit. *Radiocarbon* 55(2-3): 534-544.

Santos, G. M., et al. (2004). Magnesium perchlorate as an alternative water trap in AMS graphite sample preparation: a report on sample preparation at KCCAMS at the University of California, Irvine. *radiocarbon46* 1(165-173).

Santos, G. M. and X. Xu (2016). Bag of Tricks: A Set of Techniques and other Resources to Help 14C Laboratory Setup, Sample Processing, and Beyond. *Radiocarbon* FirstView: 1-17.

Santos, G. M. M., R B; Southon, J R; Griffin, S; Hinger, E; Zhang, D. (2007). AMS 14C Sample Preparation at the KCCAMS/UCI Facility: Status Report and Performance of Small Samples. *Radiocarbon* 49(2): 255-269.

Schneider, B., et al. (2016). Scenario-based tsunami risk assessment using a static flooding approach and high-resolution digital elevation data: An example from Muscat in Oman. *Global and Planetary Change* 139: 183-194.

Schöne, B. R. (2008). The curse of physiology—challenges and opportunities in the interpretation of geochemical data from mollusk shells. *Geo-Marine Letters* 28(5): 269-285.

Schöne, B. R., et al. (2005). Mutvei's solution: An ideal agent for resolving microgrowth structures of biogenic carbonates. *Palaeogeography, Palaeoclimatology, Palaeoecology* 228(1–2): 149-166.

Schöne, B. R., et al. (2005). Climate records from a bivalved Methuselah (Arctica islandica, Mollusca; Iceland). *Palaeogeography, Palaeoclimatology, Palaeoecology* 228(1–2): 130-148.

Schöne, B. R., et al. (2017). Effects of sample pretreatment and external contamination on bivalve shell and Carrara marble δ18O and δ13C signatures. *Palaeogeography, Palaeoclimatology, Palaeoecology* 484: 22-32.

Schöne, B. R. and D. M. Surge (2012). Bivalve Sclerochronology and Geochemistry. Part N (Revised), Volume 1 Mollusca 6 Bivalvia. P. A. Selden, Paleontological Institute University of Kansas**:** 1-24.

Schöne, B. R., et al. (2011). Annually resolved d^{13}Cshell chronologies of long-lived bivalve mollusks (Arctica islandica) reveal oceanic carbon dynamics in the temperate North Atlantic during recent centuries. *Palaeogeography, Palaeoclimatology, Palaeoecology* 302(1-2): 31-42.

Schulze-König, T., et al. (2010). BioMICADAS: Compact next generation AMS system for pharmaceutical science. *Nuclear Instruments and Methods in Physics Research Section B: Beam Interactions with Materials and Atoms* 268(7-8): 891-894.

Scourse, J. D., et al. (2012). The Marine Radiocarbon Bomb Pulse across the Temperate North Atlantic: A Compilation of Δ 14 C Time Histories from Arctica islandica Growth Increments. *Radiocarbon* 54(2): 165-186.

Searle, M. P., et al. (1983). Sedimentological and structural evolution of the Arabian continental margin in the Musandam Mountains and Dibba zone, United Arab Emirates. *GSA Bulletin* 94(12): 1381-1400.

Shirai, K., et al. (2014). Assessment of the mechanism of elemental incorporation into bivalve shells (Arctica islandica) based on elemental distribution at the microstructural scale. *Geochimica et Cosmochimica Acta* 126(0): 307-320.

Singh, A. D., et al. (2011). Productivity collapses in the Arabian Sea during glacial cold phases. *Paleoceanography* 26(3).

Sirocko, F., et al. (1993). Century scale events in monsoonal climate over the past 24,000 years. *Nature* 364: 322-324.

Sirocko, F., et al. (1991). Atmospheric summer circulation and coastal upwelling in the Arabian Sea during the Holocene and the last glaciation. *Quaternary Research* 36(1): 72-93.

Slim, F. J., et al. (1997). Leaf litter removal by the snail Terebralia palustris (Linnaeus) and sesarmid crabs in an East African mangrove forest (Gazi Bay, Kenya). *Journal of Experimental Marine Biology and Ecology* 215(1): 35-48.

Smitha, A., et al. (2014). Upwelling in the southeastern Arabian Sea as evidenced by Ekman mass transport using wind observations from OCEANSAT–II Scatterometer. *Indian Journal of Geo-Marine Science* 43: 111-116.

Soulet, G. (2015). Methods and codes for reservoir–atmosphere 14C age offset calculations. *Quaternary Geochronology* 29: 97-103.

Southon, J., et al. (2002). Marine Reservoir Corrections for the Indian Ocean and Southeast Asia. *Radiocarbon* 44(1): 167-180.

Staubwasser, M., et al. (2002). South Asian monsoon climate change and radiocarbon in the Arabian Sea during early and middle Holocene. *Paleoceanography* 17(4): 1063.

Staubwasser, M., et al. (2003). Climate change at the 4.2 ka BP termination of the Indus valley civilization and Holocene south Asian monsoon variability. *Geophysical Research Letters* 30(8).

Steinhof, A. (2016). Data Analysis at the Jena 14C Laboratory. *Radiocarbon* 55(2): 282-293.

Steinhof, A., et al. (2004). The New 14C Analysis Laboratory in Jena, Germany. *Radiocarbon* 46(1): 51-58.

Stringer, C. B., Finlayson, J.C., Barton, R.N.E., Fernández-Jalvo, Y., Cáceres, I., Sabin, R.C., Rhodes, E.J., Currant, A.P., Rodríguez-Vidal, J., Giles-Pacheco, F., Riquelme-Cantal, J.A. (2008). Neanderthal exploitation of marine mammals in Gibraltar. *Neanderthal exploitation of marine mammals in Gibraltar* 105: 14319–14324.

Stuiver, M. and T. F. Braziunas (1993). Modeling atmospheric (super 14) C influences and (super 14) C ages of marine samples to 10,000 BC. *Radiocarbon* 35(1): 137-189.

Stuiver, M., et al. (1986). Radiocarbon age calibration of marine samples back to 9000 cal yr BP. *Radiocarbon* 28(2B): 980-1021.

Styles, M., et al. (2005). Mapping ancient oceans. *Earthwise* 22: 14-15.

Sultan, S. A. R. and N. M. Elghribi (1996). Temperature inversion in the Arabian Gulf and the Gulf of Oman. *Continental Shelf Research* 16(12): 1521-1544.

Synal, H.-A., et al. (2007). MICADAS: A new compact radiocarbon AMS system. *Nuclear Instruments and Methods in Physics Research Section B: Beam Interactions with Materials and Atoms* 259: 7-13.

Synal, H.-A. and L. Wacker (2010). AMS measurement technique after 30 years: Possibilities and limitations of low energy systems. *Nuclear Instruments and Methods in Physics Research Section B: Beam Interactions with Materials and Atoms* 268(7-8): 701-707.

Taylor, R. E. and R. Berger (1967). Radiocarbon Content of Marine Shells from the Pacific Coasts of Central and South America. *Science* 158(3805): 1180-1182.

Taylor, V. K., Barton, R.N.E., Bell, M., Bouzouggar, A., Collcutt, S., Black, S., Hogue, J.T. (2011). The Epipalaeolithic (Iberomaurusian) at Grotte des Pigeons (Taforalt), Morocco: A preliminary study of the land Mollusca. *Quaternary International* 244: 5-14.

Tebano, T. and G. Paulay (2000). Variable recruitment and changing environments create a fluctuating resource: the biology of Andara uropigimelana (Bivalvia: arcidae) on Tarawa Atoll. *Atoll Research Bulletin* 488: 1-15.

Thamban, M., et al. (2007). Indian summer monsoon variability during the holocene as recorded in sediments of the Arabian Sea: Timing and implications. *Journal of Oceanography* 63(6): 1009-1020.

Twaddle, R. W., et al. (2017). Complexities in the palaeoenvironmental and archaeological interpretation of isotopic analyses of the Mud Shell Geloina erosa (Lightfoot, 1786). *Journal of Archaeological Science: Reports* 12: 613-624.

Uerpmann, H.-P. (1990). Radiocarbon Dating of shell middens in the Sultanate of Oman. *PACT* 29(IV.5): 335-347.

Uerpmann, H.-P., et al. (submitted). HLO1-South: An Early Neolithic Site in the Wadi al-Hilo (Sharjah, UAE). *Arabian Archaeology and Epigraphy*.

Uerpmann, H.-P., et al. (2013). The Neolithic period in the Central Region of the Emirate of Sharjah (UAE). *Arabian Archaeology and Epigraphy* 24(1): 102-108.

Uerpmann, M. (1992). Structuring the Late Stone Age of Southeastern Arabia. *Arabian Archaeology and Epigraphy* 3(2): 65-109.

Uerpmann, M. (2003). The dark millennium: Remarks on the final stone age in the Emirates and Oman. Archaeology of the United Arab Emirates. Proceedings of the First International Conference on the Archaeology of the U.A.E. D. T. Potts. London, Trident Press**:** 73-84.

Uerpmann, M. and H.-P. Uerpmann (1996). 'Ubaid pottery in the eastern Gulf – new evidence from Umm al-Qaiwain (U.A.E.). *Arabian Archaeology and Epigraphy* 7(2): 125-139.

Uerpmann, M., et al. (2018). HLO1-south: An Early Neolithic site in Wadi al-Hilo (Sharjah, UAE). *Arabian Archaeology and Epigraphy* 29(1): 1-9.

Ulm, S. (2002). Marine and estuarine reservoir effects in central Queensland, Australia: Determination of ΔR values. *Geoarchaeology* 17(4): 319-348.

Van Rampelbergh, M., et al. (2013). Mid- to late Holocene Indian Ocean Monsoon variability recorded in four speleothems from Socotra Island, Yemen. *Quaternary Science Reviews* 65: 129-142.

Vermeersch, P. M. and A. P. Kweakason (2008). A Holocene Prehistoric Sequence in the Egyptian Red Sea Area: The Tree Shelter, Cornell University Press.

von Bertalanffy, L. (1938). A quantitative theory of organic growth (inquiries on growth laws. II). *Human Biology* 10: 181-213.

Wacker, L., et al. (2013). A novel approach to process carbonate samples for radiocarbon measurements with helium carrier gas. *Nuclear Instruments and Methods in Physics Research Section B: Beam Interactions with Materials and Atoms* 294(0): 214-217.

Wacker, L., et al. (2010). A revolutionary graphitisation system: Fully automated, compact and simple. *Nuclear Instruments and Methods in Physics Research Section B: Beam Interactions with Materials and Atoms* 268(7-8): 931-934.

Wagner, G. A. (1995). Altersbestimmung von jungen Gesteinen und Artefakten. Stuttgart, Ferdinand Enke Verlag.

Wanamaker Jr, A. D., et al. (2008). Very Long-Lived Mollusks Confirm 17th Century AD Tephra-Based Radiocarbon Reservoir Ages for North Icelandic Shelf Waters. *Radiocarbon* 50(3): 399-412.

Wanamaker Jr, A. D., et al. (2011). Gulf of Maine shells reveal changes in seawater temperature seasonality during the Medieval Climate Anomaly and the Little Ice Age. *Palaeogeography, Palaeoclimatology, Palaeoecology* 302(1-2): 43-51.

Watanabe, T. K., et al. (2017). Past summer upwelling events in the Gulf of Oman derived from a coral geochemical record. *Scientific Reports* 7(1): 4568.

Webb, G. E. e. a. (2007). Cryptic meteoric diagenesis in freshwater bivalves: Implications for radiocarbon dating. *Geology* 35(9): 803-806.

Weninger, B., et al. (2009). The impact of rapid climate change on prehistoric societies during the Holocene in the Eastern Mediterranean. *Documenta Praehistorica* 36: 7-59.

Wohlwend, S., et al. (2017). Late Jurassic to Cretaceous evolution of the eastern Tethyan Hawasina Basin (Oman Mountains). *Sedimentology* 64(1): 87-110.

Wood, W. W. and J. L. Imes (2003). Dating of holocene ground-water recharge in western part of Abu Dhabi (United Arab Emirates): Constraints on global climate-change models. Developments in Water Science. A. S. Alsharhan and W. W. Wood, Elsevier. **50:** 379-385.

Yoloye, V. (1975). The Habits and Functional Anatomy of the West African Bloody Cockle, Anadara Senilis (L.). *Journal of Molluscan Studies* 41(4): 277-299.

Yu, S.-Y., et al. (2007). Modeling the Radiocarbon Reservoir Effect in Lacustrine Systems. *Radiocarbon* 49(3): 1241-1254.

Zazzo, A. (2014). Bone and enamel carbonate diagenesis: A radiocarbon prospective. *Palaeogeography, Palaeoclimatology, Palaeoecology* 416(0): 168-178.

Zazzo, A., et al. (2013). Can We Use Calcined Bones for Radiocarbon Dating the Paleolithic? *Radiocarbon* 55(2-3): 1409-1421.

Zazzo, A., et al. (2016). A Revised Radiocarbon Chronology of the Aceramic Shell Midden of Ra's Al-Hamra 6 (Muscat, Sultanate of Oman): Implication For Occupational Sequence, Marine Reservoir Age, and Human Mobility. *Radiocarbon* 58(2): 383-395.

Zazzo, A., et al. (2012). Variability in the marine radiocarbon reservoir effect in Muscat (Sultanate of Oman) during the 4th millennium BC: reflection of taphonomy or environment? *Journal of Archaeological Science* 39(7): 2559-2567.